Density driven Natural Convection Heat Transfer in fully immersed Liquid-Cooled Data Centre Application

YongQiang Chi

Thesis submitted in accordance with the requirements for
the degree of Doctor of Philosophy

Faculty of Engineering

School of Mechanical Engineering

December 2015

The candidate confirms that the work submitted is his/her own, except where work which has formed part of jointly authored publications has been included. The contribution of the candidate and the other authors to this work has been explicitly indicated below. The candidate confirms that appropriate credit has been given within the thesis where reference has been made to the work of others.

The work in Chapter 6 of the thesis has appeared in publication as follows:

Chi Y.Q., Summers J., Hopton P., Deakin K., Real A., Kapur N., Thompson H., (2014), *Case study of a data centre using enclosed, immersed, direct liquid-cooled servers in*: Annual IEEE Semiconductor Thermal Measurement and Management Symposium 2014, pp.164-173.

I was responsible as the primary author of the article. And the contribution of the other authors was included

Acknowledgements

This research document would not be finished without a contribution of a number of people. It is their assist and helps to make this research possible to be done.

Firstly I would like to acknowledge the tremendous input of my supervisors, Dr Jon Summers, Prof Nik Kapur and Prof Harvey Thompson. With their support in physics, mathematics and laboratory, I could then able to understand the core knowledge of natural convection and turbulence, and present them in this research.

I would also like to express my gratitude to few research students in the University of Leeds, who including Abdulmajeed Almaneea, Amirul Khan and Nicolas Delbosc. They have not only involved in the combined benchmarking project and help completing the CFD (Computational Fluid Dynamic) problem across variety of solutions, but also share their knowledge and experience of fluid dynamic during the work.

I would like to express my gratitude to the staffs and managers in Iceopote R&D Ltd. and their sub-contractor fellows including Peter Hopton, Keith Deakin, Stephan Hollingshead, Phil Astley, Paul Taylor, Paul Coates, Simon Bown and Andrei Horvat who have played an important role in assisting and pushing this project ahead. The Iceotope Company provided a laboratory space and equipment for the thermal experiment during this research. They also built a commercial HPC system for the lab of University of Leeds, School of Mechanical Engineering which deeply involved in the experiment of this research.

Finally, I would like to say thank you to my wife, KaiYi Wang, who supported me to complete this task, as always.

Abstract

Data centres are developing at a rapid pace with the continued increase in digital demands. Data centre cooling and energy efficiency is a growing topic of interest that requires new engineering solutions. To achieve both better cooling and higher efficiency, liquid-cooled computer systems are being considered as one of the best solutions.

Total liquid cooled computers are not new, but with the power densities required for supercomputers have seen resurgence in liquid cooling, in particular solutions that do not require the use of air as a cooling medium. Recently the industry has developed an advanced fully immersed liquid-cooled data centre solution to fulfil this purpose. The core technology of the design is a liquid-cooled computer node (first cooling stage), which relies on density-driven, natural convection that has challenging engineering requirements.

This thesis looks at the density-driven, natural convection from a different angle by simplifying the Navier-Stokes equations and Convection-Diffusion equation leading to the development of a Constant Thermal Gradient (CTG) model to solve the natural convection flow analytically. The CTG model yields algebraic solutions for velocity and temperature profiles, thereby it is able to give the flow characteristic length (l^*) and indicate the boundary layer thickness directly. The development and usage of the CTG model is the academic achievement in this thesis, and it provides a clearer understanding of natural convection mechanism.

This thesis also uses CFD simulation (ANSYS CFX) and laboratory experiment to analyse the heat transfer performance of the liquid-cooled system. A group of CFD simulations of a cavity convection problem has been carried out to find the appropriate approximation factor for the CTG model, hence completing the CTG model and make it ready for further analysis. A full scale CFD simulation has also been carried out to analyse the first cooling stage of the system for a given condition, and a real computer system has also been tested under the same condition. Then a three-step research work-flow has been developed to do heat transfer analysis on a natural convection based liquid-cooled system: CTG model, CFD simulation and experimental test. This thermal analysis work flow provides a knowledge base for further improvement in cooling design of the system, and this is the engineering achievement of this thesis.

In order to see the thermal advantages of the fully-immersed liquid-cooled system, other intense real-world tests on the liquid-cooled system have been carried out. One of which is a benchmark test between an advanced back-door water cooled system and a fully-immersed liquid-cooled system; and such benchmark proves the thermal benefit of the fully liquid-cooled solution. The other benchmark is a series of real-world tests on a fully immersed liquid-cooled system which aim to achieve the ASHRAE

W5 standard, and it proves the practicality of the liquid-cooled solution. The benchmark test in this thesis was published in the Semi-Therm conference.

List of figures

List of tables

Abbreviations

1-D	One dimensional / single dimensional
CAD	Computer Aided Design
CFD	Computational Fluid Dynamic
CTG	Constant Thermal Gradient / Constant Temperature Gradient (Model)
CPU	Centre Processing Unit
DDR	Double Data Ram
DIMM	Dual in-Line Memory Module
DNS	Direct Numerical Solution
ECC	Error Correcting Code
EER, eer	Energy Efficiency Ratio
GPU	Graphic Processing Unit
GPGPU	General-purpose computing on graphics processing units
HFE	Hydrofluoroether
HTC	Heat Transfer Coefficient
IPMI	Intelligent Platform Management Interface
IT	Information technology
k-ε	Kinetic - Epsilon Turbulence Model
k-ω	Kinetic - Omega Turbulence Model
LBM	Lattice Boltzmann methods
LDV	Laser Doppler Velocimetry
LES	Large Eddy Simulation
MB	MotherBoard
N-S	Navier-Stokes Equations
PDE	Partial Differential Equation
PFC	Perfluorinated compound
PFPE	Perfluoropolyether
PIV	Particle Image Velocimetry
PUE	Power Usage Effectiveness
RANS	Reynolds Averaged Navier-Stokes Equations Solution
RMS	Root Mean Square
SDRAM	Synchronous Dynamic Random-Access Memory
SHC	Specific Heat Capacity
SST	Share Stress Transport
TDP	Thermal Design Power
TKE	Turbulence Kinetic Energy

ULP	Ultra-Low-Profile
Y-Plus	Dimensionless Wall Distance, Y+

Nomenclature

a		General Equation Parameter
A	$\frac{\rho g \beta}{\mu}$	Coefficient for constant thermal gradient (CTG) model
A_Q	m^2	Surface area for heat flux
b		General Equation Parameter
B	$\frac{\rho g \beta T_0}{\mu}$	Coefficient for constant thermal gradient (CTG) model
C	$\frac{SHC \cdot \rho}{\lambda} \cdot \frac{\partial T}{\partial y}$	Coefficient for constant thermal gradient (CTG) model
C_n		Constant of Integration such as C_1, C_2, C_3 etc.
C_p	J/kg·K	Pressure Coefficient for k-ε turbulent model
$C_{\varepsilon 1}$		Dissipation Coefficient 1 for k-ε / k-ωturbulent model
$C_{\varepsilon 1}$		Dissipation Coefficient 2 for k-ε / k-ω turbulent model
C_p		Specific Heat Capacity
C_μ		Viscosity Coefficient for k-ε / k-ω turbulent model
C+		Constant for k-ε turbulent model, C+ ≈5.1
C_{TG}	$^oC/m^2$ or K/m^2	Thermal gradient Constant or Temperature Gradient Constant, $\frac{\partial T}{\partial y}$
cST	cm^2/s	CentreStokes
de		Change (differential) rate of the internal energy (W) of the medium
e		Internal Energy
E		Total Energy
err	%	Error rate
f	N	Force
f*		Force (non-dimension)
F	N	Force
g	m/s^2 or N/kg	Gravity
G	m/s^2 or N/kg	Gravity
Gr		Grashof Number
h	m	Height (Y axis), or thermal height (on gravity direction)
HTC	$W/m^2 \cdot K$	HTC, Heat Transfer Coefficient
i		Index Count for Degree of Freedom (1st DoF, or X axis direction)
j		Index Count for Degree of Freedom (2st DoF, or Y axis direction)
k		Index Count for Degree of Freedom (3st DoF, or Z axis direction)
k		Turbulence Kinetic Energy
k_c , k_f	W/m·k	Thermal Conductivity
k_v		Von Kármán Constant

k		1000, or General Scalar
K		Unit of Kelvin temperature
$\mathbf{K_{close}}$.		CTG model Coefficient for close natural convection cavity solution
l	m	Length (X axis), or thermal distant (normal to gravity direction)
*l**	m	Characteristic length scale for CTG model, also boundary thickness
l_{mix}		Mixed Length Scale
L	m	Length
n		Numbering
Nu		General Nusselt Number
Nu_h		Nusselt Number, for the gravity direction temperature and length scale
Nu_l		Nusselt Number, for the horizontal temperature and length scale (normal to gravity direction)
Nu*		Specific Nusselt Number, derivate form the constant gradient (CTG) model
m		Million, or meter
p	N/m^2 or Pa	Pressure
*p**		Pressure (non-dimension)
P	W	Power
P_k		Production of the Turbulence Kinetic Energy
Pr		Prandtl Number
$\vec{q}$	W/m^2	Local Heat Flux
Q	J	Heat Energy or Heat load, same as *E*
Q'	W	Power or Heat power
Q*	W/m^2	Heat flux
R, R^2		Root Mean Square
Ra		General Rayleigh Number
Ra_h		Rayleigh Number, for the gravity direction temperature and length scale
Ra_l		Rayleigh Number, for the horizontal temperature and length scale (normal to gravity direction)
Ra*		Specific Rayleigh Number, derivate form the constant gradient (CTG) model
Ra_{CWT}		Rayleigh number based on constant wall temperature
Ra_{CWHF}		Rayleigh number based on constant wall heat flux
Re		Reynolds Number
Re_D		Reynolds number based on the pipe diameter
t	s	Time
T	*K* or ^oC	Temperature
T_0 , T_s	*K* or ^oC	Source Temperature

T_1	*K* or ºC	Delta temperature from heated wall to middle wall on observation point, normal to gravity direction
$\overline{\boldsymbol{T_1}}$	*K* or ºC	Delta temperature value, from heated wall temperature (average) to middle wall temperature
T_l	*K* or ºC	Delta temperature from heated wall far side, normal to gravity direction (Rayleigh number for single heated wall problem)
T_∞	*K* or ºC	Reference Temperature (infinite far)
u	m/s	Velocity (general)
u*		Velocity (non-dimension)
u+		Dimensionless Velocity
ū	m/s	Mean-Velocity
ũ	m/s	Derivative (Fluctuation) Velocity
u_τ	m/s	Friction Velocity
u_{mix}	m/s	Mixed Velocity Scale
U		Velocity (non-dimension)
v	ST or m^2/s	Kinetic Viscosity
v_t	ST or m^2/s	Shear (Force) Viscosity
V	m^3	Volume
W		Surrounding Environment
x, X	m	Unknown, or X axis Displacement (Vector)
y, Y	m	Unknown, or Y axis Displacement (Vector)
Y+		Y-Plus value, Dimensionless Wall Distance
Y*	m	First layer mesh thickness
z, Z	m	Unknown, or Z axis Displacement (Vector)
ε		Dissipation of Turbulence Kinetic Energy
∇	m^{-1}	Del Operate
∇*		Del Operate (non-dimension)
$\nabla \cdot T'$		Transportation of Turbulence Kinetic Energy
Δ		Delta, Variation or Error between 2 parameter in the same unit
Δ_ρ	kg/m^3	Density Variation
Δp	Pa	Pressure Variation
Δt	s	Time change
ΔT	*K* or ºC	Delta Temperature
$\Delta L, \Delta l$	m	Distant between 2 points
α	m^2/s	Thermal diffusive
β	1/k	Thermal Expansion
μ	Pa·s	Dynamic Viscosity
μ_t	Pa·s	Shear (Force) Viscosity

ρ	kg/m^3	Density
ρ_0	kg/m^3	Initial Density
ρ_1	kg/m^3	Result Density
$\rho_{hfe7200}$	kg/m^3	Density of 3M Novec HFE 7200
$\rho_{hfe7300}$	kg/m^3	Density of 3M Novec HFE 7300
u or u_x	m/s	X axis velocity
υ or u_y	m/s	Y axis velocity
ω or u_z	m/s	Z axis velocity
$\tilde{u}\tilde{u}$		Reynolds Stress
uu		Reynolds Stress
δ		Local Layer Width
$\boldsymbol{\lambda}$	W/(m.K)	Thermal conductivity
τ	Pa	Shear Stress (Fluid)
σ	Pa	Stress (general)
σ_k		Closure coefficient (Prandtl-Schmidt number) of k.
σ_w		Closure coefficient
σ_ε		Closure coefficient
δE	W	Infinite small amount of total energy
δW	W	Infinite small amount of work that the medium has done

1. Introduction

Liquid-cooled computer systems are considered to be state-of-the-art in terms of the design for data centres and super computing solutions. In particular the fully immersed liquid-cooled design combines the performance and efficiency together and has stood out among all other high-performance computer designs. This thesis will focus on understanding and analysing such engineered system, in order to help improving the future design by reducing the operational and infrastructure costs.

The Iceotope fully-immersed liquid-cooled high-performance computer system

Iceotope have developed fully immersed liquid-cooled, enclosed and modularized computer server systems for a number of information technology requirements, such as high-performance-computer (HPC) and integrated data centre solutions. The Iceotope arrangement gives rise to a number of heat transfer stages, the first of which uses natural convection to transfer heat within a di-electric liquid (HFE or PFPE) coolant from the microelectronics to the edge of the enclosure. A second cooling stage is based on forced convection of a water-based coolant, which removes the heat from the capsule. The uniqueness of such a cooling design, especially in the first stage at the server level, requires in-depth research of the natural convection mechanism within a sealed box to both assess requirement parameters and system performance.

Aim of the research:

This PhD thesis undertakes research into the natural-convection heat transfer performance based on a fully-immersed liquid-cooled high performance computer solution. This industrially sponsored project aimed to fulfil both requirements for fundamental understanding of the thermofluid dynamics and engineering design issues of quantified heat transfer and system improvements.

Academic

A mathematical model has been developed in this thesis by a detailed mathematical analysis of the fundamentals of natural convection. The mathematical description of the flow can aid the understanding of the natural convection process in an enclosure.

Engineering

A work flow will be developed in this thesis for the related industrial application (as developed by the sponsor company). Such a work flow will include mathematical predictions, numerical analyses (via Computational Fluid dynamic, CFD) and laboratory based experiments. The development and usage of this work flow has helped the industrial sponsor design and improve the cooling performance of a natural convection based liquid-cooled computer system.

Objectives of the research

The research presented in this thesis addresses four key objectives:

1, Review of the background of the problem

Before looking into specific problems, a detailed review of background knowledge is necessary to understand computer design and the development of its cooling technique, which eventually leads to two problems: the advantage of fully immersed liquid-cooled system, and how to understand the fluid dynamics of the system.

2, Understanding the natural convection mechanism and mathematical model

Natural convection flows are usually difficult to model and analyse, (Zitzmann, T., et al, 2005) therefore this thesis explores the basic principles of fluid dynamics of such naturally convected flows. Simplifying, via certain assumptions, the Navier-Stokes equations and Convection-Diffusion equation, this work determines closed-form analytical expressions for the internal di-electric temperature profiles. Such solutions are also able to reveal some of the flow characteristics of the natural convection.

3, Analysis, testing and experiments for the problem

Following review of the mathematics of the problem, experiments and practical evaluations are also required. Specifically, Computational Fluid Dynamics (CFD) analysis is used to provide approximations for missing values to complete the mathematical model, and to compare with the result of the mathematical modelling.

4, Measurement and proof of fully immersed liquid-cooled design advantages

The other part of the practice is to run a series of experiments based on real computer systems, both air-cooled and liquid-cooled, to compare with the mathematical modelling and CFD analysis, and to try to prove the advantages of adopting a fully-immersed liquid-cooled solution in high-performance computer design.

Structure of the thesis

Excluding introduction, conclusion and reference sections, there will be 4 chapters as follows.

Chapter 2 includes a general review of the history of data centre and supercomputers design. This will provide some background knowledge of engineering approaches to data centre cooling and the reason why fully immersed liquid-cooled data centre solution is beneficial and why natural convection research is needed for such design.

In chapter 3 the mathematical knowledge and description of natural convection flow is presented. The chapter reviews density driven natural convection flow mathematically and physically, then raises the problem of mathematical modelling of the natural convection flow. Finally in this chapter a simplified expression of natural convection model (Constant Thermal Gradient model) will be given.

Based on the CTG model given in the previous chapter, chapter 4 will be a further research of natural convection modelling. A number of CFD analyses will be carried out in this chapter to find the appropriate approximation and complete Constant Thermal Gradient (CTG) model.

Chapter 5 includes the experimental section that links the theory and engineering solution together, and presents a series of case studies that compare the analytical model (CTG model), the CFD simulation and the real world experiment as an engineering work flow. Finally, chapter 6 contains results of energy efficiency testing of the fully immersed liquid-cooled computer system that proves its benefit to the industry.

In conclusion, all these chapters complete a full iteration of research and develop work, which eventually transfers in to the knowledge of doing development work for the industry.

2. Literature review- development of the data centre and its cooling design

The dictionary definition of Supercomputer is more related to a computer system usually designed for High Performance Computing (HPC), while the definition of a data centre will be that of a data-communication facility with a combination of compute, storage, tele-communication and other supporting system. Though these 2 objects are different in definition, and the term of 'supercomputer' appears to be a subset of the general concept of a 'data centre', they sometimes share similarity in design and application and will be put into the same discussion of large scale computing technology.

This chapter has four parts: The first part is a general review of data centre and supercomputer development. The second part is an in-depth discussion of data centre and supercomputer thermal / power issues. The third part is an explanation of thermal design progress from air-cooled based system towards liquid-cooled based system. The last in this chapter will be a detailed description of the fully immersed liquid-cooled data centre designs, which also explains the benefit of such design.

2.1 The blooming of data centre and supercomputer

The history of the super computer and the data centre can be traced back to the early design and the original electronic computer. One of the very first applications is the ENIAC in 1946. The ENIAC (Electronic Numerical Integrator and Computer) had more than 17,000 vacuum tube and 1500 relays; it also took 167 square meters of floor space, weighed about 27 tons and, most importantly, consumed 150kW of electrical power (Weik, 1955).

To assess the computer performance, different measurements have been introduced towards different type of computer and different requirement of calculation. But to benchmarking all types of computer, it usually use a simple base line to measure it: Floating Point Operation per Second (FLOPS). The FLOPS performance is usually measured by carrying out simple calculation such as LINPACK benchmarking, and **Figure 2-1** is some LINPACK result of top listed supercomputers in FLOPS:

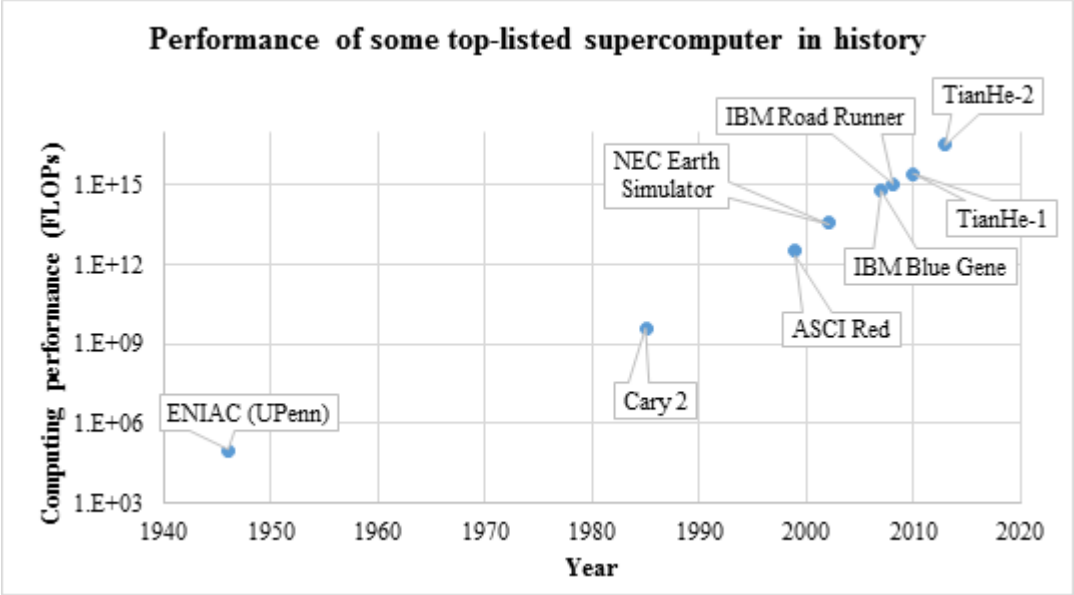

Figure 2-1 Equivalent computing performance (FLOPs) of some top-listed supercomputers in history (TOP500, 2015)

Notice: The ENIAC performance is an equivalent value. More data can be found in the appendix section

The complexity of computer design has been growing ever since the first computer, especially after the transistor and integrated circuit has been introduced. The most famous description of such is Moore's law (Moore, 1965), which stated number of transistors count in computer will double every 18 months. The law has held true over the years and the computing capability has remained exponential (**Figure 2-2**).

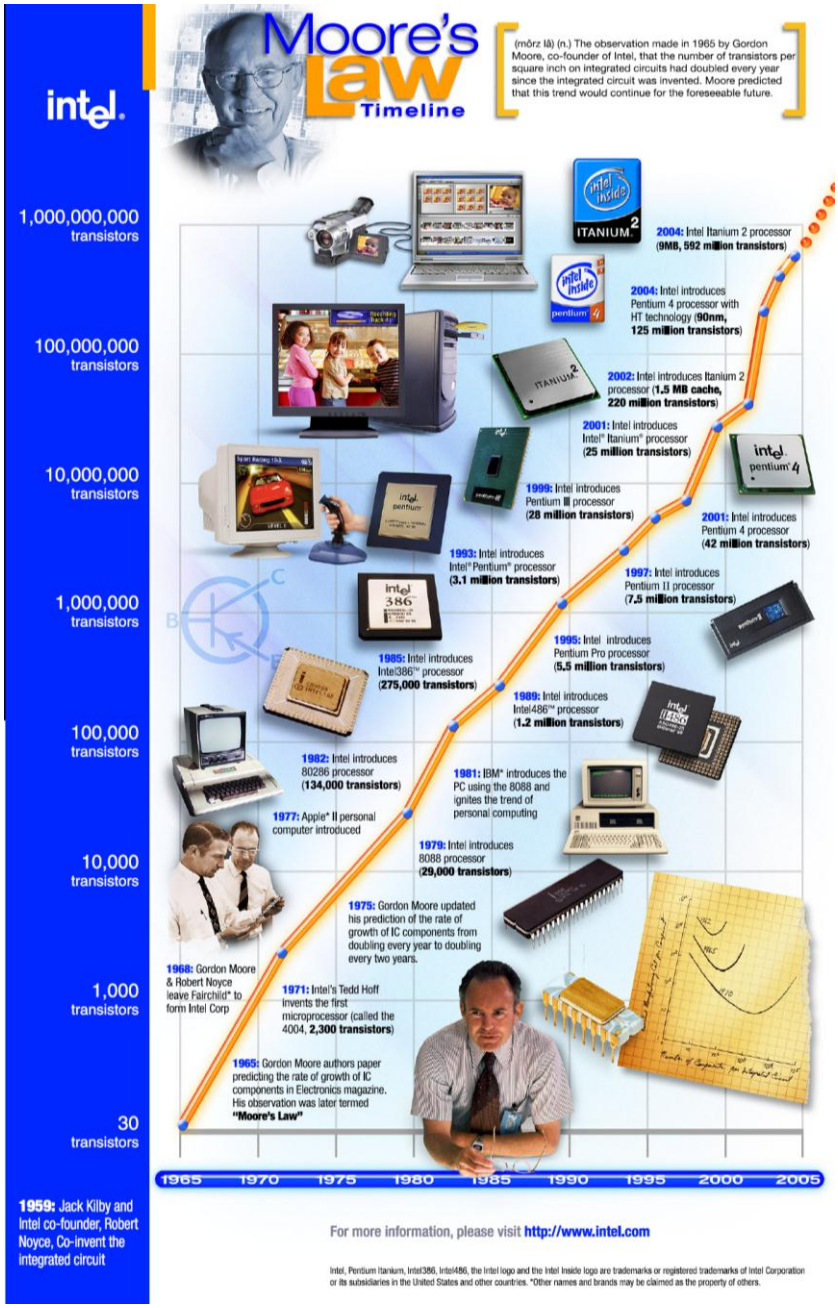

Figure 2-2 Transistor count form 1965 to 2015 following Moore's law, (Intel 2015)

Not only has the complexity of computer been growing, the usage of computer technology has increased as well. This became more evident with the growth of the Internet in recent years; computers have become one of the most important development in people's lives. This can be seen from the increasing worldwide usage of the Internet since 1996 (ITU, 2015)

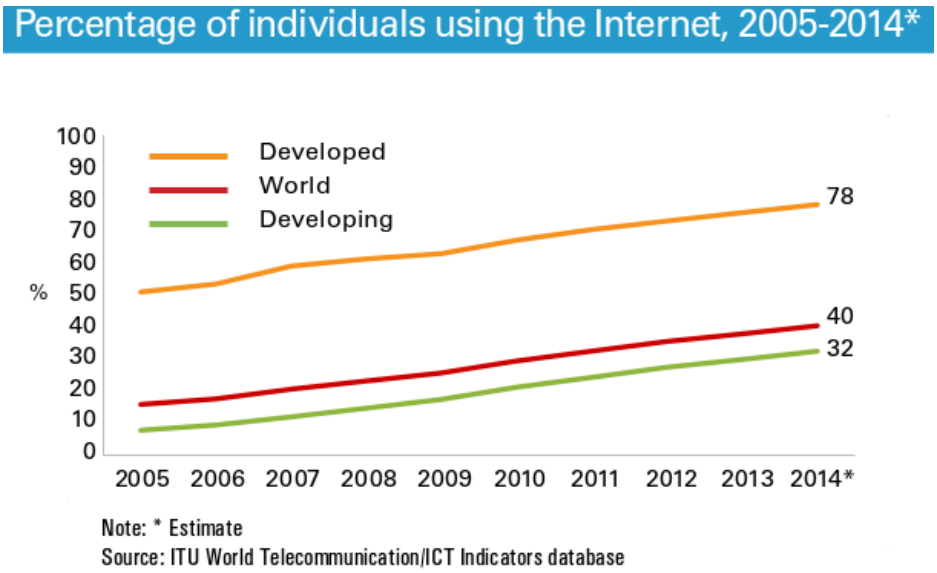

Figure 2-3 Individuals using the Internet 2005 to 2014 (ITU, 2014)

From the **Figure 2-3** it can be seen the gradually increment of internet user over the years. Also in the same research (ICT, 2014), it shows that 40% of the world population has internet access up to 2014.

Such increased usage of computers and Internet resources has led to not only greater demand for data centres, but also the changing style of data centres. Before commoditisation of computing technology, the usage of large scale and high performance computing has been dominated by the academic bodies and research bodies; 'classified' sectors (military, aero-space etc.) haves occupied a significant proportion of the applications space.. This can be seem from the application type in the TOP500 list, which list the top 500 performance (based on FLOPS) supercomputers every year. But since late 90s' more computing resource has been put into the industry bodies, and recent years the academic and research bodies took back some of the proportion again (**Figure 2-4**).

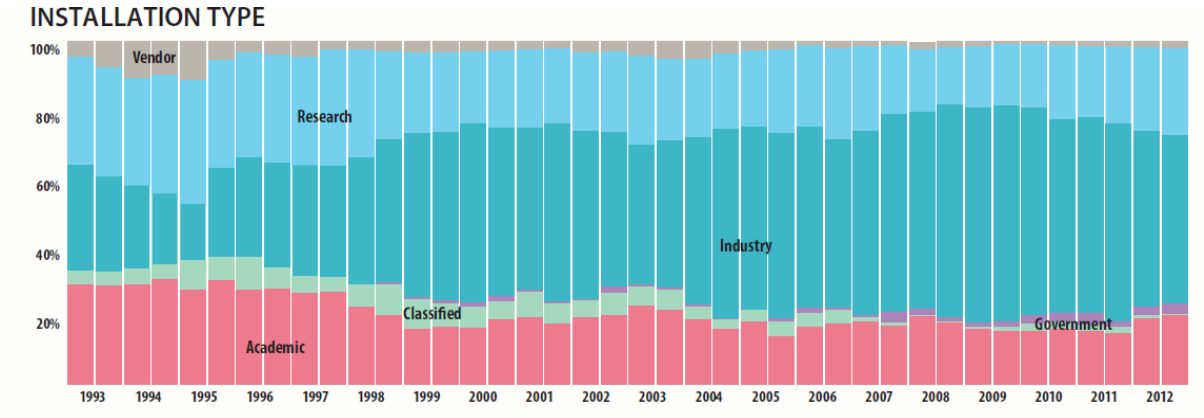

Figure 2-4 Supercomputer on the TOP500 list are used primarily I industry, research and academia. Over 50% of them go to industry (TechUK. 2013)

The changing application of supercomputers and data centres also results the change of computer design. Before the 90s, mainframe style (such as IBM-Power based solution) was more popular at the time. They were more specific built, more stable but less flexible and less performance based as well. But from the 90s, commodity based x86 style supercomputer become popular choice by data centre operators, especially from 2000s onwards where the 64-bit x86 system was introduced. The x86 system usually has more flexibility to adapt different hard ware application and different operation system (OS)

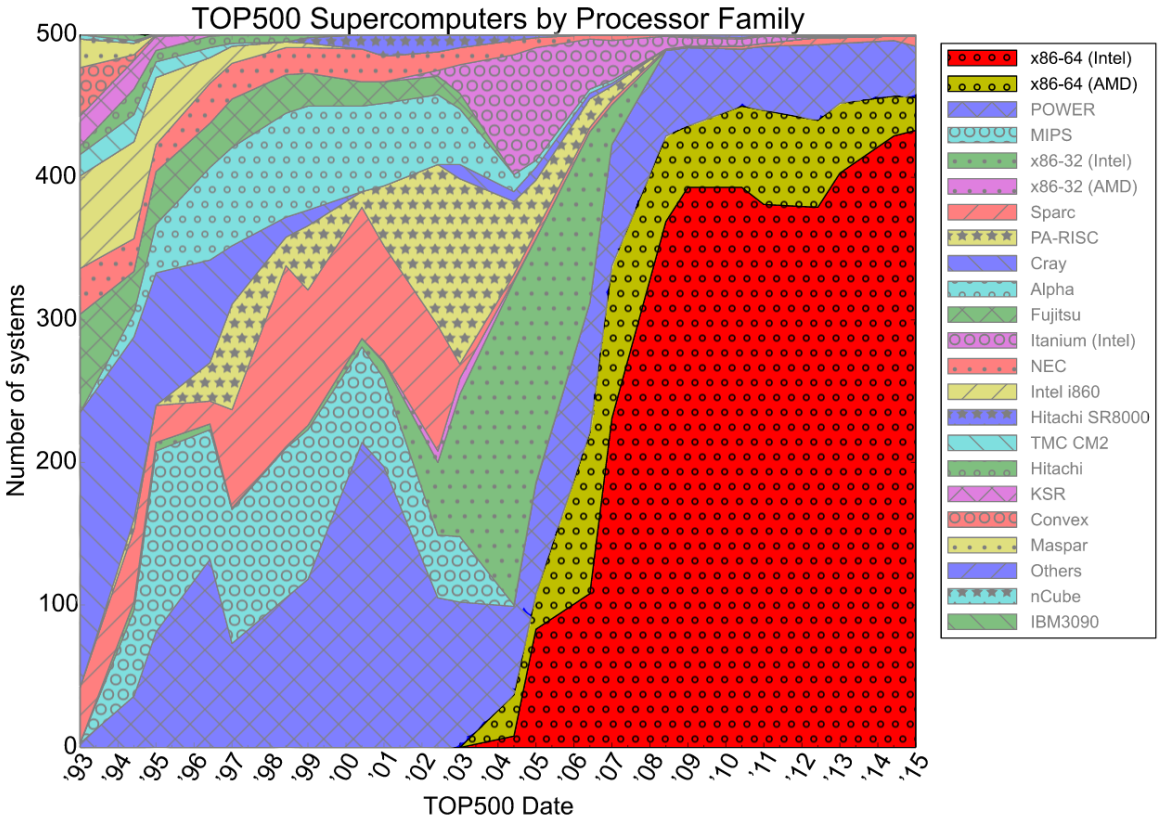

Figure 2-5 Processor family used in Top 500 supercomputers from 1993 to 2015 (TOP500, 2015)

It can be seem from the **Figure 2-5** how the processor family migrated from various proprietary providers in early 90s to becoming dominated by Intel / AMD x 86 families. So in the following sections of this research, the computer systems are based on Intel x86-64bit solution.

The increased usage and improved calculation performance (FLOPs based) eventually leads to another issue of computer design: its power consumption. In fact the power consumption of data centres has been continually increasing.

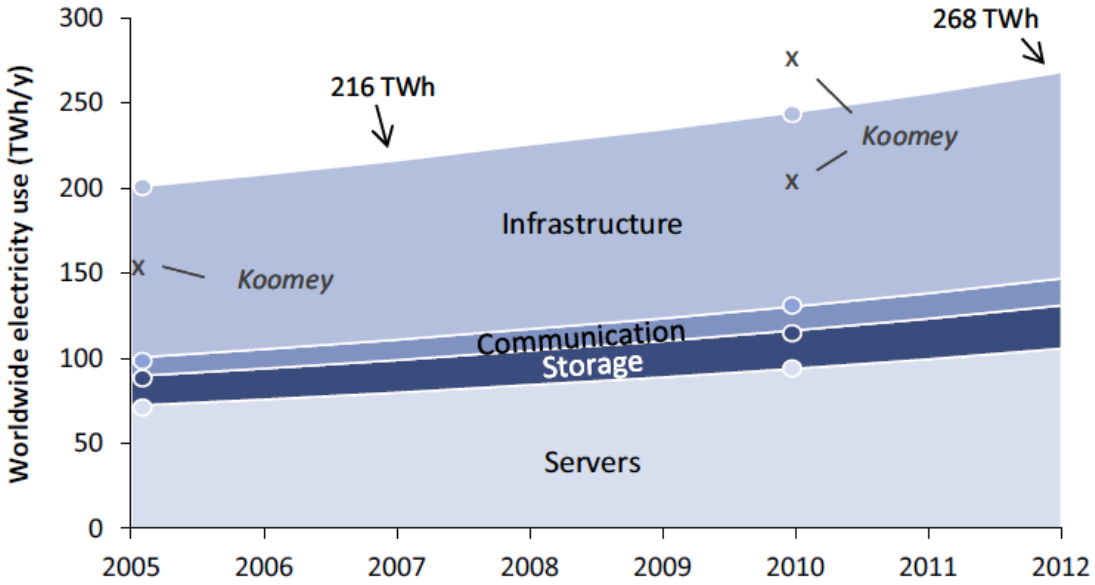

Figure 2-6 Worldwide use phase electricity consumption of data centres. Infrastructure electricity (Heddeghem, 2014)

Here is a figure that shows about a 1/3 increase in electricity power consumption of data centres worldwide between 2005 and 2012 (Heddeghem, 2014). This is the broad view about power consumption of data-communication industry, but how this increasing demand of power affect the design of supercomputers and data centres will be the topic of the next section in this chapter.

2.2 Thermal load of data centres and supercomputers

Obviously the increasing density of transistors and faster speed of integrated circuit (chip) will result a power issue, and the facing problem is not just how to handle such amount of power electronically, but also how to handle it thermally. Use the same table of top-listed super computer in history from the previous section and fill the power load and space occupation of these systems:

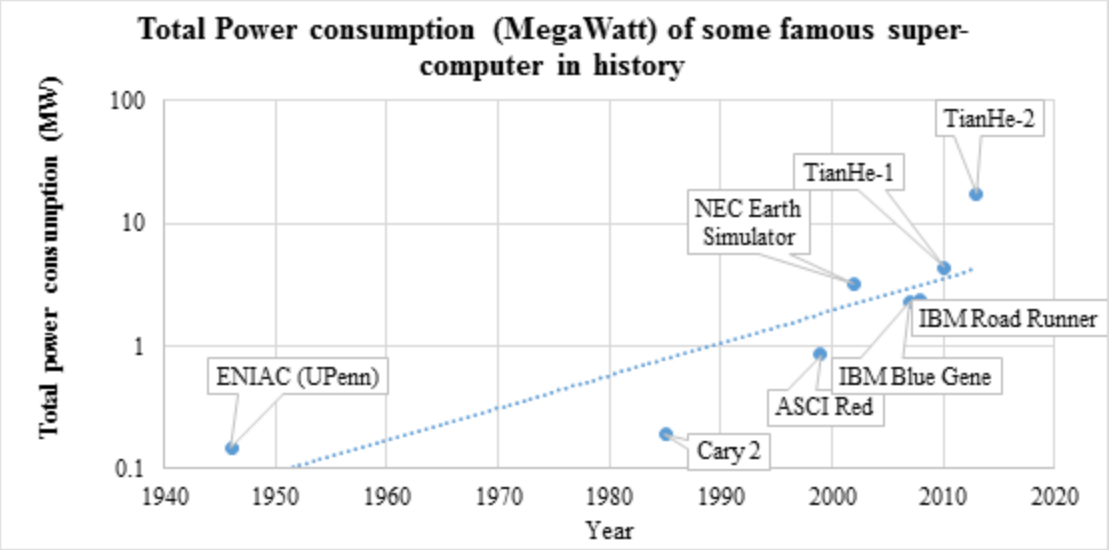

Figure 2-7 Thermal load against years of some top-listed super computer, (TOP500, 2015)

From the **Figure 2-7**, it can be seen that growth of power load of supercomputers has continued over the years at the data-centre facility scale. It is no doubt that people tried to gain more computing performance by building larger supercomputers, which demand more power. This is the view on facility level, on the other hands, the thermal load created by a single computer processor is important as well

Similar to what is expected by Moore's law, people assumed that the power load on a single computer processor would increase. And more important, the power load over surface area, or in other words, heat flux on the chip would be increase as well.

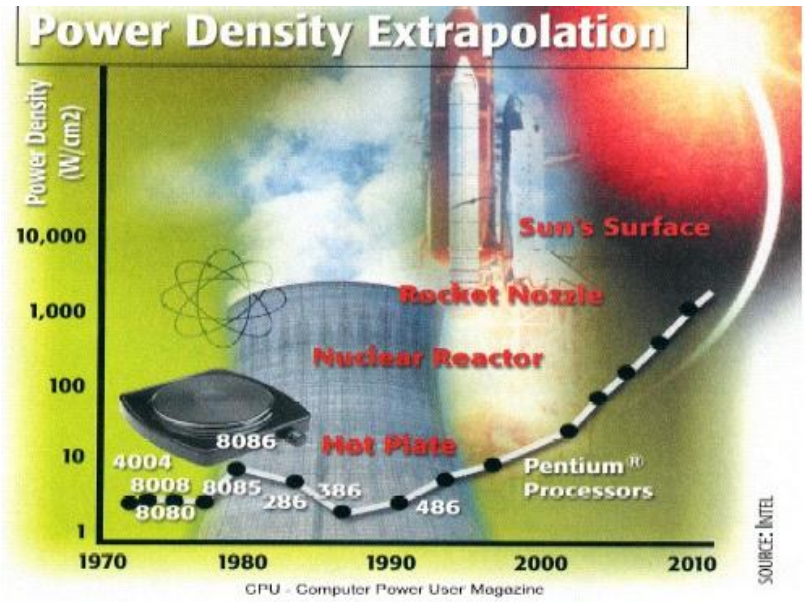

Figure 2-8 Power density / heat flux of computer processor prediction (Jurvetson S. T., 2004) (Chu, Simons and Chrysler, 1999), (Bergles, A. E, 1997)

But this has not come true. Unlike fabrication technology of integrated circuit that may seems to have no boundary of improvement and refinement, the CPU material may have a thermal load limitation. This can be seen from the recent design of Intel X86 based computer server processor (XEON family). **Table 2-1** is some data of Intel X86 based system top-listed processor from 2005 to 2015:

Code name	Year	Model	cores	Socket	TDP	Die size	frequency (Turbo)	transistors	**Flux**
Unit		Xeon		LGA	W	mm^2	GHz	Billion	**W/mm^2**
NetBrust	2005Q4	3.8E	1	604	110	135	3.8	0.169	**0.815**
Paxville	2005Q4	7041	2	604	165	206	3	0.230	**0.801**
Clovertown	2007Q3	5365	4	771	150	286	3	0.582	**0.524**
Harpertown	2008Q3	5492	4	771	150	214	3.4	0.82	**0.701**
Tulsa	2008Q4	7150N	2	604	150	435	3.5	1.328	**0.345**
Nehalem	2010Q1	7560	8	1567	130	684	2.26	2.3	**0.190**
Westmere	2011Q2	8870	10	1567	130	513	2.4	2.6	**0.253**
SandyBridge	2012Q1	2687W	8	2011	150	416	2.9 (3.8)	2.27	**0.361**
IvyBridge	2014Q1	8891V2	10	2011	155	541	3.2 (3.7)	4.31	**0.287**
Hasswell	2015Q2	8891V3	10	2011	165	661	2.8 (3.5)	5.7	**0.25**

Table 2-1 Intel top listed XEON X86 based processors specification from 2005 to 2015, (ARK Intel, 2015)

It is interesting to see that the Thermal Design Power (TDP) of these processors has not significantly increased over the years, moreover the power load has remained at a similar level since 2005, at the commencement of multi-core microprocessors. But more importantly, the heat flux based on chip die size has decreased over the years, and the **Figure 2-9** shows such tendency.

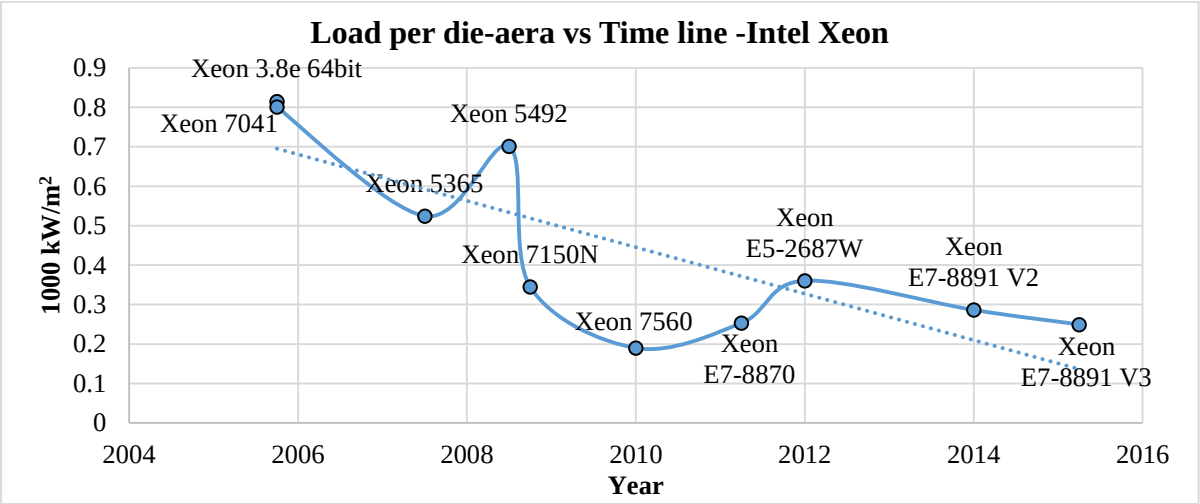

Figure 2-9 Intel top listed XEON X86 based processors die heat flux from 2005 to 2015 related to **Table 2-1**, (ARK Intel, 2015)

However, CPU (Central Processing Unit) is not the only device that carries out the computing and thermal creates the load, by the nature of parallel and vector processing, GPU (Graphic Processing

Unit) or stream processors would be more capable of running large task in small parallel sections. This has recently increased in popularity than ever, and more serious calculation has been taken place on GPGPUs (General Purpose Graphic Processing Unit) and stream processors. So a list of nVIDIA GPU (mostly the Tesla series) in different generations has been reviewed to compare the thermal load and die heat flux.

Code name	Year	Model	die	Socket	TDP	Die size	frequency	transistors	**Flux**
Unit					W	mm^2	GHz	Billion	**W/mm^2**
	2006Q1	GeForce 7800 GTX	1	PCI-E x16	86	333	0.4	0.169	**0.258**
Tesla	2007Q2	Tesla C870			170	480	0.43	0.230	**0.354**
Tesla	2009Q2	Tesla C1060			188	470	0.61	0.582	**0.4**
Fermi	2011Q3	Tesla M2090			225	435	0.65	0.82	**0.517**
Kepler	2012Q2	Tesla K20			225	551	0.706	1.328	**0.408**

Table 2-2 nVIDIA top listed GPU specification from2006 to 2015, (nVIDIA, 2015)

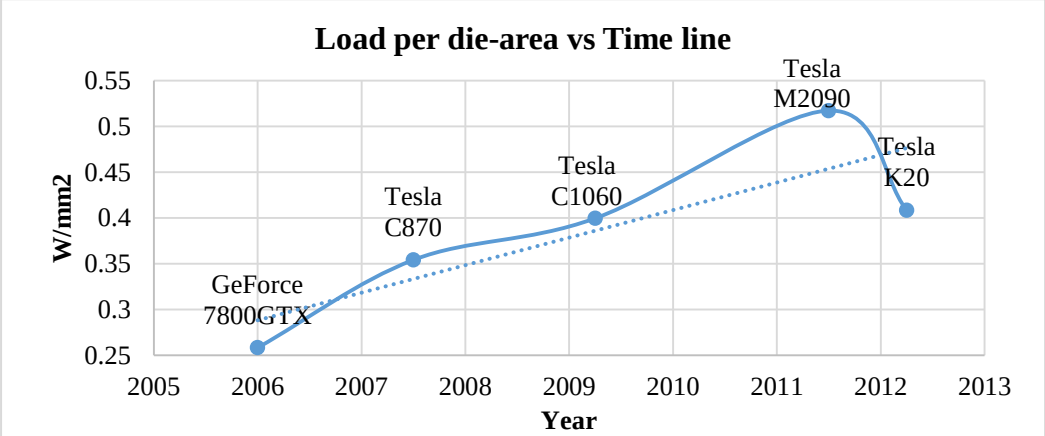

Figure 2-10 nVIDIA top listed GPU die heat flux from 2005 to 2015 related to **Table 2-2**, (nVIDIA, 2015)

The **Figure 2-10** shows the growth of thermal load and die heat flux of some nVIDIA. I contrast to Intel CPUs, which have decreasing die heat flux, the nVIDIA GPUs die heat flux has been growing until the recent released Tesla K20. Both CPU and GPU development is that their die heat flux has yet grown over 1000 kW/m^2, and this number may be the thermal barrier of the computer processor design.

Both CPU and GPU thermal issues are chip level views of the computer design, but how this thermal affects the data centre facility level would be a different case. The size of the supercomputer can be increased by putting more CPUs and GPUs into the data centre building, which may not have a physical limit in theory. But in reality, due to the practicality and economic reasons the size of data

centre cannot be expanded infinitely, so the size and power density (kW/m^2) has been added to the table of supercomputers.

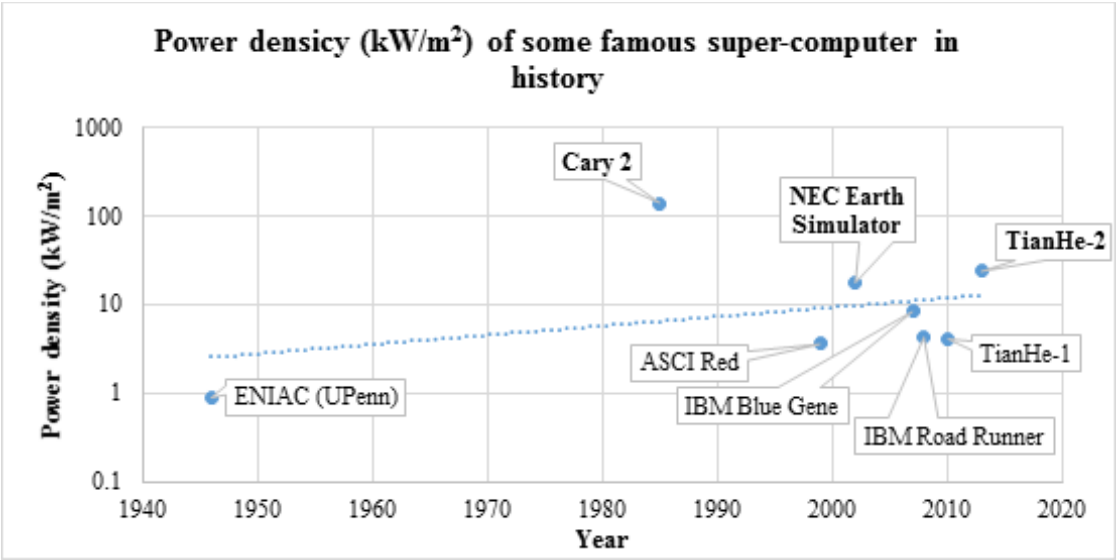

Figure 2-11 Power density against years of some top-listed super computer

From the **Figure 2-11**, it is interesting to see that the power density (kW/m^2) was not significantly increased over the years, and in fact the highest power density supercomputer among them all is the CRAY-2 from the 1980s, which it was famous for not just its superb computing performance in its era, but also its unique design to overcome the thermal problem: immersed liquid-cooled design.

Also from the same figure, the other 2nd and 3rd top power density computer was the Japanese NEC Earth Simulator in 2002 and the Chinese TianHe-2 in 2013. To overcome the problem of limited space against the need for more power, unique design was required these supercomputers. The Japanese solution for the NEC Earth Simulator is simple and straight forward: to use a huge heat sink on top of the micro-processors, this can be seen from the NEC publication on Earth Simulator (Habata, 2003):

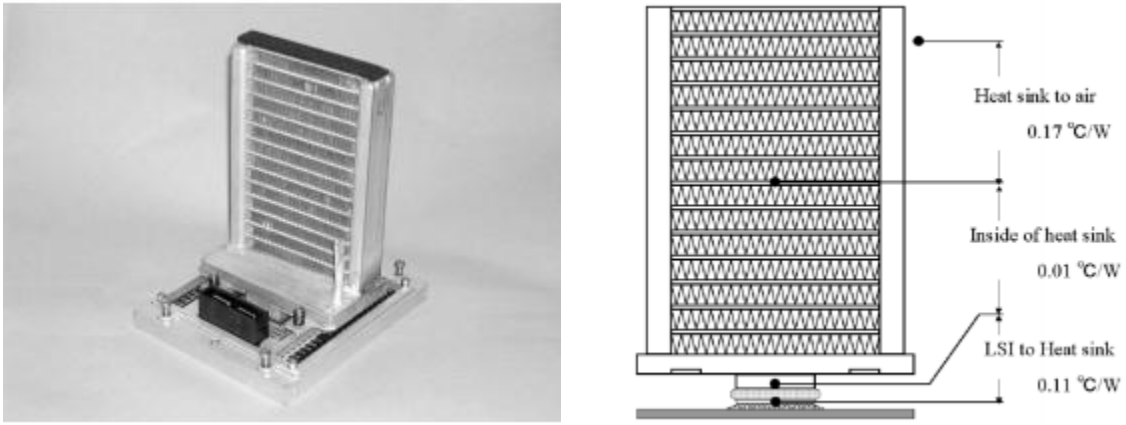

Figure 2-12 The heat sink design (right) and the view of the processor carrier board completed with

core processor and heat sink in the NEC Earth Simulator system. (Habata, 2003):

The detail design of the heat sink in the NEC Earth Simulator is not revealed, but the shape of the heat sink seems oversized and unique from the photo above. The NEC Earth Simulator is an in-house system based on NEC's own processor and carrier board design, so it has no problem to employ such a unique heat sink, but for the more common x86 based server systems a non-standard size heat sink may be a problem, especially for those based on standard cabinet design.

The Chinese TianHe 2 supercomputer is the kind of x86 based system (Intel XEON series micro-processors), in which to overcome the cooling issue it applies a more complex solution to remove the heat, namely water-cooled. Through it is not as radical as the fully immersed liquid-cooled approach adopted by the legendry CRAY-2 system, the TianHe 2 uses a more common rear-door water-cooled rack solution similar to many dense HPC approaches such as the HPC system in the University of Leeds that will mention in the latter on chapter of this thesis (Airedale, 2012)

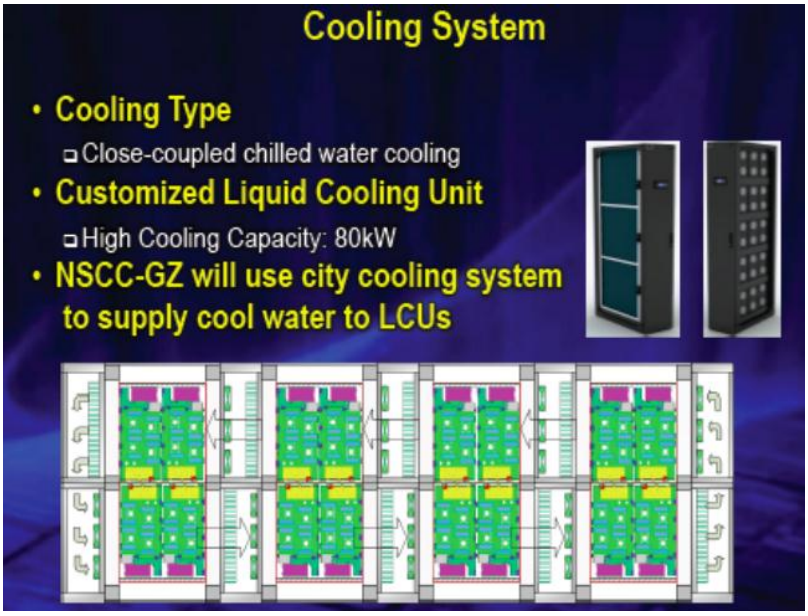

Figure 2-13 The cooling design of TianHe-2 supercomputer (Dongarra, 2013).

Another important thing that the two systems with the top power density (kW/m^2) in the list are both liquid-cooled solutions; and the Cray-2, which have the highest power density was an immersed liquid-cooled system. This shows the unique benefit to have high power density with liquid-cooled based designs, especially fully immersed liquid-cooled design. The detail of all these liquid-cooled designs will be discussed in more detail later in this thesis.

The problem of the thermal load so far is more to do with the power density in the data centre facility. But there is another issue that has risen recently, that is the energy efficiency of data centres

and supercomputers. Traditionally supercomputers are known to be large power consumers, but the relationship between computing performance and power consumption could not be a universal standard since the FLOPS of computer will change rapidly as the technology advances. So a power efficiency metrics based on the proportion of power load spend on the computing calculation has been introduce in 2007 (The Green Grid, 2007), this was the Power Usage Effectiveness (PUE) **Equation 2-1**. The term of PUE stand for Total facility power consumption over IT power consumption.

$$PUE = \frac{\text{Total Facility Power}}{\text{IT Equipment Power}} \qquad 2\text{-}1$$

The total facility power stand for the all power loads including the supporting system such as cooling, lighting and monitoring which do not join the data processing directly; the IT load is usually included the load that directly related to the computer data-processing such as server board, storage and communication devices.

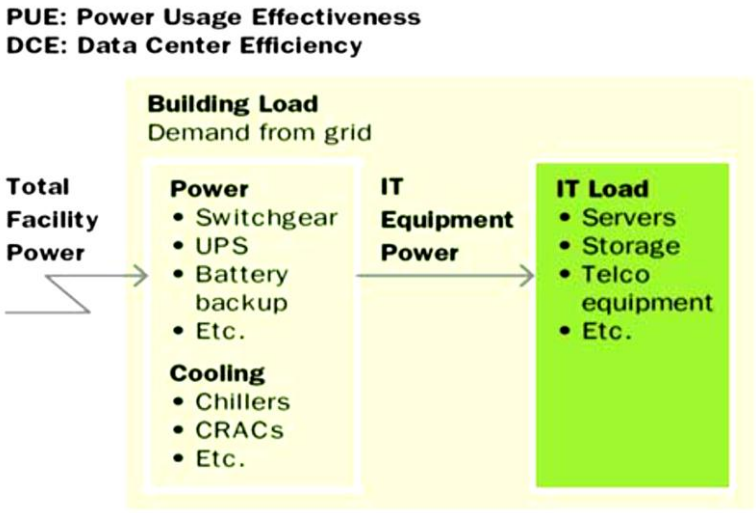

Figure 2-14 Illustration of how PUE and DCE values are calculated in a data centre (GreenGrid)

The introduce of PUE rise a new concern of power effectiveness issue for data centre design, it basically suggest proportion of power load should be spent on the computing rather than other places of a data centre. More specifically, it will be more desirable if less energy spent on cooling system in data centre design. Notice that although the PUE is popular in measuring the energy efficiency of data centres, but it needs to be careful that is an effectiveness but not efficiency figure.

All these problems add up together, the chip thermal density, the facility power density and the PUE of the data centre, is leading to a new stage of data centre design. And the key point of this issue will be the design of the cooling system in data centre and supercomputer. As some cooling

solution (air-cooled or liquid-cooled) was mentioned, the next section will focus on the specific cooling designs for data centre applications.

2.3 Design of data centre cooling system: from air-cooled to liquid-cooled

In the early days of the first electronic computers, was a vacuum tubes were used. Due to their fragility towards vibration and also the mechanical properties of glass material, the vacuum tube is difficult to cool down with a fan or a heat sink. But soon after the silicon based integrated circuit was introduced, its flat body would provide a good thermal contact surface for installing metal heat sinks in direct contact.

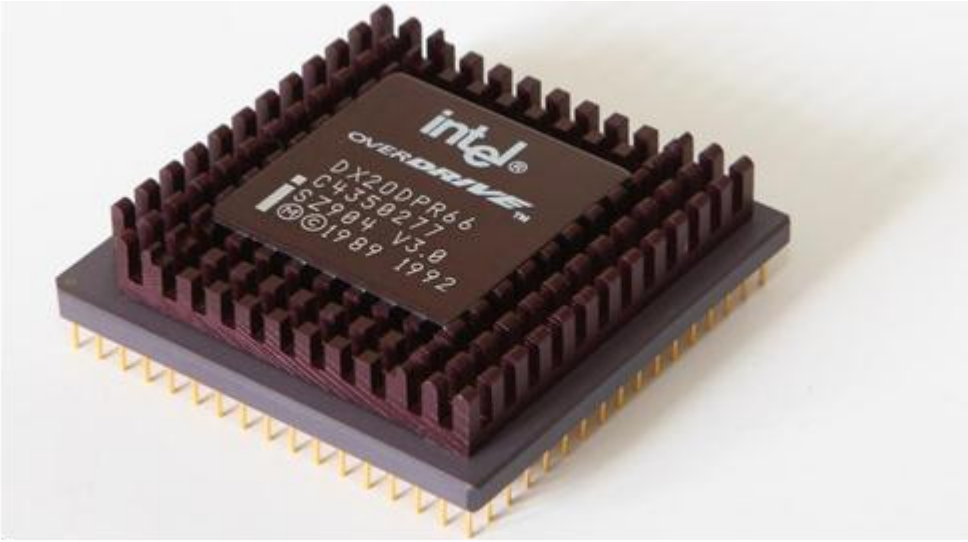

Figure 2-15 Intel 80486 DX2 'OverDrive' CPU with standard heat sink (no fan), TDP=5W (Lanzet, 2009)

The **Figure 2-15** shows a computer processor (1990s) with a standard passive heat sink on it. But soon the passive heat sink design has phased out and electric fan was added to the heat sink and form a forced convection of air flow to provide enough cooling for the processor.

Figure 2-16 Intel Pentium 'OverDrive' (P5) CPU with standard heat sink and fan, TDP =15.6W (X86-guide, 2015)

Here is the **Figure 2-16** shows an Intel PC CPU with a standard heat sink and cooling fan, the force convection with air (air-cooled) soon became a convenient cooling solution for most computer application, not because its efficiency but because its low cost and simple installation. Even now the air-cooled design is the dominated solution in most personal computer (PC) and data centre application. And the method against higher heat load with air-cooled design seems straight forward as well: bigger fan and fast air flow.

But the air is not a very ideal heat transfer media for thermal conduction or convection (Li & Kandlikar, 2015), it has low specific heat capacity (C_p) and low density. This means to deliver a certain amount of heat it requires moving a large volume of air. Moreover when the flow rate and speed of air has increase up to some point, the drag of air flow becomes significant and the pressure drop of the air flow through a limited space will increase dramatically:

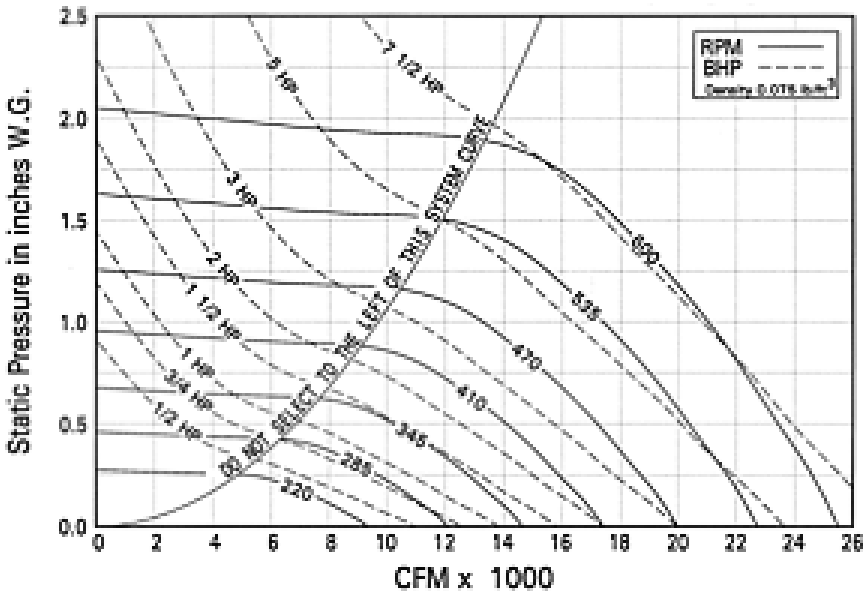

Figure 2-17 An example of fan cooling system pressure drop against the flow rate in CFM (cubic feet per minute) (Greenheck, 2015)

From the **Figure 2-17** it can be seen that the pressure drop varies non-linearly against the increasing flow rate. This eventually become another barrier of thermal design in computer cooling, the increasing system resistant of the air holds the cooling performance and result a poor power efficiency of the computer system.

To overcome the weakness of using air as a thermal agent to deliver heat energy, a better thermal agent for convection is needed. One of the option is using liquid to work as a thermal agent, and this is the starting point and liquid-cooled solution has been introduced into computer technology.

	Molecular Weight	Boiling Point(1)	Freeze Point (1)	Density (2)	SHC	Thermal Conductivity
Unit		(°C)	(°C)	Kg/m^3	J/(kg·K)	W/(m·K)
Air	28.97	N/A	N/A	1.184	1005	0.024
Water	18	100	0	1000	4181.4	0.563
	Dynamic Viscosity(2)	Kinematic Viscosity(2)	Thermal Expensive(2)	(1): At 760 mmHg		
Unit	Pa·s	cST	1/K	(2): At 25°C		
Air	1.983×10^{-5}	15.68	3.411×10^{-3}			
Water	8.9×10^{-4}	0.9	2.07×10^{-4}			

Table 2-3 The physical properties of general water and air

From the **Table 2-3** it can be seen that the Specific Heat Capacity (C_p) of water (4181.4J/kg·K) is 4 times as that of air (1005 J/kg·K), this combined the density of water (1000 kg/m^3) and air (1.184 kg/m^3), implies that the thermal load / heat capacity per unit volume (per m^3) for water (4.2×10^6 $J/m^3 \cdot K$) is 4000 time greater than that for air (1.2×10^3 $J/m^3 \cdot K$).

Liquid-cooled applications are not a new idea for engineering, and there are some simple ways of using liquid in the cooling system without changing the computer design much: one of which uses the heat pipes. (Kim etc., 2003) The original invention of heat pipe (Perkins tubes) has a much longer history than the development of computer, it is a heat transfer device designed by Jacob Perkins and his son Angier March Perkins, based on a sealed tube with liquid intermediary which transports the heat to the other side of the tube by phase-change of the liquid (Reay D.A., 1982). It was first seen as Perkins Tubes in bakers and then in locomotive since 1830s. Later on the design was improved by Samuel Dalziel Heron in 1923 (Sam Dalziel Heron, 1923) and used in the internal combustion engine with a sodium filled stem valve to improve the heat transfer. In 1963 George Grover at Los Alamos National Laboratory firstly developed the device based on capillary effect and used the term ‘heat pipe’ (Karen Freeman, 1996). Today most heat pipes are based on both

phase-change and the capillary effect (Faghri, 1995), this has the potential to increase the thermal conductivity of copper from 0.4 kW/(m·K) to 10~100 kW/(m·K). (Pastukhov, etc., 2003)

There are a number of heat pipe designs in use today, which includes different envelop material (copper, aluminium, steel, etc) different working fluid (water, Ethanol, Ammonia, R134a, alkali / liquid metal, etc.) and different heat spreading method (natural convection, phase change, pressure different, capillary effect or the combination of them). However the limitation of most heat pipe applications is that it can only transfer the heat energy in one direction, usually upward or planar, and it is rarely used for long distances greater than 1 meter. Despite the limitations, heat pipes are still popular in cooling applications, the most common type of heat pipe can be seen in commercial products making use of tubular Constant Conductance Heat Pipes (CCHPs) and flat-Vapour Chambers (flat heat pipes). These types of heat pipe have often being seen used in hot computer component heat sinks such as CPUs, GPUs and I/O controllers in computers.

Figure 2-18 Standard nVIDIA M2070 GPU unit with passive heat sink and heat pipes (nVIDIA, 2011)

The **Figure 2-18** shows an nVIDIA GPU with a big heat sink and heat pipes inside, In this case the heat pipes transfer the heat very quickly to the top of the finned heat sink for removal by the airflow. But using the liquid to transfer the heat energy over a short distant to the heat sink still far from enough for heat transfer, and using water to transport heat energy in long distant cloud improve thermal efficiency. Hence today most data centre have water circuits at the edge to reject the heat energy from inside the facility to the outside environment.

Even though there are water circuits in data centre, the majority of heat transfer inefficiencies in data centre cooling come from the part of heat transfer that still uses air as a thermal agent. So to

further improve the thermal efficiency of the system, the water or liquid should move as close to the heat source as possible, as depicted in the following figure:

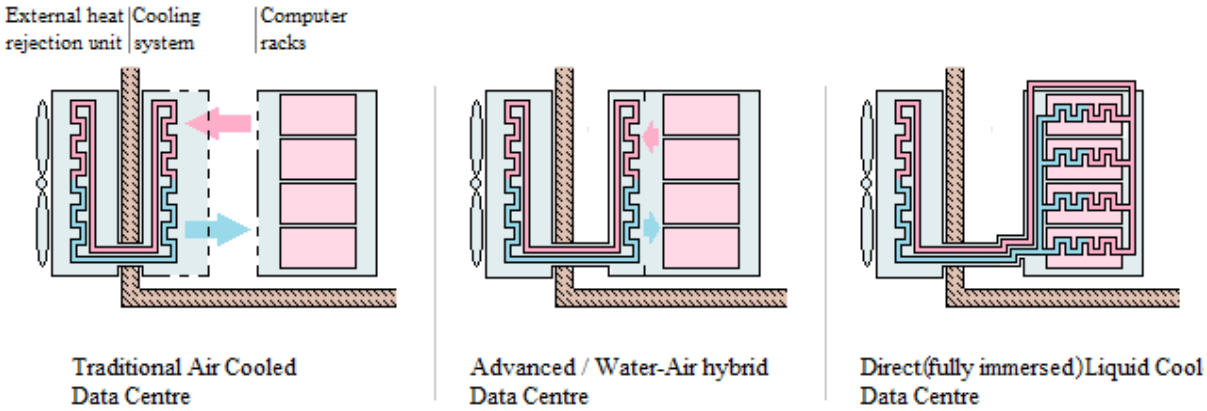

Figure 2-19 Water circuit design in data centre application: moving towards the heat source

The **Figure 2-19** demonstrates how the water circuit can be configured to move closer to the heat source within the computer systems. Originally the water is just used to transport the heat from the edge of the facility to the outside (**Figure 2-19** left). But in some advanced cooling design the water circuit can be extended into the computer cabinet and take the heat from the back of the cabinet (Figure 2-19, middle). Eventually in the direct liquid-cooled approach would reduce the need for air to take place in the heat transfer, and the water circuit takes the heat directly from the computer component (water in node solution, **Figure 2-19**, right).

The 'water in cabinet' style of data centre cooling design is one of the most common water-cooled data centre solution, this includes in-row water cooling and back-door water cooling data centre solutions (Almoli, A., et al., 2012). However both types of data centre designs are still based on air cooling and still require fans to drive air over the heat source to remove heat energy. In other words they can be described as air-cooled and water-cooled hybrid serve system.

Figure 2-20 is a typical back door heat exchanger water-cooled data centre cabinet design (US DOE, 2009):

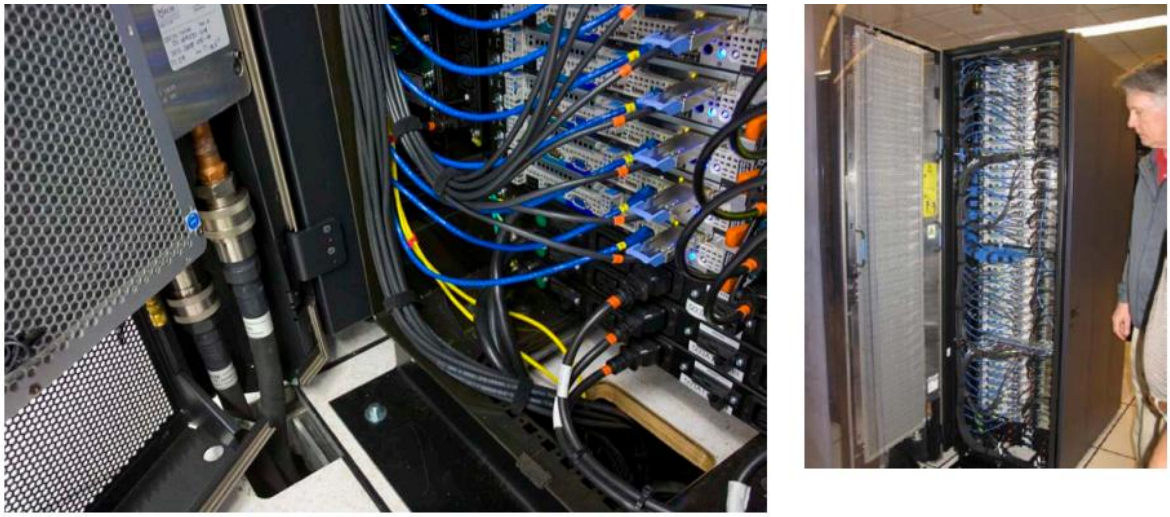

Figure 2-20 Back door heat exchanger water cooled system at Lawrence Berkeley National Laboratory (LBLN) (US DOE, 2009)

Such air-cooled and water-cooled hybrid server system in computer cabinets is a compromise between water-piping complexity and thermal loss of air heat transfer, either front-door or back-door heat exchanger design is still an air-cooled system. With low heat capacity and conductivity of air as a thermal media, it usually requires chilled water and computer room air conditioning for sufficient cooling like most other air-cooled solution. Though it is yet to be perfect, 'water in cabinet' design is currently the most popular and practical water cooled data centre so far. In previous the Chinese TianHe-2 supercomputer is a 'water in cabinet' style water system (Dongarra, 2013) which has the second highest power density (24.4 kW/m^2) in the listed supercomputers in **Figure 2-11**.

So the ultimate cooling solution should be the direct liquid-cooled that take the heat directly from the heat source to the water without using any air in the heat transfer (Iyengar, M., et al., 2012). But even with many advantages, direct / immersed liquid-cooled solution is rarely being seen in a large scale data; in fact, none of any commercial data centres / super computers more than 250kW uses direct liquid-cooling. The main problem is the engineering complexity of liquid-cooled applications whenever water meets electricity. In practice, there are few additional problems. First a liquid cooling system must have good thermal contact with the electronic component, but also remain certain amount of flexibility to allow the tolerance of PCB boards. Second, it will have complexity and reliability issue in sealing design, direct liquid-cooled design would usually have a large array piping in the system. With a design that only uses water as the thermal fluid, the leakage of water on live electronic will could pose a large threat; also such design requires the electronic connectivity goes pass the liquid through sealing, this would become a challenge too. These are the

potential reasons that slow down the development progress of direct liquid cooling technology in data centre application.

The most straight forward solution of liquids used in electronic cooling is a water cooled solution similar to that of car engines. The concept of using water to cool down heating devices is not new, but it was not until 1965 that IBM started to consider direct water cooling approaches (Kakaç, etc., 1994) for a super computer, and in 1982 when the first practical water / liquid cooled computer, the IBM 3081 was produced. Since water is a conductive material both thermally and electrically, it must not direct-contact to the electronic component. To avoid this, the approach would need complex sealing and piping, it also requires a very good thermal contact / conduction from the heat source to the water block. At the time the IBM 3081 was equipped with a radical cooling solution to face this, the Thermal Conduction Unit (Blodgett, 1982); which used helium filled metal piston to apply the contact force to the micro-processor, and transfer the waste heat into the water system. This became the first practical direct liquid cooled solution (water block solution) and no air was used in the major heat transfer process, but this can still be arguable because a helium-filled **gas** cylinder was used as heat transfer agent.

Figure 2-21 is photo of Thermal Conduction Unit (TCU) the cut-away section from the IBM 3081 main-frame computer

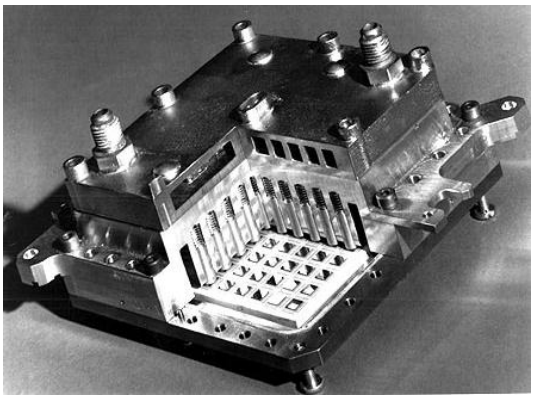

Figure 2-21 Photo of Thermal Conduction Unit (TCU) the cut-away section from the IBM 3081 (Blodgett, 1982)

Another direct-liquid solution is the use of di-electric liquid such as a mineral oil or other liquid as thermal fluid instead of water. In the material prospect it is a compromise, where water is one of the best thermal fluids for conduction as well as convection, and in reality any di-electric liquid would have poorer thermal performance than water. Yet the engineering prospect of a di-electric means that the whole electronic part of the computer can be submerged inside the liquid and the thermal contact of liquid to the electronics would be insulated. With submersion all of the heating sources can be cooled in the same environment and spread the heat load evenly. This is the design

so called fully immersed liquid-cooled solution, which firstly put into commercial by Cray with the famous Cray-2 super computer **Figure 2-22**, which was also the fastest super computer during 1985 to 1990.

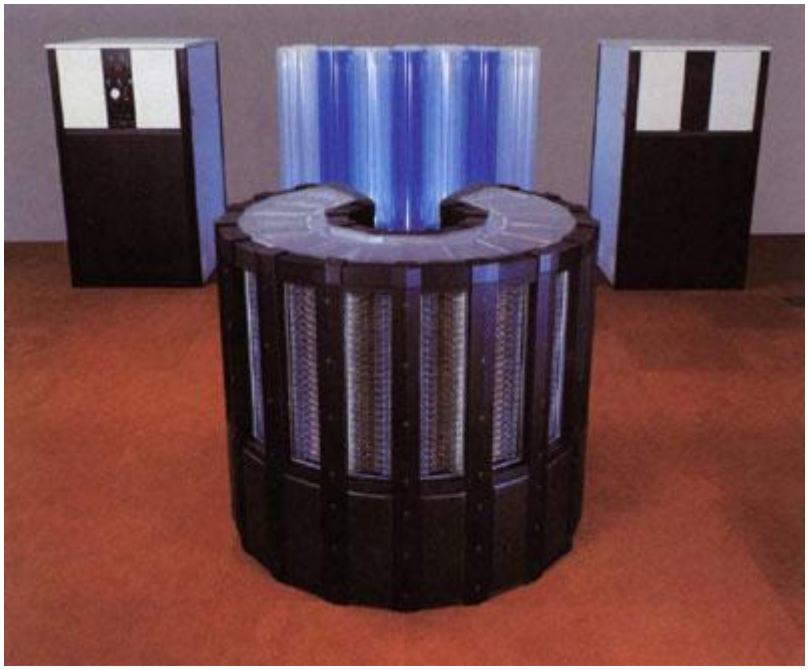

Figure 2-22 Photo of Cray-2 super computer is 1980s, (CRAY Supercomputers, 1988)

The Cray-2 system was the pioneer in computing industry in its era with many innovations, one of what is the use of a non-conductive liquid (Fluorinert™) (Computer History Museum, 2015), this led to another type of application in direct liquid-cooled design, namely the fully immersed liquid-cooled solution. Such design is able to avoid the piping issue by basically putting everything into the non-conductive coolant; in the other side it needs to deliver the signal to the outside of the liquid, which would be another challenger in sealing and cabling.

The IBM 3081 and Cary-2 are both radical solutions of the cooling problem at the time, they are symbolic of the high building costs, which for the Cray-2 was 12~17 million USD in 1985, 27~38 million USD in today's value and high running cost that was only affordable by the top ranked public bodies. The first Cray-2 (serial number 1) was delivered to the National Magnetic Fusion Energy Computer Centre at Lawrence Livermore National Laboratory (Computer History Museum, 2015). At this time most other supercomputers and data centres were using conventional air cooling method with many ventilation fans.

Liquid-cooled computers have recently become popular again with significant usage by the PC gaming enthusiast and overclocking group, which tend to modify their personal computer (PC) to water-cool in order to gain extra performance. The usual solution of such would be water-block

cooling designs, which is simply a block of metal clamped onto the hot component of the computer with water passing through it to take away the waste heat (Iyengar, M., et al., 2012). This is straight forward but a costly solution, since if the computer has a number of distributed hot spots, the water cooling system will be complex with lots of piping and sealing. Because a single water block can only cool down one component / hot spot, the water block design is usually difficult to cool down everything on the motherboard. Unless the computer server is a custom designed for water-block application, otherwise cooling air is still needed for parts without water-blocks. Never the less water blocks are efficient in cooling hot spots and still a popular concept among data centre manufactures recently.

Beside its relative complexity, one more problem of the water block design for data centre applications that requires addressing is the flow balance. Unlike a personal computer that the water loop only needed for few devices, a data-centre level solution would requires CDUs – cooling distribution units to balance the water flow.

One example is the CoolIT solution **Figure 2-23**, it combined a micro pump inside each water block powered and controlled by the motherboard fan port, and as a result each single water path is self-controlled and self-regulated. This solution also uses flexible water hoses so that the locating and contact / conduction from water block to hot spot can be ensured (CoolIT system, 2015).

Figure 2-23 CoolIT server blade with water-block cooling design (CoolIT system, 2015).

But as a typical block solution the CoolIT solution is a combination of water-cooled and air-cooled system. Notice that a typical CoolIT server blade design has 2 water route (each of 1 CPU) in a twin-processor motherboard.

The last direct liquid-cooled solution is the fully immersed liquid-cooled solution (Ohadi, MM., et al., 2012), which seems to have been silent for some time after the successful story of Cray-2 supercomputer. One reason for the silence could be that the liquid-cooled Cray-3 design became a failure in business, and before the Cray-4 was available the Cray Research became bankrupt and made this an end to its liquid-cooled series (CRAY, 1994). Other than Cray Research, very few fully-immersed liquid-cooled super computers had ever been built commercially or in large scale, and even Cray-research was not making good business on its liquid-cooled design. The problem of fully immersed liquid-cooled design, besides its high cost, is the lack of hardware flexibility and user friendliness. Also the coolant that Cray series liquid-cooled supercomputers had used was the 3M Fluorinert™ FC-70 series (FC-74) fluorocarbon-based fluid, although at the time was considered environmental friendly, lately the liquids have now became less favourable due to the growing concern of its high global warming potential and long atmosphere lifetime (UNFCCC, 1992). All these issues added together becomes a new challenge for the design of next generation fully immersed liquid-cooled solutions, but on the other hand there is growing demand for computer power and density once again calling for such designs due to their potential of having the highest facility level power density. So in recent years such type of immersed liquid-cooled designs has returned with some new technologies based on old cooling approaches.

2.4 Fully immersed liquid cooled solution with new applications

It was not until recently that the size and power of data centres and supercomputers becomes critical, and the industry starts seeking more hardware density solutions. Now they look back at fully immersed liquid-cooled solutions again, but at this time, the requirement is energy-efficiency rather than speed. Also new fluoroether based coolants such as perfluoropolyether (PFPE) and Hydrofluoroether (HFE) fluids have been introduced by different chemical engineering companies, such as Solvay and 3M. This type of liquid tends to have a lower global warming potential / shorter atmospheric lifetime also better chemical compatibility in general usage. This liquid could be a more environmental friendly replacement of the 3M Fluorinert (PFCs), and remove the barrier of using di-electrical heat transfer fluids in microelectronic cooling applications again (3M, 2015).

The basic properties of HFE 7300 liquid are presented in **Table 2-4**.

	Molecular weight	Boiling point (1)	Freeze point	Density (2)	SHC	Thermal condutivity
Unit		°C	°C	Kg/m^3	J/(kg·K)	W/(m·K)
	350	98	-35	1660	1140	0.069
	Dynamic viscosity (2)	Kinematic viscosity (2)	Thermal expensive (2)	(1) : At 760 mmHg		
Unit	Pa·s	cST	1/K	(2) : At 25oC		
	0.001176	0.71	0.00145			

Table 2-4 3M Novec HFE7300 Engineering liquid properties (3M, 2009)

According to the 3M Novec HFE7300 engineered fluid data sheet, the density has a linear relationship with the temperature:

$$\rho(T) = 2371.8 - 2.4T \qquad 2\text{-}2$$

Where T is measure in Kelvin.

In fact the other properties of 3M Novec HFE liquid can be more complex in practice. It has a large thermal expansivity constant and non-linear temperature-viscosity relationship, which could result in some difficulties with the numerical modelling. From the 3M data Sheet, most of the HFE series liquids have power-law viscosity versus temperature changes as shown in **Figure 2-24** and **Figure 2-25**.

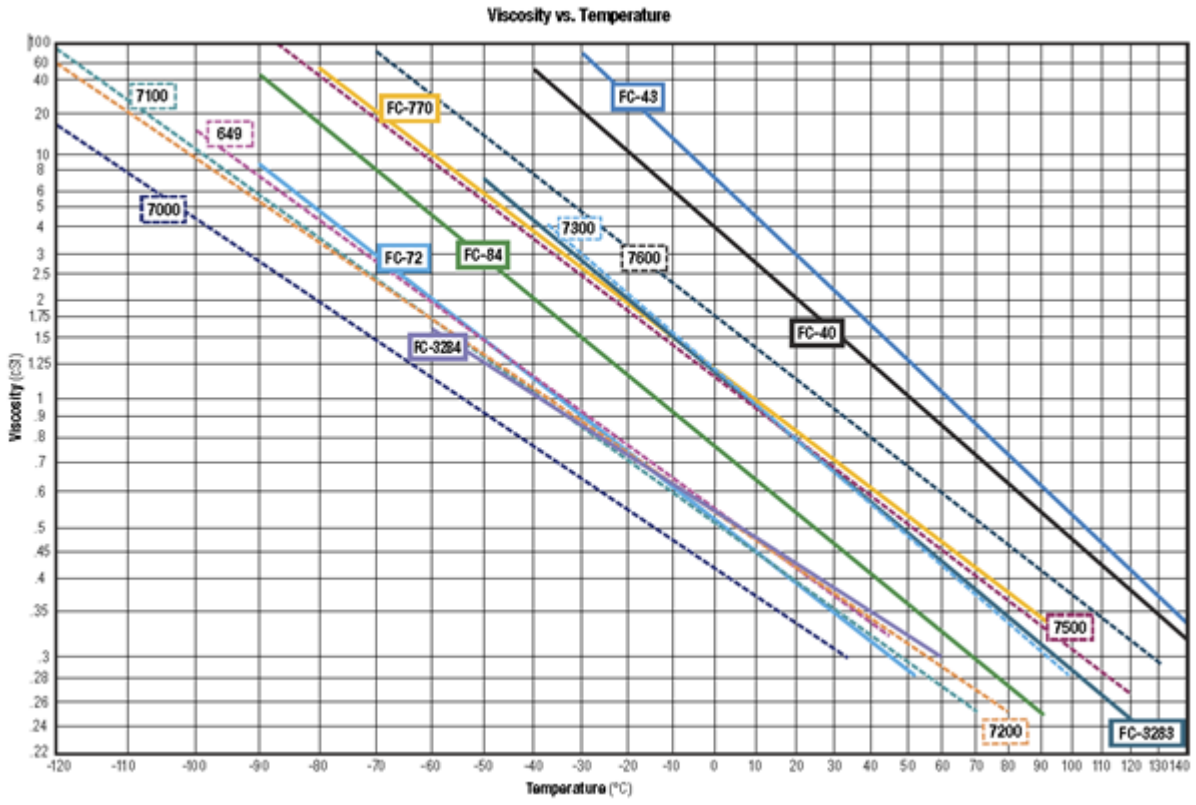

Figure 2-24 3M Novec HFE7300 Engineering liquid viscosity vs temperature (3M, 2009)

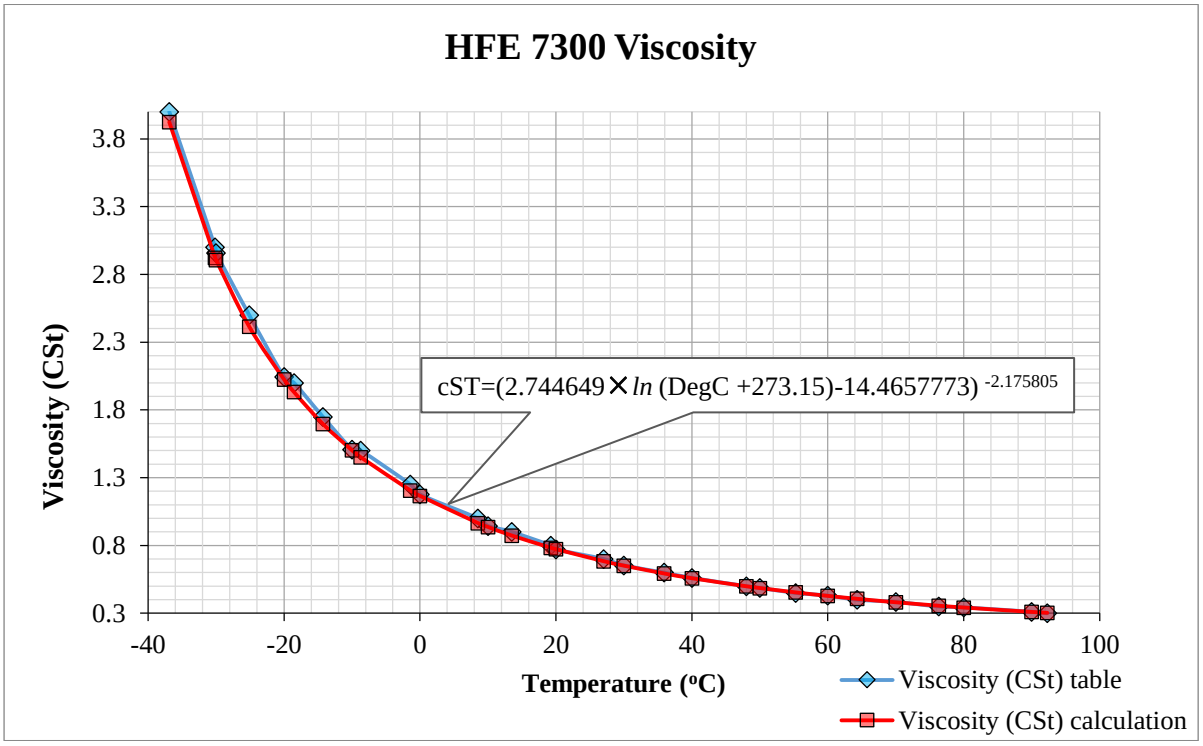

Figure 2-25 3M HFE7300 Engineering liquid viscosity vs temperature curve with Least Square approximation

From the **Figure 2-24** and **Figure 2-25** above, it can be seen that the 3M HFE coolant has a linear density correlation and power-law viscosity correlation to temperature.

Also, Solvay and other chemical engineering companies (for example, DuPont) also introduced similar fluoroether based product for the purpose of heat transfer, mainly for power electronics and manufacturing processes. The Solvay Galden HT110 (PFPE) liquid for example, has a similar property and could be used in the same application similar to the 3M HFE liquid:

	Molecular weight	Boiling point (1)	Freeze point	Density (2)	SHC	Thermal condutivity
Unit		ºC	ºC	Kg/m^3	J/(kg·K)	W/(m·K)
	580	110	-100	1710	963	0.065
	Dynamic viscosity (2)	Kinematic viscosity (2)	Thermal expensive (2)			
Unit	Pa·s	cST	1/K			
	0.001283	0.75	0.00114			

Table 2-5 Solvay Galden HT110 PFPE heat transfer liquid properties (Solvay, 2014)

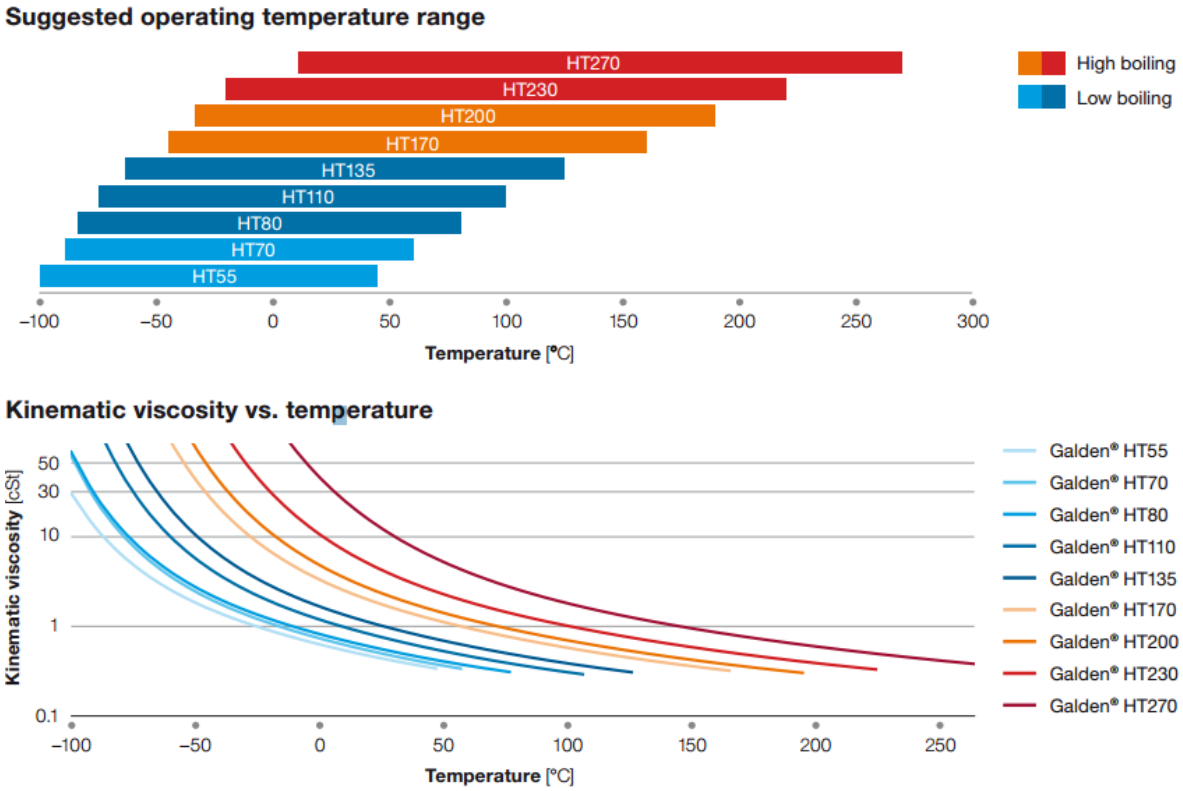

Figure 2-26 Solvay Galden HT110 PFPE heat transfer liquid viscosity vs temperature (Solvay, 2014)

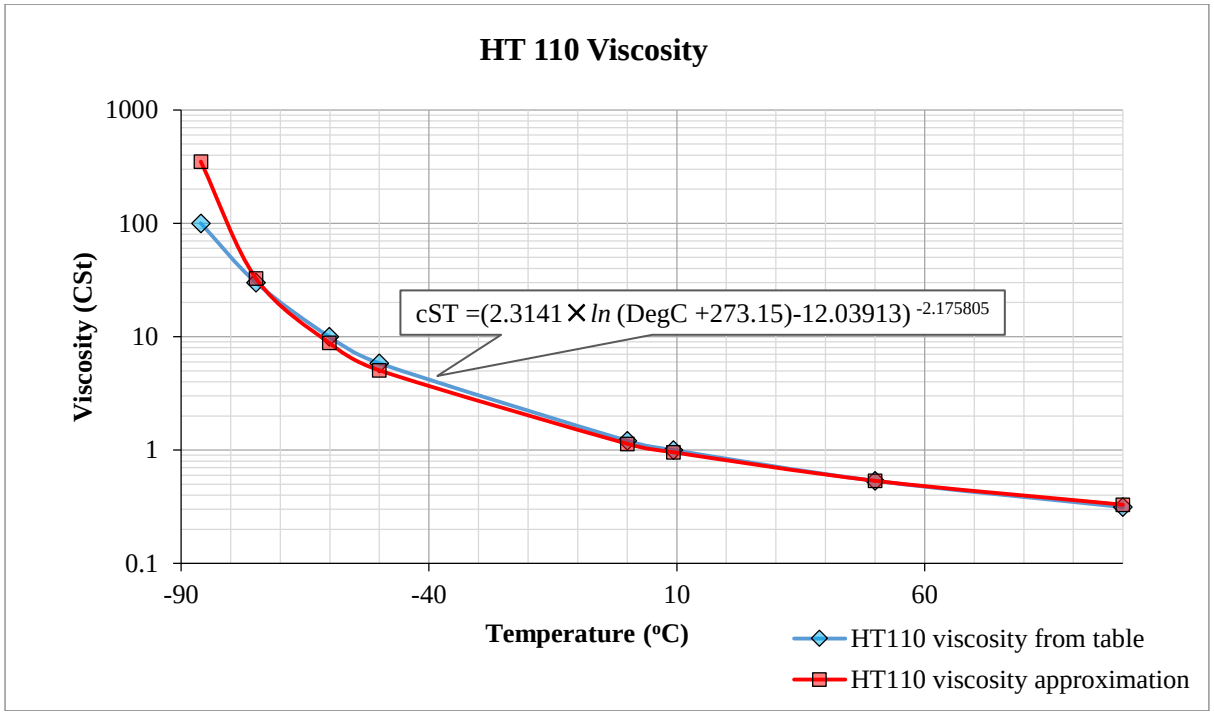

Figure 2-27 Solvay Galden HT110 PFPE heat transfer liquid liquid viscosity vs temperature curve with Least Square approximation

From the **Figure 2-27**, the Solvay PFPE coolant also has power-law viscosity correlation to temperature. It will use fixed density and viscosity value for the corresponding reference temperature later on in this thesis as well.

According to HFE 7300 and HT 110 data sheets, the viscosity of these fluorinated fluids will be increased significantly in low temperature (below 0^{o}C), and they would be better to use in a relative high temperature (above 25^{o}C) for less viscous and better fluxivity. Such liquids also have overlap temperature range with water, which make them ideal to integrate into existing data centre design, which water systems already have built in. With these fluorinate and oil based fluids, the immersed liquid-cooled concept is back again in a more fashionable manner.

Up to 2015, there are 2 types of fully immersed liquid-cooled solution that can be seen as commercial applications. The majority of which is the 'open bath' or open container solution which puts all computer electronic in the same container with the primary coolant; the secondary coolant loop (usually water) would be either work with a condenser or heat exchanger. The 3M 2-phase immersion data centre solution (3M, 2015) is an example of this type of solution:

Figure 2-28 3M open bath fully immersed 2-phase liquid-cooled data centre solution (3M, 2015)

The open bath / open container solution has the easiest position for power and signal connectivity, simply routed the wiring across the liquid surface should do the job and does not require to cable through the sealing. The pressure management of this solution should be easy as well since it is open to the atmosphere so it should be equivalent to 1 atm (standard atmosphere pressure) all the time. The real problem comes from the coolant management, as it is an open top solution, the vaporized coolant will escape to the room environment. Containing or collecting the coolant vapour will be difficult and a coolant manage system might be needed to address this, so the data-centre design may be fundamentally changed.

To avoid the coolant vapour, a non-vaporise oil coolant can be used for open bath liquid-cooled servers, for example, the Green Revolution Cooling data centre solution. It used oil based coolant

and was proved and adopted by serial customers (Varma, etc., 2014). Never the less the open bath solution is the most popular and most installed fully immersed liquid-cooled solution at the moment.

The other fully immersed liquid-cooled data centre solution, rather than the open container, is the enclosed container solution. This type of solution has a closed environment for the computer microelectronics immersed in it, one example is the Iceotope solution.

Figure 2-29 Fully immersed liquid-cooled data centre cabinet (Iceotope, 2015)

The fully immersed liquid-cooled data centre cabinet has 'static' primary coolant that only relied on natural convection to transfer the heat from the microelectronics to the liquid, and then transferred further by pumping the secondary coolant / water loop to take the heat out of the system.

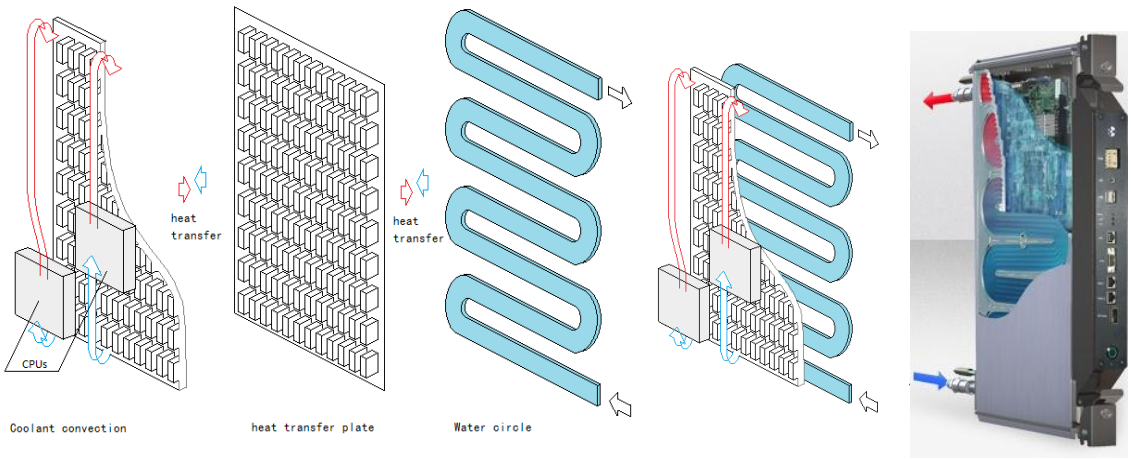

Figure 2-30 Liquid-immersed system module in detail

The module shown in **Figure 2-28** has quick connect valves that enable it to be hot-swappable in a cabinet that has a carefully designed water circulation systems that is thermally coupled to transfer

the heat to the outside environment, see **Figure 2-29**. This water circulation system can be flexible to connect with other applications, such as facility water or methods of waste heat re-use.

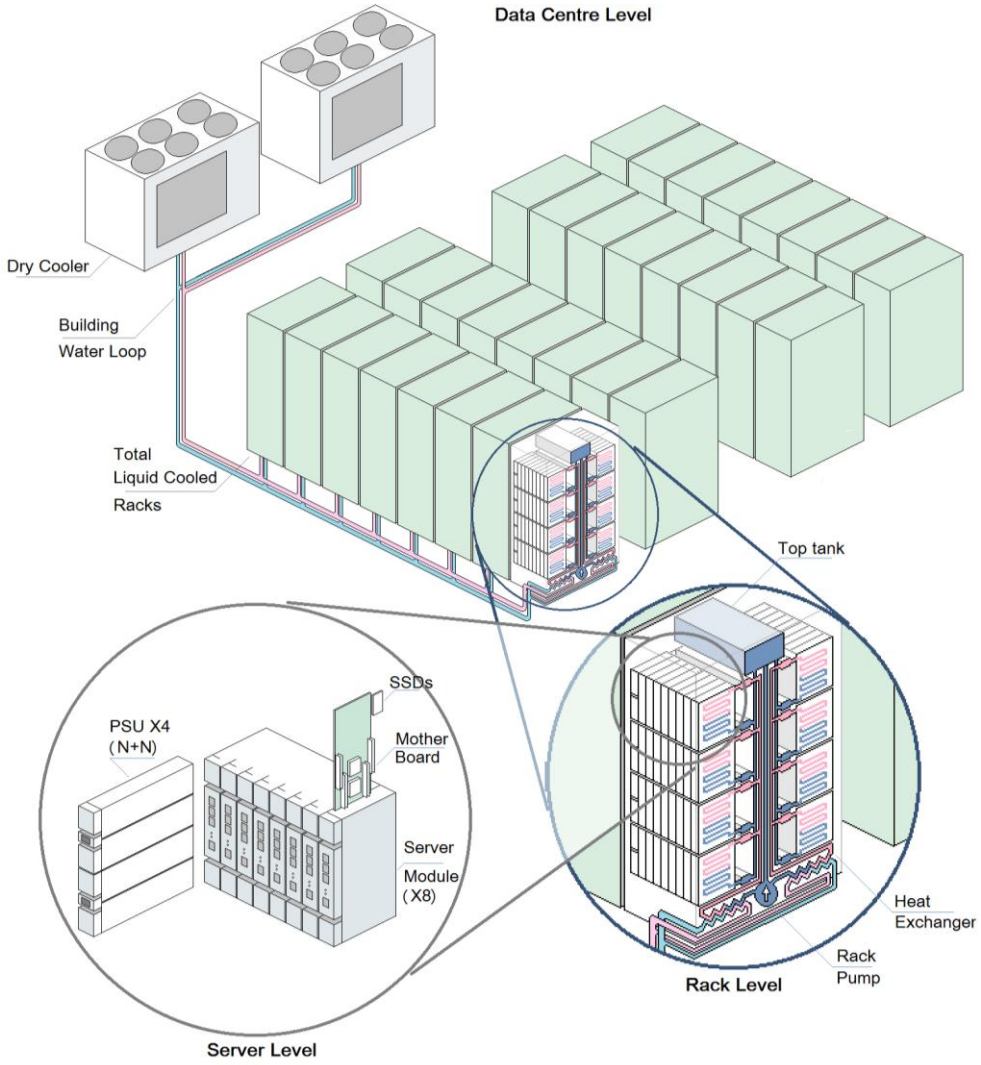

Figure 2-31 Schematic drawing of the liquid-cooled system cabinet and data centre solution

All this fully immersed liquid-cooled solutions, due their physical advantages, claimed able to achieve a high cooling effectiveness, with a PUE from 1.2 down to low as 1.01. It is also claimed to have high density as well about 60kW per cabinet. Furthermore there are some other benefits of liquid-cooled solutions:

The fully immersed enclosed liquid-cooled solution has 2 extra benefit compare to other thermal packaged solutions:

1) In the first cooling stage it is fully sealed, self-contained without any moving parts, so it can be made as a dust free, vibration free, noise free (Capozzoli, Primiceria, 2015), maintenance free and fully modularised hot swappable system.

2) A liquid-cooled data centre usually has very few rotating components (no fan) across the facility but higher thermal efficiency due to the benefit of eliminating air completely as a heat transfer agent. So the fully immersed liquid-cooled data centre solution usually has cooling effectiveness (PUE <<1.2) with a reduction in the need for extra plant in the data centre – only CDUs and insulated pipework.

To achieve these benefits with fully immersed liquid-cooled data centre solution, a careful design is needed for all aspects. Since it is a fully sealed container working in a range of temperature, the pressure inside the system must be carefully studied to avoid too much expansion. Also the design of power and signal connectivity from the inside of the seal container to the outside system will have some challenges as well. But more importantly, due to the naturally occurring free convection circuit, the heat transfer analysis for the natural convection flow is critical. The work in this thesis will concentrate in-depth on the natural convection from the point of view of the mathematical modelling, physics and its application in practice.

2.5 Summary

This chapter discussed the general concept of computer cooling and the evolution of computer cooling technology.

In terms of the conventional air-cooled method, air is the most convenient material for cooling, but air is neither good for thermal conduction nor for convection, hence a conventional air-cooled design might be limited to its power density. Also when high flow-rate electric fans and ventilation have been used in such application, some other unfavourable feature such as noise, dust, vibration will have appeared as well.

There will be two directions towards cooling performance and efficiency, one is improvement towards the heat source side (internal side) and the other is improvement towards the ambient side (external side). Generally speaking chiller or refrigeration unit can be added externally to the system to achieve extra delta temperature, which should help improving the cooling and power density of the computer system (supercomputers and data centres), but at a cost of overall power efficiency (Li, L., et al., 2016). Or in some other approach evaporative cooling can be use instead of

refrigeration in expense of water rather than power for extra cooling. Nevertheless this thesis will be focused on the internal side of cooling improvement.

To achieve both efficiency and performance at the same time, some advanced feature will be needed in large-scale high performance computer design, which are considered as ‘unconventional’ design in this thesis. Most of such unconventional method is to introduce water loop into the computer system, since water has conduction, convection and heat capacity advantage over air, it should reduce the thermal inefficiency of the cooling system. As previously explained, such option is to move the water closer to the heat source, and the ultimate goal will be eliminate air in any internal heat transfer loop to achieve direct liquid-cooled and avoid inefficiency .

One of the most common but unconventional cooling method is back-door (or front door) water cooled cabinet, it can be considered as moving the water loop into cabinet hence reducing the heat resistance to the ambient. But it can also be considered as a compromise between fully liquid (water) cooled and air-cooled, which use water to cover some of the heat transfer distant for all components and use air to cover the rest of the distant. The benefit of such application is to add cooling performance on air-cooled based system without changing it too much. The down side is that the improvement will still be limited by the basic air-cooled design and noise / vibration would still exist.

Another common but also unconventional approach is the water-block design, which brings the water loop directly onto hot spots. It can also be considered as another way of compromising water-cooled and air-cooled design, while some components are direct water-cooled all the way while others are not. The heat transfer improvement in such design would be more significant due to the water block direct contact with the hottest spots, yet air-cooling is still retained in some level and the noise / vibration remains. Even more, such design would potentially have a higher level of complexity due to extra pumping and piping.

The ultimate solution of cooling is to have everything direct liquid-cooled without air. Since water is an electrically conductive fluid, a compromise needs to be made to use di-electric fluid at the cost of poorer-than-water heat transfer properties. Other than choosing how much air or water is involved in cooling loop, now the compromise is to have material properties between air and water. Yet introducing another fluid to the cooling system usually results in sophisticated pumping and sealing design, and would be even more sophisticated if it requires phase change of the fluid.

But some design, such as the Iceotope fully immersed liquid-cooled system, uses natural convection in its first cooling stage hence sealing and pumping could be simplified. By reducing the number of pumps, energy efficiency could be improved and noise, vibration, dust could be avoided. Therefore the fully immersed liquid-cooled design would be one of the best solutions in terms of

practicality and energy efficiency. But like all other design it has its own difficulty, so the latter on chapter of this thesis will be focusing on finding solution for one of the biggest problem on fully immersed liquid-cooled computer system: the understanding and analysis of natural convection.

3. Mathematics methodology related to buoyancy driven natural convection

The core part of the fully immersed liquid-cooled computer system is the liquid-cooled computer node, which is both at the centre of computational performance and heat transfer efficiency. The computer node of the fully immersed liquid-cooled computer solution relies on density-driven natural convection flow to remove the heat energy from the microelectronic components, and then transport the heat energy to the internal water circuit located in the lid on the opposite side of the computer node. An appropriate design for the computer node would allow the system to use the highest specification computer components with high power load (Hopton and Summers, 2013), but still maintain excellent cooling efficiency.

The physics of the density-driven natural convection flow is known to be unstable and challenging to model. So in order to achieve highest computer performance as well as the required thermal efficiency, a clear understanding of the mathematics and physics of the density driven buoyancy natural convection flow is critical for this research.

This chapter is partitioned into 3 sections of work: the first section will introduce the general fluid dynamic expressions for flows that include turbulence, the second section will introduce the fluid dynamic expressions specific related to density-driven natural convection flows, and the third section will be the analytical model for density-driven natural convection flows.

Since the main focus of the research in this thesis is on the fluid dynamics of natural convection flows, it will be stated as 'natural convection' for the remainder of this thesis.

3.1 General fluid dynamic expressions

Before further research of the natural convection flow, some basic fluid dynamic principles need to be explained in order to understand the characteristic of natural convection flows. In this thesis, the fluid dynamic regime of the problem will be: sub-sonic and steady state. Also because of the unique condition of natural convection flows, especially when the flow is confined to a closed cavity, there will be some difficulty in determining whether the flow is in a turbulent state or not. This section will also discuss turbulence modelling before applying it to natural convection flows.

This section will review the general mathematical expressions for fluid dynamics within the flow regime of this research. However, the expressions in this section will not be specific to the natural convection flows.

Navier-Stokes equations

In general fluid dynamic applications, the description on fluid motion usually starts from the Navier-Stokes equations. Such equations are non-linear, partial differential equations based on a conservation of momentum (vector field) description. (Batchelor, 1967).

The Navier-Stokes (momentum) equations can be written in vector form:

$$\rho\left(\frac{\partial \vec{\mathrm{u}}}{\partial t} + \vec{\mathrm{u}} \cdot \nabla \vec{\mathrm{u}}\right) = -\nabla p + \mu \nabla^2 \vec{\mathrm{u}} + \vec{\mathrm{f}} \qquad 3\text{-}1$$

Where u is the flow velocity, ρ is the fluid density, p is the pressure, the symbol ∇ is a del operator, which is vector gradient operating on the velocity vector field in the conservation of momentum. In two dimensional Cartesian coordinates, the vector equation can be written explicitly as:

$$\rho\left(\frac{\partial u_x}{\partial t} + u_x \frac{\partial u_x}{\partial x} + u_y \frac{\partial u_x}{\partial y}\right) = -\frac{\partial p}{\partial x} + \mu\left(\frac{\partial^2 u_x}{\partial x^2} + \frac{\partial^2 u_x}{\partial y^2}\right) + \mathrm{f}_x \qquad 3\text{-}2$$

$$\rho\left(\frac{\partial u_y}{\partial t} + u_x \frac{\partial u_y}{\partial x} + u_y \frac{\partial u_y}{\partial y}\right) = -\frac{\partial p}{\partial y} + \mu\left(\frac{\partial^2 u_y}{\partial x^2} + \frac{\partial^2 u_y}{\partial y^2}\right) + \mathrm{f}_y \qquad 3\text{-}3$$

Now there are 2 equations for general 2D unknown flow field expression, but it still requires another equation to solve for the pressure term and close the equations. This is provided by the continuity equation:

$$\frac{\partial \rho}{\partial t} + \nabla \cdot (\rho \vec{u}) = 0 \qquad 3\text{-}4$$

But even if density is time independent, and the density time-derivative term in **equation 3-4** can also be temperature dependent, and then:

$$\frac{\partial \rho}{\partial t} = \frac{\partial \rho}{\partial T} \cdot \frac{DT}{Dt} \qquad 3\text{-}5$$

This will bring in the relationship for the buoyancy force expression, which can either be a full buoyancy model with temperature variable density, or a Boussinesq approximation for buoyancy model with constant density and pressure. The buoyancy expression will be discussed in the latter sections of this chapter.

With the continuity equation, the Navier-Stokes equations become closed and a solution. For easier understanding of the Navier-Stokes (**equation 3-1**), the left hand side of the equations can be seen as the inertia term (motion and position), and the right hand side can be seen as the stress and force term.

Notice that the non-linearity of the Navier-Stokes equations comes from the convective acceleration terms (u ·∇u), which is the vector field of the velocity acceleration over the position (Batchelor, 1967). Due to such characteristics the Navier-Stokes equations are very difficult to solve (Potter and Wiggert, 2008), and often require advanced computational methods for their solution.

On the other hand, fluid dynamic experiments show that under certain condition, usually with a higher velocity, the flow would become unstable. As a well-known example is the pipe flow case, which shows that the pipe scale and velocity would trigger the flow from stable (laminar) state into unstable (turbulent) state. The Reynolds number (Re) was introduced to indicate whether the flow is stable or not will be discussed in next part of this work.

Couette-Poiseuille flow

The simplified expression for laminar channel flow in an ideal condition with only one dimension of velocity considered. Assuming the flow is laminar, steady-state, incompressible, in such case, the Navier -Stokes **equation 3-3** will have only 1 expression left:

$$\frac{\partial^2 u_y}{\partial x^2} = \frac{1}{\mu} \cdot \frac{\partial p}{\partial y} \qquad 3\text{-}6$$

If the pressure gradient term is zero then the solution is called Couette flow. Now the flow has only 2nd order velocity term and 1st order pressure gradient term left (Munson, 2002):

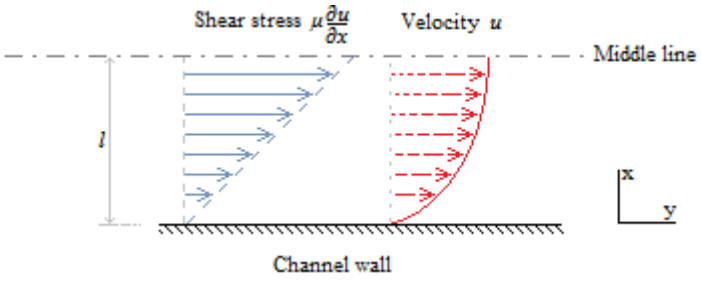

Figure 3-1 Couette (blue) and Couette-Poiseuille (red) flow in a parallel wall channel case

And with the no-slip boundary conditions

$$u_y(0) = 0\,, \qquad u_y(l) = u_0 \qquad 3\text{-}7$$

This is special condition that the Navier-Stokes equation and can be solved algebraically. The Couette–Poiseuille equation in a parallel wall channel condition has the solution for the y component of velocity:

$$u_y(x) = u_0 \cdot \frac{y}{l} + \frac{1}{2\mu} \cdot \left(\frac{\partial p}{\partial y}\right) \cdot (y^2 - l \cdot y) \quad \text{3-8}$$

Notice that such simplified form of Navier-Stokes equation is ideal to show the effect of viscous force in flow. In the latter section of this research, a mathematics solution similar to that of equation (3-8) is presented for natural convection flows.

Reynolds Number

In general fluid dynamic research, the Reynolds number (Re), named after Osborne Reynolds (Reynolds, 1883), and is used to classify the flow. The Reynolds number is a dimensionless number given as the ratio of the fluid inertial force to viscous force, that is:

$$\mathrm{Re} = \frac{\rho \cdot \mathrm{u} \cdot \mathrm{L}}{\mu} \quad \text{3-9}$$

ρ is density of the fluid

μ is the dynamic viscosity of the fluid

u is the characteristic velocity of the fluid

And L is the characteristic length scale.

In a specific 'pipe flow' case, the flow remains laminar within Reynolds number (Re) < 2300, and between 2300 to 4000 it appears transaction between lamina and turbulence state. When the Reynolds number (Re) > 4000 the pipe flow enters turbulence state and shows unstable condition (Holman, 2002). But the value of Reynolds number at transition is problem dependent.

It is also noticeable that the Reynolds number involves length scale factor (L), velocity scale factor (u) and liquid property factors of viscosity (μ or ν) with density (ρ). The flow condition is largely depends on the value of Reynolds number, which leads to the concept of dynamic similarity.

Such similarity of the Reynolds number can be described mathematically. The derivation of Reynolds number can be obtained by non-dimensionalizing the Navier-Stokes **equations 3-1**.

Then the dimensionless form of these elements would be (Fox, McDonald and Pritchard, 2006):

$$u^* = \frac{u}{U}, \quad p^* = p\frac{1}{\rho U^2}, \quad f^* = f\frac{L}{\rho U^2}, \quad \frac{\partial}{\partial t^*} = \frac{L \cdot u}{U \cdot \partial t}, \quad \nabla^* = \nabla \cdot L \qquad 3\text{-}10$$

And the unit of each element is: u = (m/s), ρ = (kg/m^3), L =(m).

Then the dimensionless form of these elements would be (Fox, McDonald and Pritchard, 2006):

$$u^* = \frac{u}{U}, \quad p^* = p\frac{1}{\rho U^2}, \quad f^* = f\frac{L}{\rho U^2}, \quad \frac{\partial}{\partial t^*} = \frac{L}{U}\frac{\partial}{\partial t}, \quad \nabla^* = \nabla \cdot L \qquad 3\text{-}11$$

The Navier-Stokes **equations 3-1** then become:

$$\frac{\partial u^*}{\partial t^*} + u^* \cdot \nabla^* u^* = -\nabla^* p^* + \frac{\mu}{\rho u L}\nabla^{*2} u^* + f^* \qquad 3\text{-}12$$

Remove the superscript of the elements and the equations become:

$$\frac{\partial u}{\partial t} + u \cdot \nabla u = -\nabla p + \frac{1}{Re}\nabla^2 u + f \qquad 3\text{-}13$$

So the dimensionless form of Navier-Stokes equations shows its relationship with Reynolds number. The Reynolds number can also be used to predict the convective flow boundary thickness for cylinder, if the convective force is:

$$\frac{\rho \cdot u^2}{L} \qquad 3\text{-}14$$

And the viscous force is:

$$\frac{\mu \cdot u}{\delta_2^2} \qquad 3\text{-}15$$

Where the variable δ_2 is the convective boundary thickness, and it can be rewritten into a dimensionless form with the Reynolds number *Re*, which:

$$\frac{L}{\delta_2} = \sqrt{\frac{\rho \cdot u \cdot L}{\mu}} = \sqrt{Re} \qquad 3\text{-}16$$

Notice that the Reynolds number might not be useful for natural convection flow, especially in a closed cavity where the mean velocity is always zero. The understanding of Reynolds number leads to the next question: how to quantify and describe such flow instabilities – i.e. turbulence in the flow. Since the Reynolds number only identifies the flow regime and similarity by its characteristic factor, or more generally speaking, the factors affect the shear force from the Navier-Stokes

equations, but not the description of turbulence within the Navier-Stokes equations. The concept of turbulence was introduced to describe such instability; it then leads to a more experimental based rather than theoretical based topic: turbulence modelling.

General heat transfer discussion

There are other factors that take parts in this research, some of them have been used in the previous chapters, and here it is a quick review of them.

There are usually 3 types of heat transfer phenomenon in the physical condition: conduction, convection and radiation. This research is based on a relative low temperature (<100°C) and low energy (<5kW in single system); also it is a closed environment heat transfer filled with liquid medium thereby the radiation effect in such type of system should be very small. The major argument of the problem is relationship between conduction and convection heat transfer in the flow system.

The thermal conduction here refers to the heat energy transfer, of more precisely, diffuse from particles to particles. It stated as the heat energy travels (diffuses) from one side (heat source) to the other side (cold source) of the body. In mathematical expression the heat conduction it can be written as:

$$\vec{q} = -\lambda \nabla T \qquad 3\text{-}17$$

Where $\vec{q}$ is the local heat flux (W/m^2) to a specific reference plate of surface and thereby it is directional towards or away from the face. In a more approximate form it can be rewritten as:

$$\vec{q} = -\lambda \cdot \frac{dT}{dl}\,, \qquad \frac{\Delta Q}{\Delta t} = -\lambda \cdot A_Q \cdot \frac{\Delta T}{\Delta l}\,, \qquad \lambda = \frac{\frac{\Delta Q}{\Delta t}}{A_Q \cdot \frac{\Delta T}{\Delta l}} \qquad 3\text{-}18$$

Where Q here is the heat energy (J), and the $\Delta Q/\Delta t$ is the power of the heat energy (J/s or W),

A_Q is the relative surface area (m^2) which the heat transfer starts and ends, and

Δl is the length that the heat energy travels through.

λ is the thermal conductivity with the unit W/(m.K)

Notice the relationship between thermal conductivity and heat load can be written as thermal resistance:

$$R_\theta = \frac{\Delta l}{A_Q \cdot \lambda} \qquad 3\text{-}19$$

In the other hands the description of heat convection usually based on the Heat Transfer Coefficient (HTC, (W/m^2·K)) which understood as the traveling of the particles which carries the heat energy with them. The heat transfer coefficient stated as the heat energy travel through (in or out) a certain surface, which mathematical expressed as:

$$HTC = \frac{Q'}{A_Q \cdot \Delta T} \qquad 3\text{-}20$$

The heat transfer coefficient (HTC) has a very close expression as the thermal conductivity; even so the inverse of the heat transfer coefficient can be the thermal resistivity (R, (m^2·K/W)) too, which is:

$$R = \frac{A_Q \cdot \Delta T}{Q'} \qquad 3\text{-}21$$

Both thermal conductivity and heat transfer coefficient are very general forms of describing heat transfer with in an ideal shape of face or volume. In fluid dynamic the delivery of energy in the fluid is a combination of conduction and convection, where the heat energy carried by the particle and transfer between particles at the same time. So the description of energy transfer in fluid leads to an extra equation coupled with the Navier-Stokes equation and forms a solution of natural convection flow, such equation is the Diffusion-convection equation, which will be discussed in the following section.

3.2 Mathematical description of density driven natural convection

Natural convection is a flow mechanism usually taking place in a closed environment with heating and cooling sources. When the flow in a closed volume heats up by the surrounding source, the heated fluid expands, reducing its density and rising upward while the cooled heavier fluid drops to the bottom of the volume. Natural convection usually formed a loop flow that the cooled fluid fed to the heat source and sustains the motion.

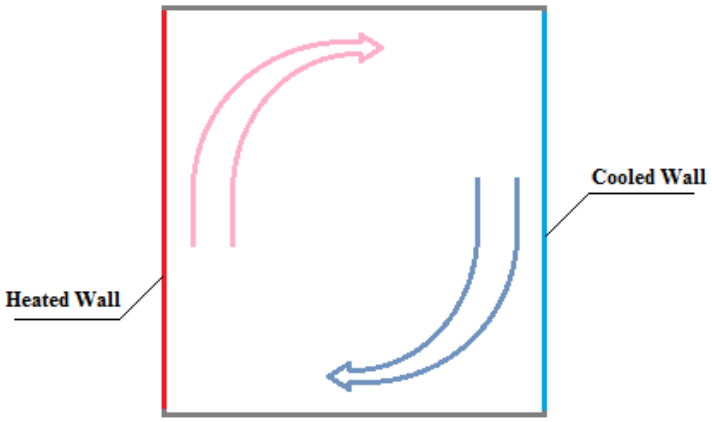

Figure 3-2 Density Driven Natural Convection in a 2-D cavity

Assuming it is incompressible fluid, the proportion of force in natural convection can be described as the combination of viscosity (shear) force as the body force, and driving (buoyancy) force as a function of a temperature (Incropera, 2011).

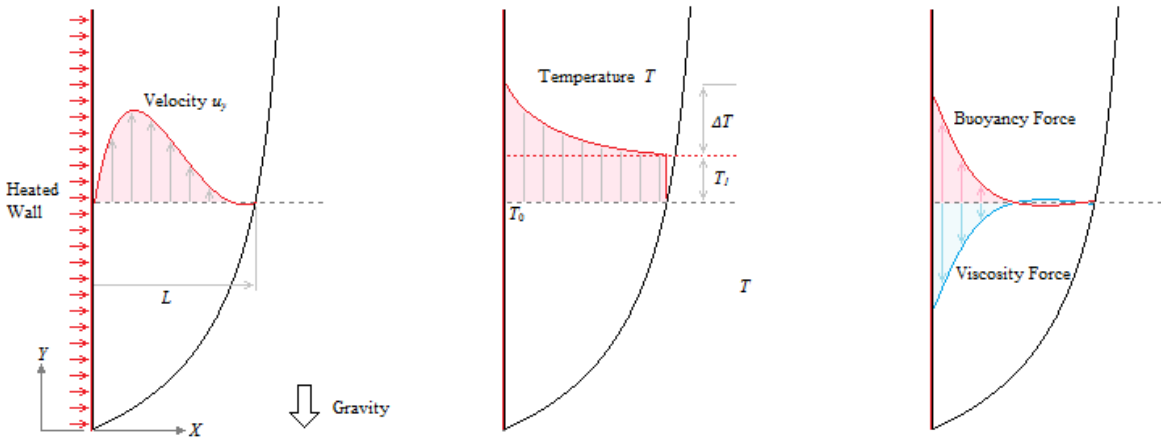

Figure 3-3 Velocity field, Temperature field and Buoyancy field of the near wall section in natural convection

Based on equation **3-1**, the density term can be rewritten in to a temperature dependent variable density:

$$\rho = \rho_0 - \Delta\rho = \rho_0 - g\beta\Delta T \qquad 3\text{-}22$$

Where β is the coefficient of thermal expansion.

Put the variable density term into the Navier-Stokes momentum equation:

$$(\rho_0 - \Delta\rho)\left(\frac{\partial \mathrm{u}}{\partial t} + \mathrm{u}\cdot\nabla\mathrm{u}\right) = -\nabla p + \mu\nabla^2\mathrm{u} + (\rho_0 - \Delta\rho)g \qquad 3\text{-}23$$

Also the pressure term can be rewritten as the hydrostatic (vertical) pressure correlated with the buoyance force, which:

$$\nabla p' = \nabla p + \rho_0 g \tag{3-24}$$

And the Navier-Stokes momentum equation can be:

$$(\rho_0 - \Delta\rho)\left(\frac{\partial \mathrm{u}}{\partial t} + \mathrm{u}\cdot\nabla\mathrm{u}\right) = -\nabla p' + \mu\nabla^2\mathrm{u} + \Delta\rho g \tag{3-25}$$

The equation above is the full buoyancy Navier-Stokes momentum equation. If the density difference is small compare to the reference density ($\Delta\rho << \rho_0$), then the Navier-Stoke momentum equation can be rewritten as:

$$\rho_0\left(\frac{\partial \mathrm{u}}{\partial t} + \mathrm{u}\cdot\nabla\mathrm{u}\right) = -\nabla p' + \mu\nabla^2\mathrm{u} + \Delta\rho g \tag{3-26}$$

This is the Boussinesq approximation (Gauthier-Villars, 1897) for buoyancy-driven flows, and if the density difference is replaced by an expression with temperature ($\Delta T = T - T_0$) and thermal expansion β:

$$\rho_0\left(\frac{\partial \mathrm{u}}{\partial t} + \mathrm{u}\cdot\nabla\mathrm{u}\right) = -\nabla p' + \mu\nabla^2\mathrm{u} + g\beta(T - T_0) \tag{3-27}$$

Where:

T_0 is the fluid reference temperature of (initial wall temperature), ΔT is the temperature difference across the medium

ρ_0 is the reference density at temperature T_0, $\Delta\rho$ is the density variation,

f is the body force, that is buoyancy force in this particular case

μ = Dynamic viscosity of the fluid, and

Up to this point the Navier-Stokes momentum equation for natural convection is governed either with full buoyancy version or Boussinesq approximation version. The full buoyancy version will be a more complex expression since the variable density affects both the time dependent and velocity terms of the Navier-Stokes equation. On the other hand the Boussinesq approximation allows the natural convection expression to retain a constant density condition, especially in the incompressible condition.

One thing should be noticed, the Boussinesq approximation is valid when the density or temperature variation relative small. The Boussinesq approximation also make the up-stream and down-stream

flow identical where only the buoyance term is different (negative to each other) in such case. But in a case like multi-phase or particle model solution, the up-stream and down-stream flow will be asymmetry, it can only uses the full buoyance expression.

Since now the source force term (buoyancy force) is no longer a constant and it is now temperature dependent. To form a complete expression for the natural convection, another equation will be needed to provide the expression for the temperature term. Hence a Convection-Diffusion equation is introduced as an expression of the conservation of energy:

$$\frac{\partial T}{\partial t} = \frac{\lambda}{C_p \cdot \rho}\left(\frac{\partial^2 T}{\partial x^2} + \frac{\partial^2 T}{\partial y^2}\right) - \left(\frac{\partial}{\partial x}(u_x T) + \frac{\partial}{\partial y}(u_x T)\right) \qquad 3\text{-}28$$

Now the natural convection expression is completed within the Navier-Stokes momentum equation and Convection-Diffusion equation together. But unlike the force convection types of problem that the temperature term is not needed in the Navier-Stokes momentum equation, and the Convection-Diffusion equation is coupled one-way to the Navier-Stokes equation velocity solution. In natural convention the temperature term will be used in the Navier-Stokes equation to calculate the velocity solution, while the velocity term will also be used in the Convection-Diffusion equation to get the temperature solution. This forms a 2-way coupling of this 2 expression, eventually increase the order of complexity.

To understand and describe the natural convection in mathematics, a method following the pipe flow in derivation Hagen–Poiseuille equation from Navier-Stokes equation would be performed in the latter on part of this work. Before taking into next step of mathematical derivation, some dimensionless numbers such as Rayleigh Number, Grashof number and Nusselt number has been introduced for natural convection.

Grashof number, Rayleigh Number, Prandtl number and Nusselt number

The Grashof number (Gr) is a dimensionless description of buoyancy influence of the flow, or more specifically, is the buoyancy force over viscosity force (Kays, Crawford and Weigand, 2004) where:

$$\mathrm{Gr}(x) = \frac{g\beta(T_s - T_0)x^3}{\nu^2} \qquad 3\text{-}29$$

The natural convection Grashof number can be obtain by non-dimensionalized the equation 3-1 (Incropera, 2011):

$$\mathbf{u}^* = \frac{\mathbf{u}}{\mathbf{U}}, \qquad \boldsymbol{p}^* = \boldsymbol{p}\frac{\mathbf{1}}{\boldsymbol{\rho}\mathbf{U}^2}, \qquad \mathbf{f}^* = \mathbf{f}\frac{\boldsymbol{L}}{\boldsymbol{\rho}\mathbf{U}^2}, \qquad \frac{\boldsymbol{\partial}}{\boldsymbol{\partial t}^*} = \frac{\boldsymbol{L}}{\mathbf{U}}\frac{\boldsymbol{\partial}}{\boldsymbol{\partial t}}, \tag{3-30}$$

$$\boldsymbol{\nabla}^* = \boldsymbol{L}\boldsymbol{\nabla}, \quad \Delta\boldsymbol{T}^* = \frac{\boldsymbol{T} - \boldsymbol{T}_\infty}{\boldsymbol{T_s} - \boldsymbol{T}_\infty}$$

$$\mathbf{u}^*\frac{\boldsymbol{\partial}\mathbf{u}^*}{\boldsymbol{\partial t}^*} + \mathbf{u}^* \cdot \boldsymbol{\nabla}^*\mathbf{u}^* = -\boldsymbol{\nabla}^*\boldsymbol{p}^* + \frac{\mathbf{1}}{\mathbf{Re}_{\boldsymbol{L}}}\boldsymbol{\nabla}^{*\mathbf{2}}\mathbf{u}^* + \left[\frac{\boldsymbol{g\beta}(\boldsymbol{T_s} - \boldsymbol{T_0})\boldsymbol{L}^{\boldsymbol{3}}}{\boldsymbol{\nu}^{\boldsymbol{2}}}\right]\frac{\boldsymbol{T}^*}{\mathbf{Re}_{\boldsymbol{L}}^{\mathbf{2}}} \tag{3-31}$$

In natural convection flow the Grashof number (Gr) play a part as that of the Reynolds number in the general non-dimensionalised Navier-Stokes equation. Also the same non-dimensionalisation method can be applied to the convection-diffusion (energy) equation:

$$\frac{\partial T}{\partial t} = \frac{\lambda}{C_p \cdot \rho}\nabla^2 T - \vec{u} \cdot \nabla T \tag{3-32}$$

It can be rewritten in a more conventional form:

$$\frac{\partial T}{\partial t} = \frac{\lambda}{C_p \cdot \rho} \cdot \frac{\partial^2 T}{\partial x_j \partial x_j} - u_j \cdot \frac{\partial T}{\partial x_j} \tag{3-33}$$

When:

$$\mathrm{u}^* = \frac{\mathrm{u}}{\mathrm{U}}, \qquad x^* = \frac{x}{\mathrm{L}}, \qquad \frac{\partial}{\partial t^*} = \frac{L}{\mathrm{U}}\frac{\partial}{\partial t}, \qquad t^* = \frac{t}{t_o}, \quad T^* = \frac{T - T_\infty}{T_s - T_\infty} \tag{3-34}$$

The energy equation can be rewritten as:

$$\frac{T_s - T_\infty}{t_o} \cdot \frac{\partial T^*}{\partial t^*} = \frac{T_s - T_\infty}{\mathrm{L}^2} \cdot \frac{\lambda}{C_p \cdot \rho} \cdot \frac{\partial^2 T^*}{\partial x^*_j \partial x^*_j} T - \frac{\mathrm{U}}{\mathrm{L}}(T_s - T_\infty) \cdot \mathrm{u}^*_j \cdot \frac{\partial T^*}{\partial \mathrm{x}^*_\mathrm{j}} \tag{3-35}$$

Eventually it can be rewritten as:

$$St \cdot \frac{\partial T^*}{\partial t^*} = \frac{T_s - T_\infty}{\mathrm{L}^2} \cdot \frac{1}{Re \cdot Pr} \cdot \frac{\partial^2 T^*}{\partial x^*_j \partial x^*_j} T - \mathrm{u}^*_j \cdot \frac{\partial T^*}{\partial \mathrm{x}^*_\mathrm{j}} \tag{3-36}$$

Which St is the Strouhal number, Re is the Reynolds number and Pr is the Prandtl number:

$$St = \frac{\mathrm{L}}{U \cdot t_o}, \qquad Re = \frac{\rho \cdot U \cdot \mathrm{L}}{\mu}, \qquad \mathrm{Pr} = \frac{\nu}{\alpha} = \frac{C_p \cdot \mu}{\lambda} \tag{3-37}$$

In fluid dynamic, the Rayleigh number (Ra) is the dimensionless factor somewhat more popular than Grashof number (Gr) in general application. Similar to Grashof number the Rayleigh number stand for convection factor over conduction factor:

$$\mathrm{Ra} = \mathrm{Gr} \cdot \mathrm{Pr} = \frac{g\beta}{\nu\alpha}(T_s - T_\infty)L^3 \tag{3-38}$$

Where:

T_s is the temperature (K or ^oC) of the heat source,

T_∞ is the temperature (K or ^oC) of far side (cold source), and

L is the reference length (m) scale here, which usually stands for the distant between the heat source and cold source.

α is the thermal diffusive (m^2/s) (Donald and Gerald, 2002).

The Rayleigh number can be rewritten in a more detailed expression:

$$\mathrm{Ra} = \frac{\rho^2 \cdot g \cdot \beta \cdot C_p \cdot \Delta T \cdot L^3}{\mu \cdot \lambda} \qquad 3\text{-}39$$

Notice that this form of Rayleigh number requires a temperature boundary condition, for a constant heat flux boundary condition, the temperature value can be changed with a thermal conductivity expression, where:

$$\lambda = \frac{Q' \cdot L}{l^2 \cdot \Delta T}\,, \qquad \mathrm{Q}^* = \frac{Q'}{L^2}\,, \qquad \rightarrow \quad \Delta T = \frac{\mathrm{Q}^* \cdot L}{\lambda} \qquad 3\text{-}40$$

And the Rayleigh number expression with wall heat load boundary condition can be rewritten as:

$$\mathrm{Ra} = \frac{\rho^2 \cdot g \cdot \beta \cdot C_p \cdot Q' \cdot L^4 \cdot}{\mu \cdot \lambda^2} \qquad 3\text{-}41$$

Notice than the Rayleigh number based on the constant wall temperature (Ra_{CWT}) and Rayleigh number based on the wall heat flux (Ra_{CWHF}) is not really equivalent and interchangeable. In most typical assumption still based on the Rayleigh number with constant wall temperature (Ra_{CWT}), so as some of the discussion. This indicate that without extra specification, the general Rayleigh number (Ra) that uses in any letter section of this work will be Rayleigh number with constant wall temperature (Ra_{CWT}).

In general engineering application the Rayleigh number is a large number usually over 1×10^6. It is also noticeable that the Rayleigh number has a cubical or quartic of length scale (L^3 or L^4), which may hint that the turbulence of the natural convection flow is largely influenced by the size scale of the environment than all other factors.

Also noticed that the Rayleigh number (Ra) has very close expression as that of Grashof number (Gr), however a thermal diffusivity (α) has been used in Rayleigh number instead of the viscosity (v) in Grashof. The factor between Rayleigh number and Grashof is that:

$$\mathrm{Ra} = \mathrm{Gr} \cdot \mathrm{Pr} \qquad 3\text{-}42$$

Where the Prandtl number (Pr), name after Ludwig Prandtl has been introduced as (White, 2006):

$$\mathrm{Pr} = \frac{\nu}{\alpha} = \frac{C_p \cdot \mu}{\lambda} \qquad 3\text{-}43$$

Where C_p is the specific heat capacity (C_p), (J/(kg·K)) , and

λ here is the thermal conductivity (W/(m.K))

Noticed that both the kinematic viscosity (ν) and thermal diffusivity (α) has the same unit (m^2/s), so the Prandtl number (Pr) is dimensionless and represent the ratio of momentum diffusivity kinematic viscosity over thermal diffusivity.

The Prandtl number does not have any factor from the flow velocity or size scale, therefore it does not represent any of the flow condition but only the fluid property itself. The higher Prandtl number of the fluid refers to greater convective heat transfer; while lower Prandtl number towards greater conductive heat transfer.

The one last dimensionless factor introduced in this section is the Nusselt number (Nu), named after Wilhelm Nusselt. It plays a similar role as the Prandtl number, which represents the convective heat transfer coefficient over the conductive heat transfer (Thermal conductivity) which:

$$\mathrm{Nu}_L = \frac{HTC \cdot L}{\lambda} \qquad 3\text{-}44$$

Where the factor HTC here is the Heat Transfer Coefficient, ($W/m^2 \cdot K$).

It is easy to find that the Nusselt number (Nu) has the same denominator as that the Prandtl number (Pr) has: thermal conductivity; while the Nusselt number has different fraction of heat transfer coefficient (HTC) multiply by a length scale L (Incropera, 2011)

It is reasonable to compare the usefulness of Nusselt number (Nu) and Prandtl number (Pr). By definition the Nusselt number has both length scale (L) and temperature scale (T) involved, which hint it should have connection with the flow condition factors such as Reynolds number (Re) or Rayleigh number (Ra), where:

$$\mathrm{Nu}_L = F(\mathrm{Re}, \mathrm{Pr}) \text{ , or } \mathrm{Nu}_L = F(\mathrm{Ra}, \mathrm{Pr}) \qquad 3\text{-}45$$

Hence the Nusselt number (Nu) can expressed as a function of Reynolds number or Rayleigh number with Prandtl number in some approximations. With a given thermal property from Prandtl

number, the Nusselt number (Nu) can evaluate geometries, condition and the environment of the flow field affects the heat transfer of the fluid.

For forced convection in turbulence pipe flow (Gnielinski cited in Incropera, 2007):

$$\mathrm{Nu}_D = \frac{\frac{f}{8}(\mathrm{Re}_D - 1000)\cdot \mathrm{Pr}}{1 + 12.7\cdot\left(\frac{f}{8}\right)\cdot\left(\mathrm{Pr}^{\frac{2}{3}} - 1\right)} \qquad 3\text{-}46$$

Where:

$$3\times 10^3 \le \mathrm{Re}_D \le 5\times 10^6\,, \qquad 0.5 \le \mathrm{Pr} \le 2\times 10^3$$

Where Re_D is the Reynolds number based on the pipe diameter, and the function f here is the Darcy friction factor that can either be obtained from the Moody chart or for smooth tubes from correlation developed by Petukhov (Incropera, 2007):

$$f = (0.79\ln(\mathrm{Re}_D) - 1.64)^{-2} \qquad 3\text{-}47$$

For a natural convection of vertical walls (Churchill and Chu cited in Incropera, 2000):

$$\mathrm{Nu}_L = 0.68 + \frac{0.67\mathrm{Ra}_L^{\frac{1}{4}}}{\left[1 + \left(\frac{0.492}{\mathrm{Pr}}\right)^{\frac{9}{16}}\right]^{\frac{4}{9}}}\,,\ \mathrm{Ra}_L \le 10^9 \qquad 3\text{-}48$$

As mentioned before, in natural convection flows it is hard to identify its velocity scale, as they usually happen in a closed environment and have zero overall mean velocity. It may be of some help to assume the Reynolds number (Re) of the natural convection is the square root of the Grashof number (Gr) where $\mathrm{Re} \approx \mathrm{Gr}^{1/2}$. However the absence of a velocity scale (u) with in Rayleigh number (Ra) and Grashof number (Gr) still results in certain difficulties to identify some parameters for numerical solution of a natural convection flow, which for example, the dimensionless wall distance (y+).

In the following section it will discuss the in-depth mathematics derivation of natural convection flow.

Log law of wall

The discussion of turbulence modelling also refers to another topic that affects the flow simulation, the turbulence flow condition near wall boundary. In general speaking the close wall fluid would

be more affected by the viscous force while the far side fluid would be mode depend on the body force. The Log law of Wall, An approximation given by Theodore von Kármán, in 1930 represent the problem (Chanson, 2009).

The near wall condition would be important, especially in natural convection flow which near wall heat transfer would dominant the flow behaviour. The near wall condition in turbulent flow usually described in the power-law near wall condition:

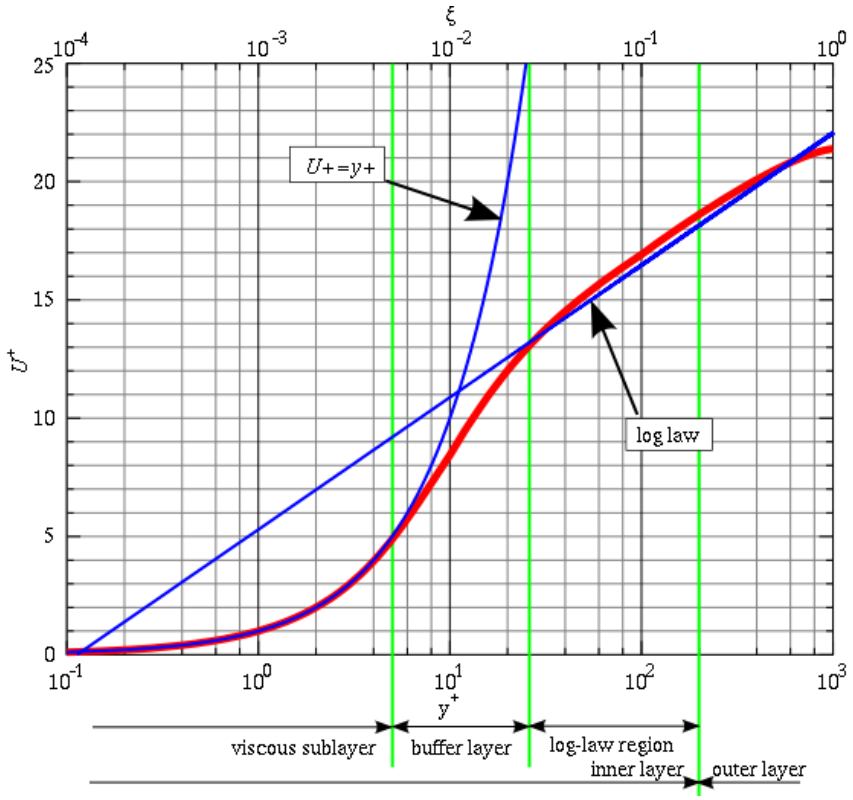

Figure 3-4 Near wall flow regime (Log law of wall)

From **Figure 3-4** it can be seen that there usually has 3 regimes to define the close wall condition: viscous sub-layer (inner), log law (outer) regime and buffer layer (middle). The logarithmic law of the wall is a self-similar solution for the mean velocity parallel to the wall, and is valid for flows at higher velocity and higher Reynolds numbers or Rayleigh number. The middle layer is an approximation that transmits from inner (scalar) to outer (power law), in some engineering applications there are only inner and outer layer in considered.

In mathematical expression the near wall condition based on dimensionless velocity and dimensionless wall distance, where for the outer layer (power law) fluid it can be:

$$\mathrm{U}^+ = \frac{1}{k_v}\ln y^+ + C^+ \qquad 3\text{-}49$$

Here:

k_v is the Von Kármán constant

$C+$ is a constant which $C+ \approx 5.1$

$y+$ is the wall coordinate: the distance Y to the wall, made dimensionless with the friction velocity u_τ and kinematic viscosity v, where:

$$y^+ = \frac{y u_\tau}{v} \quad 3\text{-}50$$

u+ is the dimensionless velocity: the velocity u parallel to the wall as a function of Y (distance from the wall), divided by the friction velocity u_τ,

$$u^+ = \frac{u}{u_\tau} \quad 3\text{-}51$$

$\tau_w$is the wall shear stress, which can be related to the stress term (τ_{ij}) in Navier-Stokes equations,

ρ is the fluid density,

u_τ is called the friction velocity or shear velocity, where:

$$u_\tau = \sqrt{\frac{\tau_\omega}{\rho}} \quad 3\text{-}52$$

For the inner layer it is simpler as it has only the scalar where:

$$U^+ = y^+ \quad 3\text{-}53$$

For most engineering solution the y+ is somewhat a guide line for the choice of turbulence model, as it defines velocity scale and length scale (wall distance) that would be observed in the solution. Also the y+ value defines the mesh density for a Computational Fluid Dynamic solution (CFD), in one hand it needs to have enough mesh resolution for the near wall boundary; on the other hand it can save some computation resource by reducing the mesh density on the less important volume. This will be an important issue in the latter on part of this research.

In general the choice of y+ would be quite relax for k-ε (kinetic - epsilon) model, as the k-ε model is usually valid for higher Reynolds number and the $y+ \approx 30$ would be sufficient. In the other hand for k-ω (kinetic - omega) model is more restricted down $y+ = 0.1 \sim 10$ due to its requirement of close wall resolution.

The reason to mention turbulent modelling and near wall condition (y+ value) is some CFD simulation in latter on work in this research will use one of the turbulent model (SST model). But

whether a relative low velocity natural flow will need turbulent modelling remains questionable. One more thing is, if there is no turbulent modelling then the near-wall flow might not necessary a power-law curve. This may require another method to describe the near-wall distant, which will be an in-depth discussion in the latter on section.

The detail of turbulent modelling method related to this research will be ln the chapter 8 Appendix.

3.3 Mathematical modelling of fully developed natural convection (constant thermal gradient model)

The goal of this section is to understand the relationship between physics and analytical model of natural convection by working on the derivation of the convection equations. Using the Hagen-Poiseuille equation of fully developed flow derivation, the flow field mathematical expression of natural convection can be simplified in a very simple manner; which, in some particular condition, could be solved without involving of CFD method.

This work is based on 2 directions of research, one is the fully developed / laminar natural convection of vertical flows (Morton, 1960) (Sinha, 1969). It starts with an anti-symmetry geometry with heated-cooled walls, and then a single heated wall with heat flux (non-uniform temperature) boundary condition. While Sinha's work is anti-symmetry but uses a uniform wall temperature boundary, and Morton's work has a heat flux wall boundary but an axis-symmetry geometry. The other direction of research is based on the work on natural convection in various vertical aspect ratios (Elder, 1965). In Elder's research it shows that the vertical aspect ratio significantly affects the flow pattern of the flow with a fixed Rayleigh number.

The following work simplifies the mathematical expressions to obtain an algebraic solution of natural convection from the Navier-Stokes equations and Convection–Diffusion equation for energy conservation, which includes relationships between flow condition and case height (aspect ratio).

Derivation of equations

The scope of the natural convection in this section base on the choice range of Rayleigh number. From **equation** 3-39, in here for Rayleigh number the characteristic length (L) defines as the total length or height (h) of the typical square cavity problem (when L= h) for the general Rayleigh number is:

$$a = \frac{\lambda}{\rho \cdot C_p}\,, \qquad v = \frac{\mu}{\rho}\,, \qquad \mathrm{Ra} = \frac{\rho^2 \cdot g \cdot \beta \cdot \Delta \mathrm{T} \cdot C_p \cdot L^3}{\mu \cdot \lambda}$$

Notice that in latter on section of this thesis, when the height scale (h , thermal length) will be more important to the problem solution, it is no longer equivalence to the length scale (h ≠ L) and could not be considered as the same length scale as L. The use of length scale will be more likely to be half length (l, thermal distant) rather than the overall length (L) of the problem, which L = 2l.

Along with the liquid physical properties such density, viscosity and gravity is known, there are 2 extra factors that states the condition: delta temperature T and characteristic length L. In other hands, the 2 variable of interest will be Y direction velocity $\vec{v}$ on X axis and temperature T on X axis.

Boundary condition (inputs)							
Wall temperature		Thermal distance Distant heated-cooled wall		Thermal length Distant against gravity			
T_1		$L = 2l$.		h			
^oC		m		m			
Properties and Constants (Typical water, 20^{o}C)							
Density	Kinematic Viscosity	Dynamic Viscosity	Thermal Conductivity	SHC	Thermal Expansion	Reference temperature	Gravity
ρ	v	μ	λ	C_p	β	T_0	$-g$
kg/m^3	m^2/s	Pa.s	W/m.K	J/kg.K	1/K	^{o}C	m/s^2
997.05	8.90×10^{-7}	8.874×10^{-4}	0.613	4181	2.07×10^{-4}	25	-9.8
Outcomes							
Velocity (Y axis)		Temperature		Flux			
v		T		Q*			
m/s		^{o}C		W/m^2			

Table 3-1 Input and output parameters that would be involved in following parts

Here the direction of gravity is always opposite to the direction of flow, but for convenience the indicator $-g$ will be use in this thesis with the value of gravity and has an absolute value of 9.8m/s^2 or 9.8 N/kg.

The concept of simplifying the natural convection problem is to reduce the dimension of the system. In the latter on section of this chapter the mathematical solution would mostly in 2-dimensional form, but here it starts with 3-dimentional velocity $\vec{u}$ vector:

$$\vec{u} = (u_x, u_y, u_z) \qquad 3\text{-}54$$

The flow direction will be on the ±Y axis within 2 vertical wall, one side of the wall is heated and the other side is cooled, with the distant between 2 walls is L = 2l. The heated fluid flow against the gravity direction (+Y) and the cooled flow follows the gravity direction (-Y).

Similar to the derivation of Couette flow from Navier-Stokes equation in a pipe flow case, there are few conditions to meet to achieve the ‘fully developed flow' state in natural convection:

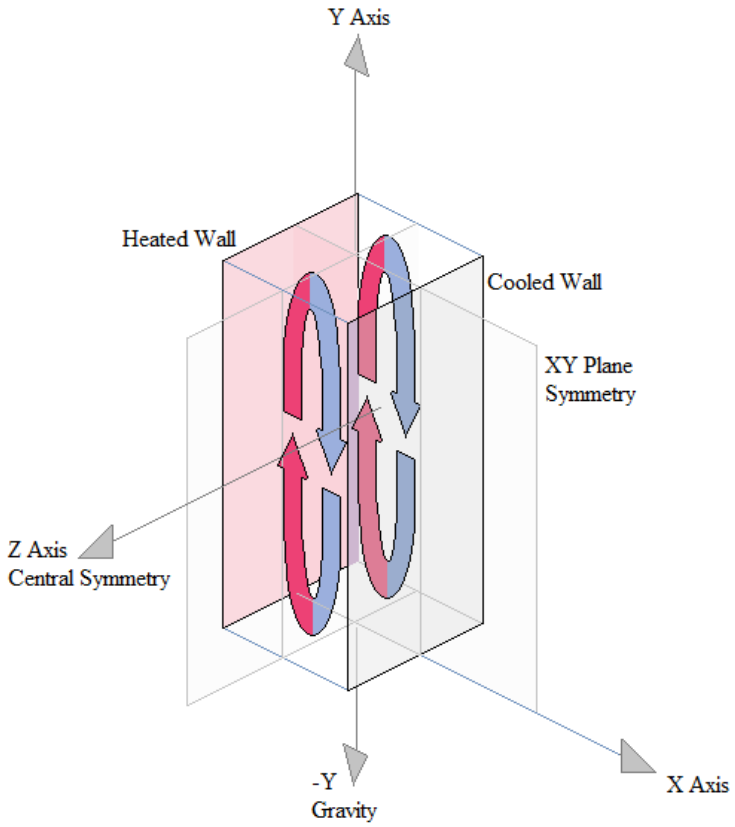

Figure 3-5 3 dimensional view of the density driven natural convection problem space

1), The flow is steady, time independent and constant in the y axis direction:

$$\frac{\partial u_y}{\partial y} = 0\,, \qquad \frac{\partial u_y}{\partial t} = 0 \tag{3-55}$$

2), All forces are balanced over time (time independent), in natural convection flow the only force term left is the buoyancy force against the gravity (y axis) direction, which:

$$\frac{\partial \mathrm{f}_y}{\partial y} = 0\,, \qquad \frac{\partial \mathrm{f}_y}{\partial t} = 0 \tag{3-56}$$

And 3), The flow is plane-symmetric on XY plane and central-symmetry on y axis, so no flow motion and force on the X and Z axis:

$$u_x = 0\,, \qquad u_z = 0\,; \qquad \mathrm{f}_x = 0\,, \qquad \mathrm{f}_z = 0$$

With these 3 conditions lined up, the dimension of the problem can be reduced and now it is possible to rewrite the 3 components of the Navier-Stokes equations (**equation 3-1**) into 1 equation:

Rewrite the 2-dimensional Navier-Stokes **equations 3-2 and equation 3-3**, with the 2-dimensional energy **equation 3-28** (Convection–diffusion equation) together forms the equations set for 2D

natural convection flow. For steady state and incompressible problem, the motions of the fluid should be consisted over time:

$$\frac{\partial u_x}{\partial t} = 0\,, \qquad \frac{\partial T}{\partial t} = 0\,, \qquad \frac{\partial u_x}{\partial x} + \frac{\partial u_y}{\partial y} = 0 \tag{3-57}$$

And:

$$\frac{\partial}{\partial x}(u_x T) + \frac{\partial}{\partial y}(u_y T) = u_x \frac{\partial T}{\partial x} + u_y \frac{\partial T}{\partial y} \tag{3-58}$$

And the pressure terms can be ignored, where (Bejan, 2013):

$$\frac{1}{\rho}\nabla p \;=\; 0 \tag{3-59}$$

Then the equations of 2D natural convection (3-2, 3-3 and 3-30) become:

$$\rho\left(u_x \frac{\partial u_x}{\partial x} + u_y \frac{\partial u_x}{\partial y}\right) = \mu\left(\frac{\partial^2 u_x}{\partial x^2} + \frac{\partial^2 u_x}{\partial y^2}\right) + \mathrm{f}_x \tag{3-60}$$

$$\rho\left(u_x \frac{\partial u_y}{\partial x} + u_y \frac{\partial u_y}{\partial y}\right) = \mu\left(\frac{\partial^2 u_y}{\partial x^2} + \frac{\partial^2 u_y}{\partial y^2}\right) + \mathrm{f}_y \tag{3-61}$$

$$0 = \frac{\lambda}{C_p \cdot \rho}\left(\frac{\partial^2 T}{\partial x^2} + \frac{\partial^2 T}{\partial y^2}\right) - \left(u_x \frac{\partial T}{\partial x} + u_y \frac{\partial T}{\partial y}\right) \tag{3-62}$$

Assume the natural convection takes place between 2 infinite-long vertical walls with the gravity against y direction, where:

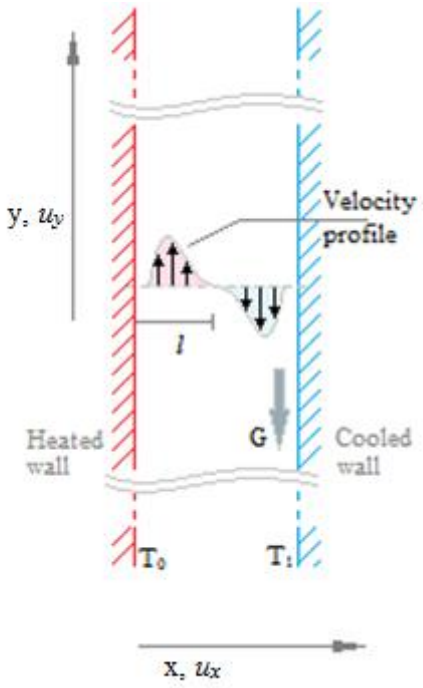

Figure 3-6 2 dimensional view of the density driven natural convection problem space

Under this assumption, in pure density driven natural convection flow the u_x velocity and the force f_x (along x axis) should always be zero, where:

$$u_x \approx 0, \qquad \mathrm{f_x} \approx 0, \qquad \rightarrow \; u_y \frac{\partial u_x}{\partial x} = 0, \qquad u_x \frac{\partial u_y}{\partial y} = 0 \tag{3-63}$$

Notice that here the x-direction velocity is assumed to be zero, when all the components with u_x are now zero value, the first Navier-Stokes equation of x-direction momentum is a zero value as well. This left only the second Navier-Stokes equation of y-direction momentum still exist since the y-direction velocity u_y is non-zero value. And the natural convection equations then reduced to:

$$\rho \cdot u_y \frac{\partial u_y}{\partial y} = \mu \left(\frac{\partial^2 u_y}{\partial x^2} + \frac{\partial^2 u_y}{\partial y^2} \right) + \mathrm{f}_y \tag{3-64}$$

$$0 = \frac{\lambda}{C_p \cdot \rho} \left(\frac{\partial^2 T}{\partial x^2} + \frac{\partial^2 T}{\partial y^2} \right) - u_y \frac{\partial T}{\partial y} \tag{3-65}$$

Also consider the natural convection flow is ‘fully developed’ on y direction which the u_y velocity dose not vary along y coordinates, therefore:

$$\frac{\partial u_y}{\partial y} = 0\,, \qquad \frac{\partial^2 u_y}{\partial y^2} = 0 \tag{3-66}$$

Up to this point, the equations of fully developed natural convection can be reduced to:

$$0 = \mu \frac{\partial^2 u_y}{\partial x^2} - \mathrm{f}_y \quad , \qquad 0 = \frac{\lambda}{C_p \cdot \rho}\left(\frac{\partial^2 T}{\partial x^2} + \frac{\partial^2 T}{\partial y^2}\right) - \nu \frac{\partial T}{\partial y} \tag{3-67}$$

This is the simplest form that Navier-Stokes equations and energy equation could be rewritten by reducing the factors and dimension of the problem, but it is still 2-dimensional system with temperature distribution on both X and Y axis.

The discussion of 'fully developed' condition leads to further simplify of temperature term ($\partial^2 T/\partial y^2$ and $\partial T/\partial y$), with the introduction of Boussinesq approximation. Ideally the buoyancy force term (full buoyancy model) in the natural convection generates the density difference of heated / cooled fluid, where:

$$\mathrm{f}_{\mathrm{buoyance}} = f(\rho - \rho_{\mathrm{ref}}) = f(\Delta\rho) \tag{3-68}$$

Such buoyancy force term leads to a complex expression since it is a function of a variable density. In small temperature changes the Boussinesq approximation could be applied instead of full buoyancy model and the buoyancy force can be simplified as a function of temperature $\mathrm{b}_{\mathrm{uoyancy}} = f$ [T(x, y)] when the density change of the fluid is insignificant:

$$\mathrm{f}(x, y) = \rho g \beta \Delta \mathrm{T} = \rho g \beta \cdot \mathrm{T}(x, y) - \rho g \beta \cdot \mathrm{T}_0 \tag{3-69}$$

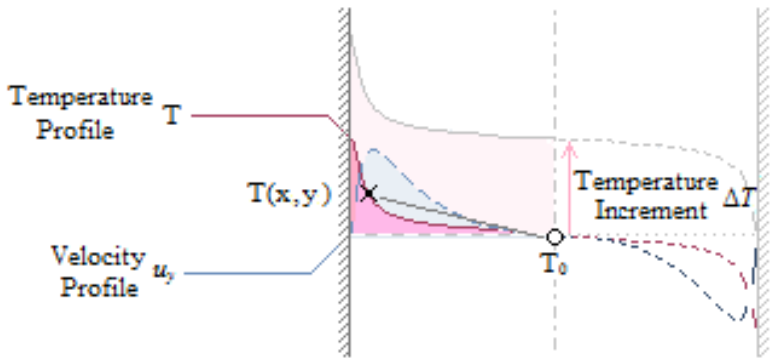

Figure 3-7 Relationship between the control point temperature T (x, y) and reference temperature T_0

Extend this to 2 dimensional case, when the fluid on the location (x_1, y_1), it heated up from temperature T(x_1, y_1) to T(x_1, y_2), and move vertically to location (x_1, y_2), the buoyancy force still based on the reference temperature T_0.

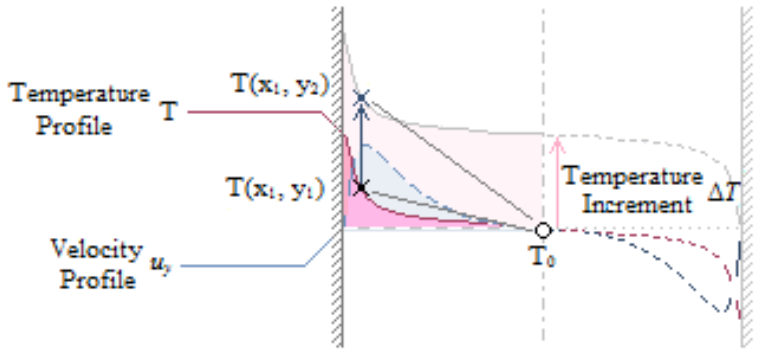

Figure 3-8 Control point moved from (x_1, y_1) to (x_1, y_2) and its temperature shifted from T(x_1, y_1) to T(x_1, y_2) but still based on the same reference temperature T_0

The uses of Boussinesq approximation retain the density as a constant under all condition, this avoids the uses of temperature dependent density ρ(T) or coordinate dependent density ρ(x,y).

The buoyancy force of the fluid control point (x_1, y_1) will be f(x_1,y_1), and in the control point (x_1, y_2) will be f(x_1,y_2), thus:

$$\mathrm{f}(x_1, y_1) = \rho g \beta \cdot \mathrm{T}(x_1, y_1) - \rho g \beta \cdot \mathrm{T}_0\,, \qquad \mathrm{f}(x_1, y_2) = \rho g \beta \cdot \mathrm{T}(x_1, y_2) - \rho g \beta \cdot \mathrm{T}_0 \qquad 3\text{-}70$$

And in this case:

$$y_1 \neq y_2 \quad \rightarrow \quad \mathrm{T}(x_1, y_1) \neq \mathrm{T}(x_1, y_2) \quad \rightarrow \quad \mathrm{f}(x_1, y_1) \neq \mathrm{f}(x_1, y_2)$$

So the buoyancy force depends on the vertical (against gravity) displacement, where the temperature of the flow control point would shift due to the increasing amount of heat load transferred into the fluid over time.

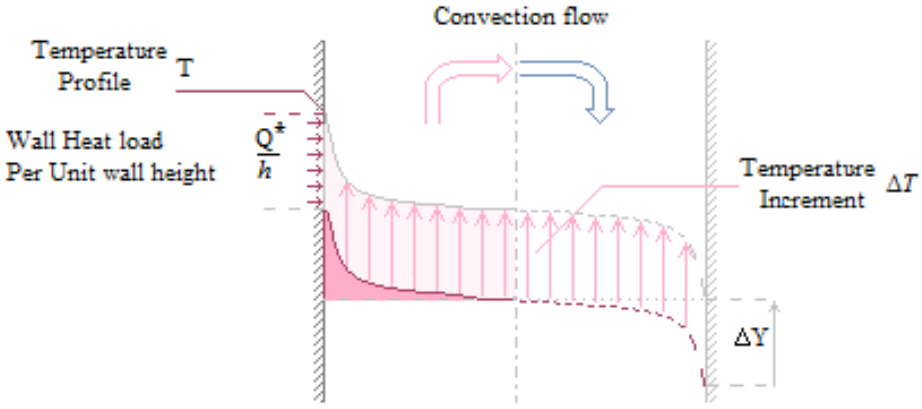

Figure 3-9 Relationship between wall heat flux (Q*) and temperature gradient $\partial T/\partial y$

This would result an increasing buoyancy force in Boussinesq approximation when the flow going upwards, if it is only based on one fixed reference temperature.

Solution with zero $\partial T/\partial y$ value, conduction model

Now the simplest assumption if the $\partial T/\partial y$ value is zero in an extreme case, where:

$$\mathrm{T}(x, y_1) = \mathrm{T}(x, y_2) \quad \rightarrow \quad \frac{\partial T}{\partial y} = 0$$

This results $\partial^2 T/\partial y^2 = 0$ as well, the coupled Navier-Stokes equations and energy equation will become:

$$\mu \frac{\partial^2 u_y}{\partial x^2} = -\rho g \beta \Delta \mathrm{T} \quad , \qquad 0 = \frac{\lambda}{C_p \cdot \rho} \cdot \frac{\partial^2 T}{\partial x^2}$$

Where:

$$\int \left(\int \frac{\partial^2 T}{\partial x^2} dx \right) dx \quad \rightarrow \quad \mathrm{T} = (\mathrm{C}_1 x + \mathrm{C}_2) \tag{3-71}$$

Give the temperature boundary condition on the heated wall x=0 and on the centre point x=*l*:

$$\begin{cases} x = 0 \\ \mathrm{T} = \mathrm{T}_0 \end{cases} and \quad \begin{cases} x = l \\ \mathrm{T} = \mathrm{T}_1 \end{cases} \quad \rightarrow \quad \mathrm{C}_1 = \frac{(\mathrm{T}_1 - \mathrm{T}_0)}{l}, \qquad \mathrm{C}_2 = \mathrm{T}_0$$

Then:

$$\mu \frac{\partial^2 u_y}{\partial x^2} = \frac{-\rho g \beta \cdot (\mathrm{T}_1 - \mathrm{T}_0) \cdot x}{l} \tag{3-72}$$

Solve **equation 3-72**, and then the y direction velocity u_y on x axis will be:

$$u_y = -\frac{\rho g \beta (\mathrm{T}_1 - \mathrm{T}_0)}{l \cdot \mu} (x^3 + \mathrm{C}_1 \cdot x^2 + \mathrm{C}_2) \tag{3-73}$$

Also put the velocity boundary condition on the heated wall x=0 and on the centre point x=*l*:

$$\begin{cases} x = 0 \\ v = 0 \end{cases} and \quad \begin{cases} x = l \\ v = 0 \end{cases} \quad \rightarrow \quad \mathrm{C}_1 = -l\,, \qquad \mathrm{C}_2 = 0$$

As the result the y direction velocity u_y profile on x axis will be:

$$u_y(x) = \frac{\rho \cdot g \cdot \beta \cdot T_1}{l \cdot \mu} \left(\frac{x^3}{6 \cdot l} - \frac{x^2}{2} + \frac{x \cdot l}{3} \right) \tag{3-74}$$

And:

$$T(x) = T_1 \left(1 - \frac{x}{l} \right) \tag{3-75}$$

Eventually the $\partial T/\partial y \rightarrow 0$ assumption leads to the collapse of energy equation (Convection–Diffusion equation) and turns the velocity solution into a cubical polynomial curve, where the heat transfer primarily is simple heat conduction. This stated as the 'conduction model' of natural convection in this research, and its maximum value of the velocity can be obtained as:

$$x_{MAX} = \pm l\left(1 - \frac{1}{\sqrt{3}}\right) \approx 0.422649 \cdot l$$

$$u_{y_{MAX}} = \frac{\sqrt{3}}{27} \cdot \frac{\rho \cdot g \cdot \beta \cdot T_1 \cdot l^2}{\mu} \approx 0.06415 \cdot \frac{\rho \cdot g \cdot \beta \cdot T_1 \cdot l^2}{\mu}$$

Under relative low Raleigh number case (for example: $Ra<10^4$) the natural convection CFD result shows increasing similarity with the conduction model with cubical curve velocity pattern. However to match scope and scale of the fluid flow closely with the conduction model, it may end up with a very low Rayleigh number (Ra <1) and / or very high aspect ratio volume ($h/l > 1\times10^4$). This might enter the regime of micro-channel fluid dynamic exceed the requirement of this research, therefore there will be not further discussion for ultra-low Rayleigh number condition in the following section. For high Raleigh number ($Ra>10^5$.), the convective heat transfer will become significant as more heat energy is contained within the flow, and the $\partial T/\partial y \rightarrow 0$ assumption is no longer valid.

Solution when $\partial T/\partial y$ is constant – Constant thermal gradient (CTG) model

To have a consisted buoyancy force despite the fluid vertical location, the force term needs to be independent from the flow y axis location, if:

$$y_1 \neq y_2 \rightarrow \quad T(x_1, y_1) = T(x_1, y_2) \quad \rightarrow \quad f(x_1, y_1) = f(x_1, y_2)$$

To achieve this, the reference temperature should only represent the same level of flow (same Y coordinates) where:

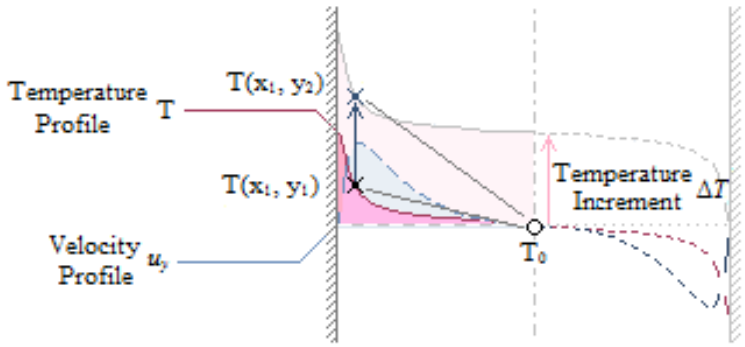

Figure 3-10 Control point moved from (x_1, y_1) to (x_1, y_2) and its temperature shifted from T(x_1, y_1) to T(x_1, y_2), based on the reference shifted temperature T(x_0, y_1) to T(x_0, y_2)

Under this assumption the vertical (Y axis, against gravity direction) temperature gradient $\partial T/\partial y$ consist in all Y location, the temperature ΔT only represent the flow in the same y coordinate level and depend on the X coordinate of the flow control point. This option avoids both Convection–diffusion equation becoming zero value and the whole expression collapse into lower order system. But the temperature gradient then has to describe with both $\partial T/\partial x$ and $\partial T/\partial y$, and also results a slightly more complex solution.

Now the coupled Navier-Stokes equation and Convection–diffusion equation can be rewritten as:

$$\mu\frac{\partial^2 u_y}{\partial x^2} = -\rho g\beta\cdot(\mathrm{T}-\mathrm{T}_0) \quad , \qquad 0 = \frac{\lambda}{C_p\cdot\rho}\cdot\frac{\partial^2 T}{\partial x^2} - u_y\frac{\partial T}{\partial y} \tag{3-76}$$

Since the reference temperature T_0 only represents the shifting of overall temperature, and when $\Delta T = T - T_0$, the expressions can be rewritten with the ΔT, which:

$$\mu\frac{\partial^2 u_y}{\partial x^2} + \rho g\beta\cdot\Delta\mathrm{T} = 0 \quad , \qquad \frac{\lambda}{C_p\cdot\rho}\cdot\frac{\partial^2(\Delta\mathrm{T}+\mathrm{T}_0)}{\partial x^2} - u_y\frac{\partial(\Delta\mathrm{T}+\mathrm{T}_0)}{\partial y} = 0 \tag{3-77}$$

Notice that the reference temperature T_0 will always be a constant value in the same problem, so the differential form of T_0 will always a zero value:

$$\mathrm{T}_0 = \text{constant}\,, \qquad \rightarrow \qquad \frac{\partial^2\mathrm{T}_0}{\partial x^2} = 0\,, \qquad \frac{\partial\mathrm{T}_0}{\partial y} = 0$$

Now the solution can be rewritten as:

$$\mu\frac{\partial^2 u_y}{\partial x^2} + \rho g\beta\cdot\Delta\mathrm{T} = 0 \quad , \qquad \frac{\lambda}{C_p\cdot\rho}\cdot\frac{\partial^2\Delta\mathrm{T}}{\partial x^2} - u_y\frac{\partial\Delta\mathrm{T}}{\partial y} = 0 \tag{3-78}$$

And for convenient if the reference temperature assumed to be zero:

$$\mathrm{T}_0 = 0\,, \qquad \Delta\mathrm{T} = \mathrm{T}-\mathrm{T}_0 = \mathrm{T}, \tag{3-79}$$

The expression can be written as the general form of the solution:

$$\mu\frac{\partial^2 u_y}{\partial x^2} + \rho g\beta\cdot\mathrm{T} = 0 \quad , \qquad \frac{\lambda}{C_p\cdot\rho}\cdot\frac{\partial^2\mathrm{T}}{\partial x^2} - u_y\frac{\partial\mathrm{T}}{\partial y} = 0\,, \ \mathrm{T}_0 = 0 \tag{3-80}$$

This should be the simplest form of the solution, although it is still a 2 dimension problem, it could be consider as a single-dimension solution by assuming the temperature gradient $\partial T/\partial y$ as a constant in all X coordinate:

$$\frac{\partial T}{\partial y} = \text{constant}$$

This is the core assumption of this paragraph and the basic setup of the constant thermal gradient (CTG) model. Because by assuming the $\partial T/\partial y$ value is a constant will remove all unknown variables other than the variables (u_y velocity and T temperature) on the X axis, thus the Navier-Stokes equation and energy equation can have an analytical solution.

Rewritten all constant coefficients in the equations, where:

$$A = \frac{\rho g \beta}{\mu}, \qquad C = \frac{C_p \cdot \rho}{\lambda} \cdot \frac{\partial T}{\partial y} \tag{3-81}$$

Then the equation set could be rewritten into a very simplified manner:

$$\frac{\partial^2 u_y}{\partial x^2} - A \cdot \mathrm{T} = 0 \tag{3-82}$$

$$\frac{\partial^2 T}{\partial x^2} - \mathrm{C} \cdot u_y = 0 \tag{3-83}$$

It is possible to rewrite this equation into a 4th order differential equation, where:

$$\frac{\partial^4 u_y}{\partial x^4} - A \cdot \frac{\partial^2 T}{\partial x^2} = 0 \quad \rightarrow \quad \frac{d^4 u_y}{dx^4} - A \cdot \mathrm{C} \cdot u_y = 0 \tag{3-84}$$

Notice that this will be a typical differential system with a parameter A×C become the damping factor. And in the special solution, if the temperature gradient $\partial T/\partial y$ is a zero value, it results the whole damping factor become zero value: A×C=0. This indicates that the value of A×C actually defines the pattern of solution in the system.

Now it has 2 variables left in 2 equations despite the $\partial T/\partial y$ value, which the solution should be closed. In the other hands, the $\partial T/\partial y$ is assumed to be a constant that does not change by x and y value. Yet $\partial T/\partial y$ is not a given value in the initial boundary condition, it should be considered as an unknown constant C_T in the equations.

$$C_T = \frac{\partial T}{\partial y}$$

Giving the boundary condition:

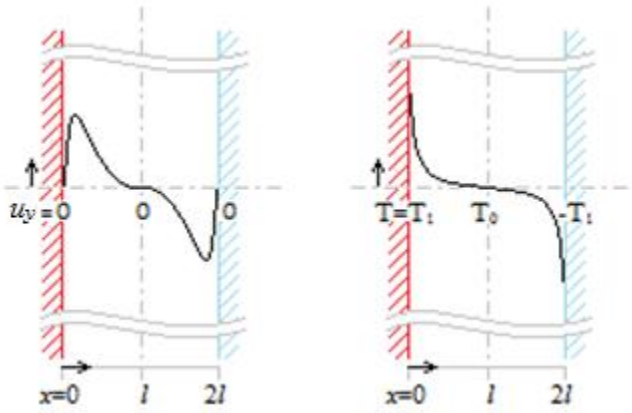

Figure 3-11 Typical velocity and temperature profile of density driven natural convection flow

$$\begin{cases} x_0 = 0, \ u_y = 0 \\ x_1 = l, \ u_y = 0 \\ x_0 = 0, \ \mathrm{T} = \mathrm{T}_1 \\ x_1 = l, \ \mathrm{T} = 0 \end{cases}$$

Equation 3-82 and **equation 3-83** can be solved as:

$$u_y(x) = \frac{T_1 \sqrt[2]{-A \cdot C}}{2}\left[\frac{e^{(2l-x)\sqrt[4]{-A\cdot C}\cdot i} - e^{x\sqrt[4]{-A\cdot C}\cdot i}}{1 - e^{2l\sqrt[4]{-A\cdot C}\cdot i}} + \frac{e^{(2l-x)\sqrt[4]{-A\cdot C}} - e^{x\sqrt[4]{-A\cdot C}}}{e^{2l\sqrt[4]{A\cdot C}} - 1}\right] \qquad 3\text{-}85$$

$$T(x) = \frac{T_1}{A \cdot C}\left[\frac{e^{(2l-x)\sqrt[4]{-A\cdot C}\cdot i} - e^{x\sqrt[4]{-A\cdot C}\cdot i}}{1 - e^{2l\sqrt[4]{-A\cdot C}\cdot i}} - \frac{e^{(2l-x)\sqrt[4]{-A\cdot C}} + e^{x\sqrt[4]{-A\cdot C}}}{e^{2l\sqrt[4]{-A\cdot C}} - 1}\right] \qquad 3\text{-}86$$

Coupling the Navier-Stokes equations and energy equation together could give the relationship between velocity and temperature of the flow. Notice that this solution was obtain with the assisted of computer mathematical software (Mathworks MatLab). Such solution could be obtained by mathematical practise such like the standard method of solving high-order Partial differential equation as well, the result should be identical and the solution method is not included in this thesis.

To understand the energy transportation of the flow, the energy equation can be rewritten into other energy forms, for example, heat flux form Q* = $f(x)$. There will be some detailed explanation latter on.

Solution of the wall heat flux Q* (W)

Consider only the same level of fluid in the natural convection has been observed in this case, for a very small amount of fluid control volume ΔV*, where:

$$\Delta V^* = \Delta(x \cdot y \cdot z) = y \cdot z \cdot dx + x \cdot z \cdot dy + x \cdot y \cdot dz \qquad 3\text{-}87$$

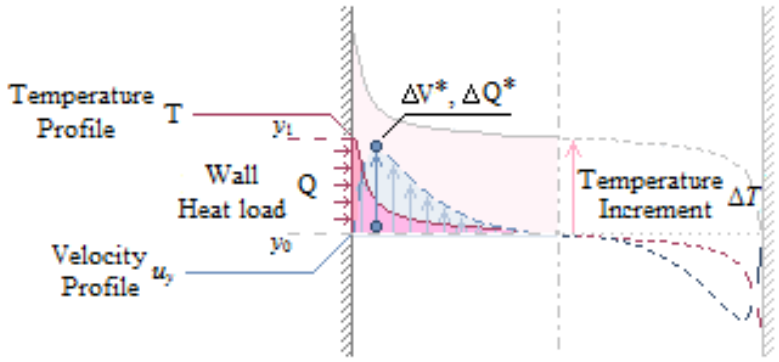

Figure 3-12 Relationship between wall heat flux (Q*), velocity profile, temperature and temperature gradient ∂T/∂y

Since the case is incompressible with Boussinesq approximation and the flow density does not vary, the control volume flow along y axis upon a distant Δy, the energy Q' (W) that such flow control volume has taken away would be:

$$\Delta Q' = \frac{\Delta V^* \cdot C_p \cdot \rho \cdot [T(x,y_1) - T(x,y_0)] \cdot u_y}{y_1 - y_0} \quad \text{3-88}$$

And

$$\Delta Q' = C_p \cdot \rho \cdot \Delta V^* \cdot \frac{[T(x,y_1) - T(x,y_0)] \cdot u_y}{y_1 - y_0} \quad \text{3-89}$$

Where:

$$y_1 - y_0 = \Delta y\,, \qquad T(x,y_1) - T(x,y_0) = \Delta T_y$$

Rewrite **equation 3-89** into a differential equation, which:

$$\frac{\Delta Q'}{\Delta V^*} = \frac{C_p \cdot \rho \cdot \Delta T \cdot u_y}{\Delta y} \;\rightarrow\; \Delta Q' = C_p \cdot \rho \cdot u_y \cdot \frac{\Delta T}{\Delta y}(yz \cdot dx + xz \cdot dy + xy \cdot dz) \quad \text{3-90}$$

Since it is a 1-dimensional fully developed flow case anti-symmetry on y axis and plane symmetry on xy plane, x and z axis heat load should be consisted in **equation 3-90**, where:

$$\frac{dQ'}{dy} = 0\,, \qquad \frac{dQ'}{dz} = 0 \qquad \rightarrow \qquad \Delta Q' = C_p \cdot \rho \cdot u_y \cdot \frac{\Delta T}{\Delta y}(y \cdot z \cdot dx + 0 + 0) \quad \text{3-91}$$

Rewrite **equation 3-91** into a partial differential form:

$$\frac{\partial \frac{Q'}{y \cdot z}}{\partial x} = C_p \cdot \rho \cdot u_y \cdot \frac{\partial T}{\partial y} \quad \text{3-92}$$

Integral the **equation 3-92** and it becomes:

$$\frac{Q'}{y \cdot z} = \int \frac{\partial \frac{Q'}{y \cdot z}}{\partial x} \cdot dx = \int C_p \cdot \rho \cdot u_y \cdot \frac{\partial T}{\partial y} \cdot dx \qquad 3\text{-}93$$

Since specific heat capacity (C_p), density (ρ) and y direction temperature gradient ($\partial T/\partial y$) are given as constants here, the only integrable value is the y velocity u_y which varies on x axis. Thus the energy **equation 3-93** can be written as a wall heat flux expression from the velocity based solution:

$$\frac{Q'}{y \cdot z} = C_p \cdot \rho \cdot \frac{\partial T}{\partial y} \cdot \int u_y \cdot dx \qquad 3\text{-}94$$

Notice that the wall heat load should be universal in both Y and Z coordinates, so the term Q/*yz* can be written in to the heat flux Q′, which:

$$\frac{Q'}{y \cdot z} = Q^* = C_p \cdot \rho \cdot \frac{\partial T}{\partial y} \cdot \int u_y \cdot dx, \quad \text{or,} \quad Q^* = C_p \cdot \rho \cdot \frac{\partial T}{\partial y} \cdot \overline{u_y} \cdot l \qquad 3\text{-}95$$

The solution of **equation 3-95** can be obtained via:

$$\int u_y \cdot dx = \mathrm{C5} + \frac{1}{2} \cdot \frac{T_1 \cdot A}{(-AC)^{\frac{3}{4}}} \cdot \left[\frac{e^{2l \cdot \sqrt[4]{-AC} - x\sqrt[4]{-AC}} + e^{x\sqrt[4]{-AC}}}{\left(e^{2l \cdot \sqrt[4]{-AC}} - 1\right)} + \frac{e^{2l \cdot \sqrt[4]{-AC} \cdot i - x\sqrt[4]{-AC} \cdot i} \cdot i + e^{x\sqrt[4]{-AC} \cdot i} \cdot i}{\left(e^{2 \cdot l \cdot \sqrt[4]{-AC} \cdot i} - 1\right)} \right] \qquad 3\text{-}96$$

And remove the constant of integration:

$$\int_0^l u_y \cdot dx = \frac{A \cdot T_1}{2 \cdot (-AC)^{\frac{3}{4}}} \cdot \frac{\left[e^{2 \cdot l \cdot \sqrt[4]{-AC}} \cdot (1 - i) + e^{2 \cdot l \cdot \sqrt[4]{-AC} \cdot i} \cdot (i - 1)\right]}{\left(e^{2 \cdot l \cdot \sqrt[4]{-AC}} + 1\right) \cdot \left(e^{2 \cdot l \cdot \sqrt[4]{-AC} \cdot i} + 1\right)} \qquad 3\text{-}97$$

Now **equation 3-97** the complete expression of the energy equation of wall heat flux solution

Also the integral of temperature field on x axis would be:

$$\int_0^l T \cdot dx = \frac{T_1}{2 \cdot \sqrt[4]{-AC}} \cdot \frac{\left[e^{2 \cdot l \cdot \sqrt[4]{-AC}} \cdot (1 + i) + e^{2 \cdot l \cdot \sqrt[4]{AC} \cdot i} \cdot (-i - 1)\right]}{\left(e^{2 \cdot l \cdot \sqrt[4]{-AC}} + 1\right) \cdot \left(e^{2 \cdot l \cdot \sqrt[4]{AC} \cdot i} + 1\right)} \qquad 3\text{-}98$$

Consider the *x* integration starts from 0 to *l*, which:

$$\frac{Q'}{y \cdot z} = C_p \cdot \rho \cdot \frac{\partial T}{\partial y} \cdot \int_0^l u_y \cdot dx \qquad 3\text{-}99$$

$$\frac{Q'}{y\cdot z}=C_p\cdot\rho\cdot\frac{\partial T}{\partial y}\cdot T_1\cdot A\cdot\frac{1}{2\cdot(-AC)^{\frac{3}{4}}}\cdot\frac{\left[e^{2l\cdot\sqrt[4]{-AC}}\cdot(1-i)+e^{2l\cdot\sqrt[4]{-AC}\cdot i}\cdot(i-1)\right]}{\left(e^{2l\cdot\sqrt[4]{-AC}}+1\right)\cdot\left(e^{2l\cdot\sqrt[4]{-AC}\cdot i}+1\right)} \quad 3\text{-}100$$

It can be simplify as:

$$\frac{Q'}{y\cdot z}=\frac{\lambda}{2}\cdot T_1\cdot\sqrt[4]{-AC}\cdot\frac{\left[e^{2\cdot l\cdot\sqrt[4]{-AC}}\cdot(1-i)+e^{2\cdot l\cdot\sqrt[4]{-AC}\cdot i}\cdot(i-1)\right]}{\left(e^{2\cdot l\cdot\sqrt[4]{-AC}}+1\right)\cdot\left(e^{2\cdot l\cdot\sqrt[4]{-AC}\cdot i}+1\right)} \quad 3\text{-}101$$

Notice that the **equation 3-101** is the general solution of natural convection wall heat flux.

Although the derivation of wall thermal heat flux equation stands alone from the energy **equation (3-101)**, it has a close relation with the energy equation, or could be considered as a transformation of energy equation (Convection-diffusion equation) under particular condition. Write down the wall thermal load **equation 3-101**:

$$\frac{\partial\frac{Q'}{y\cdot z}}{\partial x}=C_p\cdot\rho\cdot u_y\cdot\frac{\partial T}{\partial y} \quad 3\text{-}102$$

And:

$$u_y\cdot\frac{\partial T}{\partial y}=\frac{\partial\frac{Q'}{y\cdot z}}{\partial x}\cdot\frac{1}{C_p\cdot\rho} \quad 3\text{-}103$$

Put this into the original energy **equation 3-86**, then:

$$\frac{\lambda}{C_p\cdot\rho}\cdot\frac{\partial^2 T}{\partial x^2}-\frac{\partial\frac{Q'}{y\cdot z}}{\partial x}\cdot\frac{1}{C_p\cdot\rho}=0\quad\rightarrow\quad\lambda\cdot\frac{\partial^2 T}{\partial x^2}=\frac{\partial\frac{Q'}{y\cdot z}}{\partial x} \quad 3\text{-}104$$

Also the energy equation now can be written in the temperature based solution:

$$\lambda\cdot\frac{\partial T}{\partial x}=\frac{Q'}{y\cdot z} \quad 3\text{-}105$$

In this case, with the temperature gradient $\partial T/\partial y$ and velocity v removed, the equation collapse into 2nd order system again. This might hint that the fully developed convection flow will eventually turn into conduction heat transfer at some point.

Solution of the thermal energy E (J)

Similar to the pervious section of carrying out the wall thermal load equation, the expression of total energy of the flow field can be obtained as well. A heat energy term E (J) will be used instead

of the heat load expression *Q'* (W), and the heat energy E over a time scale t will become the heat load dE/d*t* =*Q'* (J/s=W).

For a small volume ΔV:

$$\Delta \mathrm{V} = \Delta(x \cdot y \cdot z) = y \cdot z \cdot dx + x \cdot z \cdot dy + x \cdot y \cdot dz \qquad 3\text{-}106$$

For a small fraction on heat energy pre volume, where:

$$\Delta E = C_p \cdot \rho \cdot T \cdot \Delta V \ , \qquad \Delta V = \Delta(x \cdot y \cdot z) \qquad 3\text{-}107$$

Then:

$$\Delta E = C_p \cdot \rho \cdot T \cdot (y \cdot z \cdot dx + x \cdot z \cdot dy + x \cdot y \cdot dz) \qquad 3\text{-}108$$

Notice that the temperature *T* is the differentiable factor of **equation 3-108** on different direction, and this part of work does not contain any 3-dimensional terms, *∂E/∂z* should be zero value where:

$$\Delta E = C_p \cdot \rho \cdot T \cdot (yz \cdot dx + xz \cdot dy + 0) \ \rightarrow \ \frac{\Delta E}{z} = C_p \cdot \rho \cdot (T \cdot y\partial x + T \cdot x\partial y) \qquad 3\text{-}109$$

Let:

$$\frac{\partial T}{\partial y} = C_T$$

In the y direction, it becomes:

$$dT = C_T \cdot dy \ \rightarrow \ T = C_T \cdot \int dy \ \rightarrow \ T = C_T \cdot y + C5 \ \rightarrow \ T = \frac{\partial T}{\partial y} \cdot y + C5 \qquad 3\text{-}110$$

Then the energy **equation (3-101)** could become:

$$\frac{\Delta E}{z} = C_p \cdot \rho \cdot [(C_T \cdot y + C5) \cdot x \cdot dy + T \cdot y \cdot dx] \qquad 3\text{-}111$$

And:

$$\frac{\Delta E}{z} = C_p \cdot \rho \cdot \frac{\partial T}{\partial y} \cdot x \cdot y \cdot dy + C_p \cdot \rho \cdot y \cdot T \cdot dx + C6 \qquad 3\text{-}112$$

Here in **equation 3-112** only the temperature *T* is the differentiable factor to the *x* derivative, hence the total energy of the fluid E would become:

$$\frac{E}{z} = C_p \cdot \rho \cdot \frac{\partial T}{\partial y} \cdot x \cdot y \cdot \int \partial y + C_p \cdot \rho \cdot y \cdot \int T \, \partial x + C6 \qquad 3\text{-}113$$

And:

$$\frac{E}{z} = C_p \cdot \rho \cdot \frac{\partial T}{\partial y} \cdot x \cdot y \cdot y + C_p \cdot \rho \cdot y \cdot \int T\, \partial x + C6 + C7 \qquad 3\text{-}114$$

Here the C6 and C7 in **equation 3-114** are constants of integration that states the initial condition of *x* derivative and *y* derivative. Considered the initial value of the integral started from a 0 temperature and 0 heat energy point, both C6 and C7 could be zero, left the total heat energy as:

$$\frac{E}{y \cdot z} = C_p \cdot \rho \cdot \left(\frac{\partial T}{\partial y} \cdot x \cdot y + \int_0^l T\, \partial x \right) \quad or \quad E' = C_p \cdot \rho \cdot l \cdot \left(\frac{\partial T}{\partial y} \cdot h + \bar{T} \right) \qquad 3\text{-}115$$

Discussion of the natural convection mathematical solution based on constant thermal gradient (CTG) model

Based on the Boussinesq approximation and the assumption of constant thermal gradient value $\partial T/\partial y$, the numerical solution can be carried out symbolically (analytical solution). There are 2 base equations of the solution which is the velocity and temperature expression. The expression of energy here is a transform from the temperature expression, which should not be considered as a third equation in the solution. Despite the properties of the fluid, there are 3 inputs / boundary conditions required for the solution: Reference distant (l), wall temperature (T_0) and y direction temperature gradient $\partial T/\partial y$. The output of the solution can be either form such as velocity, temperature or wall heat load.

The only unsolved term in this expression is the y direction temperature gradient ($\partial T/\partial y$), which could not be calculated from the equations provided from the previous section (**Equation 3-81, Equation 3-82** and **Equation 3-83**).

$$\frac{\partial^2 u_y}{\partial x^2} - A \cdot \mathrm{T} = 0\,, \qquad \frac{\partial^2 T}{\partial x^2} - \mathrm{C} \cdot u_y = 0$$

Where:

$$A = \frac{\rho \cdot g \cdot \beta}{\mu}, \qquad C = \frac{C_p \cdot \rho}{\lambda} \cdot \frac{\partial T}{\partial y}$$

The core concept will be a constant thermal gradient value:

$$\frac{\partial T}{\partial y} = \text{constant}$$

Boundary condition will be:

$$x = 0, \qquad u_y = 0$$

$$x = l, \qquad u_y = 0$$

$$x = 0, \qquad \mathrm{T} = T_1$$

$$x = l, \qquad \mathrm{T} = 0$$

So there should be an approximation of the thermal gradient value of ∂T/∂y. Such approximation will be carried out from a matrix of CFD test and will be explained later on in this research.

Notice that this solution based on the assumption of heat load on one side of the wall. Such problem (boundary condition) can be rewritten into other form: For example, equivalent heat load on both sides of the wall as in Morton's case (Morton, 1960) with comparable appearance.

And the boundary condition will be:

$$x = 0, \qquad u_y = 0$$

$$x = 2l, \qquad u_y = 0$$

$$x = 0, \qquad \mathrm{T} = T_1$$

$$x = 2l, \qquad \mathrm{T} = T_1$$

The solution of such case is too sophisticated to simplify and too complex to written down here, but it can be obtained from Matlab.

The general solution of the 2D natural convection would be given via equations (**Equation 3-85, Equation3-86** and **Equation 3-101**):

$$u_y(x) = \frac{T_1 \sqrt[2]{-A \cdot C}}{2}\left[\frac{e^{(2l-x)\sqrt[4]{-A \cdot C} \cdot i} - e^{x\sqrt[4]{-A \cdot C} \cdot i}}{1 - e^{2l\sqrt[4]{-A \cdot C} \cdot i}} + \frac{e^{(2l-x)\sqrt[4]{-A \cdot C}} - e^{x\sqrt[4]{-A \cdot C}}}{e^{2l\sqrt[4]{A \cdot C}} - 1}\right]$$

$$T(x) = \frac{T_1}{A \cdot C}\left[\frac{e^{(2l-x)\sqrt[4]{-A \cdot C} \cdot i} - e^{x\sqrt[4]{-A \cdot C} \cdot i}}{1 - e^{2l\sqrt[4]{-A \cdot C} \cdot i}} - \frac{e^{(2l-x)\sqrt[4]{-A \cdot C}} + e^{x\sqrt[4]{-A \cdot C}}}{e^{2l\sqrt[4]{-A \cdot C}} - 1}\right]$$

$$\frac{Q'}{y \cdot z} = \frac{\lambda}{2} \cdot T_1 \cdot \sqrt[4]{-AC} \cdot \frac{\left[e^{2 \cdot l \cdot \sqrt[4]{-AC}} \cdot (1 - i) + e^{2 \cdot l \cdot \sqrt[4]{-AC} \cdot i} \cdot (i - 1)\right]}{\left(e^{2 \cdot l \cdot \sqrt[4]{-AC}} + 1\right) \cdot \left(e^{2 \cdot l \cdot \sqrt[4]{-AC} \cdot i} + 1\right)}$$

The manner of the all solutions can be treated as a scaler in the front and followed by an exponential part:

$$v = \underbrace{\frac{T_1 \sqrt[2]{-AC}}{2}}_{\text{Scaler part}} \underbrace{\left(\frac{e^{(2l-x)\sqrt[4]{-AC}\cdot i} - e^{x\sqrt[4]{-AC}i}}{1 - e^{2l\sqrt[4]{-AC}\cdot i}} + \frac{e^{(2l-x)\sqrt[4]{-AC}} - e^{x\sqrt[4]{-AC}}}{e^{2l\sqrt[4]{-AC}} - 1} \right)}_{\text{Exponential part}}$$

Carefully examining the equations, it shows all components in the exponential part of energy **Equation 3-101** are assembly from a base part $l \cdot \sqrt[4]{-AC}$ or $x \cdot \sqrt[4]{-AC}$; the scalar part of the solution somehow only included some basic parameter from the liquid and the wall temperature T_1.

Hence take base part alone, where:

$$l \cdot \sqrt[4]{-AC} = l \cdot \sqrt[4]{-\frac{g \cdot \beta \cdot C_p \cdot \rho^2}{\mu \cdot \lambda} \cdot \frac{\partial T}{\partial y}} = \sqrt[4]{-\frac{g \cdot \beta \cdot C_p \cdot \rho^2 \cdot l^4}{\mu \cdot \lambda} \cdot \frac{\partial T}{\partial y}} \qquad 3\text{-}116$$

Since the term $\sqrt[4]{-AC}$ will be a complex number, it can be rewritten as a complex component multiply by a scalar which:

$$\sqrt[4]{-AC} = \sqrt[4]{-1}\sqrt[4]{AC} = \frac{\sqrt{2}}{2}(1+i) \times \sqrt[4]{AC} \qquad 3\text{-}117$$

Notice that the complex number part of the term can be considered as a constant / scalar, which should not affect characteristic of the outcome; and in the other hand, the Rayleigh number could be:

$$\mathrm{Ra} = \frac{\rho \cdot g \cdot \beta \cdot \Delta \mathrm{T}_x \cdot l^3}{v \cdot a} \quad \rightarrow \quad \mathrm{Ra} = \frac{g \cdot \beta \cdot C_p \cdot \rho^2 \cdot l^3 \cdot \Delta \mathrm{T}_x}{\mu \cdot \lambda} \qquad 3\text{-}118$$

Both parts have a noticeable similarity to each other, if let $\partial \mathrm{T}/\partial \mathrm{y} \rightarrow \Delta \mathrm{T_y}^*/\mathrm{y} \rightarrow \Delta \mathrm{T_y}^*/h$, then it could be rewritten into:

$$l \cdot \sqrt[4]{AC} = \sqrt[4]{\frac{g \cdot \beta \cdot C_p \cdot \rho^2 \cdot l^4}{\mu \cdot \lambda} \cdot \frac{\Delta \mathrm{T}_y}{h}} = \sqrt[4]{\frac{g \cdot \beta \cdot C_p \cdot \rho^2 \cdot l^3 \cdot \Delta \mathrm{T}_y}{\mu \cdot \lambda} \cdot \frac{l}{h}} \qquad 3\text{-}119$$

Then for the Rayleigh number on the vertical direction (along the gravity direction / thermal length direction), it can be:

$$Ra_h{}^* = h \cdot \sqrt[4]{AC} \qquad 3\text{-}120$$

Or the Rayleigh number on the horizontal direction (across the gravity direction / thermal distant direction), it can be:

$$Ra_h{}^* = l \cdot \sqrt[4]{AC} \tag{3-121}$$

However, the Ra* value does not yet show a straight relationship with the dynamic similarity of the flow field and heat transfer directly. Having the same Ra* value does not necessarily result an identical flow profile. This also hints that the scaler part of the solution may have greater influence to the outcome over the exponential part.

The completed expression of natural convection solution is given in this part of the research, yet there is one unsolved value in these equations, the value of thermal gradient: $\partial T/\partial y$. It was treated as a constant in the equation, but it is not be a fixed value and it should have some relationship with the condition of natural convection flow.

Also, carefully examine the energy **equation (3-101)**, it can be notice that the value of its exponential part of the **equation (3-101)** has a constant value output with a wide range of *l* value is given, where:

$$\frac{\left[e^{2\cdot l\cdot\sqrt[4]{-AC}}\cdot(1-i)+e^{2\cdot l\cdot\sqrt[4]{-AC}\cdot i}\cdot(i-1)\right]}{\left(e^{2\cdot l\cdot\sqrt[4]{-AC}}+1\right)\cdot\left(e^{2\cdot l\cdot\sqrt[4]{-AC}\cdot i}+1\right)}\approx 1-i \tag{3-122}$$

The term $\sqrt[4]{-AC}$ in **equation 3-122** can be rewritten as:

$$\sqrt[4]{-AC}=\sqrt[4]{-1}\sqrt[4]{AC}=\frac{\sqrt{2}}{2}(1+i)\times\sqrt[4]{AC} \tag{3-123}$$

Combined this with exponential part, the energy equation can be rewritten into:

$$Q^*=\frac{\lambda}{2}\cdot T_1\cdot\sqrt[4]{-AC}\frac{\left[e^{2\cdot l\cdot\sqrt[4]{-AC}}(1-i)+e^{2\cdot l\cdot\sqrt[4]{-AC}\cdot i}(i-1)\right]}{\left(e^{2\cdot l\cdot\sqrt[4]{-AC}}+1\right)\cdot\left(e^{2\cdot l\cdot\sqrt[4]{-AC}\cdot i}+1\right)}\approx\frac{\lambda}{2}\cdot T_1\cdot\frac{\sqrt{2}}{2}(1+i)(1-1i)\sqrt[4]{AC}$$

And finally the exponential part of the wall heat flux solution can be reduce to:

$$Q^*\approx\lambda\cdot T_1\cdot\frac{\sqrt{2}}{2}\cdot\sqrt[4]{AC} \tag{3-124}$$

And the complete form of the wall heat flux solution is:

$$Q^*\approx\lambda\cdot T_1\cdot\frac{\sqrt{2}}{2}\cdot\sqrt[4]{\frac{g\cdot\beta\cdot C_p\cdot\rho^2}{\mu\cdot\lambda}\cdot\frac{\partial T}{\partial y}} \tag{3-125}$$

So the energy **equation (3-101)** has been simplify into such form that can be calculated directly. Despite the fluid properties that required, the only 2 extra input parameters will be needed to define the heat flux is the heated wall to middle point temperature ΔT_x and the thermal gradient along the gravity direction $\partial T/\partial y$.

It can also be noticed that the simplified form of the energy equation has a very similar form with the heat flux over Nusselt number where:

$$Nu = \frac{HTC \cdot l}{\lambda} = \frac{Q^* \cdot l}{T \cdot \lambda} \quad \rightarrow \quad \mathrm{Q}^* = Nu \cdot \lambda \cdot T_1 \cdot \frac{1}{l} \tag{3-126}$$

Compare with the simplified energy **equation 3-124**, the term $\sqrt[4]{AC}$ can be expanded and it has a unit of (1/m)

$$\sqrt[4]{AC} = \sqrt[4]{\frac{g \cdot \beta \cdot C_p \cdot \rho^2}{\mu \cdot \lambda} \cdot \frac{\partial T}{\partial y}} \rightarrow \sqrt[4]{\left(\frac{\mathrm{m}}{\mathrm{s}^2} \cdot \frac{1}{\mathrm{K}} \cdot \frac{\mathrm{J}}{\mathrm{kg} \cdot \mathrm{K}} \cdot \frac{\mathrm{kg}^2}{\mathrm{m}^6} \cdot \frac{\mathrm{K}}{\mathrm{m}} \right)} = \sqrt[4]{\left(\frac{1}{\mathrm{m}^4} \right)} = \left(\frac{1}{\mathrm{m}} \right)$$

So the component $\sqrt[4]{AC}$ can be understood as a form of characteristic thermal distant scale, where:

$$\frac{1}{\sqrt[4]{AC}} = l^* \tag{3-127}$$

It is interesting to know that the factor A×C is also the damping factor in the original form of natural convection Navier-Stoke solution. So it is reasonable to use the A×C value as the characteristic factor (length scale) of the problem.

And:

$$Q^* \approx \lambda \cdot T_1 \cdot \frac{\sqrt{2}}{2} \cdot \sqrt[4]{AC} \quad \rightarrow \quad Q^* \approx \lambda \cdot T_1 \cdot \frac{\sqrt{2}}{2} \cdot \frac{1}{l^*} \tag{3-128}$$

If a specific Nusselt number is assumed to be the constant part in this **equation 3-128**, where:

$$Nu^* = \frac{\sqrt{2}}{2} \frac{Q^* \cdot l^*}{T_1 \cdot \lambda} \quad \rightarrow \quad Q^* \approx \lambda \cdot T_1 \cdot Nu^* \cdot \frac{1}{l^*} \tag{3-129}$$

A further assumption has made in this part of the work, as the *l** would be the specific length scale of the natural convection equation solution. Under this specific length scale the heat transfer (across the gravity direction) will be consistent since it has a constant Nusselt number value. By assuming the length scale *l** will be on the X axis (across the gravity direction), it may hint that most of the heat transfer take place within the $\sqrt{2} \cdot l^*$ regime / thickness due to the constant Nusselt number.

Also the Rayleigh number description from the previously can be rewritten in the characteristic thermal length scale form, where:

$$Ra_h{}^* = h^4 \cdot A \cdot C = \left(\frac{h}{l^*}\right)^4, \qquad \frac{l^*}{h} = \frac{1}{\sqrt[4]{Ra_h{}^*}} \tag{3-130}$$

And:

$$Ra_l{}^* = l^4 \cdot A \cdot C = \left(\frac{l}{l^*}\right)^4, \qquad \frac{l^*}{l} = \frac{1}{\sqrt[4]{Ra_h{}^*}} \tag{3-131}$$

The characteristic thermal length scale value *l** would become a very useful feature, in the following part of this work, it will look further into the heat transfer modelling base on the mathematical assumption / expression present in this section and compare with the CFD result.

3.4 Uniqueness and similarity compared with others work

Previous work has focused on a uniform wall temperature boundary, which seems to be the common method of analysing natural convection and how the original Rayleigh number was defined. Some other previous work started with uniform wall heat flux, and it requires a variation of original Rayleigh number converted into a heat flux form. A few works based on a Newtonian (variable) heating boundary, which almost equivalent to constant thermal / temperature gradient boundary. But Merkin's (1994) work was not focused on analytical solution; instead it was an asymptotic analysis.

The uniqueness of CTG (Constant Thermal Gradient) model in this thesis is that it based on an analytical solution of the Navier-Stokes equation and Convection-diffusion equation coupled together. The expression of such solution is a closed-form expression, by giving appropriate boundary condition it should be able to produce the exact value of velocity and temperature in the corresponding location. The absent of non-dimensionalization process and dimensionless factor of similarity such Ra and Gr make this work different from most other research for similar type of problem.

In terms of equation gathering, most pervious work kept the X direction u_x velocity component, and some work also kept the Y direction u_y velocity gradient. Keeping these terms help describing the developing of the convection flow, but also increase the complexity of the problem, thus some approximation method in solution method would be introduce hence there might not be a pure analytical solution with exact value result in any case. This is also true to the CTG model, through it would write down the closed-form expression of the analytical solution, it still has 3 unknowns towards 2 equations. That means an approximation still needs to be made for the last unknown value (usually is the thermal gradient value).

One of the earliest and most significant work was Sparrow and Gregg's work on laminar case (Sparrow and Gregg, 1956). They presented a Nusselt number correlation based on the exact similarity solution of the laminar boundary layer equation with Prandtl number from 0.1 to 100 (Aydin & Guessous, 2001).

$$\mathrm{Nu} = 0.616 \cdot \left(\frac{Pr^2}{0.8 + Pr}\right)^{\frac{1}{5}} \cdot {Gr^*}^{\frac{1}{5}} \tag{3-132}$$

Since Sparrow and Gregg's work, latter on researches carried on and expanded this correlation with wider range of fluid and more complex case condition, but the form of expression and correlation stay more or less the same. Here needs to mention some other important pieces of research works done by Fujii in 1975 (Fujii & Fujii, 1975), and Aydin & Guessous, 2001 (Aydin & Guessous, 2001). Which they concluded a series significant research works by the time of natural convection cases in different fluids. They also concluded the general Nusselt number correlation form would be:

$$\mathrm{Nu}_{local} = C^* \cdot (Gr^* \cdot Pr)^{\frac{1}{5}} \tag{3-133}$$

The coefficient C* will have various expression depends on different case condition and different fluid, and with experiment most of these correlations have good agreement within the range of condition they were suggested. Notice that the cases they compared seems to have more variety rather than unity, which put flat heat source and cylinder heat source together in same table.

2 more referenceable works from Goldstein & Eckert (Goldstein and Eckert, 1960) and Qureshi & Gebhart (Qureshi, Gebhart, 1964) gave the Nusselt correlation specific for water in laminar range, the correlation would be:

$$\mathrm{Nu} = 0.586 \cdot Gr^* \cdot {Pr^*}^{\frac{1}{5}}, \qquad 10^2 \le Gr^* \le 10^7 \tag{3-134}$$

(Goldstein and Eckert, 1960):

$$\mathrm{Nu} = 0.587 \cdot {Ra^*}^{\frac{1}{5}}, \qquad 1.2 \times 10^6 \le Ra^* \le 1.2 \times 10^{13} \tag{3-135}$$

Notice that most of these correlations are based on the 'open cavity' type of problem, which the coupling of cold-source is not considered.

Other than the referenceable work on Nusselt number correlation, one research work needs to be mention is Cai and Zhang's work (Cai & Zhang, 2002) on natural convection analytical solution.

This research work is somewhat similar to part of the solution that presented in this thesis: it has the same boundary condition, the setup of the boundary condition for the temperature field based on a Y-direction temperature gradient as the CTG model in this thesis.

Cai and Zhang also assumed an infinite long heated / cooled wall on Y-direction, this could be equivalent to the problem / solution in this thesis with zero-value Y-direction temperature gradient. Interestingly their result is almost same as that in this thesis, where the resulted velocity expression collapsed into a cubical polynomial equation manner. But their work did not expanded this into finite wall height and did not show more complex velocity curve that matches the natural.

Now the only remaining question of the mathematical solution is the dependence on the $\partial T/\partial y$ term, though it is assumed to be a constant, it is still an unknown value that could not be obtained from boundary or initial conditions, or from fluid properties. The next chapter will focus on how to obtain approximate thermal gradient constant ($\partial T/\partial y$) values.

3.5 Summary

The constant thermal gradient (CTG) model is an analytical solution of the Navier-Stokes equations and Convection-Diffusion equation with appropriate boundary conditions and assumptions and in this case is not based on the non-dimensionalisation versions of the equations. This means that the constant thermal gradient (CTG) model relies less on using Rayleigh and Prandtl numbers, which is different from most other natural convection studies and is also a different approach to understanding the natural convection heat transfer problem.

The non-dimensionalisation method gives a simplified expression (i.e. one based on Rayleigh number) to indicate the flow condition and dynamic similarity. But since the non-dimensionalisation method in-deed removes all the directional factors of the problem, which sometimes creates some confusion of choosing the reference point for the problem. On the other hands, algebraic solutions of the simplified Navier-Stokes equations and the Convection-Diffusion equation could give a similar but more complete description of the natural convection flow dynamic similarity in exchange of extra complexity.

Rayleigh number in general natural convection study:

$$\mathrm{Ra} = \frac{\rho^2 \cdot g \cdot \beta \cdot C_p \cdot \Delta T \cdot L^3}{\mu \cdot \lambda}$$

Notice that the length scale L here is the general characteristic length for Rayleigh number, in typical cavity problem it usually refers to the full distance between heated wall and cooled wall.

Thermal distant (*l*) or thermal length (*h*) over characteristic length scale (*l*/*l** or *h*/*l**) in CTG model:

$$\frac{l}{l^*} = \frac{\rho^2 \cdot g \cdot \beta \cdot C_p \cdot {T_y}^* \cdot l^4}{\mu \cdot \lambda \cdot h}, \qquad \frac{h}{l^*} = \frac{\rho^2 \cdot g \cdot \beta \cdot C_p \cdot {T_y}^* \cdot h^4}{\mu \cdot \lambda \cdot h}$$

Notice that the thermal distant (*l*) here is specified for CTG model in this thesis, it is the half distant between heated wall and cooled wall, which *l*=0.5L

Since now the description of in CTG model, especially Thermal distant (*l*) or thermal length (*h*) over a characteristic length scale *l*/*l** would need both vertical and horizontal length from the natural convection problem, it essentially matches 2 observations from Elder's work (Elder, 1965), namely one that different velocity profiles develop with different aspect ratios of the natural convection, and two that the middle line of the cavity has zero velocity but positive temperature gradient.

Also the concept of using a constant temperature gradient or thermal gradient is not a new idea in naturally convection flow research, it has commonly being used in geography research as the Lapse rate (Tritton, 1977). Interestingly the Lapse rate is a negative ratio that decreases with increasing height (attitude), while the constant thermal gradient (CTG) model in this research uses a positive ratio where temperature raises along with the height. But this difference could be explained by the fact that in geographical applications its scope is far greater than the general natural convection study, also in most cases heat dissipation in geographical applications would additionally be more complex.

4. Thermal gradient value ($\partial T/\partial y$) approximation

The Constant Thermal gradient (CTG) model presented in the previous chapter requires the thermal gradient ($\partial T/\partial y$) value to complete the Navier-Stokes equations and energy equation. In order to use the Constant Thermal gradient (CTG) model to numerically solve the natural convection problem, an approximation method is needed to gain the thermal gradient ($\partial T/\partial y$) value. In this part of the research, it will carry out the approximation of the thermal gradient constant C_{TG} based on CFD analysis of ideal natural convection problem (rectangular cavity case), it also compared with the Churchill and Chu's correlation of Nusselt number against the Rayleigh number to validate the model (Churchill and Chu', 1975).

To understand the scope of the problem, some pervious research has listed here as part of the reference cases. The closest research should be Elder's (Elder, 1965) work and Suslov & Paolucci's (Suslov & Paolucci, 1999) work, which all based on solutions with different aspect ratio (*h/l*). It also reference a recent benchmark work done by Dillon etc (Dillon, 2013,).

	Ra	Pr	Aspect ratio	material	
Current work	3×10^1 ~ 1×10^6	0.71, 7 and 24.6	1-32	Water, air Hydrofluoroether	CFD / Numerical
Elder's work	1×10^3 ~ 1×10^5	1000	1-60	Paraffin / silicon oil	Experiment
Suslov & Paolucci's work	6×10^3 ~ 1×10^4	0.71	1- ∞	Air/ Gas	Experiment

Table 4-1 Regime of the problem compare to some literature

The **Table 4-1** shows the scope of the research that will be carried out in this part of the work. Since the research in this section will be based on numerical and CFD solution, it can cover a wider range of the problem rather than experiments. The fluid properties continue from the previous section, which is the typical water under 20°C, the half-width of the problem case starts from l=0.00375m to 0.2288m (1:1 ~ 32:1 aspect ratio, *h/l*), this covers a wide range of Rayleigh number ($Ra \approx 3\times10^1 \sim 1\times10^6$).

It is also need to notice that, unlike general natural convection research based on Rayleigh number, the constant thermal gradient (CTG) model based on the analytical solution of the Navier-Stokes equation and Convection-Diffusion equation rather than dimentionaless method, so it is less relied on the usage or Rayleigh number and Prandtl number. Notice that this does not necessarily means the convection flow here is independent with Prandtl number, and one of the important task at the end of this chapter is the conversion of CTG model solution to an existed Nu=f(Ra) or Nu=f(Gr, Pr) correlation such as **equation 3-133** and **equation 3-134**.

4.1 Problem definition

In this section, a series of CFD analyses has been carried out based on 2 different type of basic layout: the open cavity natural convection problem and the close cavity natural convection problem. Though both these 2 cases have been popular in academic research, some even presented as a standard reference case for fluid dynamic simulation benchmarking, it is interested to see that open cavity natural convection usually has a length scale same as gravity direction, while close cavity natural convection usually use the length scale normal to the gravity direction. One of the purposes in this part of the study is to validate the constant thermal gradient (CTG) model from both open cavity and close cavity in parallel.

Open cavity case overview

The origin of open cavity problem is a vertical open channel with heated and cooled walls with flow pass through similar to a channel flow, it should have almost a fully developed vertical flow field. Since flow is anti-symmetric, only half of the domain needs to be considered. The simplified open cavity case can be setup as a vertical channel with only one side is heated wall and the other side is adiabatic wall: a half-section case with only heated section rather than full section with both heated and cooled sides. The boundary condition of the half-section open cavity case will be:

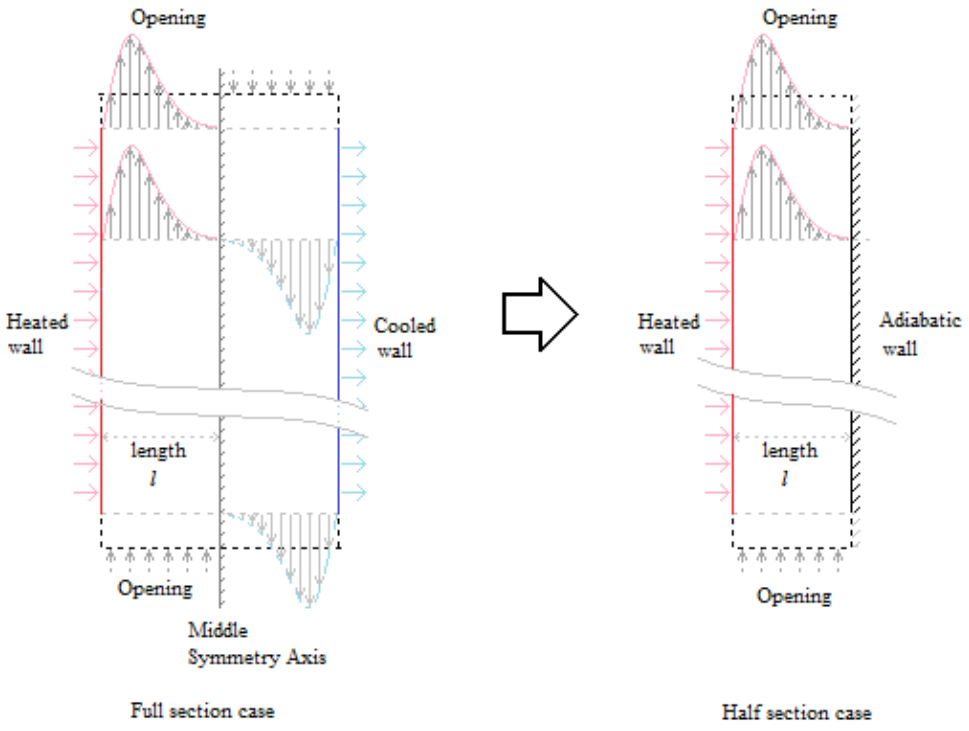

Figure 4-1 Simplification of a full open cavity natural convection case from heated-cooled wall to single heated wall model

Where in mathematical expression, the boundary condition expression is:

$$x = l \quad \rightarrow \quad u_x(l) = 0, \quad T(l) = 0$$

The problem that half-section open cavity case differ from full section case is the boundary condition of the middle line ($x=l$). In half section case the boundary that represent this line is a fixed adiabatic wall which restrict the temperature and flow velocity to zero value; for the full section (open cavity or close cavity) this there is no restriction on the middle line, the symmetry layout should naturally generate an inverse-mirror image of the other side of the flow. But in extreme condition such as turbulence / chaos flow would happen, t it may not be symmetric if it is turbulent But having a middle / adiabatic wall would be a desirable feature because of restricting the flow in one direction, but in exchange of slightly more unrealistic compare to other convection condition

As a result, the open cavity case should be very close to the ideal mathematical expression that given in the previous part of the research, and would be beneficial in modelling and approximation due to its simplicity. However the real limitation is the boundary condition on the inlet and outlet, which in these 2 section there is no heated wall. When the buoyancy force is no longer provided by the wall boundary condition, the convection flow tends to return back to typical Couette flow state as free stream channel flow. Therefore the open cavity cases suffers insufficient flow development, and the length of inlet / outlet section has an important influence to the velocity profile.

Closed cavity case overview

The other cavity problem setup in this part of flow research is the close cavity case, which can be simply understood as closed volume setup with vertical walls on the top and bottom. This results a recirculation flow within the volume despite the path and time scale of the flow, therefore should be fully developed all the time.

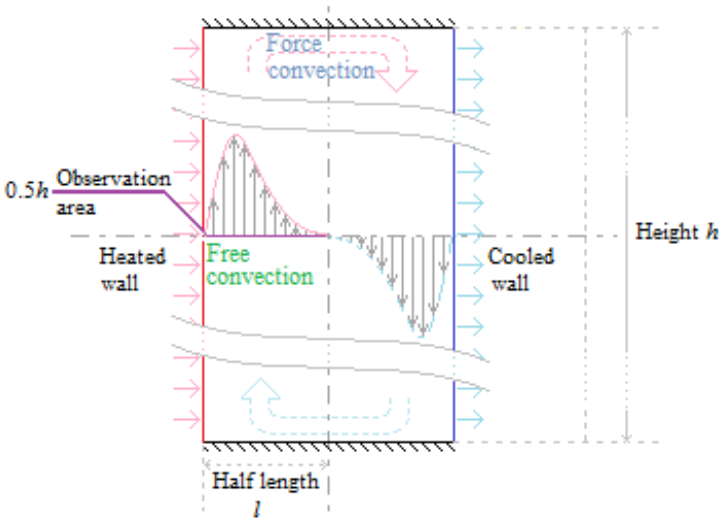

Figure 4-2 Schematic drawing of close cavity natural convection 2-D case

The problem of such setup is the changing direction in 4 corners in the cavity, which does not correspond to idealised CTG model conditions. In these corners the assumption of u_x=0 is invalid. Even more the top and bottom fluid flow horizontally without buoyance force applied on it buoyancy force assumed only appear in gravity direction), which basically turns into a force convection and become the 'short cut' of the heat transfer. Thus the close cavity case may be better suit the research of flow and heat transfer development, but also more complex and more difficult in modelling and approximation.

Basic setup parameter

A series of CFD solutions with different fluids and conditions will be carried out in the latter on section of this paragraph, so a properties table is given:

Boundary condition (inputs) for CFD / mathematics modelling								
Across the flow / gravity direction				Along the flow / Against the gravity direction				
Wall temperature		Thermal distance, half Distant heated-cooled wall		Thermal length Distant against gravity			Wall heat flux	
ΔT_x		l		H			Q*	
^oC		m		M			W/m^2	
Properties and Constants of the fluid for CFD / mathematics modelling								
Density	Kinematic Viscosity	Dynamic Viscosity	Thermal Conductivity	SHC	Thermal Expansion	Reference temperature	Gravity	Half length
ρ	v	μ	λ	C_p	β	T_0	g	d
kg/m^3	m^2/s	Pa.s	W/m.K	J/kg.K	1/K	^oC	m/s^2	m
Outcomes from CFD result								
Velocity (Y axis)		Temperature	Delta Temperature		Flux	Thermal gradient		
v		T	ΔT_x, ΔT_y		Q	dT/dy		
m/s		K or ^oC	K or ^oC		W/m^2	K/m		

Table 4-2 Input and output parameters for the problem for both CTG model and CFD analysis

Also the type of fluids and their properties is given as well in the following **Table 4-3**:

Properties and Constants (20^oC)								
	Density	Dynamic Viscosity	Thermal Conductivity	SHC	Thermal Expansion	Prandtl number	Reference temperature	Gravity
	ρ	μ	λ	C_p	B		T_0	g
	kg/m^3	Pa.s	W/m.K	J/kg.K	1/K		^oC	m/s^2
Water	997.05	8.874×10^{-4}	0.613	4181	2.07×10^{-4}	6~7	25	9.8
air	1.185	1.831×10^{-5}	0.0261	1000	3.36×10^{-3}	0.71		
HFE	1660	1.179×10^{-3}	0.069	1140	1.451×10^{-3}	19.47		

Table 4-3 Properties of fluids: general water, general air and HFE

And the CFD modelling and simulation method in this section will be:

Discretization methods	Solver model	Buoyance model	Turbulent model	Scheme	Energy model
Finite volume method	Laminar	Boussinesq approximation	N/a	Second order upwind	Thermal energy equation

Table 4-4 CFD analysis solver option

Also a mathematical solution will be calculated following CFD result, the expression of the mathematics solution would be **equation 3-85, equation 3-86** and **equation 3-101**:

$$u_y(x) = \frac{T_1 \sqrt[2]{-A \cdot C}}{2}\left[\frac{e^{(2l-x)\sqrt[4]{-A\cdot C}\cdot i} - e^{x\sqrt[4]{-A\cdot C}\cdot i}}{1 - e^{2l\sqrt[4]{-A\cdot C}\cdot i}} + \frac{e^{(2l-x)\sqrt[4]{-A\cdot C}} - e^{x\sqrt[4]{-A\cdot C}}}{e^{2l\sqrt[4]{A\cdot C}} - 1}\right]$$

$$T(x) = \frac{T_1}{A \cdot C}\left[\frac{e^{(2l-x)\sqrt[4]{-A\cdot C}\cdot i} - e^{x\sqrt[4]{-A\cdot C}\cdot i}}{1 - e^{2l\sqrt[4]{-A\cdot C}\cdot i}} - \frac{e^{(2l-x)\sqrt[4]{-A\cdot C}} + e^{x\sqrt[4]{-A\cdot C}}}{e^{2l\sqrt[4]{-A\cdot C}} - 1}\right]$$

$$\frac{Q'}{y \cdot z} = \frac{\lambda}{2} \cdot T_1 \cdot \sqrt[4]{-AC} \cdot \frac{\left[e^{2\cdot l\cdot \sqrt[4]{-AC}} \cdot (1-i) + e^{2\cdot l\cdot \sqrt[4]{-AC}\cdot i} \cdot (i-1)\right]}{\left(e^{2\cdot l\cdot \sqrt[4]{-AC}} + 1\right) \cdot \left(e^{2\cdot l\cdot \sqrt[4]{-AC}\cdot i} + 1\right)}$$

Where:

$$A = \frac{\rho \cdot g \cdot \beta}{\mu}, \qquad C = \frac{C_p \cdot \rho}{\lambda} \cdot \frac{\partial T}{\partial y}$$

Such mathematical solution can be carried out either by Matlab or Microsoft Excel (MS-Excel might suffer from difficulty in complex number solution). Notice that the thermal gradient ($\partial T/\partial y$) could not gained directly from the given condition, so at the moment this value can only come from the CFD solution.

Before entering detail simulation and analysis of the CFD modelling, the first thing to do is to determine the mesh / grid resolution as the initial of all solution. Since the length scale *l* is the only significant coordinate / displacement input in the solution expression, so it start from changing the mesh resolution related to the length scale *l* (on the X axis).

CFD verification: effect of mesh density

Unlike forced convection or other type of simple flow mechanism in similar physical regime (i.e. in similar Reynold number), natural convection usually requires finer mesh and tends to be sensitive to mesh quality. The Y+ (Y-Plus) value in turbulent flow can be useful to determine the mesh / grid close-wall resolution, but most of the cases in this research might be in laminar condition. Based on the mathematics description from previous chapter, it is possible to obtain the X direction length scale *l** (boundary layer thickness) by knowing the thermal gradient on the Y direction ($\partial T/\partial y$).

This gives the possibility to match the first layer mesh thickness with appropriate boundary layer thickness, which somehow similar to what Y+ value is taken to the turbulent flow.

Because closed cavity convection should have better flow development hence better accuracy for CFD mesh comparison. In this section, a close cavity CFD case study has been chosen and performed with various mesh setting, and here is the CFD case input parameter and boundary conditions:

	Boundary condition				Cases setup			Others	
Fluid	Flux	X axis dimension	Y axis dimension	Aspect ratio	Mid-point temperature	X Mesh count	Y Mesh count	Pr	Ra heat flux
Close cavity	Q*	$2 \times l$	h	h/l	T_0 ($x=l$)				$Ra_{(CWHF)}$
	W/m^2	m	m		°C				
water	**800**	**0.00715**	**0.0572**	**8**	0	8~256	256	6.13	1×10^5

Table 4-5 Close cavity natural convection case parameter for mesh validation

The Schematic drawing / layout of the close cavity case can be seen in **Figure 4-2**, and the result matrix with different mesh density is:

Boundary condition			Cases setup			Outcome				Others	
Heat flux	l	Aspect	X mesh count	Y mesh count	1st mesh Y*	T_1 (T_x-T_0)	$\partial T/\partial y$	T_y* (T_y^*-T_0^*)	l^*/l	Y*/l*	Error (1)
W/m^2	m	h/l			m	°C	°C/m	°C			%
800	7.15 $\times 10^{-3}$	8	8	256	1.79×10^{-3}	0.768	125.53	7.180	0.112	2.23	48.5
			16		8.94×10^{-4}	1.047	140.72	8.049	0.109	1.15	27.8
			32		4.47×10^{-4}	1.269	149.15	8.531	0.107	5.83×10^{-1}	11.2
			64		2.23×10^{-4}	1.375	151.53	8.667	0.107	2.93×10^{-1}	3.42
			128		1.12×10^{-4}	1.410	152.10	8.700	0.107	1.46×10^{-1}	0.885
			256		5.59×10^{-5}	1.420	152.23	8.708	0.107	7.32×10^{-2}	0.193
			256(2)		2.70×10^{-6}	1.417	154.09	8.814	0.107	3.55×10^{-3}	0.103

Table 4-6 Close cavity natural convection case input and outcome matrix

(1),Notice that error ratio will be: $\text{error} = 1 - \frac{Q^*_{CTG}}{Q^*_{CFD}}$. The wall heat flux Q^*_{CFD} is the input condition for the CFD simulation, and $Q^*_{CTG} = \frac{\lambda \cdot T_1}{\sqrt{2} \cdot l^*}$ is the wall heat load calculated from the constant thermal gradient (CTG) model from pervious chapter base on the characteristic length l^* obtain from the CFD simulation result. So the error ratio here basically indicate the different (in heat flux) between CFD result and constant thermal gradient (CTG) model.

The velocity and temperature profile from the observation line (Y=0.5h) will be shown in the following plot:

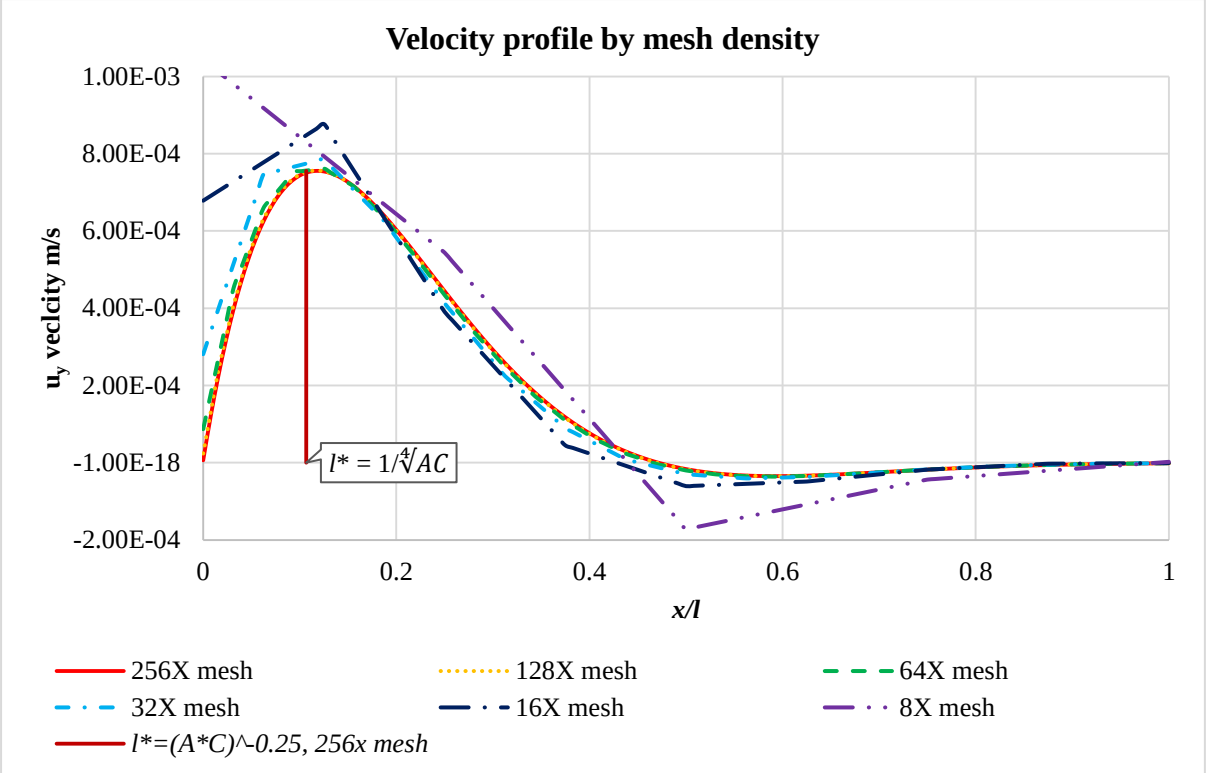

Figure 4-3 Velocity profile on the observation line (Y=0.5*h*)

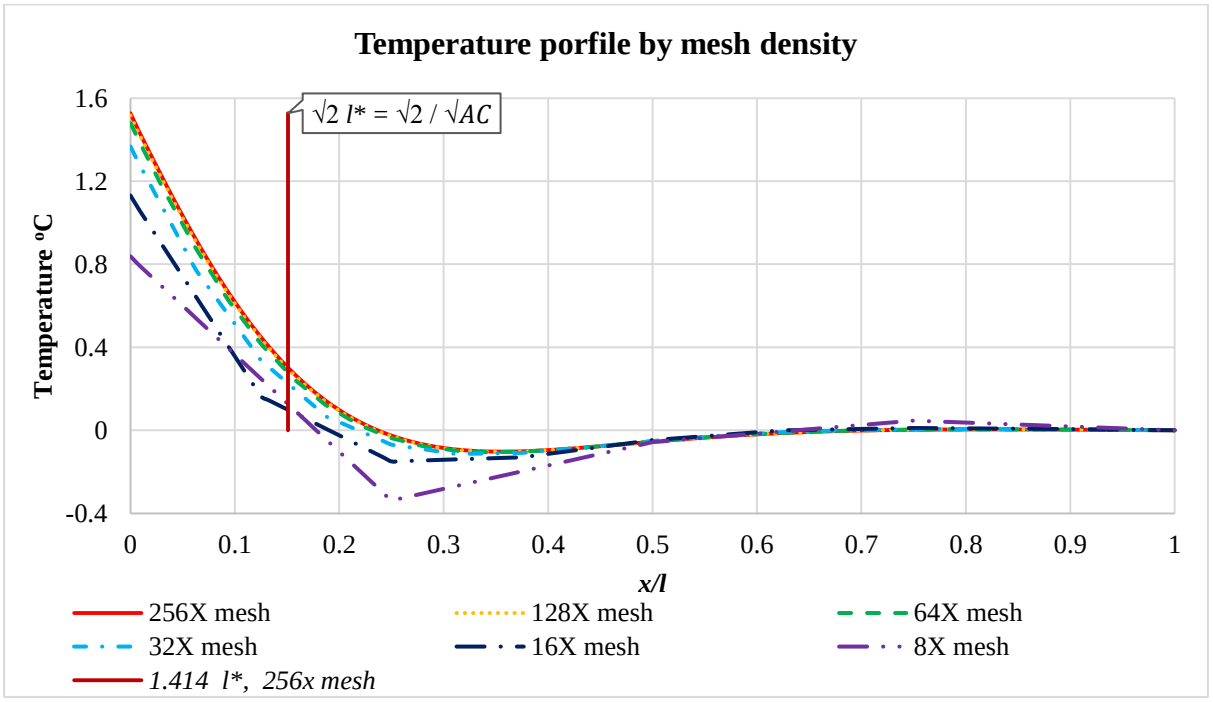

Figure 4-4 Temperature profile on the observation line (Y=0.5h)

In this case study **Figure 4-3** and **Figure 4-4** show how the mesh quality / density affect the solution, also the length scale $l^* = \sqrt[-4]{AC}$ has plotted alongside the CFD velocity solution. Recall the **equation 3-117** from the previous chapter, the length scale *l** can be rewritten as:

$$l^* = \sqrt[-4]{AC} \quad = \quad \frac{1}{\sqrt[4]{AC}} \quad = \quad \frac{1}{\sqrt[4]{\frac{\rho^2 \cdot g \cdot \beta \cdot C_p}{\mu \cdot \lambda} \frac{\partial T}{\partial y}}} \qquad 4\text{-}1$$

The length scale x=*l** happen to be (or closed to) the X direction distant when the flow has its maximum velocity (u_y) has occurred. Recall the **equation 3-84** from the previous chapter, the natural convection solution velocity expression can be written as a 4th order differential equation:

$$\frac{d^4 u_y}{dx^4} - A \cdot \mathrm{C} \cdot u_y = 0$$

Notice that the term AC is the only coefficient of the equation, which $\sqrt[-4]{-AC}$ should be one of the root of the solution. So it would be reasonable to assume that $l^* = \sqrt[-4]{AC}$ is able to represent the length scale of the problem; or more importantly, it indicates the boundary layer thickness. It is also possible to rewrite the energy equation with the length scale *l**:

$$Q^* = \frac{\lambda}{2} \cdot T_1 \cdot \sqrt[4]{-AC} \cdot \sqrt{2} \;\; \rightarrow \sqrt{2} \cdot l^* = \frac{T_1 \cdot \lambda}{Q^*} \qquad 4\text{-}2$$

It did seems like most of the heat transfer takes place within $x = (0, \sqrt{2} \cdot l^*)$ region In following section of this work will be based on this assumption. The benefit of having this $l^* = \sqrt[-4]{AC}$ as the thermal length scale is that it gives a physical definition along with simple mathematical relationship to natural convection flow solution.

Following such assumption, the first layer mesh thickness Y* should be smaller than the thermal length scale or boundary layer thickness l^* in order to represent the flow, where:

$$Y^* < l^*, \qquad \frac{Y^*}{l^*} < 1$$

Large Y*/*l** values (Y*/*l**> 1) result in a poor match result, while the smaller Y*/*l** value results in better match of input and output heat flux, and Y*/*l** < 0.1 will be desirable and it should have very small error (<0.2%) from CFD input heat flux to output heat flux; in other words it should have more than 10 mesh elements across character length scale *l** for a good CFD solution.

4.2T Observation point for thermal gradient ∂T/∂y in CFD solution

In this subsection mathematical and CFD solutions of the open and closed cavity problems will be compared for typical conditions. Since the mathematical model still cannot solve the natural convention problem alone, so the progress for the case studies in this section will be **Table 4-7**:

	CFD simulation		**CTG model calculation**
Boundary condition	Thermal distant of the problem on X axis: l (m) Aspect ratio of the problem: h/l (m)		
Input	Heat flux Q^*_{CFD} (W/m^2)		X Delta temperature T_1 (°C)
Outcome	X Delta temperature on observation point T_1 (°C) Velocity u_x (m/s) Temperature T (°C)	error cal compare	Heat flux Q^*_{CFD} (W/m^2) Velocity u_x (m/s) Temperature T (°C)

Table 4-7 Work progress of CFD and mathematical model case studies in this section

Open cavity case

The thermal gradient ($\partial T/\partial y$) in chapter 3 is assumed to be constant in the mathematic model. Yet in CFD solution, the thermal gradient ($\partial T/\partial y$) may not necessarily to be constant along Y direction (along the gravity direction). This is due to the fact that the shape of a CFD flow case (and also the real world condition) will be different from the ideal mathematic modelling.

To observe this, one typical close cavity case and one typical open cavity case has been analysed using the mathematical model and CFD. The object of this case study is to observe the thermal gradient ($\partial T/\partial y$) on the heated wall, middle line and cooled wall.

The open cavity case setup and boundary condition will be in **Table 4-8**:

	Boundary condition				Cases setup			Others	
Fluid	Flux	X axis dimension	Y axis dimension	Aspect ratio	Mid-point temperature	X Mesh count	Y Mesh count	Pr	Ra heat flux
Close cavity	Q*	$2 \times l$	h	h/l	T_0 ($x=l$)				$Ra_{(CWHF)}$
	W/m^2	m	m		°C				
water	**800**	**0.00715**	**0.0572**	**8**	0	256	256	6.13	1×10^5

Table 4-8 Open cavity natural convection case setup and boundary condition

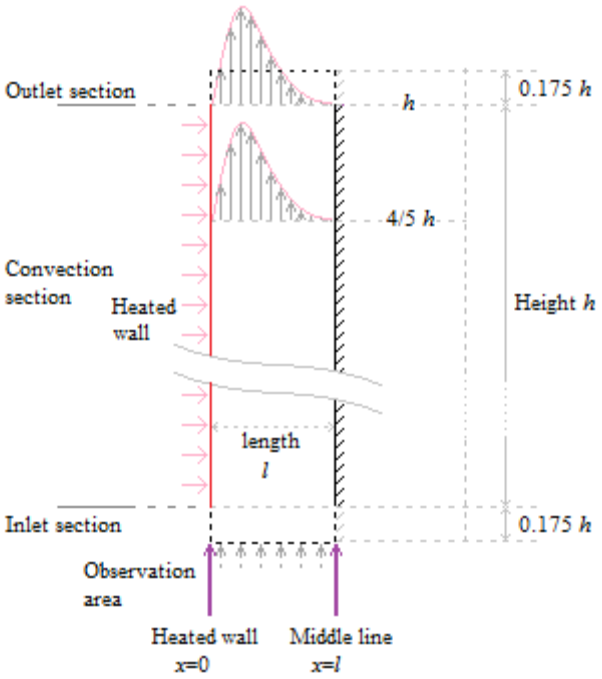

Figure 4-5 Schematic drawing of open cavity natural convection 2-D case

The temperature plot along the Y axis is shown in the following **Figure 4-6**:

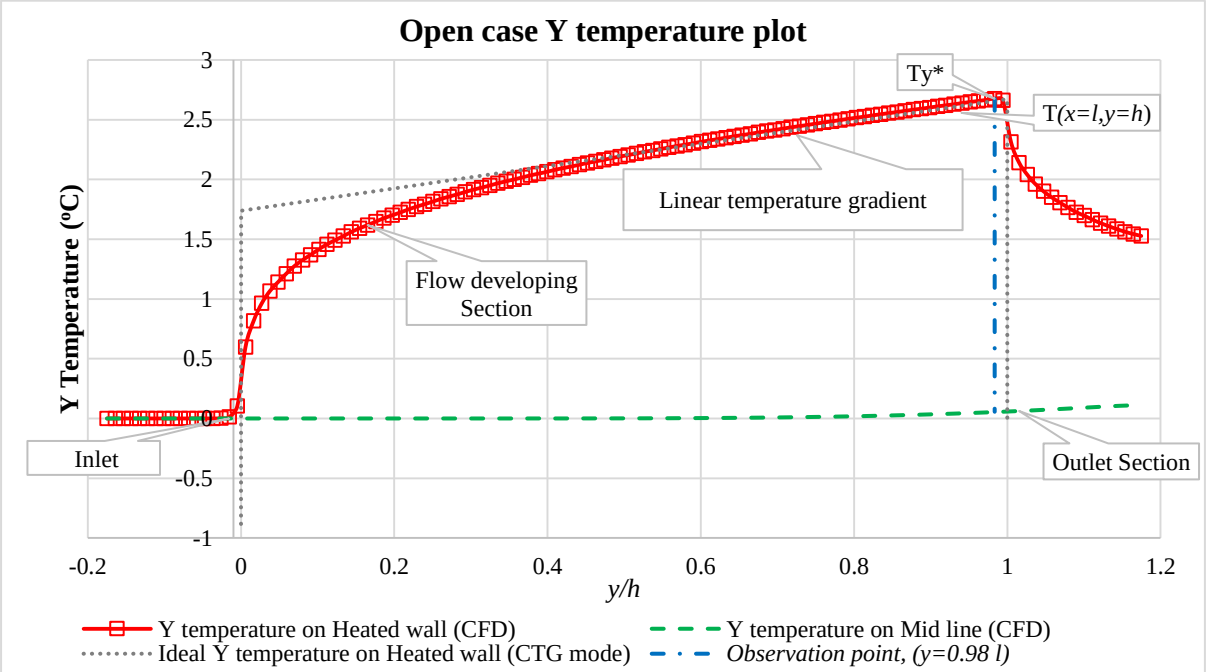

Figure 4-6 Temperature vs Y coordinate plot of the typical open cavity natural convection case.

From the temperature plot diagram in **Figure 4-6**, the dash line is the ideal temperature distribution on the heated wall (Y direction), based on the concept of constant thermal gradient (CTG) model. It can be seen in open cavity case CFD solution, the temperature gradient $\partial T/\partial y$ is not entirely constant and significantly influenced by the inlet and outlet section.

Because it still needs to obtain the temperature gradient $\partial T/\partial y$ value from the CFD result, the $\partial T/\partial y$ value from the CFD result is not entirely constant along the Y axis. It would be better to obtain the $\partial T/\partial y$ value from the point that the thermal gradient is almost linear. So the reference / observation point is chosen to be the highest point on the heated wall before entering the non-linear section (T_1 at x=0, y*→*h*). The exact location of this observation point would be various depends on the condition of the case, but in most cases it is around y=0.7*h*~0.99*h*.

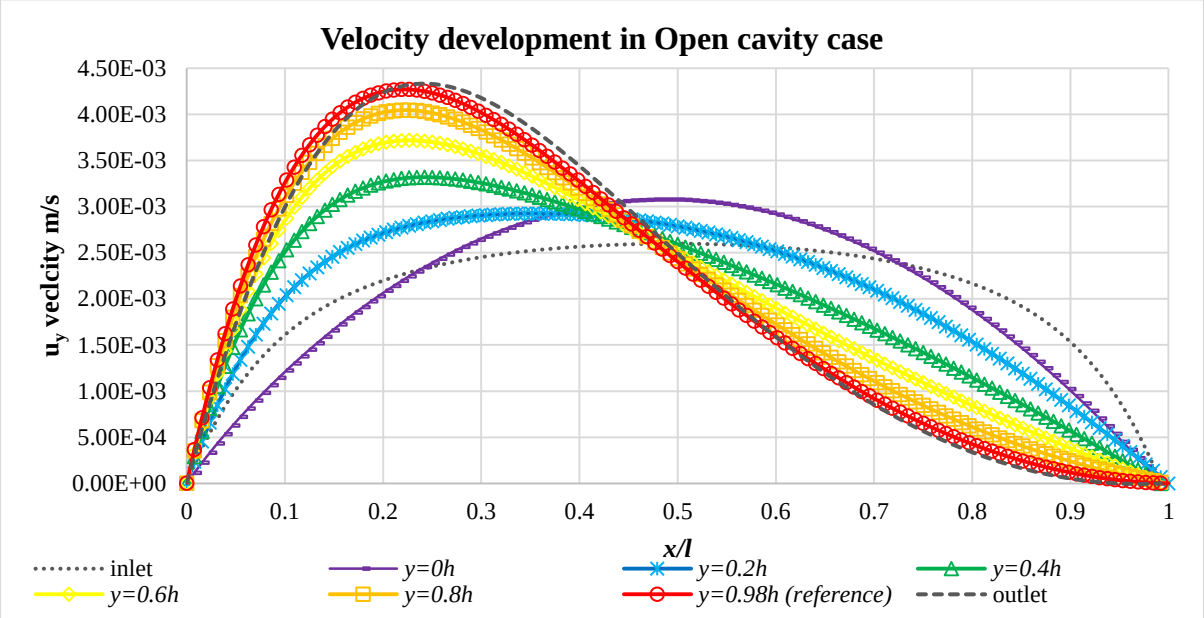

Figure 4-7 Velocity vs X coordinate plot of the typical open cavity natural convection case

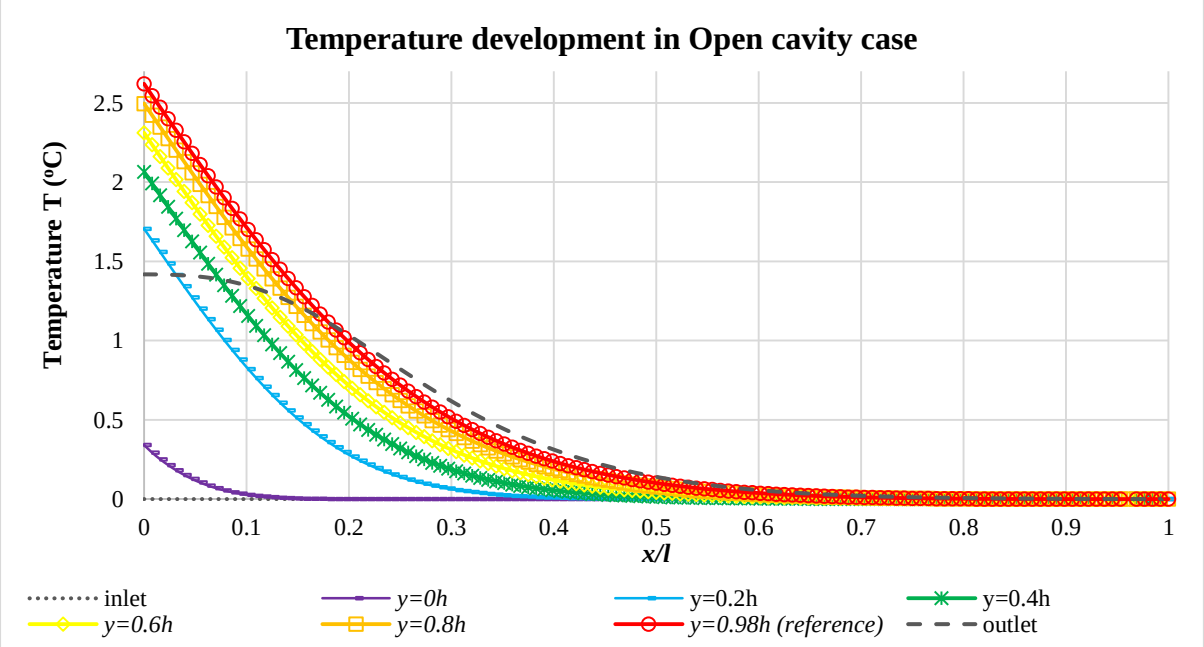

Figure 4-8 Temperature vs X coordinate plot of the typical open cavity natural convection case

From the velocity and temperature plot in **Figure 4-7** and **Figure 4-8**, it can see how the flow develops along the Y axis (along the gravity direction). In this particular open cavity case (h/l =8, l=0.0715, Q*=800W/m^2 with water), the observation point is chosen to be y=0.98h, this is the point has most developed flow before affected by the outlet condition. Obtain the delta temperature T_1= T(0, 0.98h) – T(l, 0.98h), and temperature gradient $\partial T/\partial y$ from the observation point (x=0, y=0.98h). With T_1 and $\partial T/\partial y$ value known, the velocity and temperature profile can be calculated from the **equation 3-85, equation 3-86** and **equation 3-101**:

Table 4-9 is the data matrix to setup the test; the boundary condition will be applied to both the CFD simulation and CTG model calculation:

Boundary condition			Cases setup	Outcome				Others	
Heat flux	l	Aspect	mesh count	$\Delta T_{0.98h}$ (T_{x1}-T_{x0})	$\partial T/\partial y$	T_y* (T_y^*-T_0^*)	l^*/l	Y*/l*	Error (1)
W/m^2	m	h/l		ºC	ºC/m	ºC			%
800	7.15×10^{-3}	8	256 ×256	2.62	15.425	0.8823	5.29	9.99 ×10^{-4}	3.92

Table 4-9 Open cavity case CFD simulation input and outcome matrix

The velocity and temperature plot from the observation point will be shown in the following diagram **Figure 4-9**:

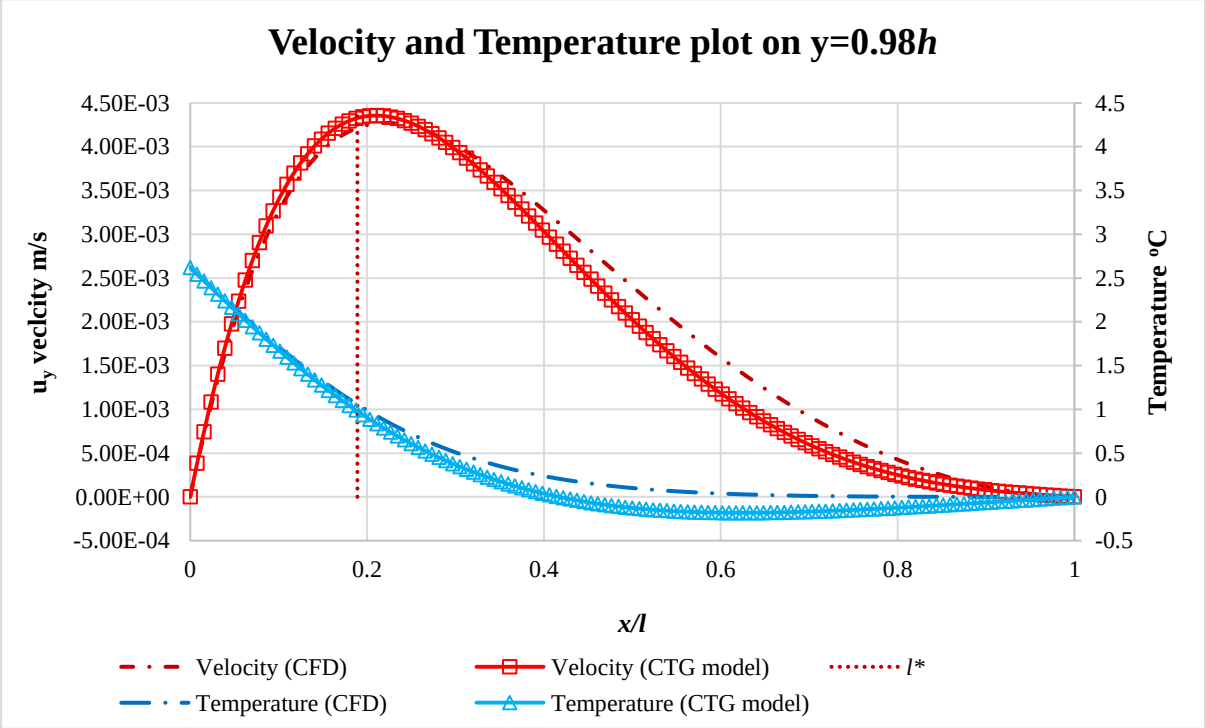

Figure 4-9 Open cavity natural convection case velocity and temperature plot in observation point (Typical case)

From **Figure 4-9** above, the velocity and temperature curve calculated by constant thermal gradient (CTG) model matches the CFD result in open cavity case quite well, through it still requires the $\partial T/\partial y$ value from the CFD model to carry out the calculation. Also the flow profile from the CTG model seems to have further flow development, which pushed the peak velocity point more towards the heated wall.

Closed cavity case

In closed cavity case, the problem setup and observation point is slightly different from the open cavity case such as **Figure 4-10**. The X axis length l is the half length of the (closed) cavity, the observation point for T_1 and temperature gradient $\partial T/\partial y$ is the middle axis across the Y axis ($y=0.5h$), and the observation line for Y temperature plot are heated wall ($x=0$), cooled wall ($x=2l$) and middle line ($x=l$).

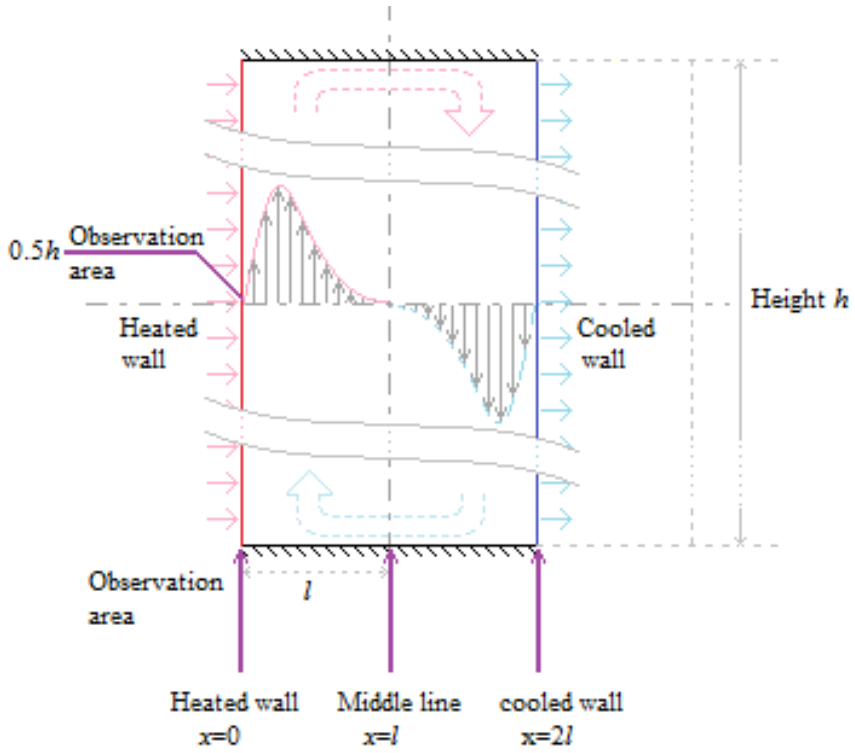

Figure 4-10 Schematic drawing of close cavity natural convection 2-D case

The temperature plot along the Y axis is shown in the following **Figure 4-11**:

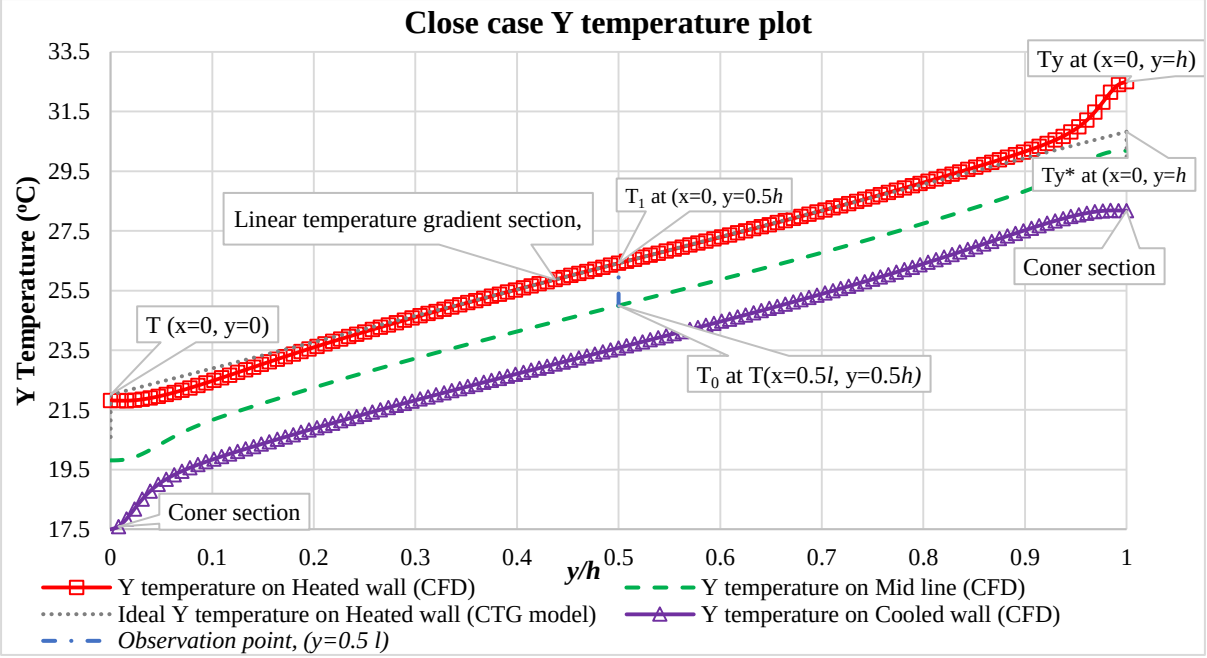

Figure 4-11 Temperature vs Y coordinate plot of the typical close cavity natural convection case

Form **Figure 4-11**, in closed cavity case, the 4 corners generate the non-linear effect to the temperature gradient, but in general the temperature gradient in the cavity case is effectively linear. The top and bottom wall do not have the buoyancy force generated for the convection flow, the flow in these places act as force convection which transfer the heat from the heated wall to the cooled wall, hence improves the heat transfer. General speaking the close cavity case seems closer to the ideal natural convection case of CTG model, especially the aspect ratio is large (h/l >>1). Part of the reason may be the flow has infinite long path to develop in a closed circle condition, so there is no obvious developing section. This can be seen from the velocity and temperature plot from different height of the CFD solution **Figure 4-12** and **Figure 4-13**:

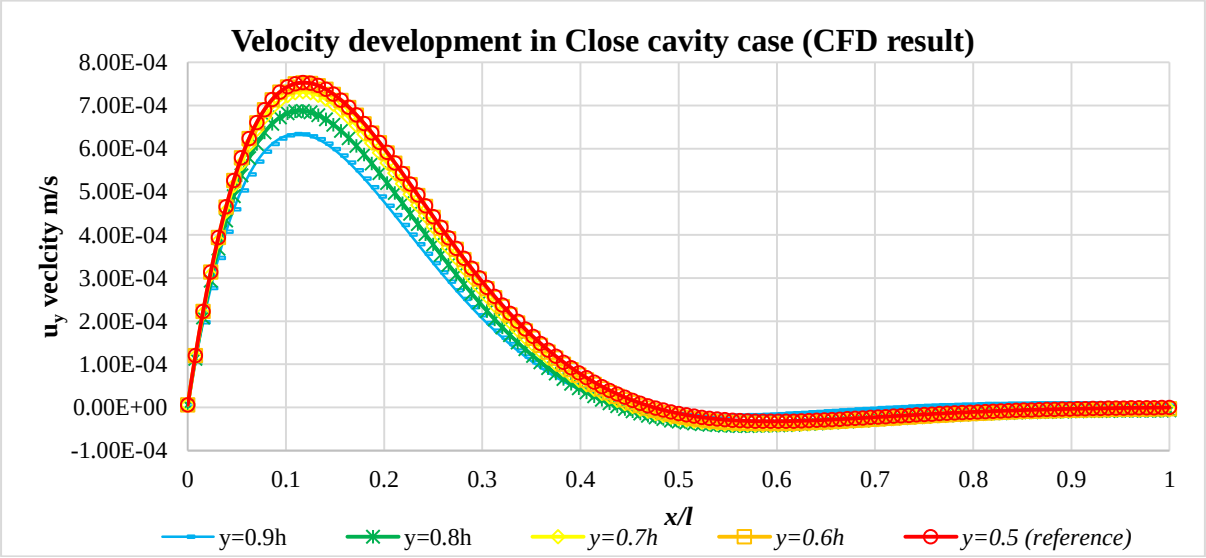

Figure 4-12 Velocity vs X coordinate plot of the typical close cavity natural convection case

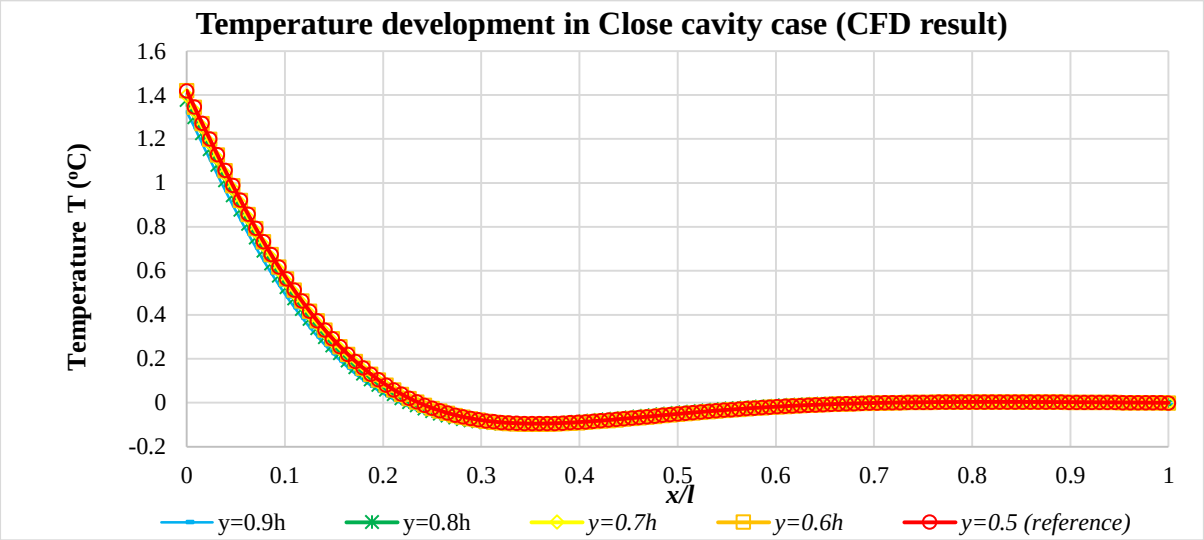

Figure 4-13 Temperature vs X coordinate plot of the typical close cavity natural convection case

Table 4-10 is the boundary conditions and outcome from the close cavity CFD simulation.

Boundary condition			Cases setup	Outcome				Others	
Heat flux	l	Aspect	mesh count	T_1	$\partial T/\partial y$	T_y^* (T_y^*-T_0^*)	l/l^*	Y^*/l^*	Error (1)
W/m^2	m	h/l		ºC	ºC/m	ºC			%
800	7.15×10^{-3}	8	256 ×256	1.417	154.09	8.814	9.35	3.55×10^{-3}	0.10

Table 4-10 Close cavity case CFD simulation input and outcome matrix

In the same way as open cavity cases, from **Figure 4-12** and **Figure 4-13** the Y velocity and temperature of the close cavity case on the reference line (y=0.5*h*) can be obtained with the wall temperature T_1 and temperature gradient $\partial T/\partial y$ value known.

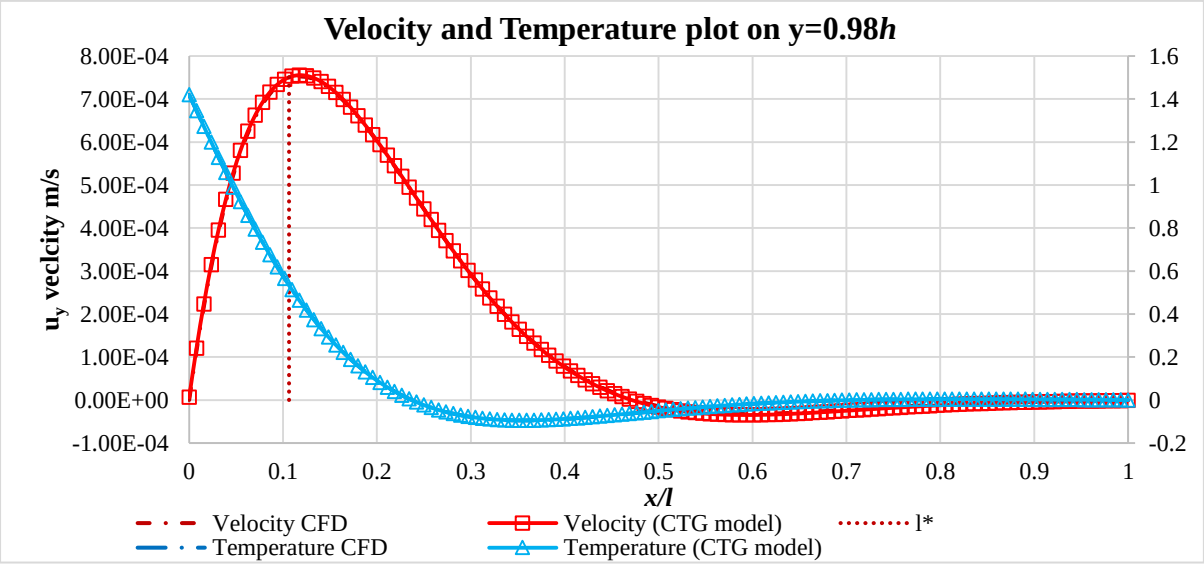

Figure 4-14 Close cavity natural convection case velocity and temperature plot in observation point (Typical case)

Figure 4-14 is the velocity and temperature plot from CFD result and CTG model calculation. In the close cavity case, the velocity and temperature result seems to have a good match between CFD and CTG mathematical modelling; this may due to the reason that a close cavity case has recirculation flow hence results better development of the flow.

Up to this point, it can be seen there is a very good match between the CFD result and the mathematics modelling on velocity and temperature calculation. This means it just need 3 parameters to match / justify the convection flow: the X-axis temperature delta from the wall to the middle-point (T_1), the Y-axis temperature gradient ($\partial T/\partial y$), and the distance between heated wall to middle line (l).

The influence of wall heat flux case study

In this section, two series of tests for open cavity and close cavity will be carried out. In this case study, all other input and boundary condition is fixed except the value of wall heat flux. Both open cavity and close cavity problem will have 5 iterations of test and compare the velocity and temperature plot from the observation point.

Also another task of this case study (and the following case as well) is to validate whether the characteristic length l^* universally matches all cases and conditions. Notice that in this part of case study only CFD result will be used and discussed.

First part is the open cavity case, same condition and dimension with various wall heat flux, here is the condition / result matrix **Table 4-11**:

Boundary condition			Outcome				Others	
Heat flux Q^*_{CFD}	l	Aspect	T_1	$\partial T/\partial y$	T_y^*	l/l^*	Error [1]	Case Setup:
W/m^2	m	h/l	°C	°C/m	°C		%	Water
50	2.86	2	0.328	0.7134	0.0977	11.24	4.13	Open Cavity
200	$\times 10^{-2}$		0.994	2.054	0.2811	14.64	5.13	$Y^*/l^* < 10^{-3}$
800			3.017	6.057	0.8122	19.2	5.51	Mesh count
3200			9.154	18.13	2.491	25.26	5.61	512×512
12800			27.72	54.57	7.508	33.33	5.82	$Y_{ref}=0.95h$

Table 4-11 Open cavity case CFD simulation input and outcome matrix for heat flux case study

[1] Error rate calculated as Error = 1- Q^*_{CTG} / Q^*_{CFD}

The velocity profile from the CFD at the observation point will be given in **Figure 4-15**

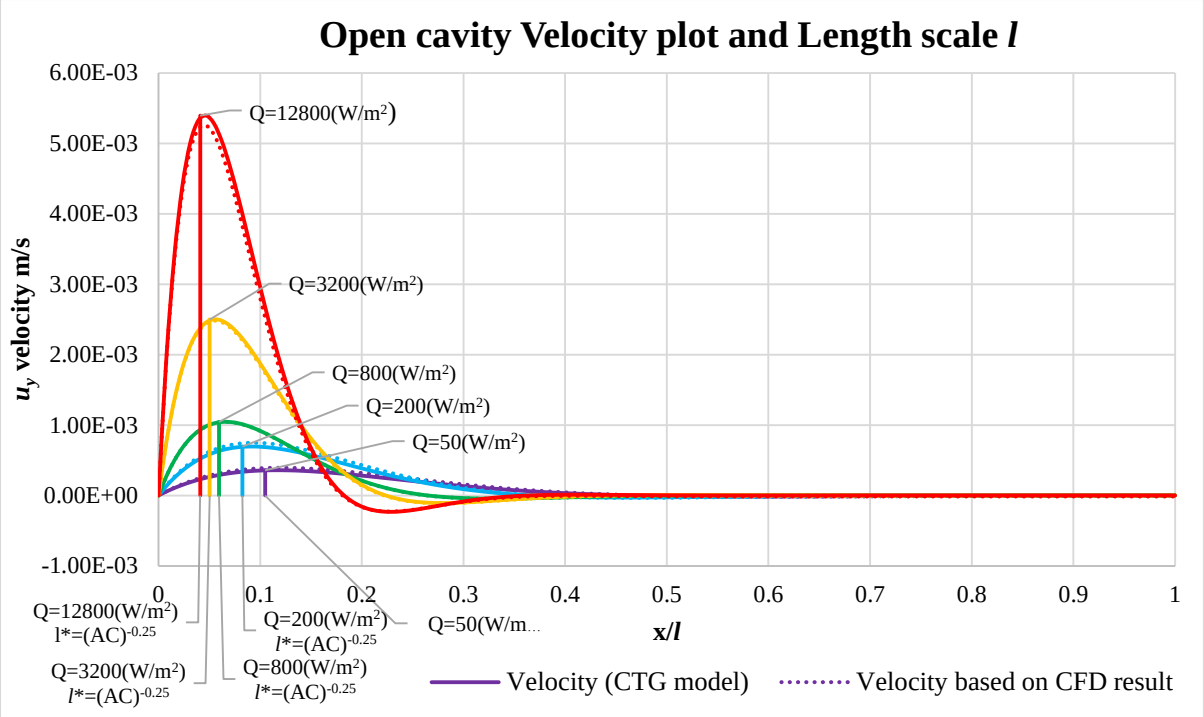

Figure 4-15 Open cavity case, heat flux case study, CFD result velocity plot on $Y_{ref}=0.95h$

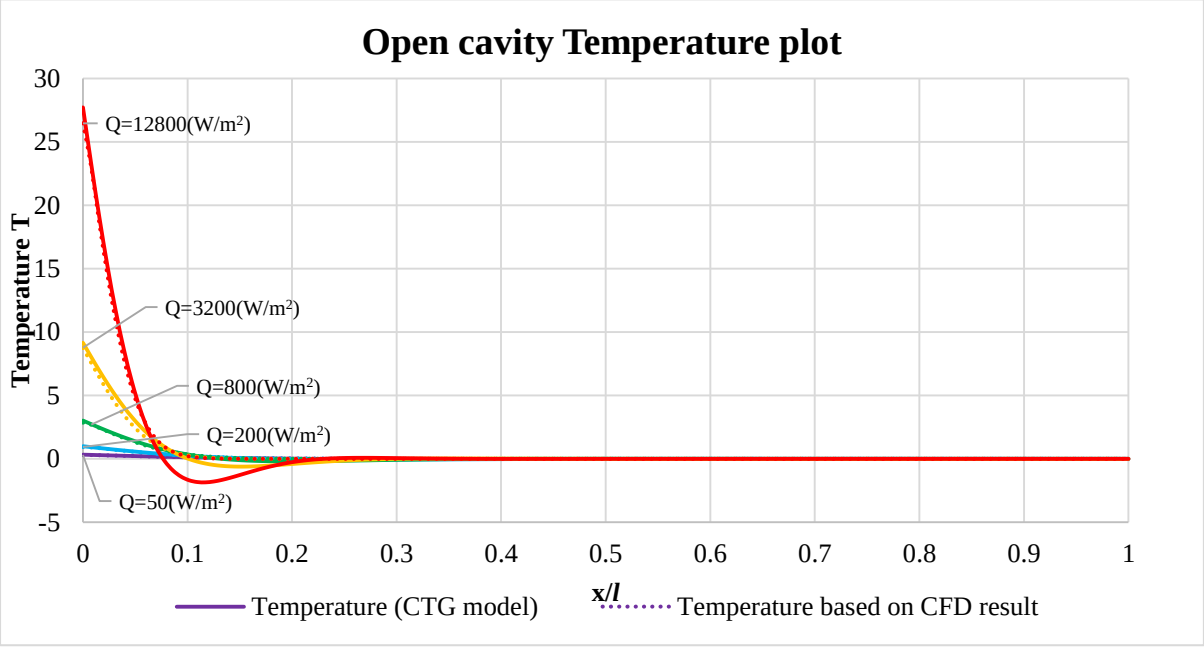

Figure 4-16 Open cavity case, heat flux case study, CFD result temperature plot on Yref=0.95h

From the velocity and temperature plot **Figure 4-16**, it can be seen the outcome of open cavity case velocity and temperature from both CFD simulation and CTG model loosely match each other.

Second part is the closed cavity case with various wall heat flux, here is the condition / result matrix **Table 4-12**:

Boundary condition			Outcome				Others	
Heat flux Q^*_{CFD}	l	Aspect	T_1	$\partial T/\partial y$	T_y^*	l/l^*	Error (1)	Case Setup:
W/m^2	m	h/l	°C	°C/m	°C		%	Water
50	1.43 $\times 10^{-2}$	2	0.1748	10.16	1.162	9.526	0.13	Close Cavity
200			0.5482	26.59	3.042	12.12	0.33	$Y^*/l^*<10^{-3}$
800			1.584	98.09	11.22	16.79	0.22	Mesh count
3200			5.317	193.0	22.08	19.89	0.83	512×512
12800			17.19	432.71	49.50	24.34	2.0	$Y_{ref}=0.5h$

Table 4-12 Close cavity case CFD simulation input and outcome matrix for heat flux case study

[1] Error rate calculated as Error = 1- Q^*_{CTG} / Q^*_{CFD}

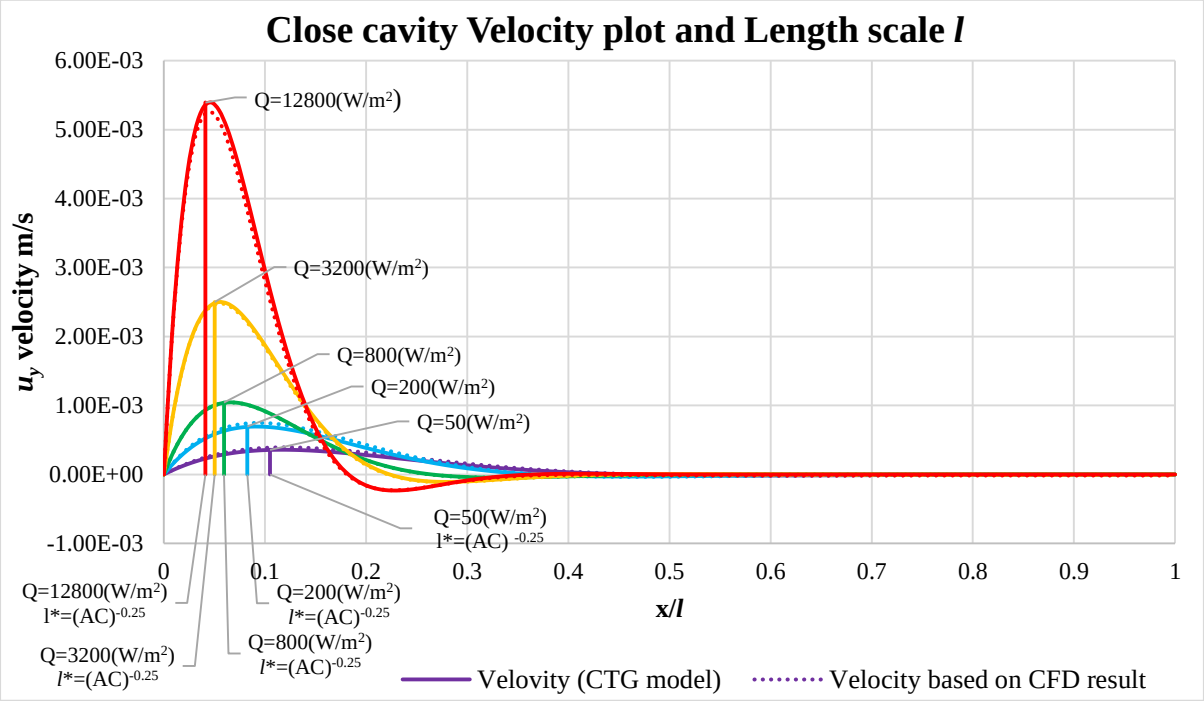

Figure 4-17 Close cavity case, heat flux case study, CFD result velocity plot on $Y_{ref}=0.5h$

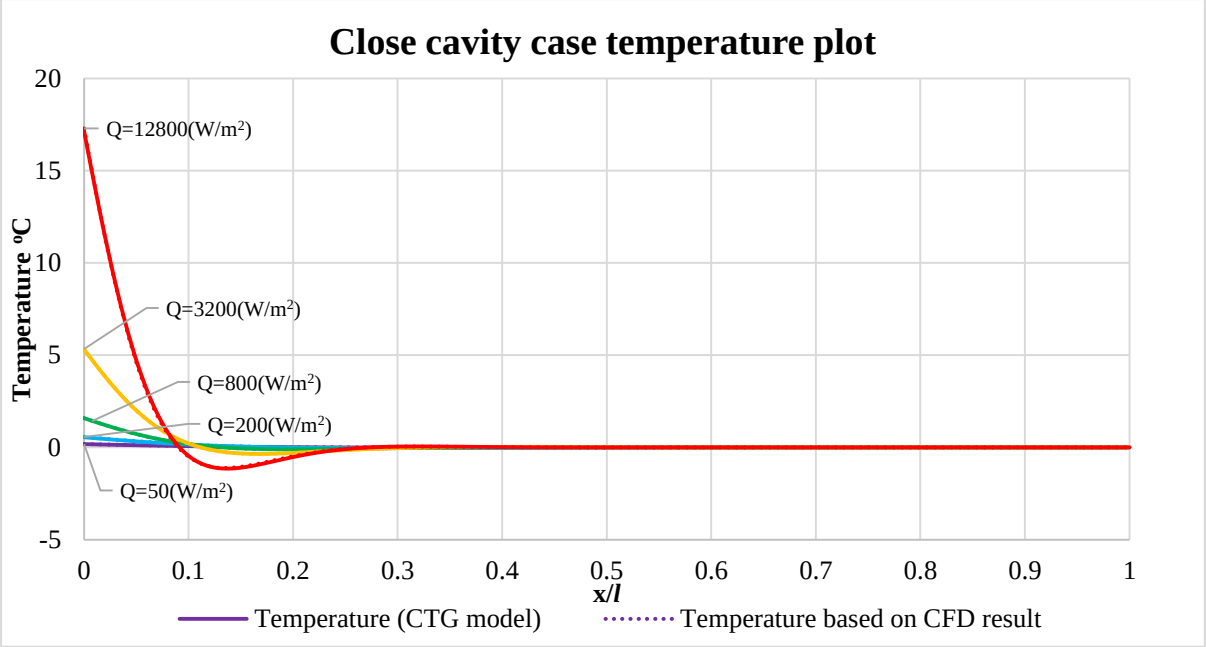

Figure 4-18 Close cavity case, heat flux case study, CFD result temperature plot on Y_{ref}=0.5h

Notice: the thermal distance *l* in the closed cavity case (heated-wall to middle line distant across the gravity) is different from that in the open cavity case.

From the velocity and temperature plot **Figure 4-17** and **Figure 4-18**, the outcome of closed cavity case has very good match between CFD simulation and CTG model. This again shows the close cavity case has better flow development.

For observation of characteristic length scale $(l^* = \sqrt[-4]{A \cdot C})$, in all cases the *l** distant has always match the distance to the maximum flow velocity (u_y = max).

It is also noticeable that there is a negative peak captured in the velocity plot profile, especially from the closed cavity cases. This will be more significant when the *l*/*l** scale (work as $\sqrt[4]{Ra^*}$) value is large. In the CTG model it was simplified to have only one dimension flow, and in the CFD simulation results so far they were set to avoid complex and unstable flow so it does not have a significant effect to the outcome of this research. But it would be possible in some other configurations such negative flow velocity could cause a local recirculation, or even chaotic flow.

If the simplification of Navier-Stokes equation is a 4 order system as the **equation 3-84**:

$$\frac{d^4 u_y}{dx^4} - A \cdot \mathrm{C} \cdot u_y = 0$$

If the coefficient A×C in this equation consider as the damping factor of the oscillatory system, it could be possible to obtain the overshoot scale and distant with analytical solution. But it will be very difficult to have the analytical solution of the overshoot value since it is a 4th order system.

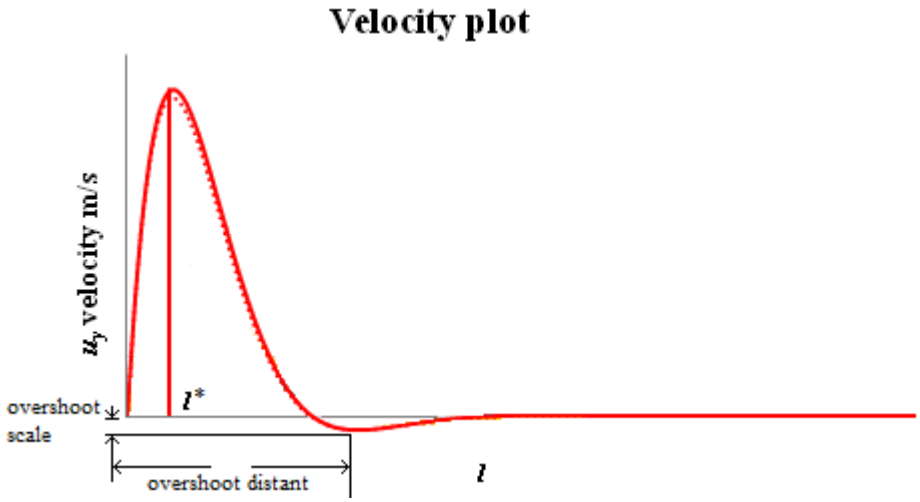

Figure 4-19 Overshoot of the velocity curve

The overshoot of the velocity and temperature curve may be related to the chaotic flow of natural convection, never the less the effect of this negative velocity is not a major concern here, in this thesis it is focus on the characteristic length scale l^*. It does not have a large l/l^* scale that goes in to the chaotic flow regime; and will not have further discussion on this topic.

4.3 $\partial T/\partial y$ approximation for Constant thermal gradient (CTG) model in open cavity case

In this part of case study, a matrix of CFD solution will be carried out with different parameter to show the relationship of temperature difference between X direction (across the gravity direction) and Y direction (along gravity direction). For the X direction temperature T_1, it is the delta temperature between the heated wall and the middle line in the same height (h) of the cavity. The reference line for the T_1 temperature in open cavity problem it is $y=0.8h \sim 0.98h$ (depends on flow development), and for the close cavity problem it is: $y=0.5h$.

For the Y direction temperature, it is slightly more complex. Ideally the delta temperature $\Delta T_y = T(0, h)-T(0, 0)$ should be taken from the top to bottom of the heated wall. However this temperature will be affected by the inlet / outlet section in the open cavity cases, or by the corner effect in the close cavity cases; instead it will use the temperature gradient $\partial T/\partial y$ read from the reference line and multiply by the height (h) of the cavity to have the linear delta temperature $\Delta T_y^*(x=0)$, where:

$$T_y{}^* = \frac{\partial T}{\partial y} \times h \qquad 4\text{-}3$$

Up to this point by using outcome (T_1, and $\partial T/\partial y$) from the CFD result as an input of the constant thermal gradient (CTG) model, the constant thermal gradient (CTG) model can closely match the CFD result. The key point now is the value of thermal gradient $\partial T/\partial y$, this is not the boundary condition of natural convection case. So finding the appropriate approximation of the thermal gradient $\partial T/\partial y$ is the key to complete the constant thermal gradient (CTG) model.

Since there are only 3 values needed for the constant thermal gradient (CTG) model, and the thermal gradient ($\partial T/\partial y$) value is one of these value that have been looking for, the relationship between these 3 factors will be the task in this part of the study.

In the following case study will be a number of CFD simulations in 2 types: First type of CFD simulation will have fixed thermal distance (l) with various heat flux (Q*) and aspect ratio (h/l), this results different wall delta temperature T_1 and different thermal gradient $\partial T/\partial y$ for study. The second type will be a fixed heat load (Q*), fixed thermal length (h) but various thermal distant (l), this again results different wall delta temperature T_1 and different thermal gradient $\partial T/\partial y$ for study. The thermal gradient $\partial T/\partial y$ can be converted to a Y axis temperature delta T_y* with the **equation 4-3**, and by studying the temperature plot map T_1 against T_y*, the relationship between thermal gradient $\partial T/\partial y$ and other factors should be reveal.

Open cavity CFD case study: fixed thermal distant (*l*) with variable heat flux (Q*) and variable aspect ratio (*h/l*)

In this section, a series of CFD simulations with fixed thermal distant (l), and various values of the heat flux (Q*) and aspect ratio (h/l) will be carried out, the outcome will be T_1 and T_y*.

Step 1, Open cavity natural convection case with water. The CFD simulation conditions and matrix of results of the open cavity natural convection case with water and fixed thermal distant (l) is given in the following **Table 4-13**:

Boundary condition			Outcome				Others	
Heat flux	l	Aspect	T_1	$\partial T/\partial y$	T_y*	l/l*	Error	Case setup:
W/m^2	m	h/l	^{o}C	^{o}C/m	^{o}C		%	
50	1.43×10^{-2}	1	**0.2459**	2.158	**0.0617**	12.93	0.13	Water
200			**0.7487**	6.331	**0.1811**	16.93	0.33	
800			**2.277**	18.72	**0.5353**	22.20	0.22	Open Cavity
3200			**6.917**	55.96	**1.600**	29.19	0.83	
12800			**20.98**	168.7	**4.825**	38.46	2.0	$Y^*/l^*<10^{-3}$
50		2	**0.2843**	1.229	**0.0703**	11.24	0.13	
200			**0.8638**	3.541	**0.2025**	14.64	0.33	Mesh count 512×512
800			**2.624**	10.48	**0.5993**	19.20	0.22	
3200			**7.964**	31.42	**1.797**	25.27	0.83	
12800			**24.13**	94.74	**5.419**	33.29	2.0	Ref. point Y=0.95h
50		4	**0.3280**	0.7134	**0.0816**	9.808	0.13	
200			**0.9940**	2.054	**0.2350**	12.78	0.33	
800			**3.017**	6.057	**0.6930**	16.74	0.22	
3200			**9.154**	18.13	**2.074**	22.02	0.83	
12800			**27.72**	54.57	**6.243**	29.01	2.0	
50		8	**0.3775**	0.4220	**0.0965**	8.601	0.13	
200			**1.142**	1.193	**0.2729**	11.15	0.33	
800			**3.462**	3.485	**0.7974**	14.58	0.22	
3200			**10.50**	10.37	**2.373**	19.15	0.83	
12800			**31.79**	31.13	**7.124**	25.21	2.0	
50		16	**0.4345**	0.2547	**0.1165**	7.581	0.13	
200			**1.312**	0.7029	**0.3216**	9.771	0.33	
800			**3.974**	2.028	**0.9282**	12.74	0.22	
3200			**12.04**	5.992	**2.742**	16.70	0.83	
12800			**36.43**	17.94	**8.211**	21.96	2.0	

Table 4-13 Open cavity case CFD simulation matrix based on water with fixed thermal distant (l), variable heat flux (Q*) and variable aspect ratio (h/l)

Notice: the Error rate in table and all other similar part of the thesis defined as the:

$$\text{error} = 1 - \frac{\text{CTG model Output Heat Flux}}{\text{CFD Input Heat Flux}} \qquad 4\text{-}4$$

Plot the natural convection cases temperature result points T_1 and T_y* of water:

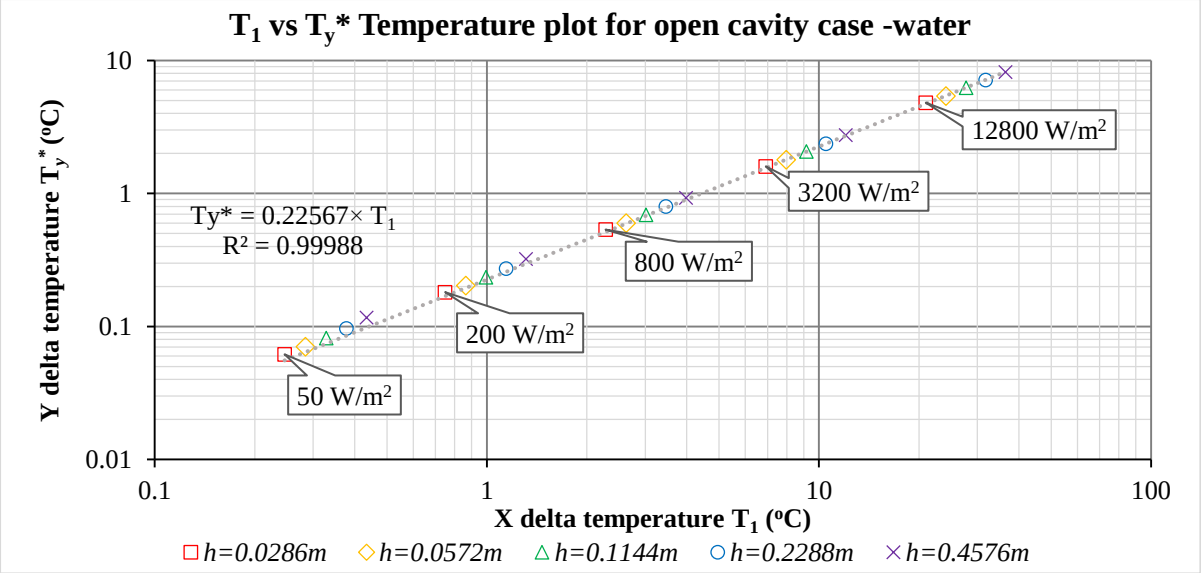

Figure 4-20 Open cavity case T_1 vs T_y* temperature plot based on water with fixed thermal distant (*l*), variable heat flux (Q*) and variable aspect ratio (*h/l*)

From the **Table 4-13**, despite different input of heat flux (Q*) and cavity height (*h*, thermal length), the relationship between T_1 and Ty* tends to be very linear all the time. It is possible to use linear scaler approximation with only 1 scalar coefficient to represent the temperature X and Y temperature relationship, any this can be the approximation expression for the thermal gradient value $\partial T/\partial y$.

Step 2, Open cavity natural convection case with air. Due to the reason that air has poorer thermal performance, the heat flux Q* applied for the air convection will be smaller than that of for the liquid. The CFD simulation conditions and result matrix of open cavity natural convection with air and fixed thermal distant (*l*) will be shown in the following **Table 4-14**:

Boundary condition			Outcome				Others	
Heat flux	l	Aspect	T_1	$\partial T/\partial y$	T_y*	l/l*	Error	Case setup:
W/m^2	m	h/l	°C	°C/m	°C		%	
4	1.43×10^{-2}	1	**1.178**	12.94	**0.370**	5.384	2.30	Air
16			**3.710**	37.98	**1.086**	7.047	5.43	
64			**11.46**	107.9	**3.087**	9.150	5.75	Open Cavity
256			**35.13**	314.7	**9.000**	11.96	5.88	
1024			**107.1**	933.6	**26.70**	15.69	5.92	$Y^*/l^*<10^{-3}$
4		2	**1.356**	8.846	**0.5060**	4.896	7.09	
16			**4.294**	23.85	**1.364**	6.274	8.65	Mesh count 512×512
64			**13.43**	64.53	**3.691**	8.046	8.91	
256			**41.28**	183.4	**10.49**	10.45	8.71	
1024			**125.9**	539.4	**30.86**	13.68	8.52	Ref. point Y=0.95h
4		4	**1.523**	5.911	**0.6762**	4.426	8.75	
16			**4.850**	14.62	**1.673**	5.551	8.57	
64			**15.28**	38.36	**4.388**	7.065	8.84	
256			**47.51**	105.5	**12.07**	9.097	8.95	
1024			**145.1**	309.9	**35.45**	11.91	8.90	
4		8	**1.684**	3.751	**0.8582**	3.951	7.34	
16			**5.493**	9.074	**2.076**	4.927	9.15	
64			**17.22**	23.53	**5.38**	6.252	8.56	
256			**54.72**	61.10	**13.98**	7.937	9.47	
1024			**167.7**	175.4	**40.13**	10.33	9.19	
4		16	**1.822**	2.412	**1.104**	3.538	3.97	
16			**6.136**	5.776	**2.643**	4.401	8.91	
64			**20.07**	13.59	**6.217**	5.450	10.3	
256			**62.42**	36.23	**16.58**	6.965	9.59	
1024			**191.8**	101.1	**46.28**	9.002	8.79	

Table 4-14 Open cavity case CFD simulation matrix based on air with fixed thermal distant (l), variable heat flux (Q*) and variable aspect ratio (h/l)

And plot the natural convection cases temperature result points T_1 and T_y* of air:

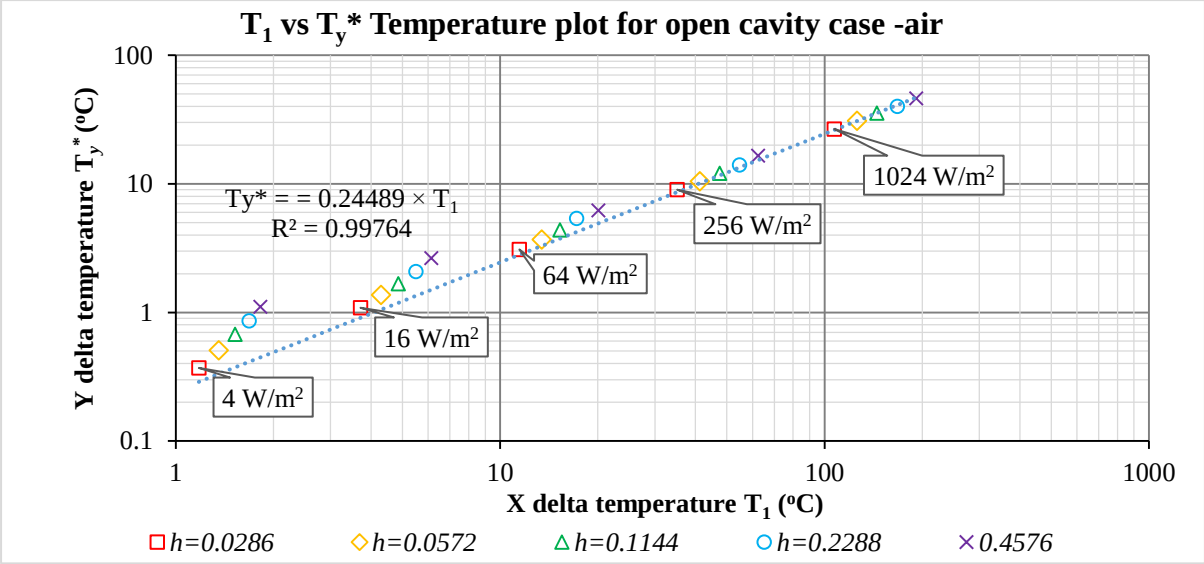

Figure 4-21 Open cavity case T_1 vs T_y* temperature plot based on air with fixed thermal distant (l), variable heat flux (Q*) and variable aspect ratio (h/l)

From the table above, the CFD solution of open cavity natural convection case with air does not has a good linear relationship between T_1 and T_y* temperature value. This may be related to the property of air, its low density results a large boundary layer thickness (*l**, characteristic length), hence affect the outcome of the temperature result. Whether the reason, or it is related to the Prandt number (Pr), there will be some discussion in the latter on part of case study of open cavity natural convection with variable thermal distant (*l*).

Step 3, Open cavity natural convection case with HFE liquid. The HFE liquid has a much greater thermal expansion ratio (β), with greater buoyance force, or in other words, greater Rayleigh number (Ra). Therefore the choice of cavity size of the HFE liquid natural convection case study is smaller in order to compensate the thermal expansion ratio. The CFD simulation conditions and result matrix of open cavity natural convection with HFE and fixed thermal distant (*l*) will be shown in the following **Table 4-15**:

Boundary condition			Outcome				Others	
Heat flux	*l*	Aspect	T_1	$\partial T/\partial y$	T_y*	*l*/*l**	Error	Case setup:
W/m^2	m	*h*/*l*	°C	°C/m	°C		%	
12.5	1.43×10^{-2}	1	**0.1915**	3.274	**0.0468**	17.55	8.27	HFE
50			**0.5811**	9.570	**0.1368**	22.95	8.99	
200			**1.764**	28.38	**0.4059**	30.12	9.36	Open Cavity
800			**5.356**	85.08	**1.217**	39.63	9.48	
3200			**16.24**	251.3	**3.594**	51.96	1.01	Y*/*l**<10^{-3}
12.5		2	**0.2207**	1.854	**0.0530**	15.23	8.28	
50			**0.6692**	5.442	**0.1556**	19.93	8.99	Mesh count 512×512
200			**2.029**	16.10	**0.4604**	26.14	9.51	
800			**6.153**	48.22	**1.379**	34.39	9.76	
3200			**18.66**	145.3	**4.154**	45.30	9.87	Ref. point Y=0.95*h*
12.5		4	**0.2413**	1.006	**0.0575**	13.07	1.39	
50			**0.7309**	2.947	**0.1686**	17.10	1.47	
200			**2.216**	8.743	**0.5001**	22.44	1.52	
800			**6.719**	26.21	**1.499**	29.53	1.54	
3200			**20.40**	78.96	**4.517**	38.90	1.54	
12.5		8	**0.2927**	0.6308	**0.0722**	11.63	7.08	
50			**0.8846**	1.828	**0.2092**	15.17	8.40	
200			**2.678**	5.376	**0.6150**	19.87	9.22	
800			**8.117**	15.99	**1.830**	26.10	9.67	
3200			**24.61**	47.99	**5.490**	34.34	9.88	
12.5		16	**0.3195**	0.3464	**0.0793**	10.01	1.27	
50			**0.9651**	1.000	**0.2289**	13.05	1.41	
200			**2.922**	2.930	**0.6703**	17.07	1.49	
800			**8.857**	8.708	**1.992**	22.42	1.53	
3200			**26.84**	26.13	**5.978**	29.50	1.56	

Table 4-15 Open cavity case CFD simulation matrix based on HFE with fixed thermal distant (*l*), variable heat flux (Q*) and variable aspect ratio (*h*/*l*)

And plot the natural convection cases temperature result points T_1 and T_y* of HFE liquid:

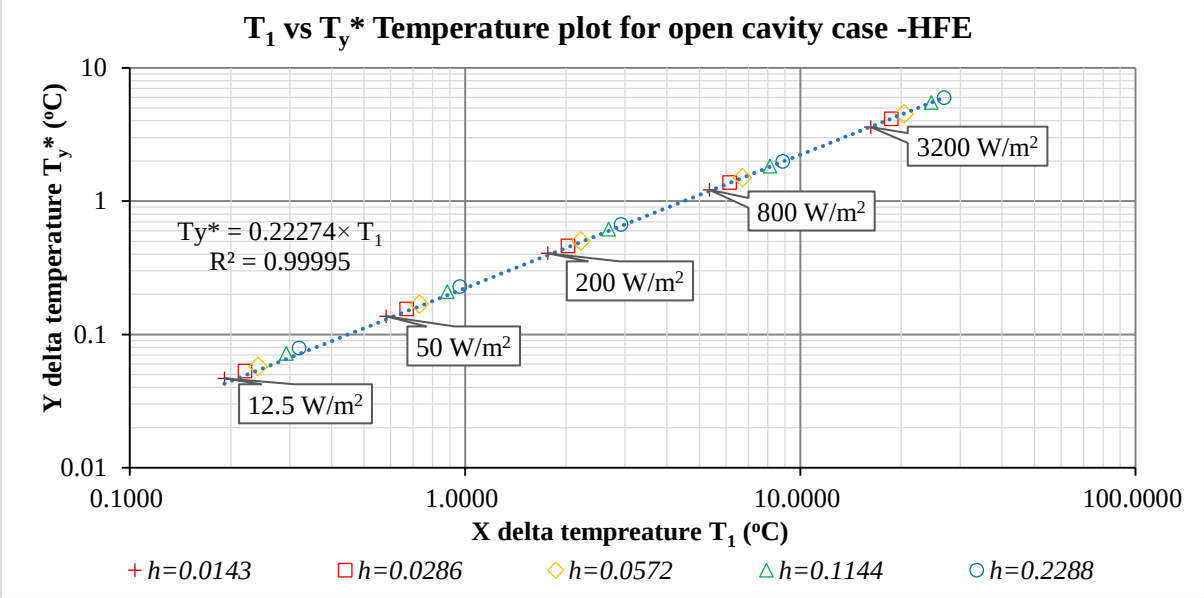

Figure 4-22 Open cavity case T_1 vs T_y* temperature plot based on HFE with fixed thermal distant (*l*), variable heat flux (Q*) and variable aspect ratio (*h/l*)

Similar to the natural convection case result with water, the HFE liquid result has very linear temperature plot as well. Since the temperature result from all 3 types of fluid seems to be in the same flow regime, they can be put into the same plot for comparison **Figure 4-23**:

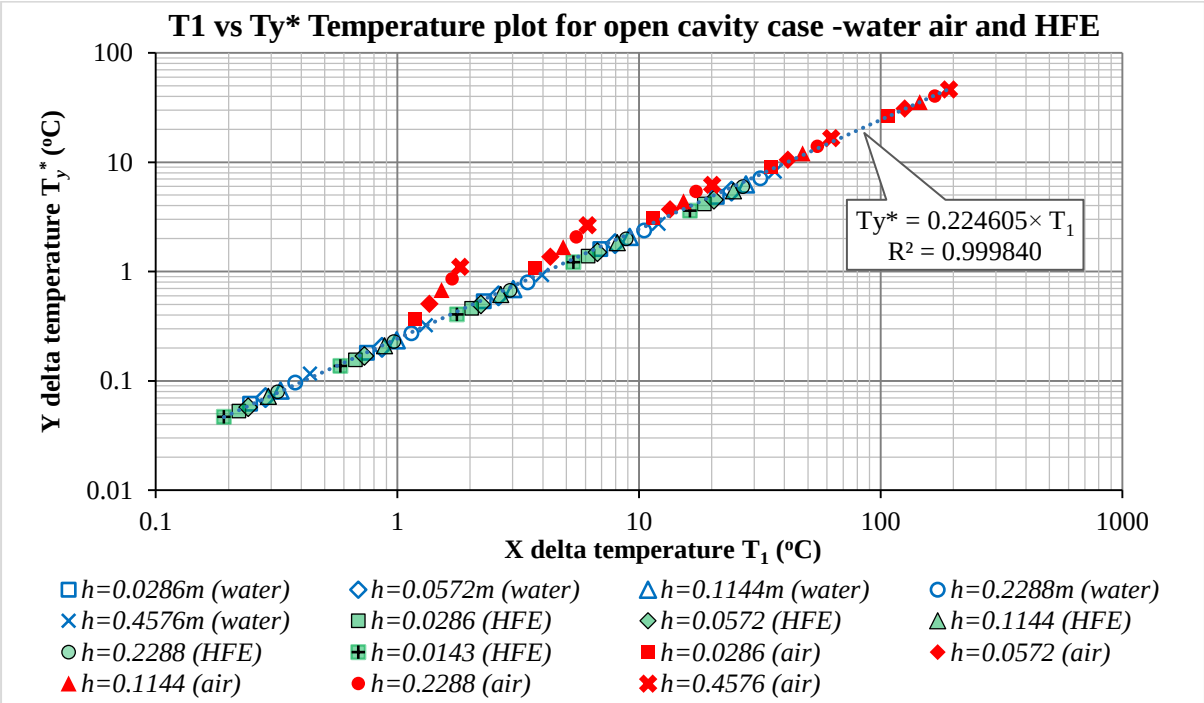

Figure 4-23 Open cavity case T_1 vs T_y* temperature plot based on water, air and HFE with fixed thermal distant (*l*), variable heat flux (Q*) and variable aspect ratio (*h/l*)

It can be seen from the **Figure 4-24**, most of the temperature point fits in a single linear line, use least square method to approximated the Ty* and $\partial T/\partial y^*$ calculation is given:

$$T_y^* = 0.224605 \times T_1 \qquad 4\text{-}5$$

And it can be rewritten with the thermal gradient ($\partial T/\partial y$) value:

$$\frac{\partial T}{\partial y} \approx C_{TG} \times \frac{T_1}{h}, \qquad C_{TG} = 0.224605 \qquad 4\text{-}6$$

Now the thermal gradient ($\partial T/\partial y$) value can be a universal expression to natural convection problem independent to the material and fluid that was used. The scaler of the linear expression C_{TG} =0.22465 now is the thermal gradient constant of the CTG model. This could be a universal expression but the relation between temperature and different thermal distant (*l*) has yet to be discussed, so in the next section it will focus on the relationship between temperature (T_1, T_y*) and thermal distant (*l*), and followed by the discussion of the thermal gradient ($\partial T/\partial y$) approximation.

Discussion of the CTG model for Open cavity natural convection problems

The previous section showed that the relationship between temperatures (T_1, T_y*) and thermal distance (*l*) needed to be identified before building the CTG model. In this section a number of CFD simulations for open cavity natural convection (water) with variable thermal distant (*l*), but fixed heat flux (Q*) and fixed thermal length (*h*) are presented.

Boundary condition			Outcome				Others	
Heat flux	*l*	Aspect	T_1	$\partial T/\partial y$	T_y*	*l*/*l** ($Ra^{*0.25}$)	Error (1)	Case setup: Water
W/m^2	m	*h*/*l*	°C	°C/m	°C		%	
3200	2.29×10^{-1}	0.5	**9.055**	18.09	**2.069**	176.1	6.6	Open Cavity
	1.14×10^{-1}	1	**8.954**	18.24	**2.087**	88.22	7.4	
	5.72×10^{-2}	2	**9.059**	18.09	**2.070**	44.02	6.5	Y*/*l**<10^{-3}
	2.86×10^{-2}	6	**9.067**	18.22	**2.084**	22.05	6.2	
	1.43×10^{-2}	8	**9.037**	19.36	**2.214**	11.19	5.1	Mesh count 512×512
	7.15×10^{-3}	16	**9.046**	24.36	**2.787**	5.927	5.6	
	3.58×10^{-3}	32	**7.846**	41.87	**4.790**	3.393	1.2	Ref. point Y=0.95*h*
	1.79×10^{-3}	64	**4.594**	93.99	**10.75**	2.077	28	
	8.94×10^{-4}	128	**2.356**	0.80	**0.092**	0.3158	89	

Table 4-16 Open cavity case CFD simulation matrix based on water with fixed heat flux (Q*) and fixed aspect ratio (*h*/*l*), but variable thermal distant (*l*)

Plot the temperature result points T_1 and Ty* from the variable thermal distant (*l*) open cavity water convection case along with the temperature plot from **Figure 4-20**:

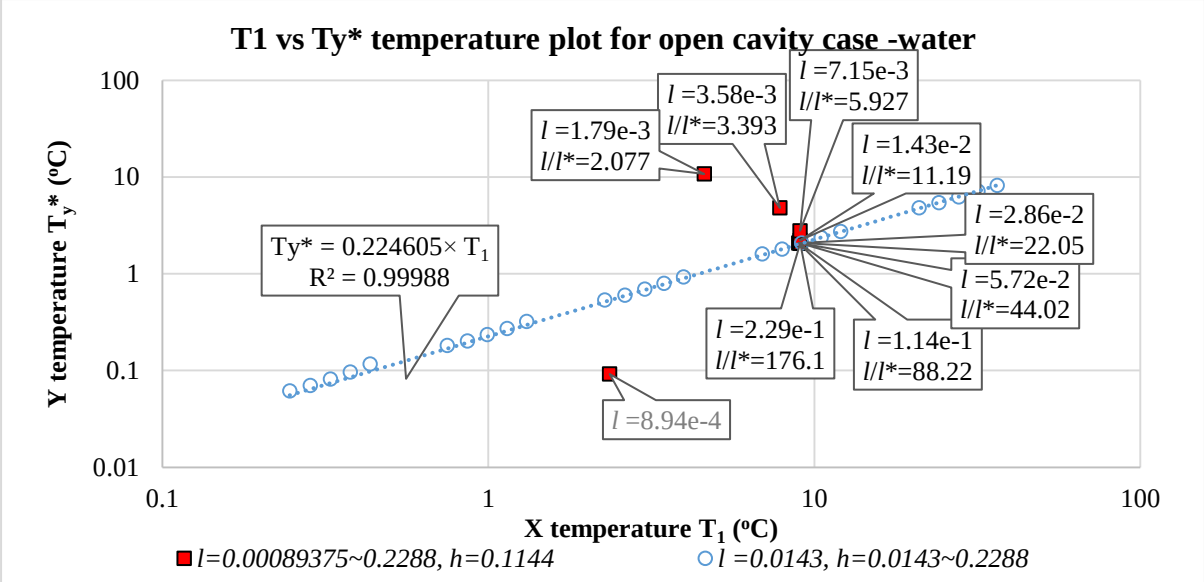

Figure 4-24 Open cavity case T_1 vs T_y* temperature plot based on water with fixed heat flux (Q*) and fixed aspect ratio (*h*/*l*), but variable thermal distant (*l*)

It can be seen from **Figure 4-24** when *l*/*l**>5 most of the temperature point (T_1 vs T_y*) will gather at almost the same location in the temperature map. Despite the changes of the thermal distant *l*, the heat transfer of the natural convection case would have little variation as the thermal distant *l* is greater than 5 ×*l**. For a better observation, the velocity profile against the physical X coordinate of the case study is given as well:

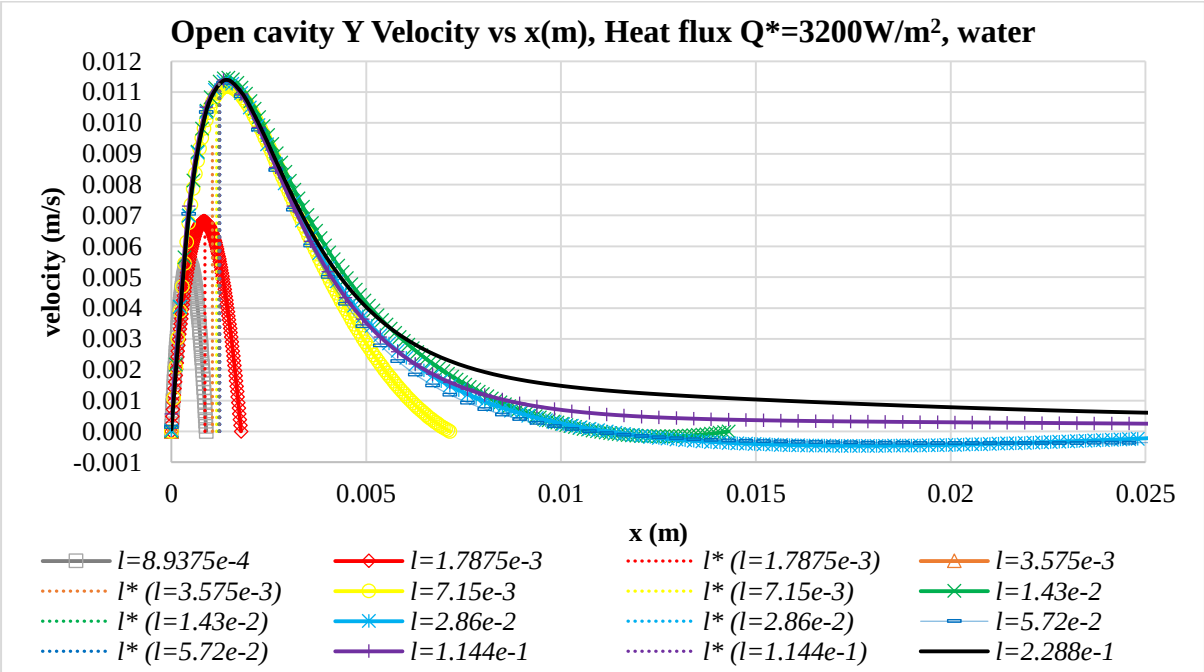

Figure 4-25 Open cavity case velocity plot based on water with fixed heat flux (Q*) and fixed aspect ratio (*h*/*l*), but variable thermal distant (*l*)

From **Figure 4-25**, it also shows the velocity plot overlap in the same curve when the thermal distant is larger: $l > 7.15\times10^{-3}$m, but the actual value of the thermal distant (l) will be problem dependent. It is better to use the characteristic length scale l^* as the base factor. That is to say, the **equation 4-5** and **equation 4-6** will be valid when:

$$\frac{l}{l^*} > 5 \tag{4-7}$$

This along with the **equation 3-85, equation 3-86** and **equation 3-101** (general natural convection expressions), also with **equation 4-5** and **equation 4-6** (CTG model approximation) forms the complete solution of density driven natural convection in open cavity cases.

Notice that the CTG model will have poorer agreement with the CFD when the thermal distant $l < 5\ l^*$, but this usually means a very small value of thermal distant, for example in the previous case (**Table 4-16**), the distant $l < 5\ l^*$ results a very small convection cavity of $l< 10$ mm, which exceed the regime of interest in this thesis.

Interestingly, the l/l^* expression can be rewritten as **equation 3-120** and **equation 3-121**:

$$\frac{l}{l^*} = \sqrt[4]{\frac{\rho^2 \cdot g \cdot \beta \cdot C_p}{\mu \cdot \lambda} \cdot \frac{\partial \mathrm{T}}{\partial y} \cdot l^4}$$

And use the constant thermal gradient approximation (C_{TG}) to rewrite the gradient value $\partial T/\partial y$, which:

$$\frac{l}{l^*} = \sqrt[4]{\frac{\mathrm{C_{tc}} \cdot l}{h} \cdot \frac{\rho^2 \cdot g \cdot \beta \cdot C_p}{\mu \cdot \lambda} \cdot T_1 \cdot l^3} = \sqrt[4]{\frac{\mathrm{C_{tc}} \cdot l}{h}} \cdot \sqrt[4]{\frac{\rho^2 \cdot g \cdot \beta \cdot C_p}{\mu \cdot \lambda} \cdot T_1 \cdot l^3} \tag{4-8}$$

It has the same expression as the Rayleigh number (Ra_l) based on the X direction wall distant, thus the thermal distant scale should (l/l^*) can be used to describe natural convection as well:

$$\frac{l}{l^*} = \sqrt[4]{\frac{\mathrm{C_{tc}} \cdot l}{h} \cdot {Ra^*}_l} \tag{4-9}$$

One more observation of this length scale and thermal distant expression is that, to represent the complete scaling and similarity problem, both X direction coordinate (thermal distant, l) and Y direction coordinate (thermal length, h) will be needed. The precise expression of Rayleigh number should be:

$$Ra = \frac{\rho^2 \cdot g \cdot \beta \cdot C_p \cdot l^4 \cdot \Delta T}{\mu \cdot \lambda \cdot h} \tag{4-10}$$

This expression / approximation is also possible to describe single heated wall natural convection case without the middle wall. Unfortunately it is not quite possible to give the exact expression when l=∞, the exponential-complex part of the equation may result an invalid value:

$$l = \infty\,, \qquad e^{(2l-x)\sqrt[4]{-A\cdot C}\cdot i} \to e^{\infty+\infty i}$$

It only need to give a large thermal distant value, which:

$$\frac{l}{l^*} \to \infty$$

The thermal distant l still need to be a real value, but as it could be large value and the solution will be very close to a single heated wall case. And for a natural convection problem like open cavity and single heated wall case, the thermal distant l may be irrelevant to the solution as long as it is large, and it does not appear in the energy equation solution as well.

It is also possible to rewrite the energy equation into general Nusselt number form (Ra^*_h and Nu^*_h). Firstly writing down the Rayleigh number expression for a single heated wall:

$$Ra_h = \frac{\rho^2 \cdot g \cdot \beta \cdot C_p}{\mu \cdot \lambda} \cdot \Delta T_l \cdot h^3 \qquad 4\text{-}11$$

The reference temperature T_l in this expression is be the difference between heated wall temperature and the far side bulk temperature (constant wall temperature condition). For simplification, the delta temperature far side temperature T_0 for the delta temperature ΔT_l will be zero value, which:

$$\Delta T_l = T_l - T_0\,, \qquad T_0 = 0 \quad \to \quad \Delta T_l = T_l$$

Notice that general Rayleigh number and Nusselt number correlation has constant wall temperature T_l for boundary condition. But the constant thermal gradient in this research based on constant wall heat flux assumption and uses the reference point heated wall delta temperature T_1. It is possible to obtain the average heated wall temperature $\overline{T_1}$ from Reference point temperature T_1 and thermal gradient $\partial T/\partial y$, which:

$$\overline{T_1} = T_1\left(1 - \frac{h}{2}\cdot\frac{\partial \mathrm{T}}{\partial y}\right) \qquad 4\text{-}12$$

In the other hands, the average heated wall temperature $\overline{T_1}$ can be loosely used as the reference temperature for Rayleigh number calculation:

$$Ra_h = \frac{\rho^2 \cdot g \cdot \beta \cdot C_p}{\mu \cdot \lambda} \cdot h^3 \cdot \overline{T_1} = \frac{\rho^2 \cdot g \cdot \beta \cdot C_p}{\mu \cdot \lambda} \cdot h^3 \cdot T_1\left(1 - \frac{h}{2}\cdot\frac{\partial \mathrm{T}}{\partial y}\right) \qquad 4\text{-}13$$

With the Rayleigh number, the Nusselt number (Nu_h) can be calculated by the correlation that in given by Churchill & Chu (1975), which:

$$\overline{\mathrm{Nu}_h} = 0.68 + \frac{0.67 \cdot \sqrt[4]{Ra_h}}{\left[1 + \left(\frac{0.492}{Pr}\right)^{\frac{9}{16}}\right]^{\frac{4}{9}}} \qquad 4\text{-}14$$

It is also possible to use the heat flux from the constant thermal gradient model to calculate the Nusselt number. Since this is a different method to calculate the Nusselt number, it will be given as a specific Nussult number $\mathrm{Nu}_h{}^*$, which:

$$\mathrm{Q}^* \approx \frac{\lambda \cdot T_1}{\sqrt{2} \cdot l^*}, \qquad \mathrm{Nu}^*{}_h = \frac{\mathrm{Q}^*}{T_1} \cdot \frac{h}{\lambda} \quad \rightarrow \quad \mathrm{Nu}^*{}_h = \frac{h}{\sqrt{2} \cdot l^*} \qquad 4\text{-}15$$

And with the length scale:

$$l^* = \sqrt[-4]{\frac{\rho^2 \cdot g \cdot \beta \cdot C_p}{\mu \cdot \lambda} \cdot \frac{\partial \mathrm{T}}{\partial y}} \qquad 4\text{-}16$$

Finally the specific Nusselt number $Nu_h{}^*$ derived from constant thermal gradient model can be rewritten as:

$$\mathrm{Nu}_h{}^* = \frac{h}{\sqrt{2}} \cdot \sqrt[4]{\frac{\rho^2 \cdot g \cdot \beta \cdot C_p}{\mu \cdot \lambda} \cdot \frac{\partial \mathrm{T}}{\partial y}} \qquad 4\text{-}17$$

Noticed that the Nusselt number calculated from the constant thermal gradient model shares significant similarity with the Rayleigh number Ra_h. So a specific Rayleigh number for constant thermal gradient model $\mathrm{Ra}_h{}^*$ can be:

$$\mathrm{Ra}_h{}^* = \frac{\rho^2 \cdot g \cdot \beta \cdot C_p}{\mu \cdot \lambda} \cdot \frac{\partial \mathrm{T}}{\partial y} \cdot h^4 \quad \rightarrow \quad \mathrm{Ra}_h{}^* = \mathrm{C_{TG}}{}^* \cdot \frac{\rho^2 \cdot g \cdot \beta \cdot C_p}{\mu \cdot \lambda} \cdot T_1 \cdot h^3 \qquad 4\text{-}18$$

So this specific Rayleigh number for open cavity solution only needs the thermal length along the gravity direction (h) as the length scale. Also it can rewrite the specific Nusselt number expression with Rah component:

$$\mathrm{Nu}_h{}^* = \frac{h \cdot \sqrt[4]{\mathrm{C_{TG}} \cdot \frac{\rho^2 \cdot g \cdot \beta \cdot C_p}{\mu \cdot \lambda} \cdot \frac{T_1}{h}}}{\sqrt{2}} = \frac{\mathrm{Ra}_h{}^*}{\sqrt{2}} \qquad 4\text{-}19$$

In the open cavity problem, the specific Rayleigh number Ra_h* is closely related to the calculation on Nusselt number. It can be written in terms of the thermal length scale *l** and the thermal height *h*: (**equation 3-131**)

$$\mathrm{Ra}_h{}^* = \left(\frac{h}{l^*}\right)^4$$

It indicates the ratio between the free convection flow travelling distant *h* (thermal height) and free convection flow boundary thickness, or even loosely understood as the intensity of the free convection flow.

Using the temperature data from the open cavity convention case with water, the Nusselt number from constant thermal gradient model can be compared with Churchill & Chu's correlation:

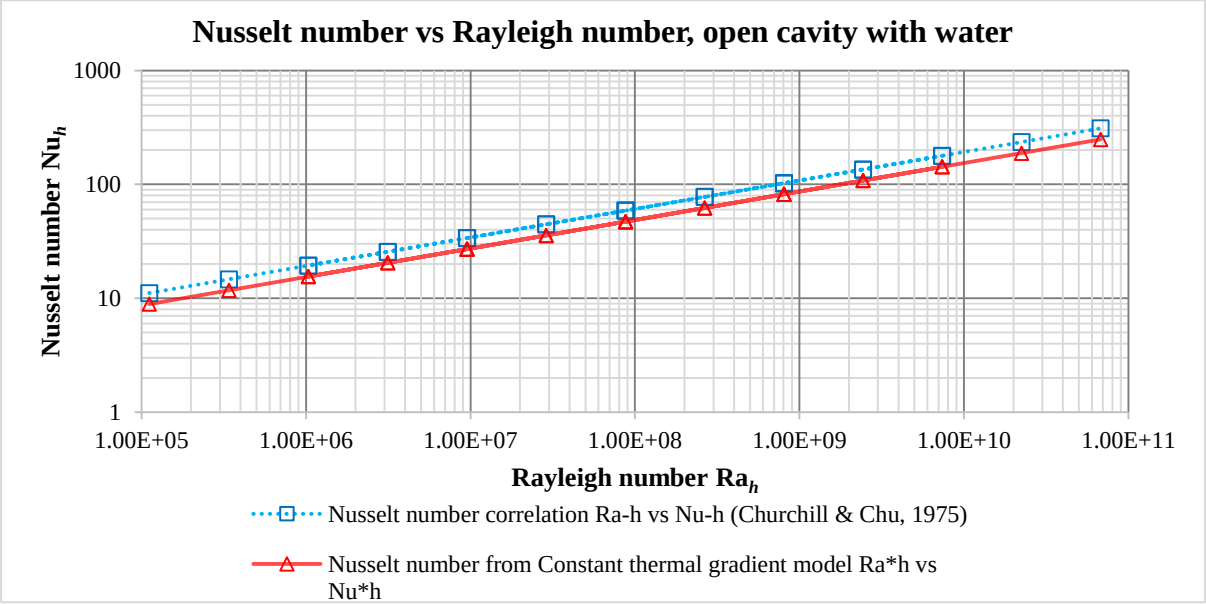

Figure 4-26 Nusselt number vs Rayleigh number correlation comparison

It can be seen there is a constant shift between the Nusselt number derived from the energy equation of the constant thermal gradient model matches and the Nusselt number correlation present by Churchill & Chu (1975). This shift value is indeed the thermal gradient constant C_{TG} value, the C_{TG} value obtain from the CFD result in this research is C_{TG} (CFD) =0.224605, and the C_{TG} value approximation for Churchill & Chu's correlation would be C_{TG} (Churchill & Chu) =0.54836, where:

$$\overline{\mathrm{Nu}_h} = 0.68 + \frac{0.67 \cdot \sqrt[4]{Ra_h}}{\left[1 + \left(\frac{0.492}{Pr}\right)^{\frac{9}{16}}\right]^{\frac{4}{9}}} \approx \frac{\sqrt[4]{\mathrm{C}_{\mathrm{TG(C)}} \cdot Ra_h}}{\sqrt{2}}, \qquad \mathrm{C}_{\mathrm{TG(C)}} = 0.54836 \qquad 4\text{-}20$$

The reason of the shift between 2 Nusselt number approximation methods may due to their different boundary conditions?: the constant thermal gradient model uses heat flux wall condition and assumed to have a variable wall temperature (constant gradient), while Churchill & Chu's correlation is based on a constant wall temperature boundary. From the Nu vs Ra plot and the shifting value between the methods means that these 2 Nusselt number methods are linearly related and can be converted from one to another with a simple linear approximation.

It is also interesting to know that the specific Rayleigh number Ra_l^* based on the thermal distant *l* (distant between walls) as the length scale, may depend on the flow regime. On the other hand, the specific Rayleigh number Ra^*_h based on the thermal length *h* (height along the gravity) seems to be less useful at the moment. Still it may be more useful to take both Ra^*_l and Ra^*_h based on thermal distant (*l*) and thermal height (*h*) to represent the complete view of the convection case.

To compare with the constant heat flux case from other pervious research, the CTG model energy expression can be rewrite into a similar manner as the $Nu_{(CWHF)}$ and $Ra_{(CWHF)}$ correlation. Now the original CTG model heat flux is (**equation 3-125**):

$$\mathrm{Q}^* \approx \frac{\lambda \cdot T_1}{\sqrt{2} \cdot l^*} = \frac{\lambda \cdot T_1}{\sqrt{2}} \cdot \sqrt[4]{\frac{\rho^2 \cdot g \cdot \beta \cdot C_p}{\mu \cdot \lambda} \cdot \frac{\partial \mathrm{T}}{\partial y}} = \frac{\lambda \cdot T_1}{\sqrt{2}} \cdot \sqrt[4]{\frac{\rho^2 \cdot g \cdot \beta \cdot C_p \cdot \mathrm{C_{TG}} \cdot T_1}{\mu \cdot \lambda \cdot h}}$$

Rewrite the order of the equation and put the T_1 temperature to the left hand side:

$$T_1^{\frac{5}{4}} = \frac{\sqrt{2} \cdot \mathrm{Q}^*}{\lambda} \cdot \sqrt[4]{\frac{\mu \cdot \lambda \cdot h}{\rho^2 \cdot g \cdot \beta \cdot C_p \cdot \mathrm{C_{TG}}^*}} \quad , \qquad T_1 = \left(\frac{\sqrt{2} \cdot \mathrm{Q}^*}{\lambda}\right)^{\frac{4}{5}} \cdot \sqrt[5]{\frac{\mu \cdot \lambda \cdot h}{\rho^2 \cdot g \cdot \beta \cdot C_p \cdot \mathrm{C_{TG}}^*}}$$

Now put the temperature T_1 back into the specific Nusselt number Nu_h^* expression, which:

$$\mathrm{Nu}^*_h = \frac{\mathrm{Q}^*}{T_1} \cdot \frac{h}{\lambda} = \mathrm{Q}^* \cdot \frac{h}{\lambda} \left(\frac{\lambda}{\sqrt{2} \cdot \mathrm{Q}^*}\right)^{\frac{4}{5}} \cdot \sqrt[-5]{\frac{\rho^2 \cdot g \cdot \beta \cdot C_p \cdot \mathrm{C_{TG}}}{\mu \cdot \lambda \cdot h}}$$

This can be further reduced into:

$$\mathrm{Nu}^*_h = \left(\frac{1}{2}\right)^{\frac{2}{5}} \cdot \sqrt[5]{\mathrm{C_{TG}}} \cdot \sqrt[5]{\frac{\rho^2 \cdot g \cdot \beta \cdot C_p \cdot \mathrm{Q}^* \cdot h^4}{\mu \cdot \lambda^2}} \qquad \text{4-21}$$

Given the constant of CTG model C_{TG}=0.54836, the end result of Nusselt number Nu_h^* now is:

$$\mathrm{Nu}^*_h = 0.672 \cdot \sqrt[5]{\frac{\rho^2 \cdot g \cdot \beta \cdot C_p \cdot \mathrm{Q}^* \cdot h^4}{\mu \cdot \lambda^2}} \qquad \text{4-22}$$

Notice that the right part of the expression is identical to the Rayleigh number for constant wall heat flux Ra(CWHF), which make this expression rather close to Qureshi and Gebhart's work (Qureshi and Gebhart, 1978), which was:

$$\mathrm{Nu}^*_{l} = 0.587 \cdot \sqrt[5]{Ra_{(\mathrm{CWHF})}}$$

And also close to Goldstein and Eckert's work (Goldstein and Eckert, 1960) which was:

$$\mathrm{Nu}^*_{l} = 0.586 \cdot \sqrt[5]{Gr_{(\mathrm{CWHF})} \cdot Pr}$$

Consider Qureshi and Gebhart's work based on a case with a fixed height of 1.835m, and the *l* distance in their case of the Rayleigh number actually refers to the point of observation height over the inlet section, and their work was more focused on the developing stage of the flow. In this thesis the *h* refers to the overall height of the problem and it only looked into the fully-developed stage of the flow. Thus the outcomes of the Nusselt number are different in this comparison.

Such outcome of the energy equation of CTG model also match Aydin and Guessous's suggestion (Aydin, Guessous, 2001):

$$\mathrm{Nu}_{local} = C^* \cdot (Gr^* \cdot Pr)^{\frac{1}{5}}$$

The importance of such practice of rewriting the CTG model energy into Nusselt number correlation is that it could be reverse used. In face a Nusselt number correlation can be rewritten into a single C_{TG} value and could be used in the CTG model analytical solution expression. For example combine Qureshi and Gebhart's correlation and equation 4-20 together, the C_{TG} value for Qureshi and Gebhart's correlation ($C_{Qureshi}$) could be:

$$\left(\frac{1}{2}\right)^{\frac{2}{5}} \cdot \sqrt[5]{\mathrm{C}_{\mathrm{Qureshi}}} = 0.587\,, \qquad \mathrm{C}_{\mathrm{Qureshi}} = 0.2788$$

As a result, a number of Nusselt number correlations that fits Aydin and Guessous's assumption could be used to obtain the C_{TG} value for analytical solution, thus the usage of CTG model can be expanded.

Close cavity CFD case study: fixed thermal distant (*l*) with variable heat flux (Q*) and variable aspect ratio (*h/l*)

Follows the open cavity case studies, a matrix of CFD simulations with fixed thermal distant (*l*), various of heat flux (Q*) and aspect ratio (*h/l*) will be carried out for the closed case and the outcome will be T_1 and T_y*.

Step 4, Close cavity natural convection case with water. The CFD simulation conditions and result matrix of open cavity natural convection with water and fixed thermal distant (*l*) will be shown in the following table:

Boundary condition			Outcome				Others	
Heat flux	*l*	Aspect	T_1	$\partial T/\partial y$	T_y*	*l*/*l**	Error	Case Setup:
W/m^2	m	*h/l*	^{o}C	^{o}C/m	^{o}C		%	
50	2.86×10^{-2}	2	**0.1566**	14.42	**0.4123**	10.40	2.27	Water
200			**0.4624**	49.78	**1.424**	14.17	1.66	
800			**1.377**	174.1	**4.978**	19.38	1.13	Close Cavity
3200			**4.406**	412.8	**11.80**	24.05	6.25	
12800			**14.02**	914.7	**26.16**	29.34	3.56	Y*/*l**<10^{-3}
50		4	**0.1602**	14.51	**0.8301**	10.41	0.13	
200			**0.4823**	44.74	**2.559**	13.80	0.13	Mesh count 512×512
800			**1.478**	129.1	**7.383**	17.99	0.26	
3200			**4.678**	323.8	**18.52**	22.63	0.71	
12800			**15.49**	626.6	**35.84**	26.70	3.07	Ref. point Y=0.5*h*
50		8	**0.1747**	10.16	**1.162**	9.526	0.13	
200			**0.5482**	26.59	**3.042**	12.12	0.33	
800			**1.584**	98.09	**11.22**	16.79	0.22	
3200			**5.317**	193.0	**22.08**	19.89	0.83	
12800			**17.18**	432.7	**49.50**	24.34	1.98	
50		16	**0.2016**	5.707	**1.306**	8.247	0.21	
200			**0.6087**	17.55	**4.016**	10.92	0.24	
800			**1.819**	54.77	**12.53**	14.52	0.95	
3200			**6.133**	108.8	**24.90**	17.23	0.87	
12800			**19.35**	273.8	**62.65**	21.71	1.52	
50		32	**0.2427**	2.709	**1.240**	6.846	0.28	
200			**0.7060**	9.696	**4.437**	9.416	0.25	
800			**2.092**	31.23	**14.29**	12.61	1.04	
3200			**7.282**	54.43	**24.91**	14.49	1.02	
12800			**22.06**	163.8	**74.95**	19.09	1.27	

Table 4-17 Close cavity case CFD simulation matrix based on water with fixed thermal distant (*l*), variable heat flux (Q*) and variable aspect ratio (*h/l*)

Plot the temperature result points T_1 and T_y* of water convection in close cavity convection (water):

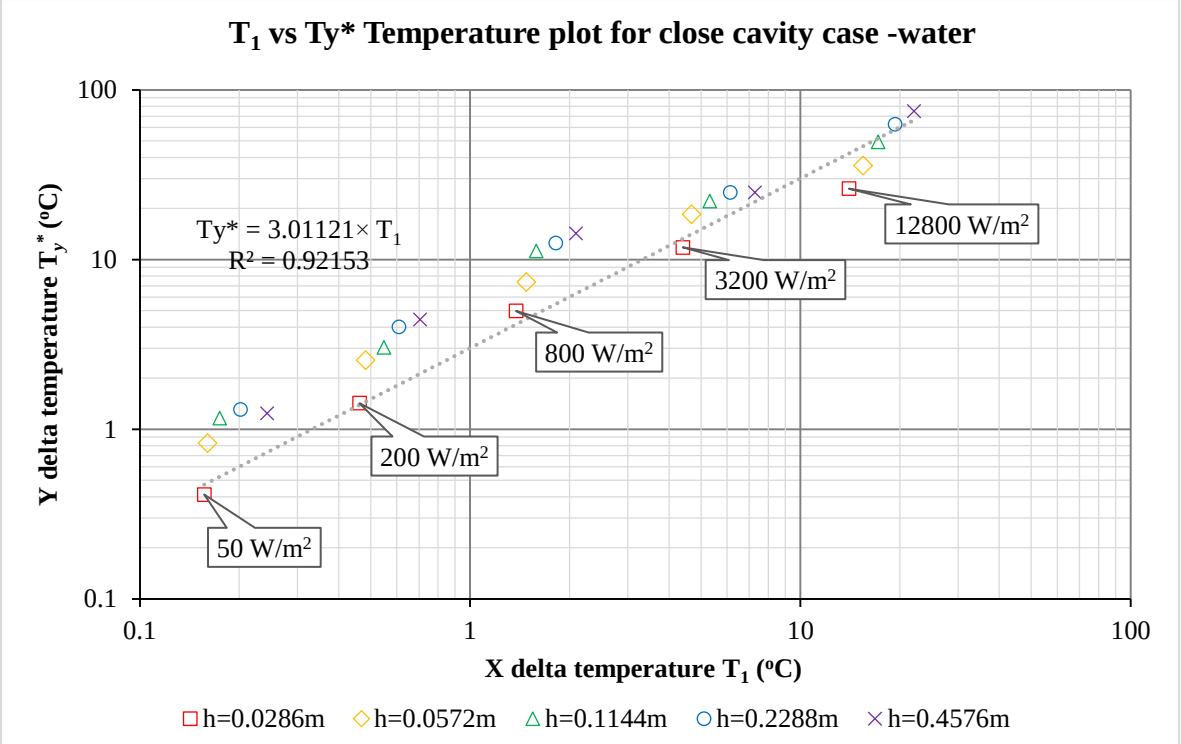

Figure 4-27 Close cavity case T_1 vs T_y* temperature plot based on water with fixed thermal distant (l), variable heat flux (Q*) and variable aspect ratio (h/l)

From the **Figure 4-27** it can be seen that the closed cavity natural convection case does not have a linear relationship between T_1 and T_y* temperature like the open cavity cases. Therefore it may not be possible to use the same method as the open cavity cases to approximate the thermal gradient value $\partial T/\partial y$ with the close cavity cases.

Step 5, Close cavity natural convection case with air. Here are the conditions and result matrix:

Boundary condition			Outcome				Others	
Heat flux	l	Aspect	T_1	$\partial T/\partial y$	T_y*	l/l*	Error	Case setup:
W/m^2	m	h/l	^{o}C	^{o}C/m	^{o}C		%	
12.5	1.43×10^{-2}	2	**2.284**	154.7	**4.426**	10.40	18.0	Air
50			**6.708**	427.1	**12.21**	14.17	11.7	
200			**19.54**	1397	**39.97**	19.38	9.45	Close Cavity
800			**56.81**	4623	**132.2**	24.05	7.26	
3200			**163.1**	17257	**493.5**	29.34	7.00	$Y^*/l^*<10^{-3}$
12.5		4	**2.290**	127.3	**7.280**	10.41	12.7	
50			**6.640**	375.6	**21.48**	13.80	7.10	Mesh count 512×512
200			**19.33**	1306	**74.70**	17.99	6.45	
800			**54.62**	5217	**298.4**	22.63	6.30	
3200			**250.2**	9440	**539.9**	26.70	4.12	Ref. point $Y=0.5h$
12.5		8	**2.262**	103.2	**11.81**	9.526	5.64	
50			**6.878**	326.5	**37.36**	12.12	7.12	
200			**19.92**	1171	**133.9**	16.79	6.75	
800			**59.12**	4101	**469.2**	19.89	8.33	
3200			**235.3**	8118	**928.7**	24.34	27.9	
12.5		16	**2.511**	62.85	**14.38**	8.247	3.62	
50			**7.544**	224.8	**51.43**	10.92	7.01	
200			**21.66**	839.1	**192.0**	14.52	6.76	
800			**66.68**	2399	**548.8**	17.23	6.85	
3200			**217.6**	4759	**1089**	21.71	3.47	
12.5		32	**2.836**	35.89	**16.42**	6.846	1.72	
50			**8.896**	111.0	**50.80**	9.416	5.8	
200			**25.82**	417.7	**191.1**	12.61	6.91	
800			**77.80**	1300	**594.7**	14.49	6.92	
3200			**253.0**	2792	**1278**	19.09	5.29	

Table 4-18 Close cavity case CFD simulation matrix based on air with fixed thermal distant (*l*), variable heat flux (Q*) and variable aspect ratio (*h/l*)

Plot the temperature result points T_1 and T_y* of air convection in close cavity convection:

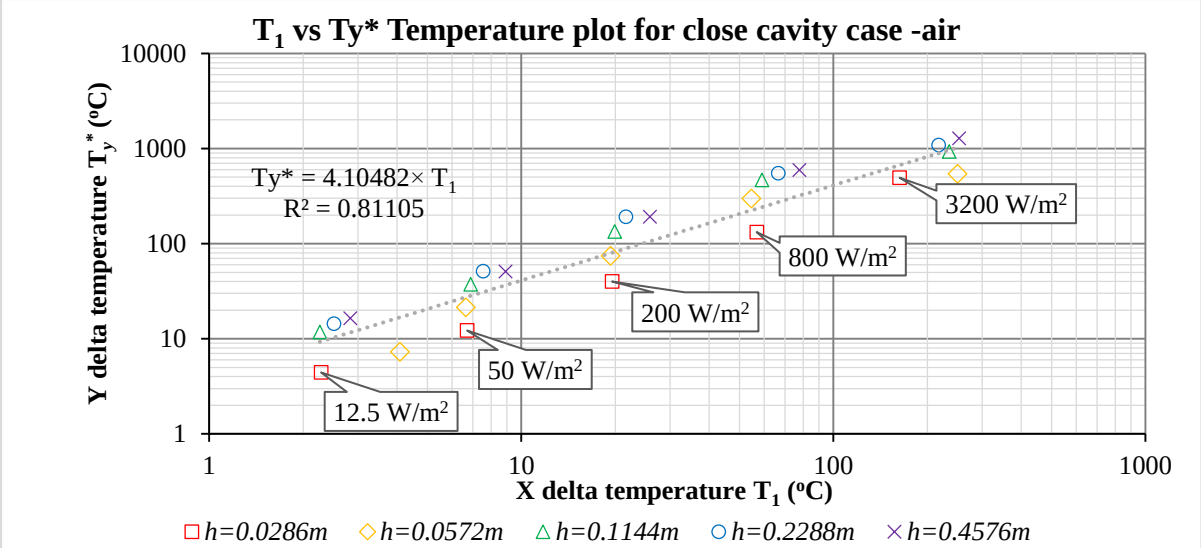

Figure 4-28 Close cavity case T_1 vs T_y* temperature plot based on air with fixed thermal distant (*l*), variable heat flux (Q*) and variable aspect ratio (*h*/*l*)

Step 6, Close cavity natural convection case with HFE liquid. The conditions and result matrix are given below:

Boundary condition			Outcome				Others	
Heat flux	*l*	Aspect	T_1	$\partial T/\partial y$	T_y*	*l*/*l**	Error	Case setup:
W/m²	m	*h*/*l*	ºC	ºC/m	ºC		%	
12.5	7.15 ×10⁻³	2	**0.1304**	20.52	**0.293**	13.89	1.13	HFE
50			**0.3792**	56.99	**0.815**	17.93	7.22	
200			**1.177**	150.0	**2.146**	22.83	8.27	Close Cavity
800			**3.668**	379.8	**5.432**	28.80	9.88	
3200			**11.43**	942.2	**13.47**	36.15	11.9	Y*/*l**<10⁻³
12.5		4	**0.1496**	11.87	**0.3394**	12.11	1.11	
50			**0.4692**	30.22	**0.8643**	15.30	2.04	Mesh count 512×512
200			**1.468**	74.39	**2.127**	19.16	4.05	
800			**4.574**	180.8	**5.172**	23.93	6.64	
3200			**14.24**	496.2	**14.19**	30.79	6.49	Ref. point Y=0.5*h*
12.5		8	**0.174**	6.283	**0.3594**	10.33	1.69	
50			**0.547**	15.48	**0.8855**	12.94	3.43	
200			**1.701**	38.15	**2.182**	16.21	5.87	
800			**5.304**	92.16	**5.271**	20.22	8.55	
3200			**16.522**	256.5	**14.67**	26.11	8.01	
12.5		16	**0.2032**	3.329	**0.3809**	8.813	2.22	
50			**0.6344**	8.814	**1.008**	11.24	2.66	
200			**1.972**	20.81	**2.381**	13.94	6.23	
800			**6.006**	60.25	**6.893**	18.18	6.88	
3200			**18.74**	138.7	**15.87**	22.39	10.5	
12.5		32	**0.235**	1.795	**0.4106**	7.552	2.99	
50			**0.748**	4.783	**1.094**	9.648	1.54	
200			**2.379**	15.03	**3.438**	12.85	4.27	
800			**6.841**	51.27	**11.73**	17.46	1.87	
3200			**21.08**	135.6	**31.02**	22.26	0.63	

Table 4-19 Close cavity case CFD simulation matrix based on HFE with fixed thermal distant (*l*), variable heat flux (Q*) and variable aspect ratio (*h/l*)

Plot the temperature result points T_1 and T_y* of HFE fluid convection in close cavity convection:

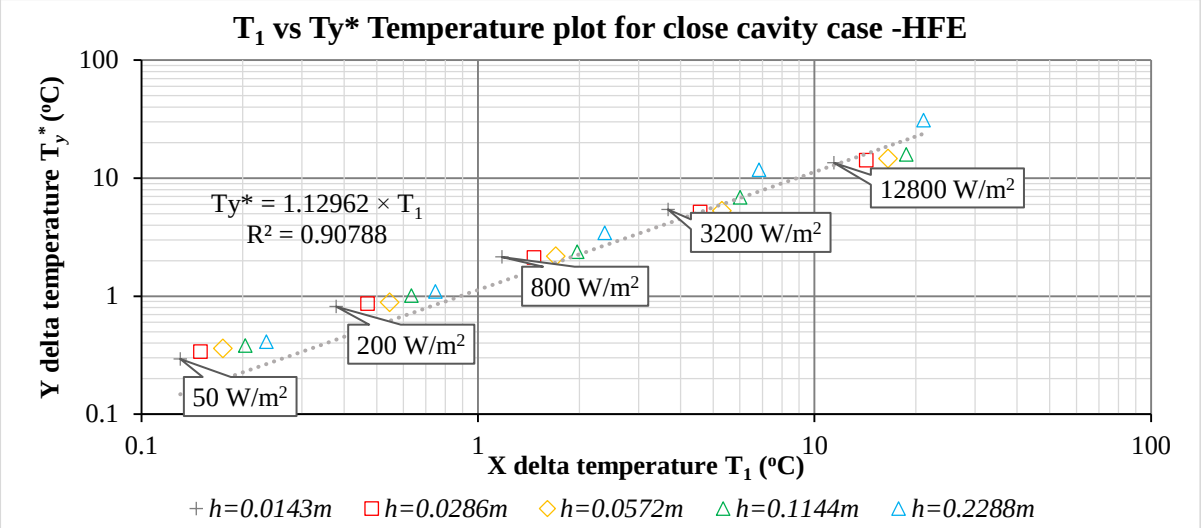

Figure 4-29 Close cavity case T_1 vs T_y* temperature plot based on HFE with fixed thermal distant (*l*), variable heat flux (Q*) and variable aspect ratio (*h/l*)

Gather all the temperature from different cases (water, air and HFE) and put them into the same plot.

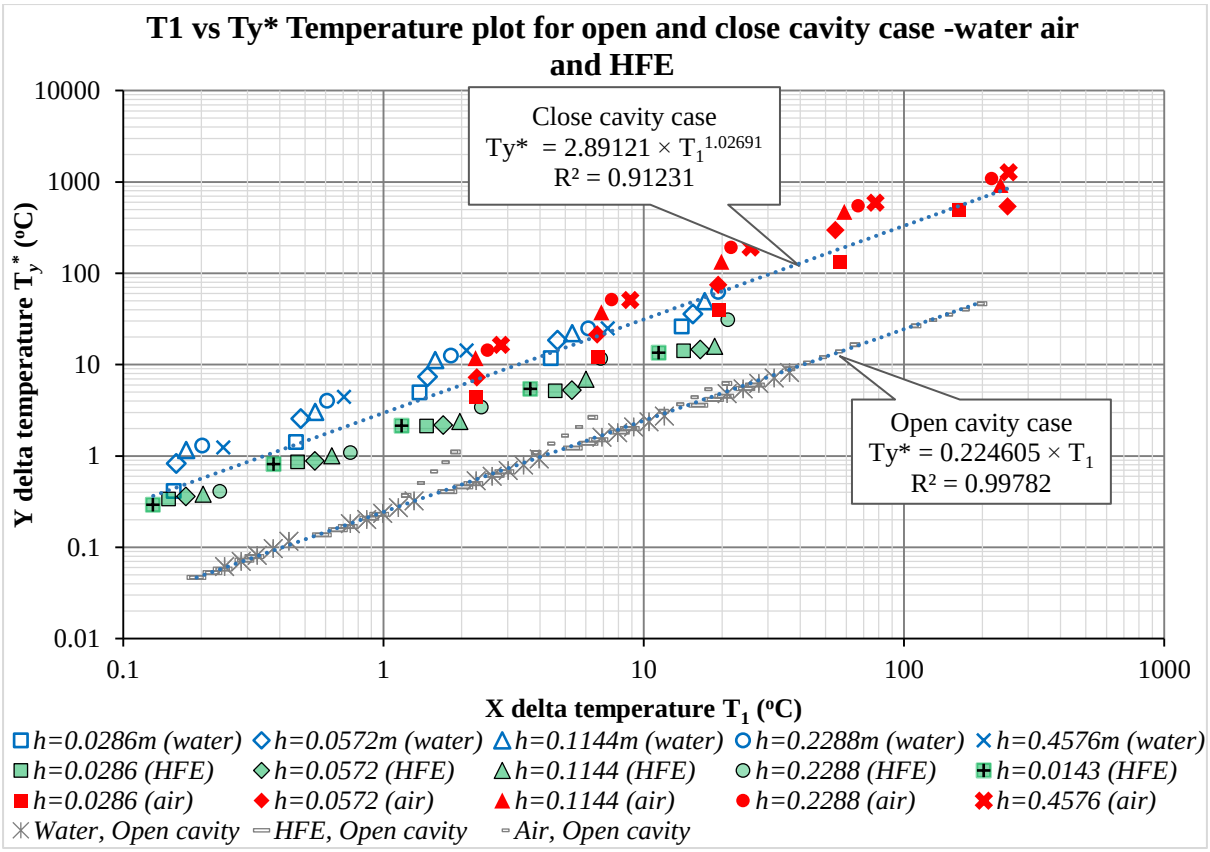

Figure 4-30 Close and Close cavity case T_1 vs T_y* temperature plot based on water, air and HFE with fixed thermal distant (*l*), variable heat flux (Q*) and variable aspect ratio (*h/l*)

I t can be seen from **Figure 4-30** that temperature plot has less consistency in close cavity convection cases than for the open cavity cases. This may due to the extra forced convection section from the top and bottom side of the close cavity cases, therefore using just one linear correlation to approximate the temperature field may result in a poor match.

In the previous section of open cavity natural convection case study, the Rayleigh number Ra_h with thermal height (*h*) is used for the heat transfer problem, and the Rayleigh number with thermal distant (*l*) is used to determine the flow regime. But that was based on the assumption that the thermal distant (*l*) is irrelevant to the heat transfer in the open cavity case ($l > 5\ l^*$). In the close cavity problem, if there is heat transfer in the vertical direction (across the gravity direction), that the thermal distant (*l*) in no longer independent, and it will affect both flow regime and heat transfer.

4.4 CTG model for the closed cavity problem

The CTG model is now applied to the closed cavity problem. Once again, a simple scalar correlation is used to approximate the X axis and Y axis temperature relationship with one constant parameter introduced for the solution.

To observe the impact of the thermal distant (*l*) on the CTG model solution a number of CFD simulations for close cavity natural convection with variable thermal distant (*l*), but fixed heat flux (Q*) and fixed thermal length (*h*) are presented.

Table 4-20 is the condition and solution table for the water convection case:

Boundary condition			Outcome				Others	
Heat flux	*l*	Aspect	T_1	$\partial T/\partial y$	T_y*	*l*/*l** ($Ra^{*0.25}$)	Error (1)	Case setup: Water
W/m^2	m	*h*/*l*	°C	°C/m	°C		%	
3200	∞	0	9.154	18.13	2.074	∞	5.47	Close Cavity
	4.58×10^{-1}	0.25	7.485	38.33	4.385	424.85	6.81	
	2.29×10^{-1}	0.5	7.227	43.76	5.006	219.6	6.99	Y*/*l** $<10^{-3}$
	1.14×10^{-1}	1	6.941	54.44	6.228	116	5.65	
	5.72×10^{-2}	2	6.471	80.98	9.265	64.03	2.85	Mesh count 512×512
	2.86×10^{-2}	6	5.88	128.4	14.69	35.92	0.97	
	1.43×10^{-2}	8	5.317	193	22.08	19.89	0.83	
	7.15×10^{-3}	16	5.548	216	24.71	10.29	6.43	Ref. point Y=0.5*h*
	3.58×10^{-3}	32	5.755	184.9	21.15	4.919	6.19	
	1.79×10^{-3}	64	6.041	175.2	20.04	2.426	9.98	
	8.94×10^{-4}	128	4.712	0.7152	0.0869	0.3104	78.1	

Table 4-20 Close cavity case CFD simulation matrix based on water with fixed heat flux (Q*) and fixed aspect ratio (*h*/*l*), but variable thermal distant (*l*)

Plot the temperature points (T_1 vs Ty*) with variable thermal distant (*l*) in red (dark) square dots. The back ground of the **Figure 4-31** is the open cavity and closed cavity with thermal distant (*l*) but different input heat flux (Q*) and different thermal length (*h*).

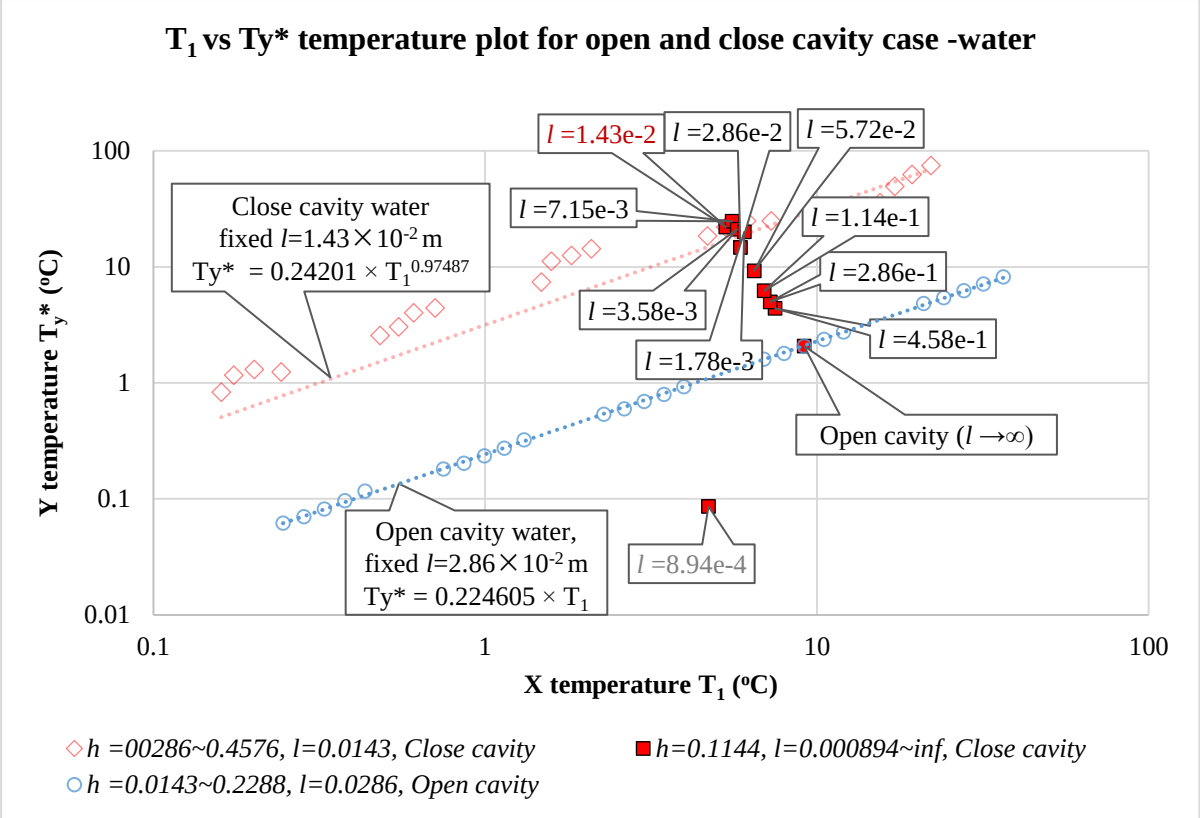

Figure 4-31 Close cavity case T_1 vs T_y* temperature plot based on water with fixed heat flux (Q*) and fixed aspect ratio (*h*/*l*), but variable thermal distant (*l*)

From **Figure 4-31**, the red (dark) square dot represents the CFD solution with different thermal distant (*l*) but same heat flux (Q) and same thermal length (*h*). This temperature points (T_1 vs Ty*) has a linear appearance, and there appears to be a linear relationship between the close cavity case and the open cavity case. And as the thermal length scale value *l*/*l** grows, the temperature point moves towards the open cavity solution. In order to have an approximation for the relationship between temperature scale and length scale of the close cavity problem 2 assumptions have been made here:

The inverse of thermal distant scale *l**/*l* would have a linear relationship with the slop ratio of the temperature scale Ty*/T_1.The temperature from the open cavity solution would be equivalent to a close cavity solution when $l \to \infty$, thus $l^*/l \to 0$.

It is also interesting to know that the thermal length scale *l** is an expression based on the vertical (along the gravity direction) thermal height *h* and vertical temperature Ty*, it represents the horizontal thickness of boundary layer in vertical natural / free convection flow. On the other hands the thermal distant *l* should be closely related to the horizontal forced convection flow of the case,

because they are in the same direction. The ratio between thermal length scale *l** and thermal distant *l* could be simply interpreted as the ratio between free convection and force convection.

The curve Ty^*/T_1 against l^*/l from the solution matrix (close cavity problem with water, various thermal distance *l*, fixed thermal height *h*, and fixed wall heat flux Q*) is plotted in **Figure 4-23**

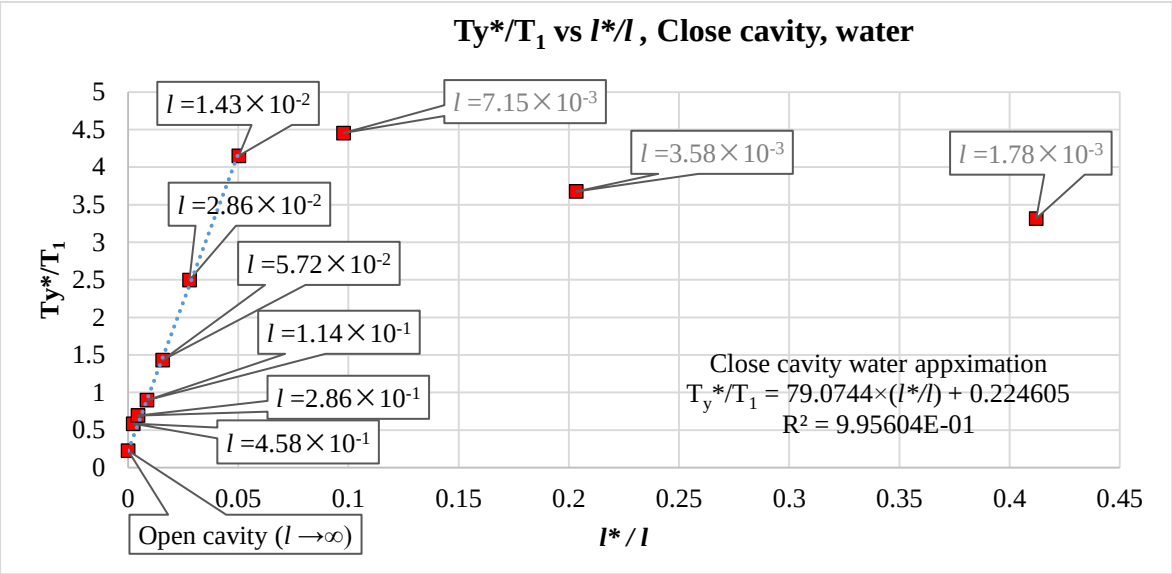

Figure 4-32 Close cavity case T_y^* / T_1 vs l^* / l plot based on water with fixed heat flux (Q*) and fixed aspect ratio (h/l), but variable thermal distance (l)

From the **Figure 4-23**, in the region $10\ l^* < l < \infty$, this section of T_y^* / T_1 vs l^* / l curve is approximately linear. The close cavity temperature approximation correlation can be given as:

$$\frac{T_y^*}{T_1} = \mathrm{K}_{close} \cdot \frac{l^*}{l} + C_{close}\,, \qquad \frac{l^*}{l} < 0.1 \tag{4-23}$$

When $0 < \frac{l^*}{l} < 0.1$, the correlation between temperature ratio Ty^*/T_1 and length scale ratio l^*/l seems to be linear and the temperature ratio Ty^*/T_1 would reach the maximum value with the thermal distant value between $0.1 < \frac{l^*}{l} < 0.5$.

And when the thermal distant (l) towards infinite vale, $l \to \infty$ and $\frac{l^*}{l} \to 0$ this correlation should be equivalent to the open cavity case, the constant for close cavity solution C_{close} should become the thermal gradient constant C_{TG} from the open cavity solution:

$$l \to 0\,, \qquad \frac{l^*}{l} = 0\,, \qquad \frac{T_y^*}{T_1} = C_{close} = C_{TG} \tag{4-24}$$

Also the scalar K_{close} can be estimated as:

$$\mathrm{K}_{close}(\text{water}) \approx 79.0744 \qquad \text{4-25}$$

Expand the close cavity temperature correlation **equation 4-25** with the specific length scale (l^*) equation:

$$l^* = \sqrt[-4]{\frac{\rho^2 \cdot g \cdot \beta \cdot C_p}{\mu \cdot \lambda} \cdot \frac{\partial T}{\partial y}} \qquad \text{4-26}$$

For close cavity problem, the thermal gradient $\partial T/\partial y$ is no longer linearly related to the heated wall temperature T_1, so it would be rewritten as the Y direction temperature difference over the thermal height of the case:

$$\frac{\partial T}{\partial y} \to \frac{T_y{}^*}{h}, \qquad l^* = \sqrt[-4]{\frac{\rho^2 \cdot g \cdot \beta \cdot C_p}{\mu \cdot \lambda} \cdot \frac{T_y{}^*}{h}} \qquad \text{4-27}$$

Put this back in the correlation **equation 4-21**:

$$\frac{T_y{}^*}{T_1} = \frac{\mathrm{K}_{close}}{l} \cdot \frac{1}{\sqrt[4]{\frac{\rho^2 \cdot g \cdot \beta \cdot C_p}{\mu \cdot \lambda} \cdot \frac{T_y{}^*}{h}}} + C_{TG} \qquad \text{4-28}$$

The **equation 4-28** is the general thermal gradient expression of CTG model for closed cavity natural convection. To make the model valid, 2 constants will be needed for the solution: The thermal gradient constant C_{TG} and the close cavity scalar. Notice that this model will also be valid for the open cavity solution, where the thermal distance is assumed to be infinite ($l \to \infty$), and the model collapses to a scalar model (**equation 4-4**):

$$\frac{T_y{}^*}{T_1} = C_{TG}$$

In this research, the thermal gradient constant value C_{TG}= 0.224605 is a least square approximation calculated from different CFD results. The close cavity scalar will be vary depending on the fluid properties, but it can use the same least square approximation method from different CFD results. For water this close cavity scalar is $K_{close\ water}$ = 79.0744

Also the Constant thermal gradient model expression can be rewritten as a 5th order quintic (polynomial) function of Y direction temperature if the T_1 temperature value is known (T_1 temperature solution):

$$0 = \left(\sqrt[4]{T_y{}^*}\right)^5 - C_{TG} \cdot T_1 \cdot \sqrt[4]{T_y{}^*} - \frac{\mathrm{K}_{close} \cdot T_1}{l} \cdot \frac{1}{\sqrt[4]{\frac{\rho^2 \cdot g \cdot \beta \cdot C_p}{\mu \cdot \lambda \cdot h}}} \qquad 4\text{-}29$$

Or combined with the energy equation, it became a 6 degree sextic (polynomial) function if only the heat flux value Q* is known (Q* is the heat flux solution):

$$0 = \left(\sqrt[4]{T_y{}^*}\right)^6 - \sqrt{2} \cdot \frac{Q^* \cdot C_{TG}}{\lambda} \cdot \frac{1}{\sqrt[4]{\frac{\rho^2 g\beta \cdot C_p}{\mu \cdot \lambda \cdot h}}} \cdot \sqrt[4]{T_y{}^*} - \sqrt{2} \cdot \frac{\mathrm{K}_{close} \cdot Q^*}{\lambda \cdot l} \cdot \frac{1}{\sqrt[2]{\frac{\rho^2 g\beta \cdot C_p}{\mu \cdot \lambda \cdot h}}} \qquad 4\text{-}30$$

In both **equations 4-29** and **equation 4-30** the only unknown variable is the Y direction delta temperature T_y*, it can be solved either by knowing the X direction delta temperature T_1 (**equations 4-29**), or the heated wall heat flux Q* (**equation 4-30**). These approximation equations are high degree polynomial functions and the solution can be obtained using Matlab.

To validate the model, a comparison between the CTG model solution and CFD temperature solution will be carried out. The CFD solution matrix will be using the one from the previous section (step 4, **Table 4-17**), and the CTG model will use the same input as the CFD solution (heat flux Q*, thermal distant *l* and thermal length *h*). Both CFD and CTG solutions will predict T_1 and T_y*, and the input and outcome matrix will be shown in the following table:

Input			Outcome (Close cavity, water)					
Heat flux	l	Aspect	CFD T_1	CTG model T_1	CFD $\partial T/\partial y$	CTG model $\partial T/\partial y$	CFD T_y*	CTG model T_y*
W/m^2	m	h/l	^oC	^oC	$^oC/m$	$^oC/m$	^oC	^oC
50	1.43 $\times 10^{-2}$	2	**0.1566**	**0.133**	14.42	30.39	**0.4123**	**0.87**
200			**0.4624**	**0.422**	49.78	77.04	**1.424**	**2.2**
800			**1.377**	**1.34**	174.1	195.59	**4.978**	**5.59**
3200			**4.406**	**4.23**	412.8	497.47	**11.8**	**14.23**
12800			**14.02**	**13.39**	914.7	1268.24	**26.16**	**36.27**
50		4	**0.1602**	**0.149**	14.51	19.1	**0.8301**	**1.09**
200			**0.4823**	**0.474**	44.74	48.38	**2.559**	**2.77**
800			**1.478**	**1.5**	129.1	122.73	**7.383**	**7.02**
3200			**4.678**	**4.76**	323.8	311.85	**18.52**	**17.84**
12800			**15.49**	**15.06**	626.6	794.05	**35.84**	**45.42**
50		8	**0.1747**	**0.168**	10.16	12	**1.162**	**1.37**
200			**0.5482**	**0.532**	26.59	30.39	**3.042**	**3.48**
800			**1.584**	**1.69**	98.09	77.04	**11.22**	**8.81**
3200			**5.317**	**5.34**	193	195.59	**22.08**	**22.38**
12800			**17.18**	**16.93**	432.7	497.48	**49.5**	**56.91**
50		16	**0.2016**	**0.188**	5.707	7.55	**1.306**	**1.73**
200			**0.6087**	**0.597**	17.55	19.1	**4.016**	**4.37**
800			**1.819**	**1.89**	54.77	48.38	**12.53**	**11.07**
3200			**6.133**	**6**	108.8	122.73	**24.9**	**28.08**
12800			**19.35**	**19.02**	273.8	311.85	**62.65**	**71.35**
50		32	**0.2427**	**0.212**	2.709	4.75	**1.24**	**2.17**
200			**0.706**	**0.671**	9.696	12	**4.437**	**5.49**
800			**2.092**	**2.13**	31.23	30.39	**14.29**	**13.91**
3200			**7.282**	**6.75**	54.43	77.04	**24.91**	**35.25**
12800			**22.06**	**21.37**	163.8	195.59	**74.95**	**89.5**

Table 4-21 Close cavity case CFD simulation and CTG model solution matrix based on water with fixed thermal distance (l), variable heat flux (Q*) and variable aspect ratio (h/l)

The plot of the Y axis temperature against the X axis temperature from both CFD solution and Constant thermal gradient model solution is given in **Figure 4-23**:

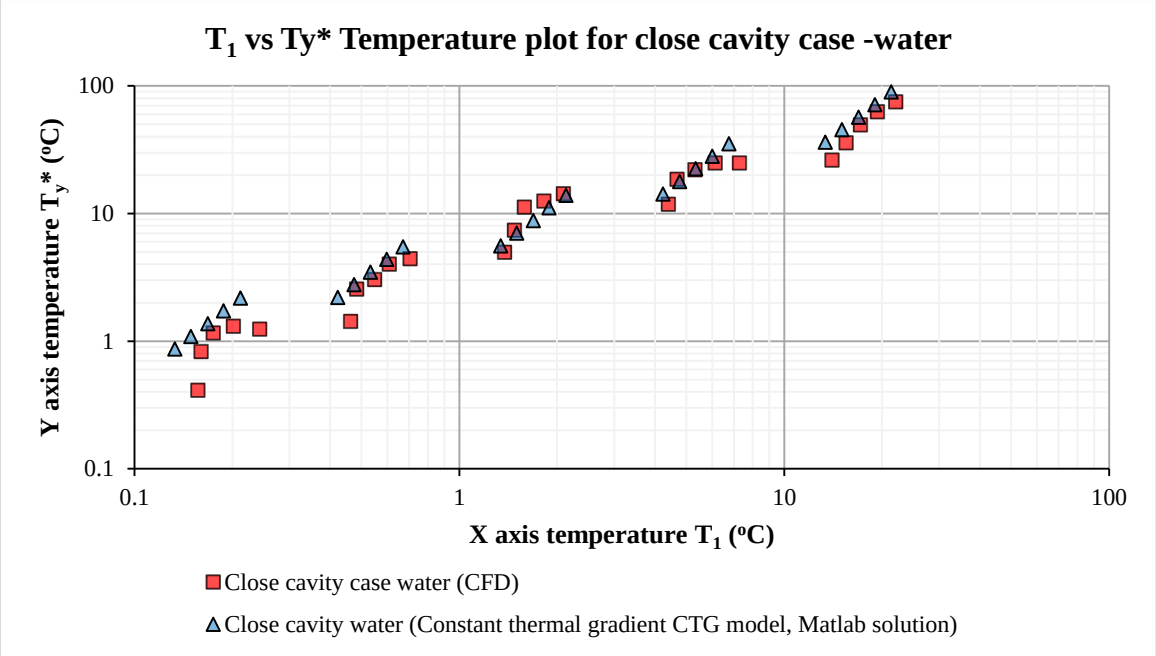

Figure 4-33 Close cavity case T_1 vs T_y* temperature plot based on water with fixed thermal distant (*l*), variable heat flux (Q*) and aspect ratio (*h/l*), CFD simulation and CTG model solution

It can be seen from **Figure 2-1** that the C_{TG} model has a reasonable good agreement with the CFD solution. From previously discussed in close cavity problem should be a combination of free convection in vertical direction and forced convection in horizontal direction, the relationship on both length scale should be more complex that a linear equation.

CTG model for closed cavity problem, HFE

Unlike the approximation for the open cavity solution that can use the same thermal gradient constant (C_{TG}) for all fluid (water, air and HFE), the approximation for close cavity scalar K_{close} cannot be universal for all fluids. This might be because the closed cavity problem is a combination of free convection and forced convection, the closed cavity scalar K_{close} may somehow be related to the ratio of free convection and forced convection, or related to the Prandtl number which refers to the ratio between viscous diffusion and thermal diffusion. But because only 3 types of fluid was used in the case study, it is difficult to find out the relationship between close cavity scalar K_{close} and Prandtl number Pr, so in here it only calculated the K_{close} value from the CFD solution.

A case study with different thermal distance (*l*) and same heated wall heat flux (Q*) and same thermal length (*h*) will be carried out. Here is the condition and solution table:

Boundary condition			Outcome				Others	
Heat flux	l	Aspect	T_1	$\partial T/\partial y$	T_y*	l/l* ($Ra^{*0.25}$)	Error (1)	Case setup: HFE
W/m^2	m	h/l	°C	°C/m	°C		%	
800	∞	0	8.117	15.99	2.074	N/a	9.67	Close Cavity
	1.14×10^{-1}	1	6.707	30.14	3.448	245	12.5	$Y^*/l^*<10^{-3}$
	5.72×10^{-2}	2	6.550	34.96	3.999	127	11.4	
	2.86×10^{-2}	6	6.328	39.20	4.484	65.3	11.9	Mesh count 512×512
	1.43×10^{-2}	8	6.333	45.88	5.248	34.0	8.28	
	7.15×10^{-3}	16	6.006	60.25	6.893	18.2	6.88	
	3.58×10^{-3}	32	5.579	99.41	11.37	10.3	1.96	Ref. point $Y=0.5h$
	1.79×10^{-3}	64	5.204	141.2	16.15	5.62	1.82	
	8.94×10^{-4}	128	5.181	177.7	20.32	2.98	5.26	
	4.47×10^{-4}	256	5.153	4.808	0.55	0.604	57.5	

Table 4-22 Close cavity case CFD simulation matrix based on HFE with fixed heat flux (Q*) and fixed aspect ratio (h/l), but variable thermal distant (l)

The following figures shows a plot of the temperature points (T_1 vs Ty*) from 4 fixed thermal distance (l) cases studies: open cavity with water, close cavity with water, open cavity with HFE and closed cavity HFE, along with a variable thermal distance (l) temperature result of HFE liquid closed cavity CFD solution:

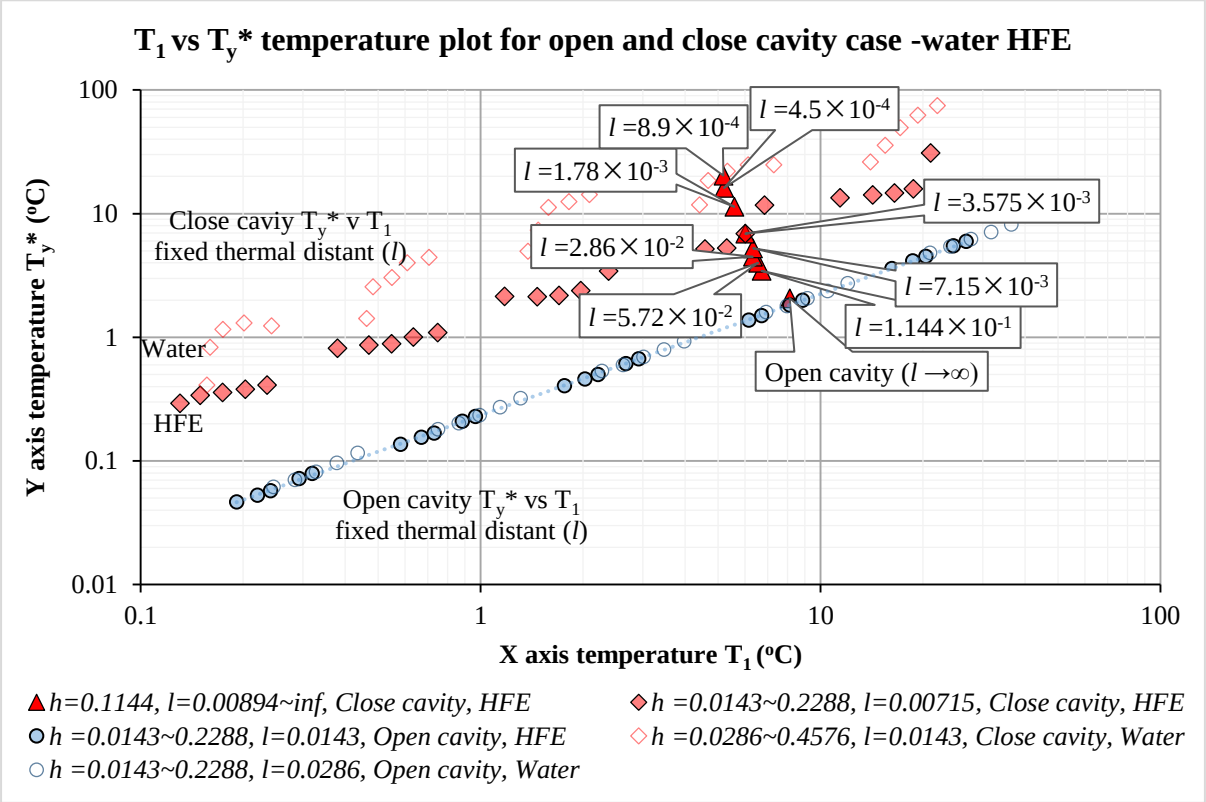

Figure 4-34 Closed cavity case T_1 vs T_y* temperature plot based on HFE with fixed heat flux (Q*) and fixed aspect ratio (h/l), but variable thermal distance (l)

It can be seen that the temperature plot with variable thermal distance (l) but the same thermal height (h) and heat flux (Q*) from the closed cavity HFE solution has a linear appearance similar to the close cavity water solution.

To obtain the close cavity temperature approximation correlation scale K_{close} (HFE), it will need the temperature curve T_y^*/T_1 against l^*/l from the solution matrix. Plot this curve from the CFD result with HFE liquid in blue (dark) triangle dots, (with various thermal distant l, fixed thermal height h, and fixed wall heat flux Q*), the back ground dots are the CFD result with water.

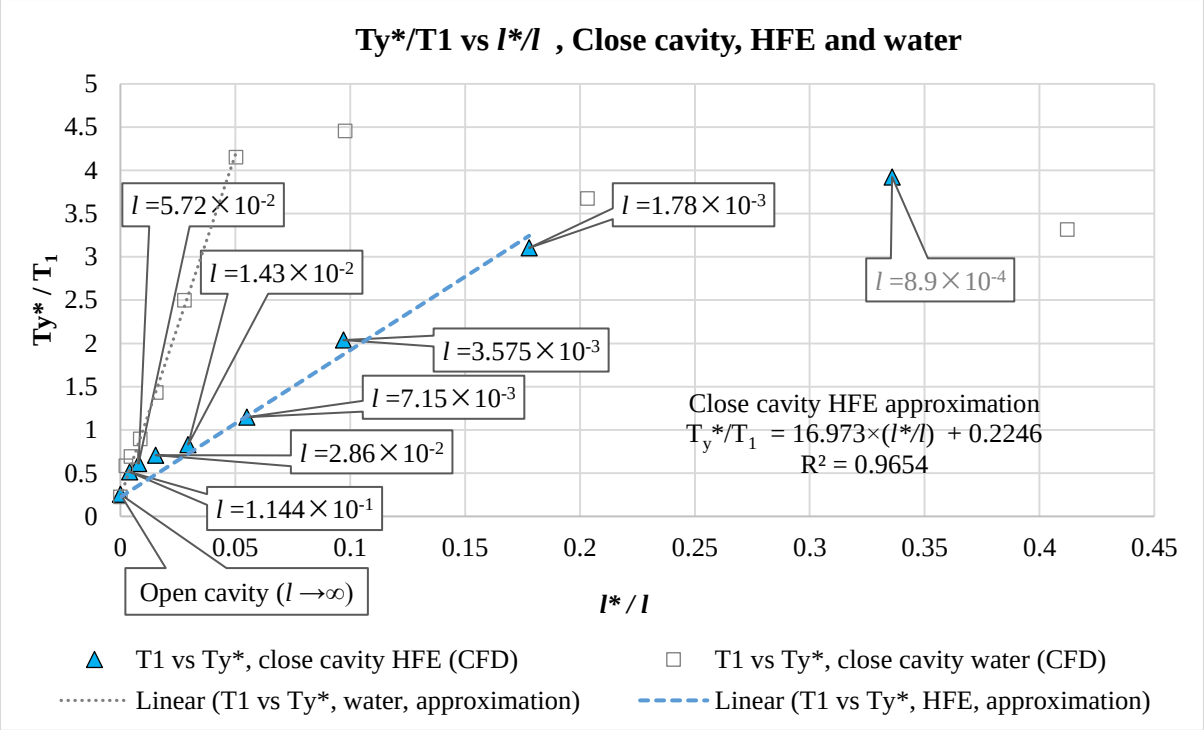

Figure 4-35 Close cavity case T_y^* / T_1 vs l^* / l plot based on HFE with fixed heat flux (Q*) and fixed aspect ratio (h/l), but variable thermal distant (l)

It can be seen that the temperature scale ratio against length scale ratio curve (T_y^* / T_1 vs l^* / l) with the HFE has quite a different slope from the curve with the water, therefore a different K_{close} value will be used for the close cavity HFE problem, which:

$$K_{close}(\text{HFE}) \approx 16.973 \qquad 4\text{-}31$$

There will be a comparison between the CTG model and CFD solutions for the HFE liquid. The CFD solution matrix will be using step 6, **Table 4-19**, and the CTG model will use the same input as the CFD solution (heat flux Q*, thermal distant l and thermal length h). Both CFD and CTG solutions will predict (T_1 and T_y^*), and the result are shown in the following table:

Input			Outcome (Close cavity, HFE)					
Heat flux	l	Aspect	CFD T_1	CTG model T_1	CFD $\partial T/\partial y$	CTG model $\partial T/\partial y$	CFD T_y*	CTG model T_y*
W/m^2	m	h/l	°C	°C	°C/m	°C/m	°C	°C
12.5	7.15 $\times 10^{-3}$	2	**0.1304**	**0.142**	20.52	15.29	**0.293**	**0.219**
50			**0.3792**	**0.448**	56.99	39.52	**0.815**	**0.565**
200			**1.1774**	**1.411**	150.0	102.8	**2.146**	**1.47**
800			**3.6679**	**4.44**	379.8	268.9	**5.432**	**3.85**
3200			**11.430**	**13.92**	942.2	709.4	**13.47**	**10.15**
12.5		4	**0.1496**	**0.16**	11.87	9.53	**0.3394**	**0.272**
50			**0.4692**	**0.504**	30.22	24.56	**0.8643**	**0.703**
200			**1.4677**	**1.59**	74.39	63.67	**2.127**	**1.82**
800			**4.5745**	**4.75**	180.8	166.1	**5.172**	**5**
3200			**14.240**	**15.72**	496.2	436.3	**14.19**	**12.48**
12.5		8	**0.1743**	**0.18**	6.283	5.94	**0.3594**	**0.34**
50			**0.5467**	**0.568**	15.48	15.29	**0.8855**	**0.874**
200			**1.7014**	**1.79**	38.15	39.5	**2.182**	**2.26**
800			**5.3036**	**5.64**	92.16	102.7	**5.271**	**5.88**
3200			**16.522**	**17.75**	256.5	268.9	**14.67**	**15.38**
12.5		16	**0.2032**	**0.202**	3.329	3.71	**0.3809**	**0.424**
50			**0.6344**	**0.639**	8.814	9.53	**1.008**	**1.09**
200			**1.9721**	**2.02**	20.81	24.56	**2.381**	**2.81**
800			**6.0057**	**6.40**	60.25	63.67	**6.893**	**7.28**
3200			**18.744**	**20.02**	138.7	166.1	**15.87**	**19**
12.5		32	**0.2353**	**0.227**	1.795	2.319	**0.4106**	**0.531**
50			**0.7477**	**0.719**	4.783	5.94	**1.094**	**1.36**
200			**2.3790**	**2.271**	15.03	15.29	**3.438**	**3.5**
800			**6.8408**	**7.17**	51.27	35.52	**11.73**	**9.04**
3200			**21.077**	**22.57**	135.6	102.7	**31.02**	**22.5**

Table 4-23 Close cavity case CFD simulation and CTG model solution matrix based on HFE with fixed thermal distant (l), variable heat flux (Q*) and variable aspect ratio (h/l)

The following **Figure 4-36** is a plot of the Y axis temperature against the X axis temperature from the CFD and CTG solutions for HFE liquid:

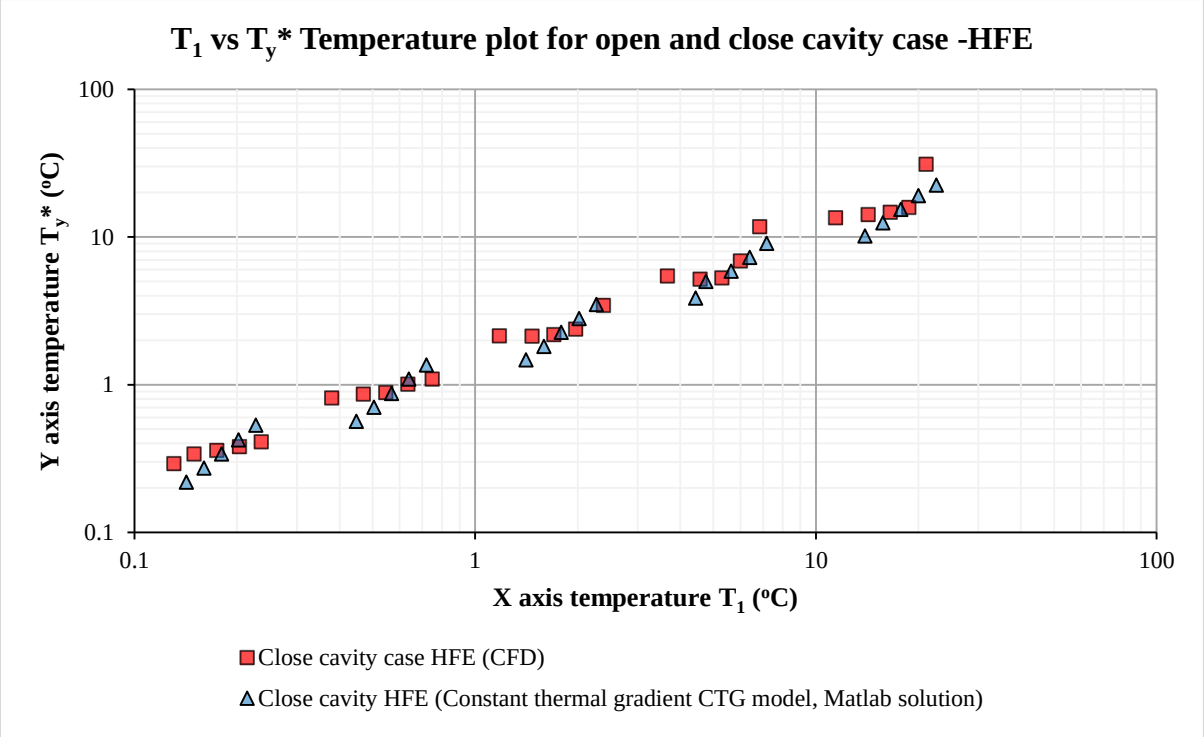

Figure 4-36 Close cavity case T_1 vs T_y* temperature plot based on HFE with fixed thermal distant (*l*), variable heat flux (Q*) and aspect ratio (*h/l*)

From the table **4-23** and figure **4-35** above, the CTG solution of the closed cavity problem with HFE liquid agrees reasonably with the CFD result. Though the CTG model for the closed cavity problem only added one more constant parameter (K_{close}, close cavity scale) to the open cavity solution, it gives a reasonable approximation to the CFD solution.

4.5 Summary

This chapter provides the thermal gradient value $\partial T/\partial y$ by introduction the thermal gradient constant C_{TG} to the open cavity solution. The CTG model and approximation seems to match Churchill & Chu's correlation of Nusselt number quite well.

For closed cavity problem a cavity scale parameter (K_{close}), is introduced to combine both free convection and forced convection; the approximation for close cavity problems is poorer and the close cavity scale (K_{close}) value will be different when different fluid is used.

The analytical solution of the CTG model of natural convection is:

$$u_y(x) = \frac{T_1 \sqrt[2]{-A \cdot C}}{2}\left[\frac{e^{(2l-x)\sqrt[4]{-A\cdot C}\cdot i} - e^{x\sqrt[4]{-A\cdot C}\cdot i}}{1 - e^{2l\sqrt[4]{-A\cdot C}\cdot i}} + \frac{e^{(2l-x)\sqrt[4]{-A\cdot C}} - e^{x\sqrt[4]{-A\cdot C}}}{e^{2l\sqrt[4]{A\cdot C}} - 1}\right]$$

$$T(x) = \frac{T_1}{A \cdot C}\left[\frac{e^{(2l-x)\sqrt[4]{-A\cdot C}\cdot i} - e^{x\sqrt[4]{-A\cdot C}\cdot i}}{1 - e^{2l\sqrt[4]{-A\cdot C}\cdot i}} - \frac{e^{(2l-x)\sqrt[4]{-A\cdot C}} + e^{x\sqrt[4]{-A\cdot C}}}{e^{2l\sqrt[4]{A\cdot C}} - 1}\right]$$

$$\mathrm{Q}^* \approx \frac{\lambda \cdot T_1}{\sqrt{2} \cdot l^*}$$

Where

$$l^* = \sqrt[-4]{A \cdot C}\,, \qquad A = \frac{\rho \cdot g \cdot \beta}{\mu}\,, \qquad C = \frac{C_p \cdot \rho}{\lambda} \cdot \frac{\partial T}{\partial y}$$

For the open cavity problem, the CTG model is:

$$\frac{\partial T}{\partial y} = \frac{T_y{}^*}{h} = \mathrm{C_{tc}} \cdot \frac{T_1}{h}\,, \qquad \mathrm{C_{TG}}^* = 0.224605\,, \qquad \frac{l}{l^*} > 5$$

And for close cavity problem, the complete CTG model (thermal gradient equation) is:

$$\frac{T_y{}^*}{T_1} = \mathrm{K}_{close} \cdot \frac{l^*}{l} + \mathrm{C_{TG}}^*\,, \qquad \frac{\partial T}{\partial y} = \frac{T_y{}^*}{h}, \qquad \frac{l}{l^*} > 10$$

And the close cavity scalar $\mathrm{K_{close}}$ is:

$$\mathrm{K}_{close}(\mathrm{water}) = 79.0744\,, \qquad \mathrm{K}_{close}(\mathrm{HFE}) = 16.973$$

Generally speaking the CTG model contains two temperature figures, one is vertical temperature distribution (along gravity direction) that uses a simple scalar (thermal gradient, $\partial T/\partial y$) to represent, and the other one is the horizontal temperature distribution (normal to gravity direction) derived from the solution of energy equation of the problem. A 2D temperature map and velocity profile can be calculated from the given fluid properties, cavity dimension and heat load.

For open cavity problem it is simple and straight forward, the relationship between T_1 and $T_y{}^*$ is a linear expression without the length scale involved, so a simple equation can have the temperature (T_1) vs heat flux (Q*) solution. For close cavity problem its more complex, the relationship between 2 temperature figures is non-linear and it requires solving a high degree polynomial functions (equation 4-27) in order to obtain a temperature (T_1) vs heat flux (Q*) solution. Notice that solution of a polynomial functions higher than 5 degree would be difficult to achieve. So rather than

spending time to solve difficult but known problem, in this thesis it uses computer assisted mathematics software to obtain the result.

The next chapter will use the CTG model in practice. It will be used to predict the thermal regime of a liquid-cooled computer system, and guide the selection of the convection boundary layer thickness for CFD meshing control.

5. Constant thermal gradient (CTG) model and CFD analysis compare with CFD analysis and laboratory experiment

The goal of this chapter is to develop an engineering methodology for predicting and analysing the thermal performance of the Iceotope liquid-cooled computer system. The fully immersed liquid-cooled system has as its core technology the self-contained computer node with Hydrofluoroether (HFE) or PFPE type of coolant, which relies on natural convection for waste heat removal in the first cooling stage. In order to achieve this, the thermal design of the system will be important since natural convection is unstable and difficult to analyse, this makes the design work critical to the fully-immersed liquid-cooled compute solution.

In previous chapter a Constant Thermal Gradient (CTG) model has been developed, with an approximated C_{TG} and K value this model can be used in predicting the natural convection flow heat transfer efficiency. And in this chapter, a heat transfer case study will be given to compare the CTG model prediction, the CFD analysis and the laboratory experiment. More important such pattern of prediction, analysis and experiment will form a work flow for establishing new design or improvement for fully-immersed liquid-cooled systems.

5.1 Overview of the problem setup

Natural convection is complicated by its instability and the difficulty of finding the right length scale and velocity scale for the specific problem. The natural convection flow, especially in an enclosed environment, would have a zero mean velocity due to its recalculating flow; so it would be difficult to obtain the reference velocity in the first place.

The CTG model is used to analyse the heat transfer problem. It can give heated wall temperature from the corresponding heat flux, as well as the free convection boundary layer thickness l^* as well. This could make the understanding of the convection flow easy and straight forward, and the boundary layer thickness l^* will be a very useful feature for validating the CFD meshing quality.

In this case study, a thermal experimental test has been setup in the Iceotope Company with a real running system, and in parallel a corresponding CFD model has been constructed to compare the experimental test data. In the CFD test the heat sink on the lower CPU has been switched to a cheaper alternative aluminium heat sink with thicker fins, instead of the original copper heat sink with thinner fins. And the result will be presented to the company for the consideration of their new design with reduced cost.

The experimental tests and analyses are based on a running computer thermal test system within Iceotope Ltd. It was a small scale liquid-cooled computer system (8-nodes rack) linked with a thermal controlled heat rejection unit that will provide a constant temperature water supply for the test.

A schematic diagram of the test device used for the CFD and experimental comparisons is given in **Figure 5-1**:

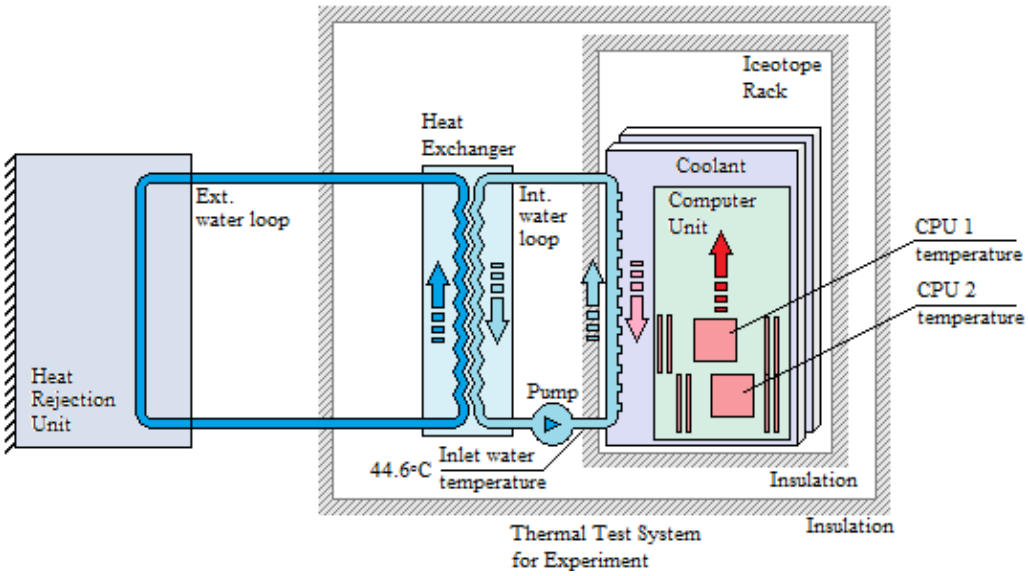

Figure 5-1 Schematic drawing of the thermal test system basic layout

The principles behind the system design have been discussed in the previous section of this thesis, so there is no need to explain it again. The thermal test system in this experiment was modified from a commercial based 1C system. The basic structure in terms of thermal design and mechanical design is based on the original commercial model, but the metal cover of the system has been removed and extra insulation has been added to improve the measurement accuracy. In total there are 2 more layers of insulation than a commercial unit: one layer of insulation added on each computer nodes so they does not significantly affect each other, another layer of insulation has been added from the outside to cover the whole system to prevent heat leakage to the ambient.

Another difference of the thermal test system compared to the commercial unit will be the electronic system, the power supply for the thermal test system use a laboratory power supply with higher power (voltage) accuracy instead of commercial power supply, and also a lab-view based sensor monitor system has been installed to the test unit.

Externally there is heat rejection unit / water chiller connected to the external water loop in order to provide a stable cooling for the test system. Notice that there is a heat exchanger to separate the

external and internal water systems, and in this research the only concern in the thermal test system, therefore the efficiency of the heat rejection unit is irrelevant. In fact, only the temperature and flow rate on the supply water from the heat exchanger (internal loop) to the computer node is fixed.

Requirement and description of the test

The goal of this part of the study is not just run the thermal test computer system; instead it will aim to provide an engineering procedure for the industry to predict the thermal performance of their design before putting together a real system and run a test traial. Commercial requirements, mean that the tests have to have relatively low economical cost and labour cost. Therefore the cost of the CFD simulation should not be significant higher than the experimental test. The resource spent on experimental test is easy to track and record, while the CFD simulation software and computing resource is difficult to calculate. So only the labour time of the CFD simulation and experimental test will be recorded and compared in this study.

The core part of the test is experiment and analysis the cooling performance of the computer system (**Figure 5-2**, **Figure 5-3**), in this test an Intel based server board computer has been used. The choice of mother board is Intel S2600 series server board, with 2 Intel Xeon E2690-v3 CPUs on it.

Figure 5-2 Intel S2600 series motherboard real item top view photo

The temperature and heat load on the CPUs will be the major observation point since they will have the most critical condition among all components / heat source in the system. The detailed heat motherboard component load will be shown in **Table 5-1**:

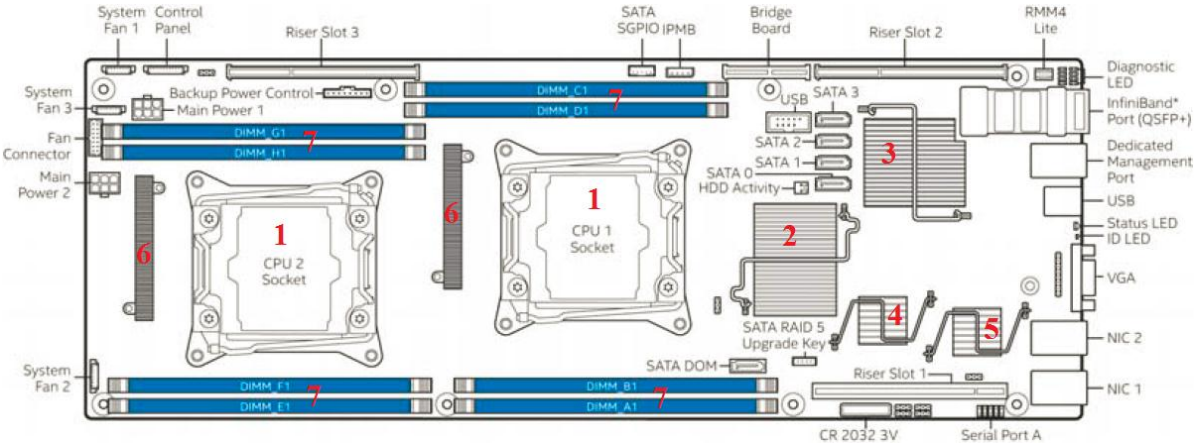

Figure 5-3 Schematic drawing of the server motherboard with numbering indicate the heat load components described in Table 5-1

	Type	Make	Model	Quantity	TDP	Sub Total	T max
	MotherBoard	Intel	S2600 series	1			
1	CPU	Intel	E5-2690-v3	2	135 W	270W	99 ºC
2	Chipset	Intel	Intel C600/612	1		69 W	>90 ºC
3	BMC chip			1			>90 ºC
4	Ethernet controller		Intel I350	1			>90 ºC
5	Video chip		Matrox G200	1			>90 ºC
6	Voltage regulater	N/a	N/a	2	10W	20 W	>100 ºC
7	DDR3 memory	Samsung	8GB	8	5W	40 W	>90 ºC
Total						399 W	

Table 5-1 Computer server board with major component heat load data, component refers to Figure 5-3. Notice TDP refers to Thermal-Design-Power

Only 2 motherboards with identical configuration are used in the test, the water supply temperature measured from the exit of the heat exchanger is 44.6 ºC, with a flow rate about 4L/min, and the water flow rate to each single system will be 2L/min. The test / benchmark software is the Power Thermal Utility (Intel PTU) for the Xeon series CPUs, which can provide an ideal heat load to the major components as well as temperature and power load tracking of the components as well.

The heat sink used in the test is one important factor, the original fully immersed liquid-cooled compute system uses a copper heat sink (90 ×90mm base) with thin skived fins (0.3mm thickness × 75 fins). This is a relatively expensive heat sink with large surface area. Because the fully immersed liquid-cooled computer node positioned the motherboard vertically in the coolant container and relay on natural convection to cool it down, it will be reasonable to assume the lower processor (CPU #2) has lower temperature than the higher processor (CPU #1). So it may be possible to replace the lower processor heat sink from a high cost copper heat sink with a lower

cost aluminium heat sink (0.6mm thickness × 16 fins), and as long as all processors retain its temperature below the design tolerance temperature.

Schematic drawing of the processor heat sink will be using in the following test

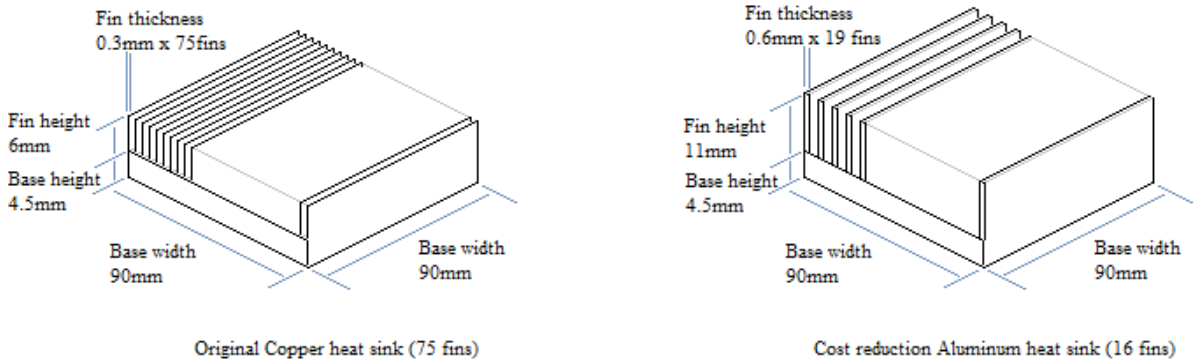

Figure 5-4 Schematic drawing of copper heat sink and 'reduce cost' aluminum heat sink

The copper heat sink (thin fin) in the left has a surface area about 0.0971m^2, and the aluminium heat sink heat sink (thick fin) in the right has a surface area about 0.0426 m^2 (**Figure 5-5**)

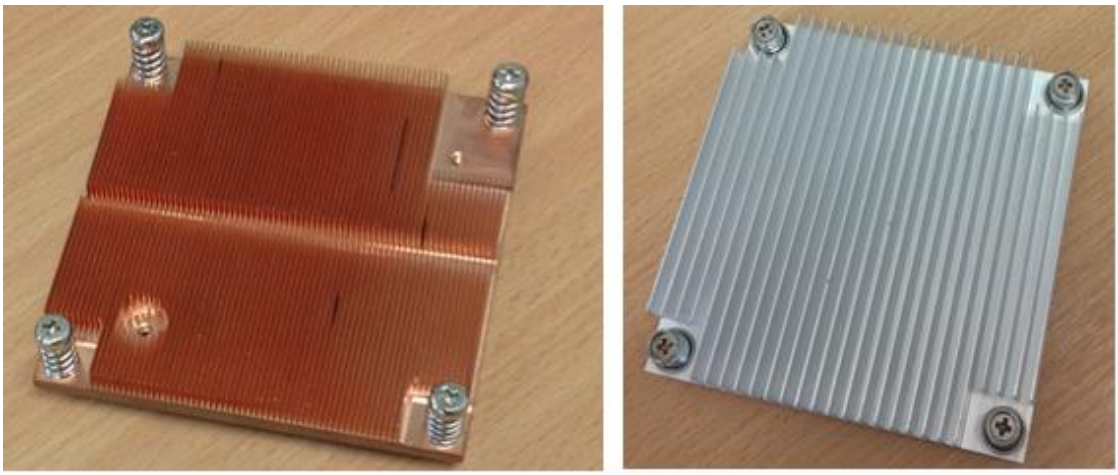

Figure 5-5 The copper heat sink (left) and 'reduce cost' aluminum heat sink (right)

In parallel, a CFD model will be constructed to simulate the heat transfer of the system and the choice of CFD software will be CFX. The reason to choose CFX is because its user friendly interface to industry, which the sponsor company of this thesis has experience to operate this software as well.

In the previous sections of the research only laminar (non-turbulent) model has been used, but in this part of the work comparison simulation between laminar and K-omega (SST) turbulent model will be carried out as well.

To configure the numerical model for the test, the dimension and geometry of the system will be needed. Usually CFD simulation for natural convection is sensitive and unstable, so the geometry of the model needs to be simplified to allow ideal mesh quality and resolution for the simulation. Thus only important dimension will be retained in the model, most of unnecessary detail can be simplified.

Here is the basic layout, orientation and dimension of the fully immersed liquid-cooled computer node (**Figure 5-6**):

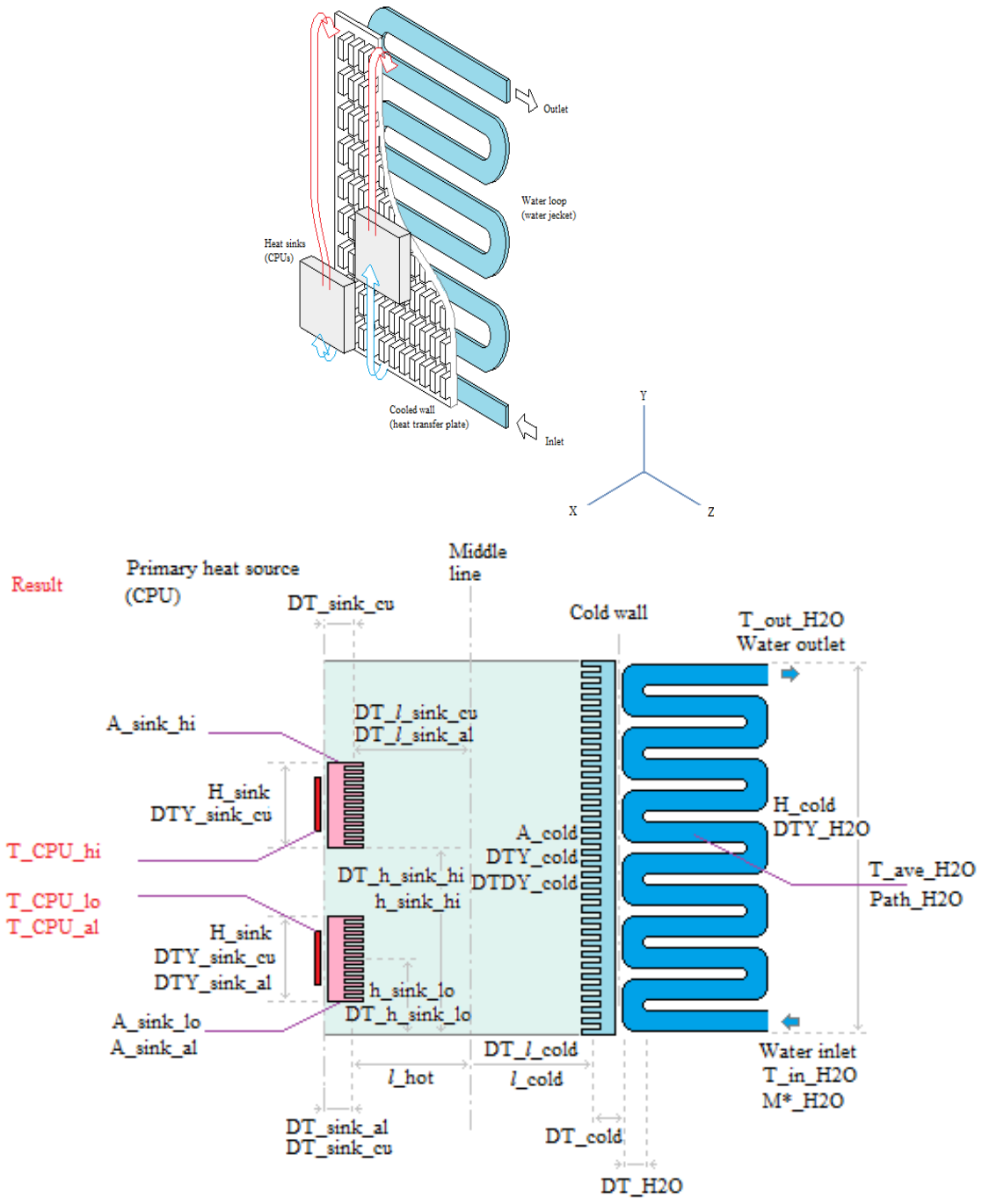

Figure 5-6 Schematic drawing of the internal layout and dimensions of the fully immersed liquid-

cooled computer node

It is also important to know that in the fully immersed liquid-cooled computer node the coolant is not filled to the top level, it usually left about 10%~30% empty as an expansion gap for the system (filled to 380mm in this case). The cooled side (with water jacket) of the system internal will have fins and extension surface as well, the surface area that submerged in the coolant is about 0.2564 m^2.

The choice of the coolant will be a custom blend of Solvay Galden Perfluoropolyether Fluorinated (PFPE) Fluids. Through the Perfluoropolyether liquid has different chemical formula from the hydrofluoroether liquid, it has similar physical property and in most condition they can be interchangeable.

The choice of liquid reference temperature is 60 ^oC. Notice that the PFPE liquid viscosity has a non-linear dependence on temperature (Solvay, 2015) but quite linear density changes vs temperature, it can be calculated as:

$$\text{Viscosity (CSt)} = (2.307499 \times \ln K - 11.99818)^{-2.175805} \quad 5\text{-}1$$

$$\text{Density } \rho = 2286.3 - 2 \times K \quad 5\text{-}2$$

Here K is the temperature in Kelvin. In the following Table 5-2 the density and viscosity of the PFPE liquid is calculated by **equation 5-1** and **equation 5-2**.

Table of liquid properties:

Prosperities and Constants (20^{o}C)							
	Density	Dynamic Viscosity	Thermal Conductivity	SHC	Thermal Expansion	Prandtl number	Reference temperature
	ρ	μ	λ	C_p	β	Pr	T_0
	kg/m^3	Pa.s	W/m.K	J/kg.K	1/K		^{o}C
Water	ρ_H2O 997.05	μ_H2O 8.874×10^{-4}	λ_ H2O 0.613	SHC_ H2O 4181	β_ H2O 2.07×10^{-4}	6~7	T_0_ H2O 25
HFE	1660	1.179×10^{-3}	0.069	1140	1.451×10^{-3}	19.47	25
	1572.2	6.731×10^{-4}	0.063	1140	1.526×10^{-3}		60
PFPE	1690	1.268×10^{-3}	0.065	971.3	1.01×10^{-3}	17.26	25
	ρ_PFPE 1620	**μ_PFPE 7.745×10^{-4}**	**λ_PFPE 0.063**	**SHC_PFPE 1078**	***β_PFPE* 1.235×10^{-3}**		**T_0_PFPE 60**

Table 5-2 Table of general fluid properties for the case study

Up to this point, all the detail and data that require for modelling has collected and ready to procced to the next part of calculation.

	Configuration	CTG model	CFD model	Experiment
Normal node	CPU 1 copper CPU 2 copper	Yes	Laminar and SST	Yes
Reduce cost node	CPU 1 copper CPU 2 aluminium	Yes	Laminar	No

Table 5-3 CFD simulation plan / schedule

5.2 CFD solution based on the CTG model

Before constructing the CFD model, a numerical solution based on the Constant Thermal gradient model will be carried out to get the approximate reference temperature ($T_{reference}$), CPU temperature, temperature gradient (Y axis) and the free convection boundary layer thickness . Having this number calculated before the CFD modelling will help building mesh and reduce the model setup time, therefore reduce the time consumption of the work.

Thermal performance prediction based on CTG model

Gather all geometry dimensions together, the surface area can be obtain from the heat sink geometry in figure 5-4, the heat load of each heat sink will be the CPU's TDP value, then the heat flux on the heat sink surface can be calculated from the heat flux and surface area. The thermal distance (*l*) is the half distance from the fin centre to the cooled wall from the figure 5-6. And the thermal length (*h*) is the base width of the heat sink in the figure 5-4. With the heat flux (Q*), thermal distant (*l*) and thermal height (*h*), the temperature of the heat sink can be calculated with the thermal gradient (CTG) model

Solid body dimension & condition	Load	area	Heat flux	Middle line distant	Height	Y axis location
	Q		Q*	*l*	*h*	$Y_{(part)}$
	W	m^2	W/m^2	m	m	m
Cooled wall	Q'_cold 399	A_cold 0.2564	**Q*_cold 1556.16**	***l*_cold 0.00925**	**H_cold 0.38**	h_cold 0.190
Heat sink low (cooper)	Q'_sink 135	A_sink_lo 0.0971	**Q*_cu 1390.32**	***l*_hot 0.00925**	**H_sink 0.09**	h_sink_lo 0.08724
Heat sink high (copper)		A_sink_hi 0.0971				h_sink_hi 0.21521
Heat sink low (Aluminium)		A_sink_al 0.0426	**Q*_al 3169.01**			h_sink_lo 0.08724

Table 5-4 Metal heatsink basic dimension and heat load

Then the solid material temperature gain $\mathbf{T_{solid}}$ can be calculated:

	Material	Thermal conductivity	Average thickness	Area (base)	Load	Heat flux (base)	Temperature increase T_{solid}
unit		W/(m.K)	m	m^2	W	W/m2	^oC
Cooled wall	Al	λ_AL 237	l_t_cold 0.00385	A_base_cold 0.076	Q'_cold 399	Q*_base_cold 5250	**DT_cold 0.09**
Heat sink (thin)	Cu	λ_Cu 401	l_t_sink_cu 0.0075	A_base_sink 0.0081	Q'_sink 135	Q*_base_sink 1.67×10^4	**DT_sink_cu 0.3**
Heat sink (thick)	Al	λ_AL 237	l_t_sink_al 0.01				**DT_sink_al 0.7**

Table 5-5 Conduction calculation of the heat sink

Here is the table of water thermal properties and result $\mathbf{Ty_{water}}$ based on Specific Heat Capacity:

Water data properties	SHC	Flow rate	Inlet temperature	Outlet temperature	DT/DY (water)	Wall height	Water Ty
Unit	J/kg.K	L/min	^oC	^oC	^oC /m	m	^oC
	SHC_ H2O 4181	M*_H2O 2	T_in_H2O 44.6	T_out_H2O 47.62	DTDY_H2O 7.945	H_H2O 0.38	**DTY_H2O 3.02**

Table 5-6 Water temperature calculated from the flow rate

On the cooled wall side with a water jacket, it is necessary to calculate the temperature increase due to forced convection. In this section the forced convection Nusselt number (Nu_D) is correlated with the Reynolds number (Re_D) to approximate the corresponding temperature difference of the water-to-metal interface:

$$\mathrm{Nu}_D = 0.023 \times \mathrm{Re}_D^{\frac{4}{5}} \times \mathrm{Pr}_{water} = \frac{Q^* \times \text{thickness}}{T} \quad 5\text{-}3$$

$$\mathrm{Re}_D = \frac{\rho \times v \times D}{\mu} \quad 5\text{-}4$$

There are the Reynolds number for circular pipe and the Dittus-Boelter equation (Equation 5-2, Incropera, 2007) approximation for Nusselt number. But these 2 equations require a circular cross-section and the water jacket cross-section is close to rectangular shape. So a transformation equation to give the equivalent shape / flow velocity scale will be needed (White, 2011):

$$\mathrm{D} \approx 2 \times \frac{\text{thickness} \times \text{width}}{\text{thickness} + \text{width}} \quad 5\text{-}5$$

Here is the Schematic drawing of the water channel of the computer node. Noticed that is not completely rectangular shape so the cross-section area is slightly less than thickness × width:

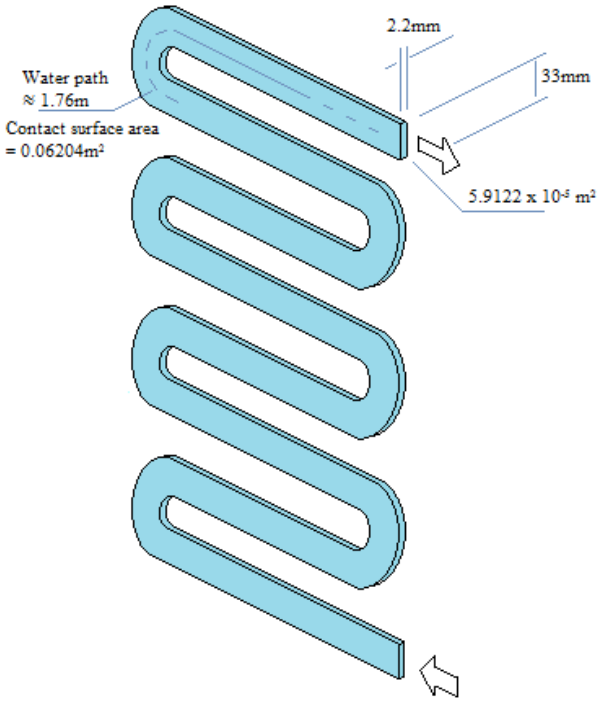

Figure 5-7 Schematic drawing of the cooling water volume with dimensions

So the table of force convection calculation and interface temperature $\mathbf{T_{face}}$ result will be:

Force convection	Heat load	Contact Area	Flux	Flow rate	Velocity	
Unit	W	m^2	W/m^2	L/min	m/s	
	Q'_cold 399	A_H2O 0.06204	Q*_H2O 6431	M*_H2O 2	U_H2O 0.564	
Force convection	Water path lengtyh	Cross section Diameter	Nu	Re	Pr	Interface temperature
Unit	m	Mm				°C
	Path_H2O 1.76	D_H2O 8.26	Nu_H2O 50.11	Re_H2O 5626	Pr_H2O ≈7	**DT_H2O 0.283**

Figure 5-8 Water temperature delta calculated from the Dittus-Boelter equation

The design of the water channel on the cooling loop of the Iceotope liquid-cooled node is reasonable long with extended surface, it should have little heat resistance and lead to little additional temperature increase.

Now all data for the computer module temperature calculation is ready. The CPU to heat sink interface temperature can be calculated from the (CTG) model. Because only temperature result is needed, only the energy **equation 3-131** and thermal gradient **equation 4-25** will be used:

$$Q^* \approx \frac{\lambda \cdot T_1}{\sqrt{2}} \sqrt[4]{\frac{\rho^2 \cdot g \cdot \beta \cdot C_p}{\mu \cdot \lambda} \cdot \frac{T_y^*}{h}}$$

$$\frac{T_y{}^*}{T_1} = \frac{\mathrm{K}_{close}}{l \cdot \sqrt[4]{\frac{\rho^2 \cdot g \cdot \beta \cdot C_p}{\mu \cdot \lambda} \cdot \frac{T_y{}^*}{h}}} + C_{close}\,, \qquad \mathrm{C_{TG}}^* = 0.224605\,, \qquad \mathrm{K}_{close}(\mathrm{HFE}) = 16.973$$

$$0 = \left(\sqrt[4]{T_y{}^*}\right)^6 - \sqrt{2} \cdot \frac{Q^* \cdot C_{TG}}{\lambda \cdot \sqrt[4]{\frac{\rho^2 g \cdot \beta \cdot C_p}{\mu \cdot \lambda \cdot h}}} \cdot \sqrt[4]{T_y{}^*} - \sqrt{2} \cdot \frac{\mathrm{K}_{close} \cdot Q^*}{\lambda \cdot l \cdot \sqrt[2]{\frac{\rho^2 g \cdot \beta \cdot C_p}{\mu \cdot \lambda \cdot h}}} \qquad 5\text{-}6$$

Notice that these 2 equations form a high degree polynomial expression, and have an analytical solution (by Matlab in this case). The result matrix shows as:

CTG model calculation	Input			Output			
	Q*	*l*	*H*	**T_Y***	**T_1**	**DT/DY**	***l****
	W/m^2	m	M	°C	°C	°C/m	mm
Cold plate	Q*_cold 1556.16	*l*_cold 0.00925	H_cold 0.38	**DTY_cold 15.41**	**DT_*l*_cold 15.12**	**DTDY_cold 40.56**	**0.43**
Copper Heat sink	Q*_cu 1390.32	*l*_hot 0.00925	H_sink 0.09	**DTY_sink_cu 9.05**	**DT_*l*_sink_cu 10.77**	**DTDY_cu 100.61**	**0.35**
Aluminium Heat sink	Q*_al 3169.01	*l*_hot 0.00925	H_sink 0.09	**DTY_sink_al 16.3**	**DT_*l*_sink_al 21.18**	**DTDY_al 181.42**	**0.44**

Thermal stack calculation						
Input	Copper heat sink low		Aluminium heat sink low		Copper heat sink high	
	T_in_H20	44.6				
	DTY_H2O × 0.5	3.02 × 0.5				
	DT_H2O	0.283				
	DT_cold	0.09				
	DT_*l*_cold	15.12				
	DT_*l*_cu	10.77	DT_*l*_al	21.18	DT_*l*_cu	10.77
	DTDY_cold × h_sink_lo	40.56 ×0.04224			D DTDY_cold × h_sink_hi	40.56 × 0.1702
	DTY_sink_cu	9.05	DTY_sink_al	16.3	DTY_sink_cu	9.05
	DT_sink_cu	0.3	DT_sink_al	0.7	DT_sink_cu	0.3
Output (Sum)	**T_CPU_lo**	**83.44**	**T_CPU_al**	**101.5**	**T_CPU_hi**	**88.63**
Thermal resistance	**R_CPU_lo (°C/W)**	**0.2877**	**R_CPU_al (°C/W)**	**0.4215**	**R_CPU_hi (°C/W)**	**0.3262**

Table 5-7 CTG model calculation of heat sink temperature

Notice that the upper CPU (1) is pre-heated by the lower CPU (2), but it is difficult to calculate the pre-heated value with the simple CTG model. Ideally the heat transfer of 2 separated but vertically stacked heat sinks could be considered as one single heat sink with double thermal height (*h*), and

in this way the pre-heated upper CPU (1) heat sink can be taken as the upper half of the elongated counterpart.

The calculation of CPU temperature and characteristic length scale *l** is now known. The exact average coolant temperature would be difficult to obtain, but since the hottest part in the coolant is about 90 ^{o}C and the coldest part is about 45^{o}C, it is reasonable to use a middle temperature T_0=60^{o}C as the reference (average) temperature for the latter on CFD modelling. Also the characteristic length scale (boundary layer thickness) *l** is given between 0.31~0.43mm, so the first layer mesh thickness Y* must be smaller than the *l** value. And for greater reliability of the CFD solution, the Y*/*l** should be close to 0.1

The next step is to build a CFD model and compare the temperature calculation from CTG model. Also the reference temperature and the length scale (*l*) obtained from the CTG model will be a useful guide for CFD meshing and modelling.

Construction and running the CFD model

In this part of the study a series of CFD simulation will be using CFX, and a laminar / K-omega (SST) turbulence model. In general the CFD modelling for natural convection flow has convergence problems due to its 4-th order nature. Also K-omega (SST) turbulent model is a 2-equation single order (only have 1st order velocity term) system, it might not able to reduce the instability of a 4-order system such as natural convection flow.

Step 1, Create geometry

The first step of the work will be building the geometry model for the CFD simulation. In order to have an all-hexahedral and all-sweep mesh for better convergence, only simple shape and important feature has retained in the geometry of the model:

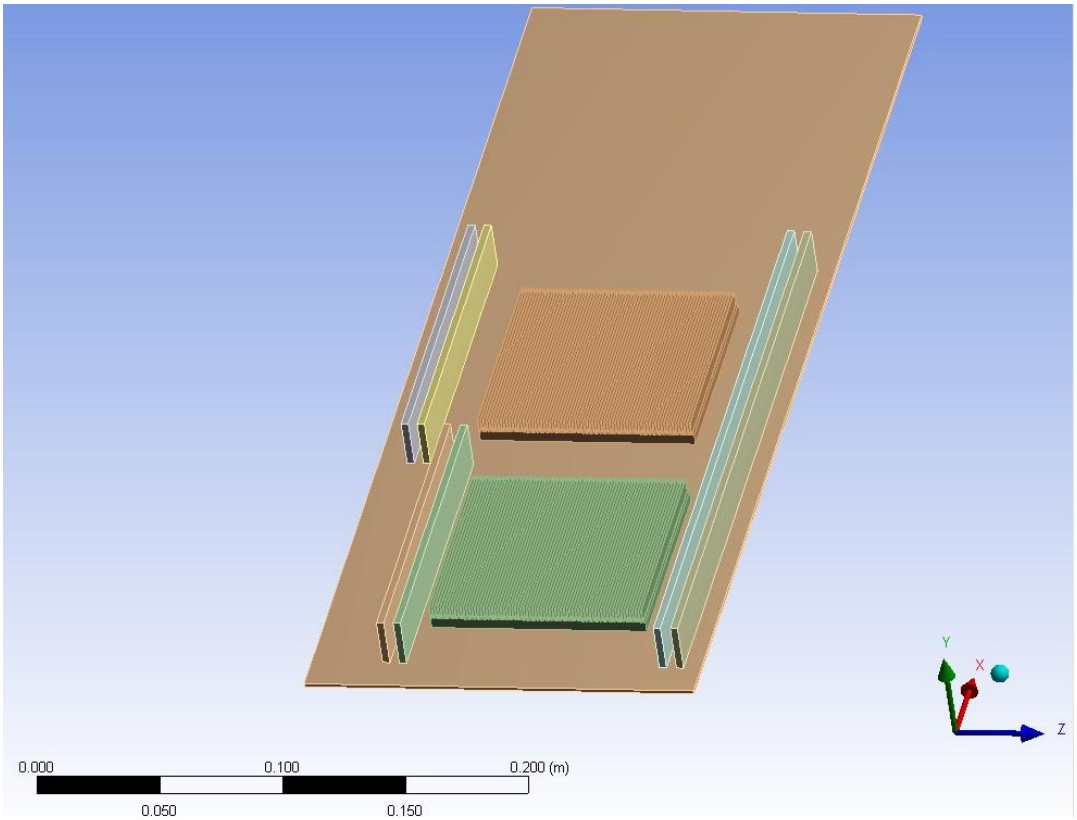

Figure 5-9 3D geometry model for CFD simulation

In the mother board geometry for CFD modelling, only the CPU, heat sink and dimms have been retained.

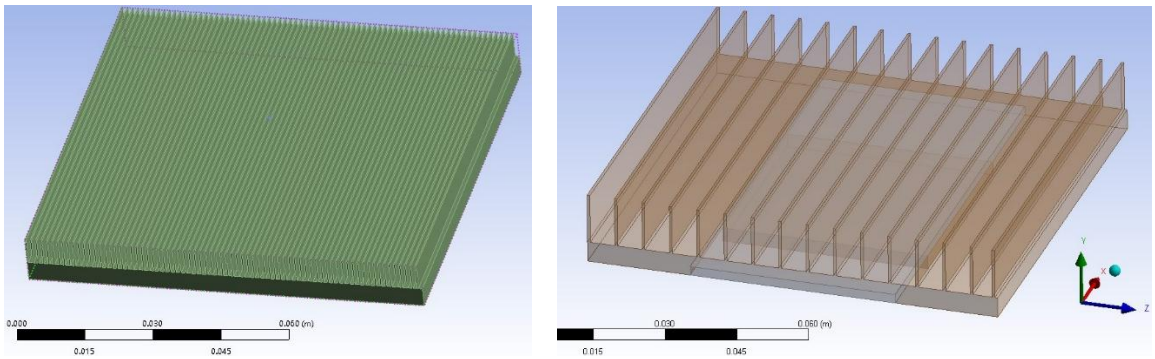

Figure 5-10 3D geometry of copper heat sink and ‘reduce cost’ aluminum heat sink

The figure 5-10 is the detail of CPU heat sink geometry, left hand side is the thin fin copper heat sink, right hand side is the thick fin aluminium heat sink.

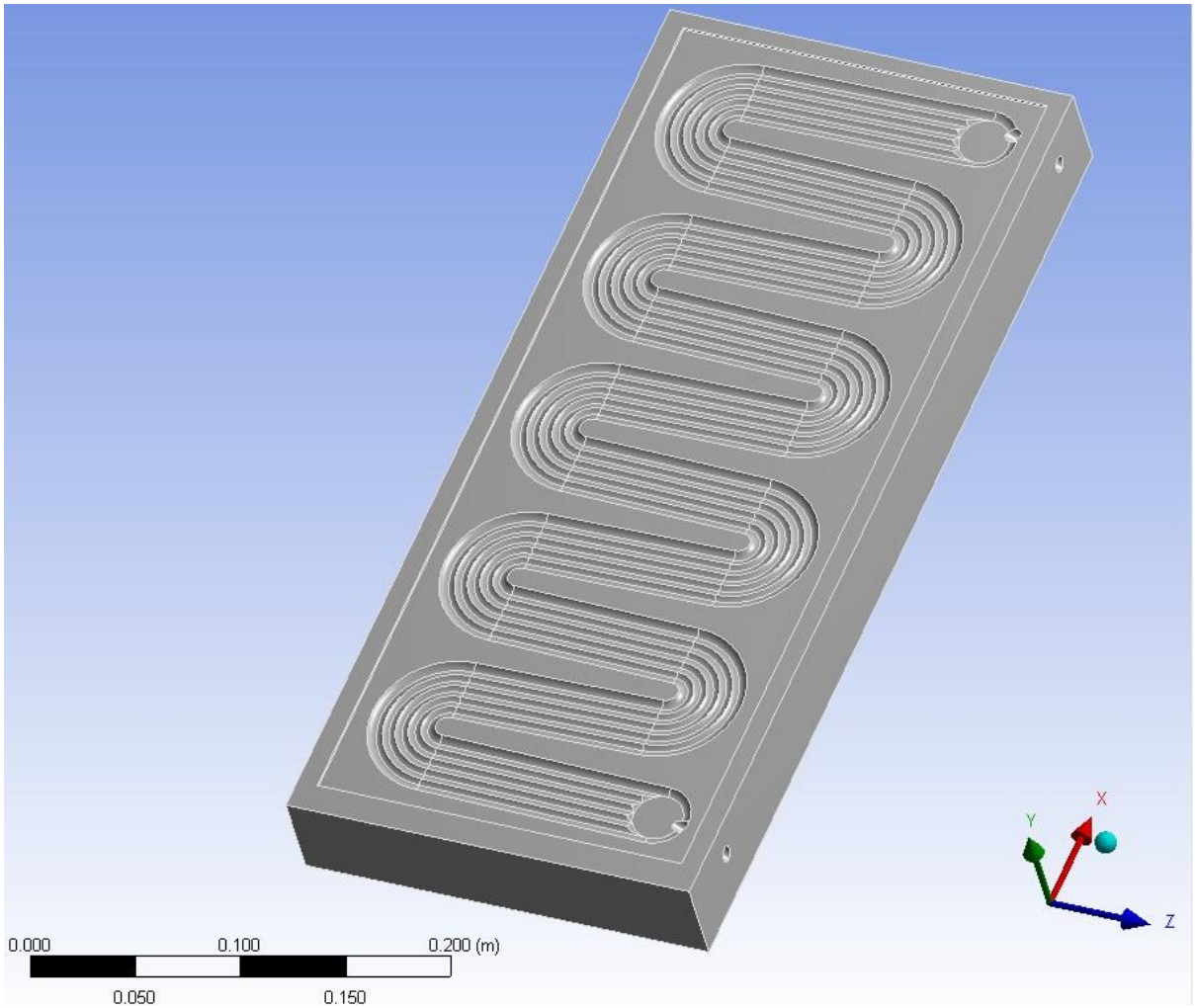

Figure 5-11 3D geometry of computer node container with water channel detail

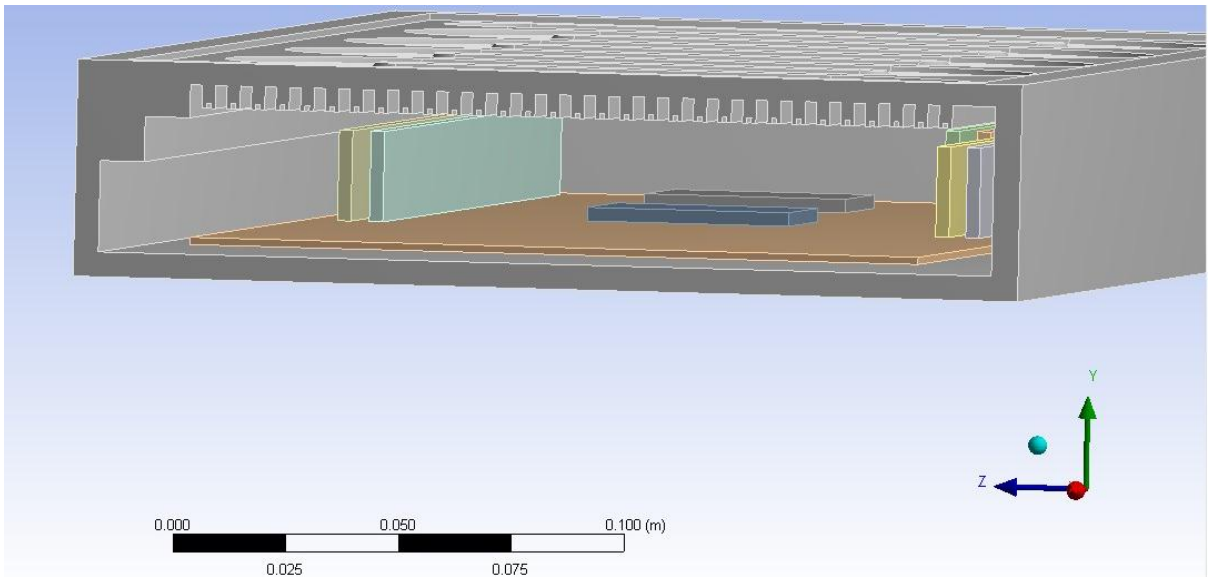

Figure 5-12 3D geometry detail of the internal of computer node container, the cooled wall has fins for heat transfer.

Step 2, building the mesh for CFD solution

After having the basic geometry built, the next step is constructing the mesh for simulation. Natural convetion flow usually tends to be unstable and have poor convergence, so a high quality (low skewness) mesh will be critical. Also from the previous calculation from the (CTG) model the boundary layer thickness (l^*) would be around 0.31~0.43mm, to achieve first layer mesh thinner than 0.3mm will require very fine and detailed mesh structure. Therefore all- hexahedral mesh for coolant body will be desirable before making the CFD file into an unmanageable size.

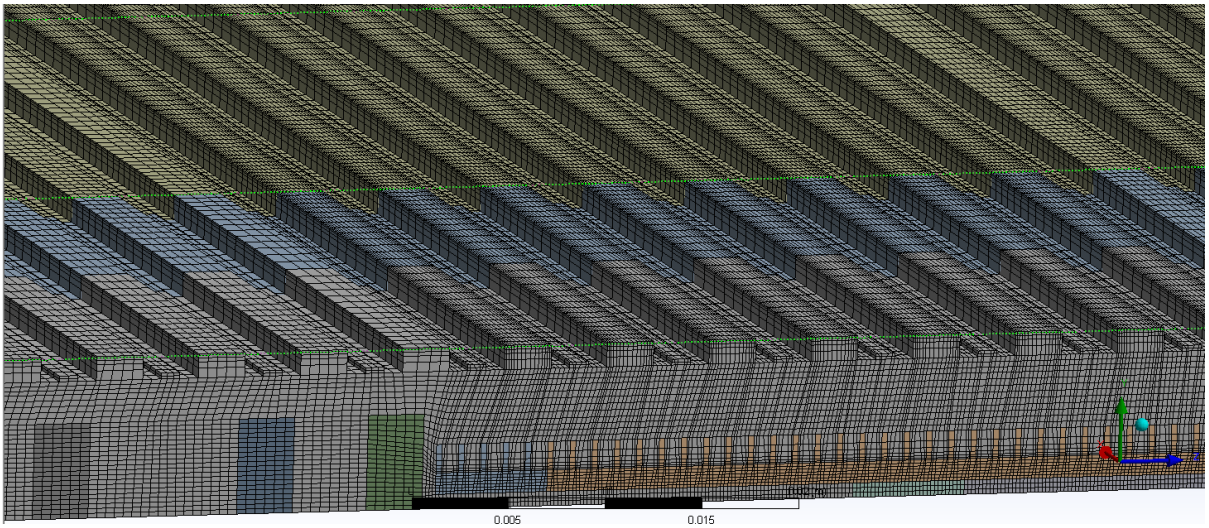

Figure 5-13 Detail of the coolant body mesh cross section.

The meshing method uses a multi-body mesh with 1:1 connection so there will be not loss between different sections.

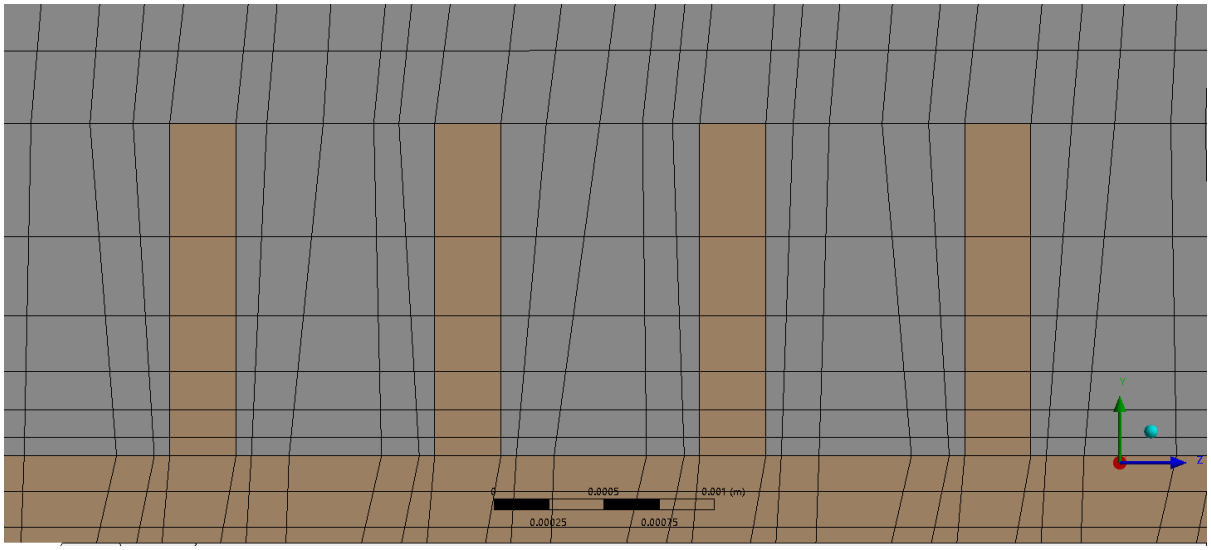

Figure 5-14 Detail section of the mesh layer near solid body,

Notice that from **Figure 5-14** it can see the first mesh thickness is about 0.1mm.

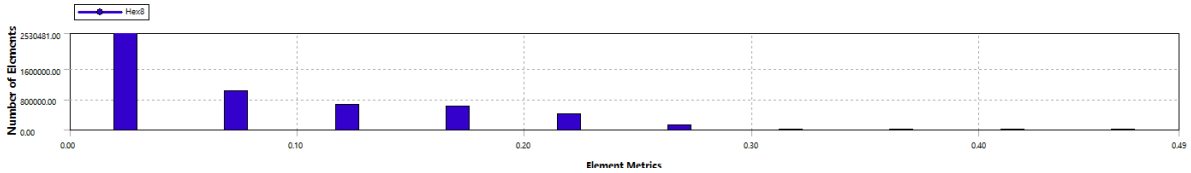

Figure 5-15 Mesh quality check in the mesher (Ansys meshing), it can be seen most elements has low skewness (skewness calculated in Ansys meshing).

Coolant	Nodes	elements	Average skewness	Max skewness	First layer Y*
With Copper heat sink	5.7 million	5.33 million	0.077	0.488	$\approx 1\times10^{-5}$ mm
Aluminium Heat sink	5.4 million	5.06 million	0.0406	0.815	$\approx 1\times10^{-5}$ mm
Overall	6.96 million	7.64 million			

Table 5-8 Mesh file statistics for CFD simulation

From the mesh quality **Table 5-8**, it can be seen that the average mesh skewness is very low for all cases.

Step 3 Setting up and running the CFD solution

The method of CFD simulation will be shown in **Table 5-9**:

Discretization methods	Solver model	Buoyance model	Turbulent model	Scheme	Energy model
Finite volume method	RANS	Boussinesq Approximation 60ºC ref	Laminar SST	Second order upwind	Thermal energy equation

Table 5-9 CFD simulation basic configurations

Setup the CFD model in CFX-Pre, and run the model with a relative low relaxation factor (0.5x time scale), the model should take 24-48 hours to finish. Usually the momentum and heat transfer will have some difficulty of reaching 1×10^{-4}residual (CFX default converging point), so the convergence condition would be more based on the monitor of temperature and heat flux point. One of the useful methods is to monitor the heat load of the water outlet. Because the computer node have 399W thermal load, the water outlet should carry the same load as well. The water outlet thermal load can be calculated by the Specific heat capacity of the water, outlet flow rate and outlet temperature. When the outlet thermal load has an error smaller than 1% (about 4W) compare to the overall system heat load, it can considered as converged:

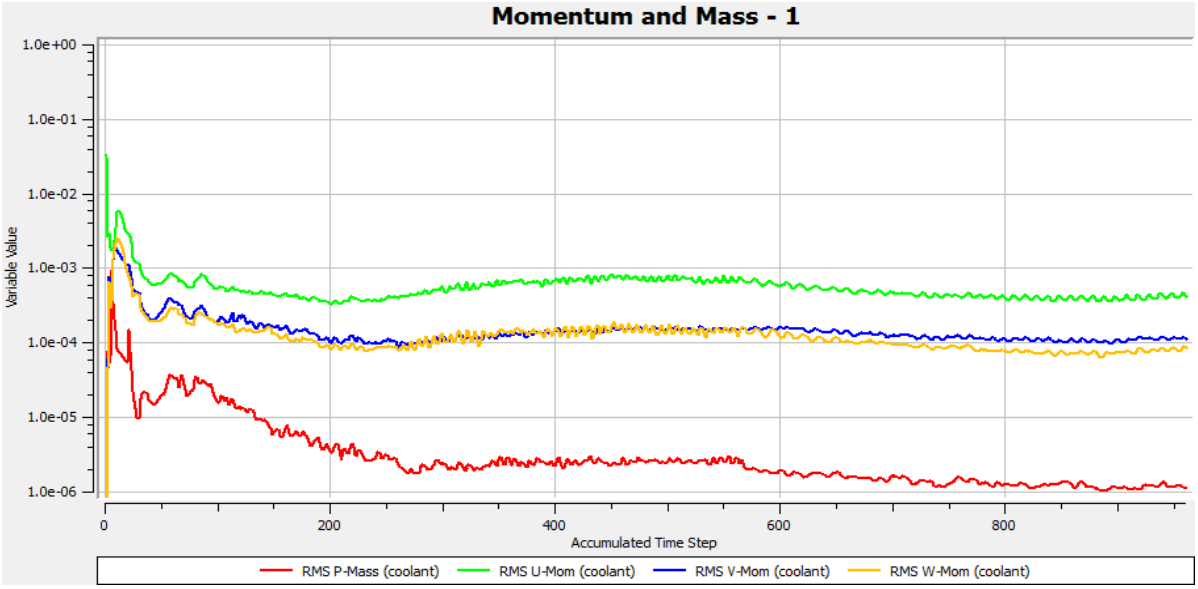

Figure 5-16 Momentum and Mass residual plot of CFD simulation

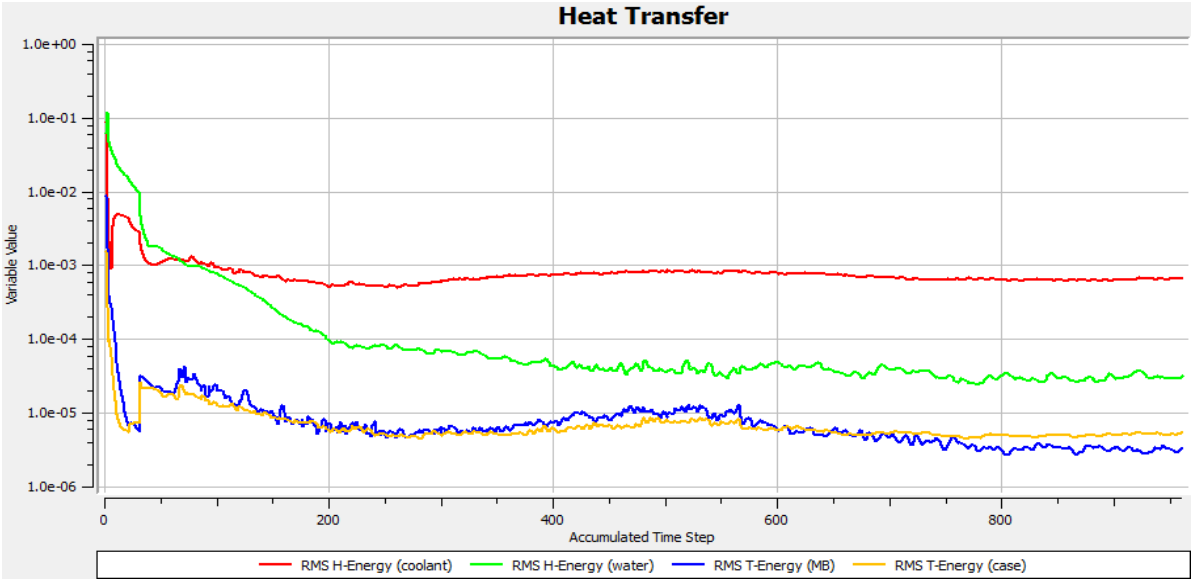

Figure 5-17 Heat transfer residual plot of CFD simulation

From the **Figure 5-17** above, it can be seen the high residual of momentum and heat transfer.

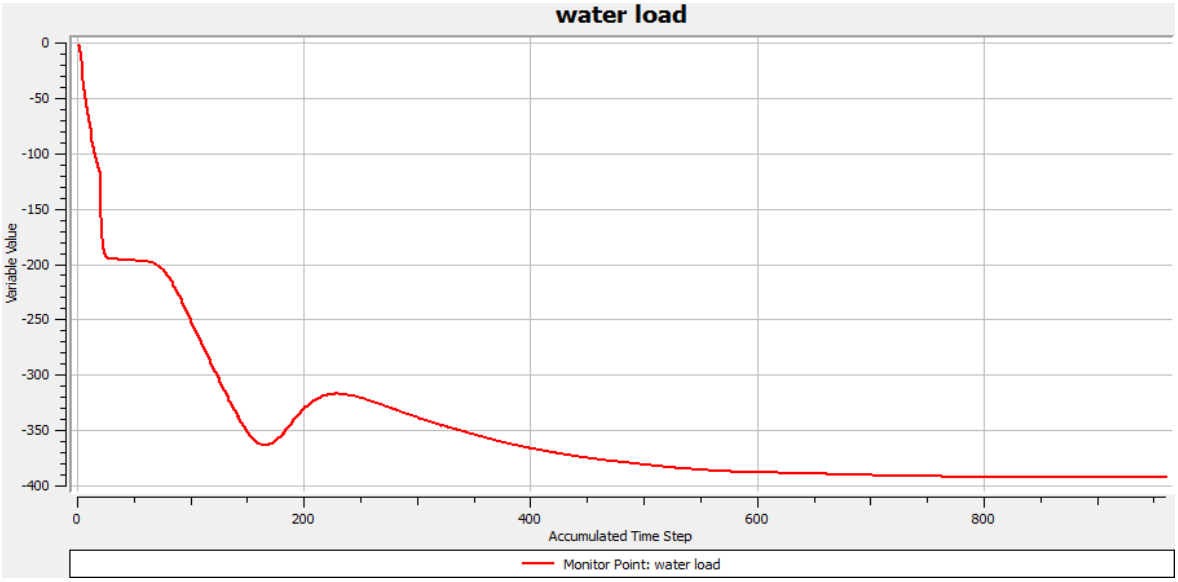

Figure 5-18 Water thermal load plot from CFD simulation over iterations

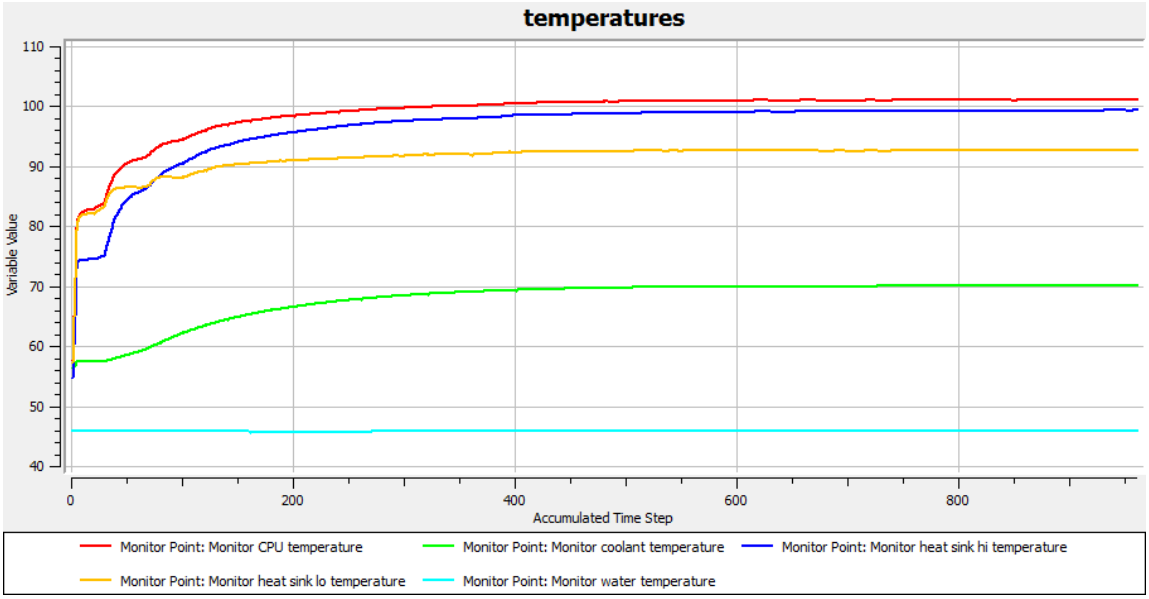

Figure 5-19 Major component temperature plot from CFD simulation over iterations

From the residual plot **Figure 5-19**, it can be seen that the monitor temperature point and the water outlet heat load does not change anymore. At this point the model can be considered as converged.

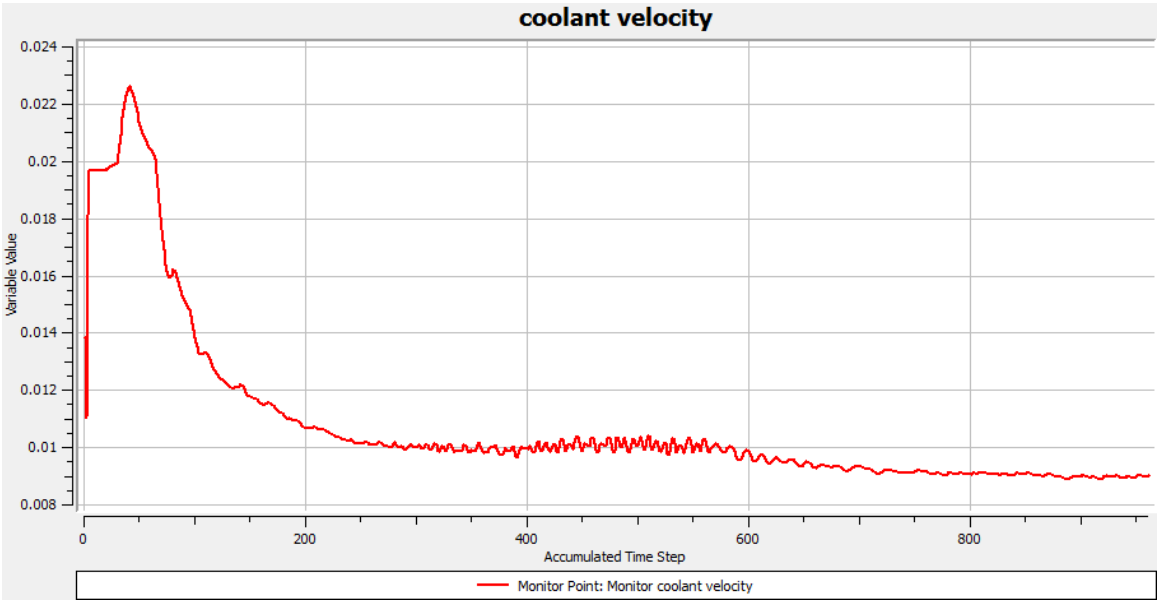

Figure 5-20 Average / nominal coolant velocity plot from CFD simulation over iterations

The **Figure 5-20** is the coolant average velocity, it can be seen that the velocity scale plot stabilized

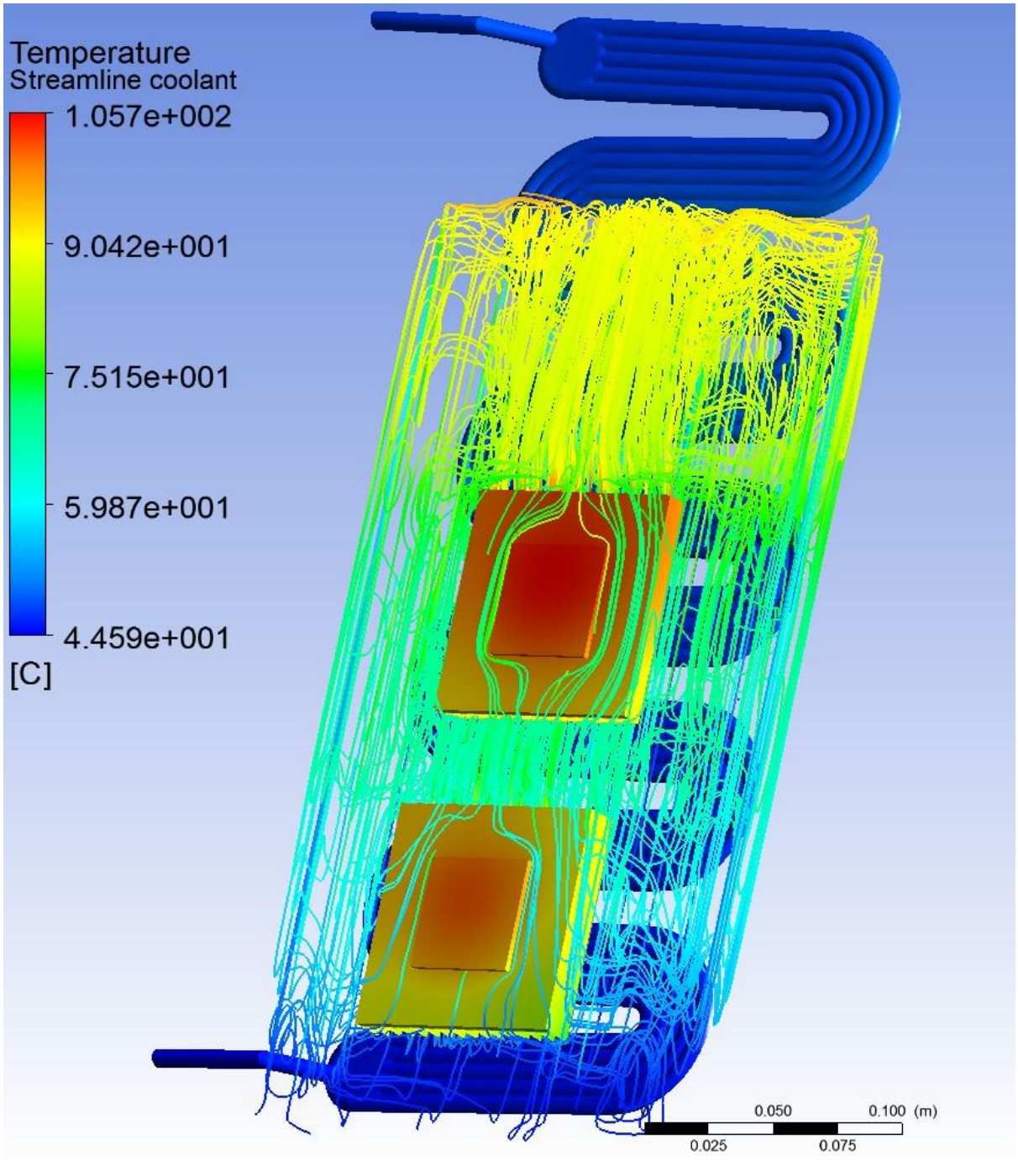

Figure 5-21 An exampleCFD simulation graphical result (coolant stream line)

The **Figure 5-21** is the flow path line with temperature colure rendering, the convection flow pattern can be seen easily.

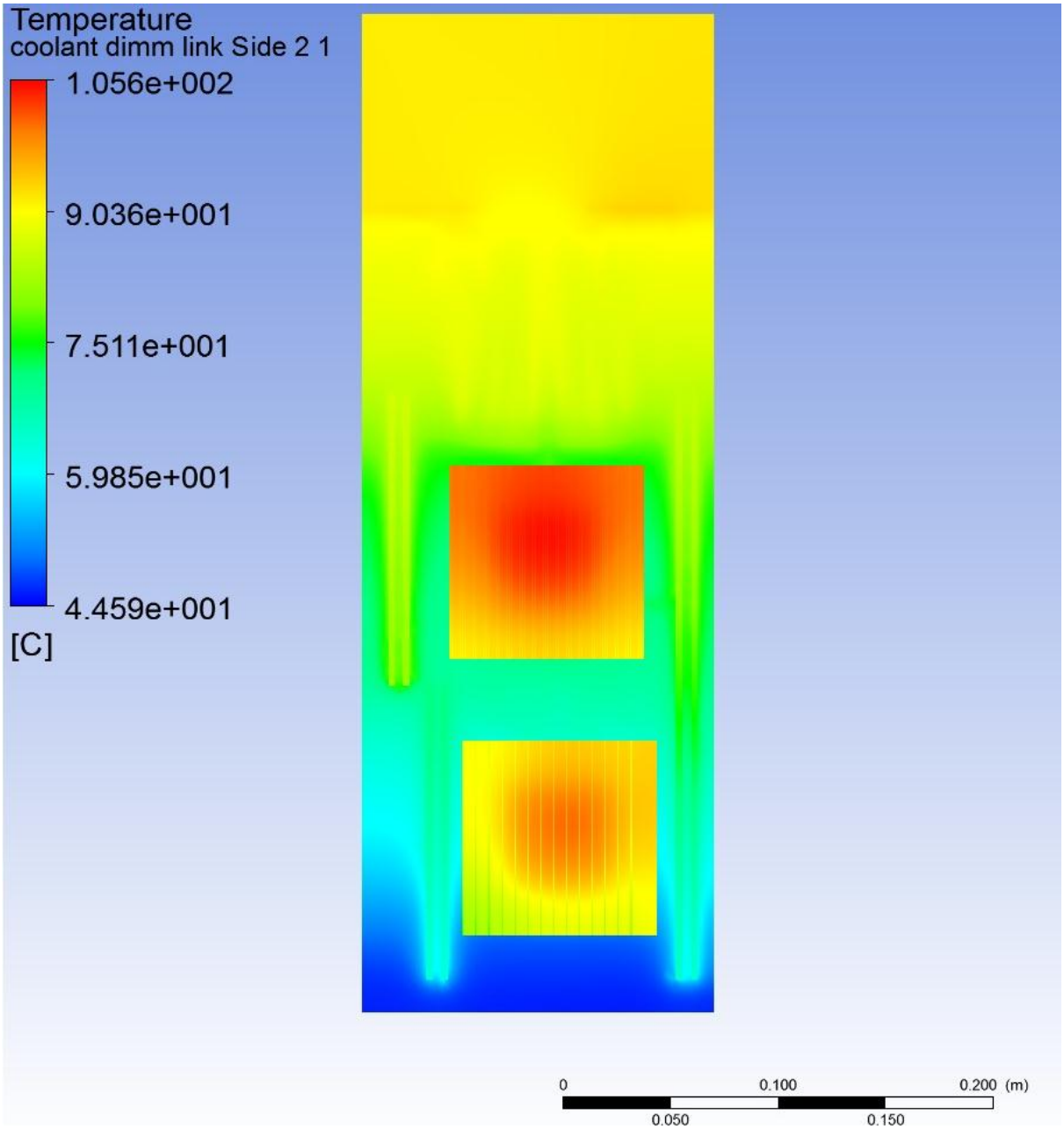

Figure 5-22 CFD simulation graphical result (motherboard temperature)

The **Figure 5-22** is the temperature colour contour plot. It can be seen the top CPU (CPU 1) is overheated, with a temperature slightly over 100°C. From data sheet this the Intel Xeon E5-2690-v3 processor should perform below 99 °C.

A total of 3 CFD simulations has been carried out, the result matrix shown as:

Temperature °C	Water inlet	Water outlet	Water load	CPU 1	CPU 2	Memory average	Coolant average	Water metal interface	Coolant metal interface
Copper sink laminar	44.6	47.41	395W	**102.5**	**86.2**	73.1	70.2	41.42	41.72
Copper sink SST		47.41	392W	**102.4**	**85.1**	73.3	69.8	41.42	41.71
Aluminium Sink laminar		47.42	393W	**101.5**	**97.1**	73.7	70.1	41.41	41.71

Table 5-10 CFD simulation result matrix

It can be seen from **Table 5-10**, the top CPU (1) temperature is somewhere around 100°C, and the lower CPU (2) for copper heat sink is about 86°C, 16~17°C lower than the top CPU temperature.

To validate the mesh resolution for the flow, a vertical cross line in the centre of the CPU fin area has been use to plot the velocity profile:

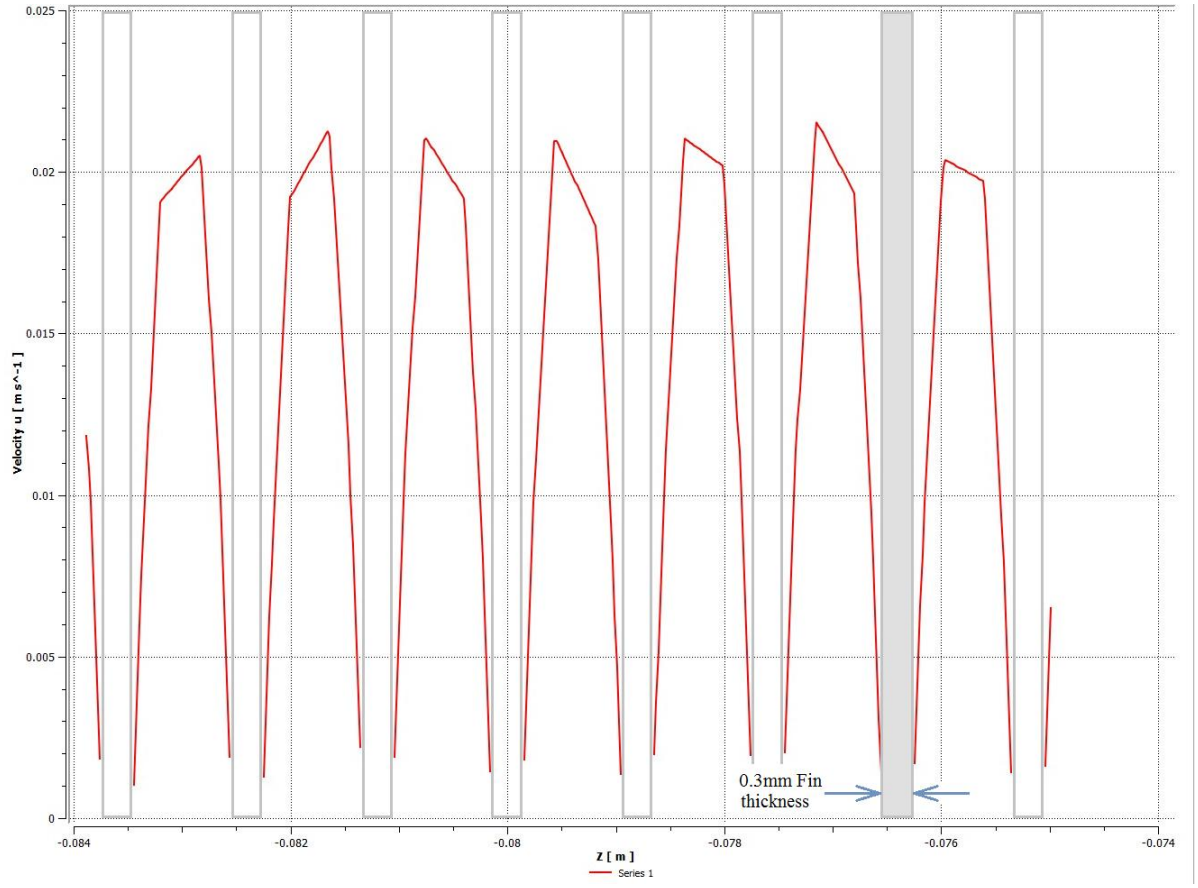

Figure 5-23 CFD simulation result: coolant velocity profile between fin, cooper heat sink

From **Figure 5-23**, it shows the vertical direction velocity curve / profile between CPU (1) heat sink fins. The velocity curve shows the relative low resolution near the fin wall boundary, because there are only 5 elements across the fin pitch. Also the natural convection boundary layer thickness

(characteristic length scale, l^*) calculated in the constant thermal gradient (CTG) model is about 0.31~0.39mm, and the pitch l_{pitch} between fins is 0.9mm. So the boundaries of 2 facing fin wall would be merged when:

$$l_{\text{pitch}} \rightarrow 2 \times l^*$$

Thus, only a single peak velocity profile between fins on the thin-fin copper heat sink can be observed.

For the thicker, cheaper aluminium heat sink design, because the fin pitch is much larger (4.2mm pitch), and the natural convection boundary layer thickness (characteristic length scale, l^*) calculated in the CTG model is about 0.31~0.44mm, it should be possible to see a twin-peak velocity profile between fins similar to Morton's case (Morton B.R., 1960) with both sided heated walls:

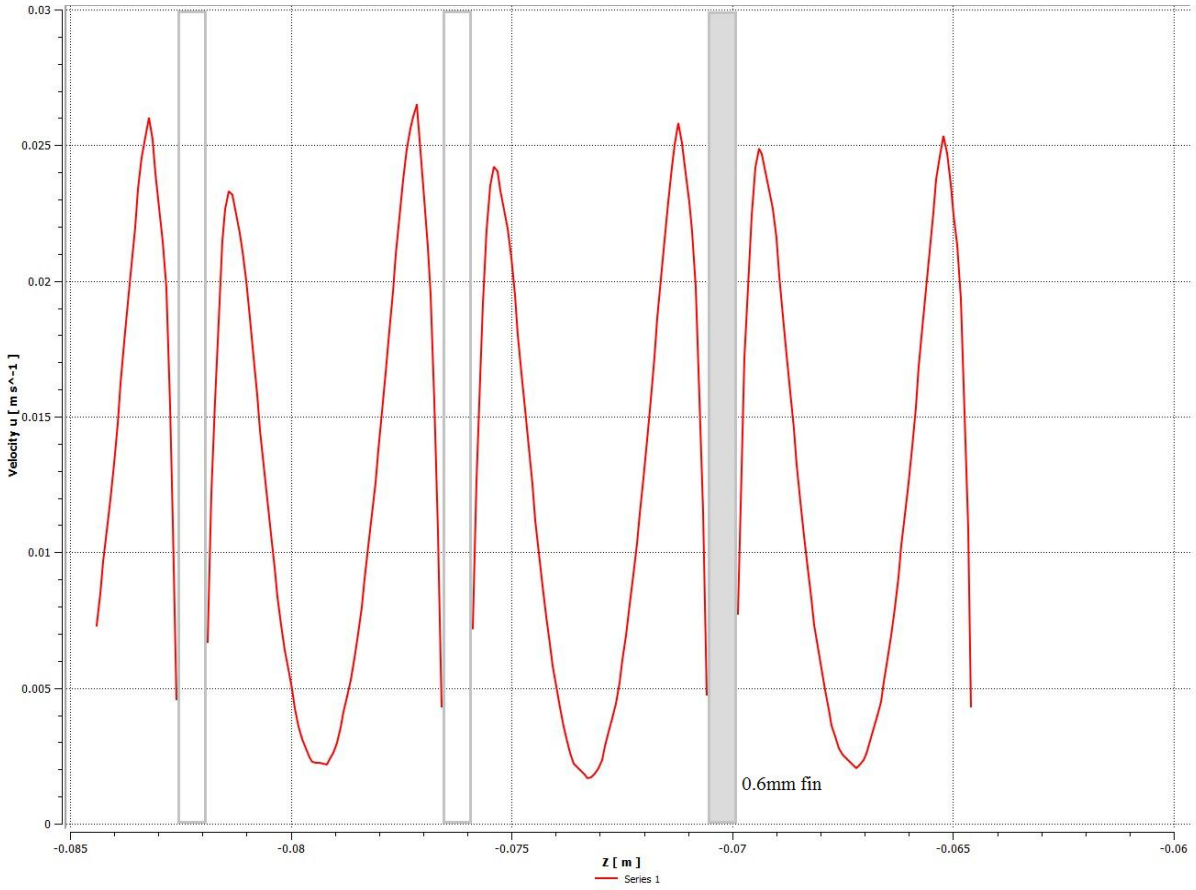

Figure 5-24 CFD simulation result: coolant velocity profile between fin, aluminum heat sink

The **Figure 5-24** is the cross section Y direction velocity profile on the thick-fin aluminium heat sink, the twin-peak shape can be observe and the distant from the fin wall to the velocity peak is about 0.4~0.6mm, somewhat close to the CTG model prediction of 0.44mm.

5.3 Experimental test with the liquid-cooled computer thermal test system

The last section of this chapter is an experimental test of the liquid-cooled computer node in the Iceotope Company.

The thermal test system in the Iceotope Company is shown in the following figure:

Figure 5-25 Photo of the thermal test unit in the Iceotope company lab

The **Figure 5-25** shows the fully immersed liquid-cooled thermal test unit with the external case and insulation removed, the blue part is the computer node. Notice that the insulation panel will put back to the thermal test unit during the experiment.

The **Figure 5-26** is the photo of the heat rejection unit with chiller.

Figure 5-26 Heat rejection unit in the lab which can provide constant water temperature

From the **Figure 5-26** it can be seen that the heat rejection unit is a relative small unit

The user interface of Intel Power Thermal Utility for Intel server system:.

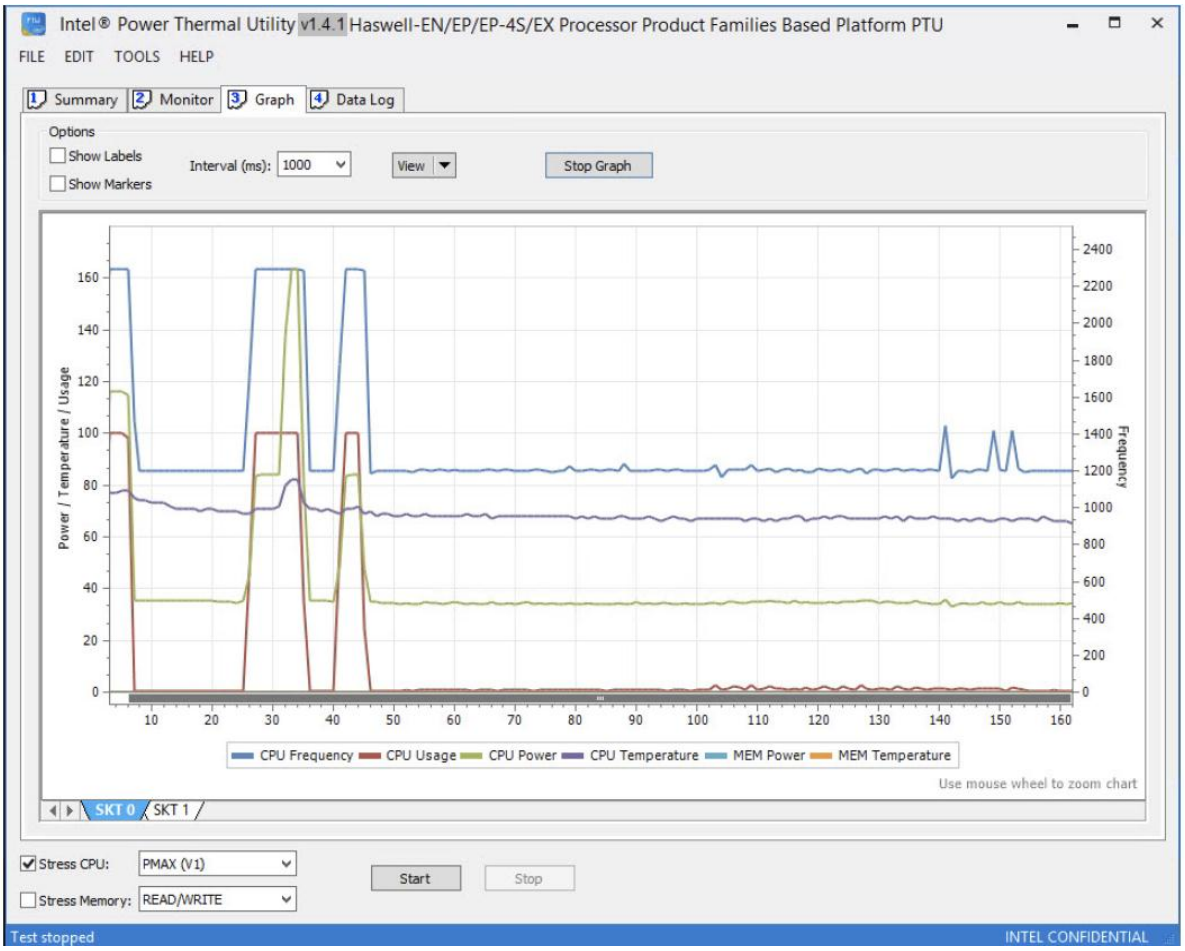

Figure 5-27 User Interface of the Intel Power Thermal Utility software

The Intel Power Thermal Utility software is a thermal performance testing software specific for Intel system. Though it is a commercially confidential system and provided by Intel for the Iceotope company internal usage, some of the detail of the software may not be available in this work.

The reason to choose this software is simply because its convenience, due to its ability of stressing the system with power / thermal load and recording the temperature and power consumption data at the same time. In the matter of providing thermal load to the computer system only, it provides similar capabilities as some other software or method such Linpak or StressLinux.

The setup of the test is simple and straight forward, basically put on the insulation, set the cooling temperature on the heat rejection unit and put the thermal load with the Intel Power Thermal Utility software on the system. After continuously running the computer system for 12 hours, the result is:

Inlet water	Outlet	CPU 1	CPU 2	Memory high	Memory low
Temperature ^{o}C					
44.6	48.2	92	84	67	63

Table 5-11 Temperature test result from the liquid-cooled system thermal test unit

The table 5-11 is the experimental result of the thermal test unit, compare to the CFD result from table 5-10 it can be seen that the temperature reading from the experiment is smaller than the simulation. This could be reasonable because that in reality it is difficult to insulate the heat loss perfectly.

5.4 Evaluation and prediction of the aluminium heat sink performance

The purpose of this section is to predict the performance of the new design before the experiment test, in here there is 2 methods to achieve this: mathematical calculation and CFD simulation. But in the end it still needs some physical experiment or test to evaluate the accuracy of these predictions.

The simulation and experimental data is summarised in the following evaluation table:

		Prediction	Simulation		Test
Temperature ^{o}C	Configuration	CTG model	CFD model		Experiment
			Laminar	SST	
Normal node	CPU 1 copper	88.63	102.5	102.4	92
	CPU 2 copper	83.44	86.2	85.1	84
	Memory high		73.1	73.3	67
	Memory high				63
Reduce cost node	CPU 1 copper	88.63	101.5		
	CPU 2 aluminium	101.5	97.1		
	Memory high		73.7		
	Memory high				

Table 5-12 Temperature result gathered from all prediction / simulations and test data

From **Table 5-12**, the CTG model calculation and CFD simulation result shows an acceptable accuracy (less than 10% difference) compare to the experimental data. But a CFD model can give a complete view of the whole system, while the mathematical model can only calculate some important value such as the temperature and heat load. And furthermore the CTG model can only calculate the heat transfer on vertical systems (along gravity direction), and at the moment it cannot solve the problem on horizontal system.

It is also important to compare the time consumption (labour cost) for all different stages of work

It is also important to compare the time consumption (labour cost) for all different stages of work:

Cost in time (per person, per test)	CTG model calculation	CFD	Experiment

Setup time	15 min	7-9 days (meshing)	3-5 days
Test time	0	2-3 days	12 hours

Table 5-13 Time consumption of different engineering methods

5.5 Summary

In this chapter, the comparison between CTG model predictions, CFD analysis and laboratory experiment has been carried out. Both CTG model and CFD analysis provides a reasonable close result compare to the laboratory experiment, and in this particular problem the result from CTG model seems even closer to the real world.

An interesting point to note is that running the CFD simulation is actually more time consuming (about double) than having a test system setup and run the experiment. But this will only be possible if the task is to improvement the system with exchangeable parts, also an existed working system is required. So for some simple engineering design, it might be faster to do calculation and then go straight into experiment, and skip the simulation stage. In other hands, some design may be difficult or too costly to work on experiment then CFD simulation is the only method to preview the result.

6. Thermal test and case study of the fully immersed liquid-cooled computer systems

In previous chapter, systematic thermal analyses and experiments have validated the thermal performance of the fully immersed liquid-cooled computer system. But this is based on a single computer node and investigates the thermal efficiency in an ideal condition.

In this chapter there will be a real-time experiment on some fabricated of real liquid-cooled computer systems. The purpose of the thermal test is to reveal the true potential of liquid-cooled computer system which refers back to the chapter 2 about the development and achievement of computer cooling technology

Two types of .measurement matrix will be used in the experiments of this chapter. One of which is the Power Usage Effectiveness (PUE), which is more related to the usage of energy in data-centre and. The other one is ASHREA W5 standard, which more towards the thermal tolerance of the system and the capability of reusing the waste heat.

6.1 Case study of the fully immersed liquid-cooled data centre system compare to rear-door water cooled system

The benefit of having a high power load electronic system liquid-cooled is not just to provide better cooling, but also reduced energy consumption in the cooling system and better management of the waste heat. Or in an easier way to understand it, a fully immersed liquid-cooled data centre system should have lower PUE (Power Usage Effectiveness) and able to work in a water inlet higher temperate.

Recall the equation in chapter 2, the PUE calculation (**equation 2-1**) should be:

$$PUE = \frac{\text{Total Facility Power}}{\text{IT Equipment Power}}$$

Originally Iceotope claimed that the pPUE of their liquid-cooled data centre cabinet was below 1.1, and with the possibility of running 45ºC inlet water as the cooling water it will fulfil the ASHRAE W4/W5 standard. Notice: The concept of pPUE stand for total energy within a boundary divided by the IT equipment energy within that boundary (The GreenGrid, 2011), and in this case the pPUE only takes account the computer server cabinet power consumption as the total power in the PUE equation. This should be consider as good thermal efficiency and good thermal management in all

data centre standard, and determining whether this can be achieved in a real running environment is the major task in this chapter.

Overview of the fully immersed liquid-cooled computer system

Historically the University of Leeds acquired a small scale Iceotope fully immersed liquid-cooled computer cabinet as part of the laboratory equipment since 2012. Unlike the thermal test system used in the Iceotope Company lab which was specific for thermal test, the system in the University of Leeds was a commercial based system. This computer system served 2 purposes for the university: an experimental test system for the university to study fully immersed liquid-cooled computer thermal behaviour, and also extra computation resource added to the university main data centre. Note that part of the CFD simulation in this research was actually done using this Iceotope system.

The experiments in this section are based on the Iceotope Company provided fully immersed Liquid-cooled computer server system for data centre solution. It is the first liquid cooled available commercially, which aims to provide a high efficiency data centre solution with lower PUE and free cooling for data centre users. This liquid-cooled computer system was a full cabinet with a relatively small scale computer system inside with 11computer nodes and 4 power supply unit (2×2 PSU) located in the university's mechanical engineering department main lab. Since the system has a relative small power load (about 3kW in total), it can use passive heat rejection unit without fans rather than standard heat rejection unit with fans and chiller.

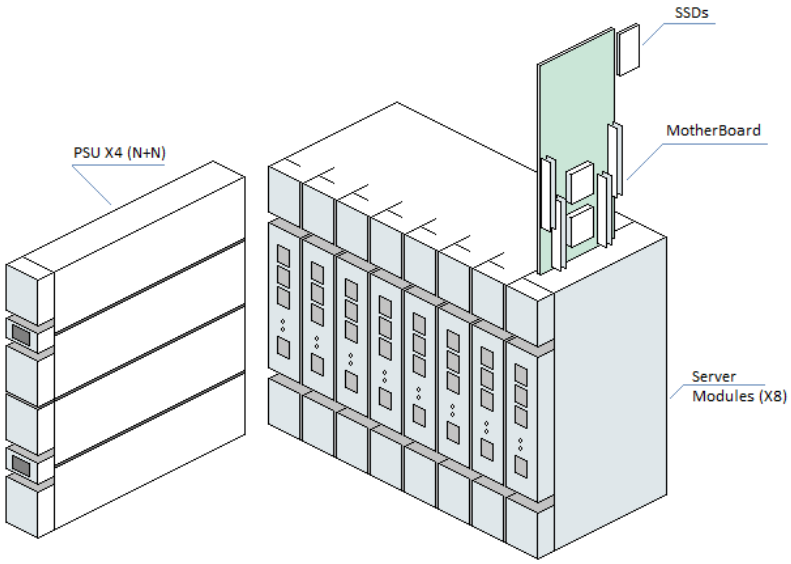

Figure 6-1 Schematic drawing of the computer node with the power pack

The drawing above explains the basic layout of the computer system: for high power systems it will take 2x2 power pack towards 8 high power computer nodes, but for low power system only 1x2 power pack will be needed

Figure 6-2 Photo of the full immersed liquid-cooled computer cabinet (left) with 11 nodes and passive radiator (right) in the university lab

The photo above (**Figure 6-2**) shows the basic system layout, and in the top shelf of the cabinet there is a network switch and a 3-phase power distribution unit (PDU). The PDU of the system is also possible to work as a power meter which provide some very useful information during the test. The other characteristic of the system is the 2x redundancy twin liquid-cooled power supply design, each power package has 2 individual power supply unit (1.6kW each). In ordinary running condition there will be one PSU under load and another standby, but it will automatic swap power if one has failure. This is quite different from the thermal test unit in the Iceotope Company which use a single adjustable laboratory power supply unit for the job.

This liquid-cooled computer system has 3-years running history up to the period of finishing this thesis (from late 2012 to late 2015). It had a mid-life span IT upgrade of the system in 2014 (end of 2nd year), this including upgrade to some of the computer nodes which significantly improve the computing capability. The active duty of this computer system would be ended in the late 2016, which would fulfil a typical 4 years duty of a computer system.

There will be 2 parts of energy efficiency experiments in this chapter, they were carried out at 2 separate times. The first experiment was the thermal efficiency tests focussing on PUE (Power

Usage Effectiveness), it was carried out before the IT upgrade so the computation performance was lower (in FLOPS) but the thermal load was almost identical. The second experiment was more of a reliability test aim to achieve the ASHRAE W5 standard that requires a continuous running with 45°C inlet water temperature for more than 24 hours.

Thermal efficiency test base on pPUE (partial Power Usage Effectiveness) of the fully immersed liquid-cooled computer system

The concept of the thermal efficiency experiment in this section is to construct a methodology compare the pPUE (partial Power Usage Effectiveness) (The GreenGrid, 2011) between a fully immersed liquid-cooled computer server system and an air-cooled based back-door water-cooled computer server system.

Notice: The concept of pPUE stand for total energy within a boundary divided by the IT equipment energy within that boundary (The GreenGrid, 2011). In this section the boundary for pPUE included the computer unit (CPU, motherboard, etc) all equipment that maintains the necessarily running of the data centre computer system such as PSU, HRU and UPS; but excluded some general data centre facility building level equipment such like lighting.

HRU stands for Heat Rejection Unit, UPS stands for Uninterruptible power supply

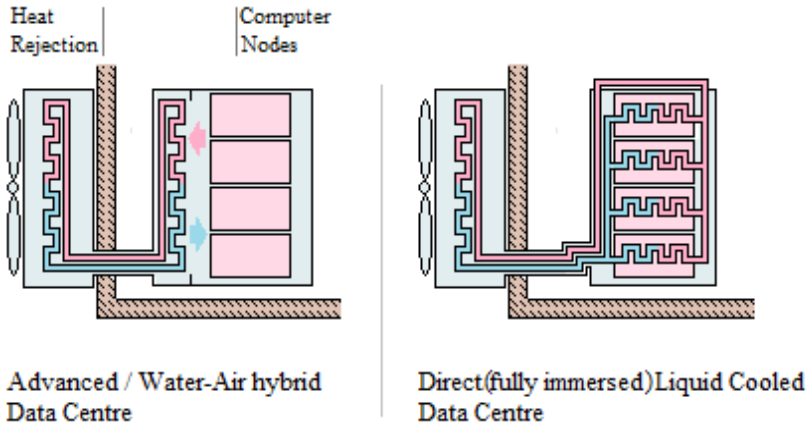

Figure 6-3 Schematic drawing of back-door water-cooled system (left) and fully immersed liquid-cooled system (right)

The **Figure 6-3** shows the major different (thermal path) between a fully immersed liquid-cooled computer server system and an air-cooled based back-door water-cooled computer server system. The University of Leeds has both types of computer server system. The Iceotope based liquid-cooled cabinet was mention previously in the lab was a stand-alone unit that runs in a laboratory environment. The Airedale based back door water-cooled cabinets, in the other hands, mixed with

other air-cooled system as a mid-term IT upgrade to the university's main HPC data centre (**Figure 6-4**).

Figure 6-4 Photo of the HPC servers in the University of Leeds' server room

But in reality this 2 types of system rarely have anything in common. In this case to study 2 computer system in the university, they are very different from the basic element of computer component to the overall facility configuration. It is also a common case that some of the HPC (High Performance Computing) data centre user does not have their computer system constructed in the same time and same spec. In a real data centre it would not be surprising to see new system and old system in the same place, or even air-cooled and water-cooled systems in the same room as well.

Real system	Back door water-cooled system	Fully immersed liquid-cooled system
Capacity (W)	84kW (28kW X3)	3KW
Computer system	Mixture of Sun, Dell and Intel	SuperMicro
CPU / GPU	Intel / AMD / nVIDIA / Others	Intel / AMD
Rack cooling method	Airedale back-door water cooled	Rack cooling method
External heat exhaust	Airedale free cooling	Passive air cooled

Table 6-1 Different between the actual back door water-cooled system and fully immersed liquid-cooled system installation

To compare this put these 2 different systems into one comparison means it need to put them into the same condition, same scale and same workload. It is also difficult to achieve physically because not only their difference in configuration, but also their different locations. This leads to the idea of collecting the thermal test result from 2 different computer systems, and then scale up these results to construct 2 Hypothetical systems with 2 different cooling method, but have identical computer and electronics components in order to have fair comparison.

Here is the configuration table of hypothetical liquid-cooled and air-cooled system will based on identical hardware systems:

Hypothetical system	Back door water-cooled system	Fully immersed liquid-cooled system
Capacity range	240kW	240kW
Computer system	SuperMicro X9D seires	SuperMicro X9D seires
CPU / GPU	Intel (E5-2670)	Intel (E5-2670)
Rack cooling method	back-door water cooled (Airedale OnRak 28Kw)	Fully liquid cooled (Iceotope)
External heat rejection	Airedale free cooling	Airedale free cooling

Table 6-2 hypothetical air-cooled system and liquid-cooled system configuration

In **Table 6-2** the fully immersed liquid-cooled system has been scaled up to match the same size of the back door water-cooled system, and they are assumed to use the same mother-board / CPU solution (SuperMicro X9D with Intel XEON E5-2670), same power supply (Super Macro PWS-1K62P 1R) and the same heat rejection unit (Airedale Ultima Compact FreeCool). With such assumptions the only physical difference in the 2 sides would only be the computer and rack cooling method, which eventually give the idea of how much energy efficiency can be improved by just switched the Back door water-cooled solution into fully immersed liquid-cooled solution in data centre.

It also needs to mention here that the heat rejection unit (Airedale Ultima Compact FreeCool unit) can work in 2 modes, either in the free-cooling mode which works purely as a fanned radiator, or a water chiller which costs extra energy to provide a negative temperature difference for better cooling.

The experiments to build the scaled up Hypothetical data centre system have individual tests of an air-cooled computer node for the back door water-cooled system, and a liquid-cooled computer node for the fully immersed liquid-cooled system. They have to be exactly the same computer system but in 2 different enclosure, and which eventually will but into 2 completely different data centre model. There will be a detailed explanation of the sensor point and measurements later in this chapter.

Thermal test of the liquid-cooled computer node in fully immersed liquid-cooled system.

This part of work aims to gain the energy efficiency result from a running fully immersed liquid-cooled system.

Firstly consider the computer components (IT) in the system: There are 11 computer nodes in the fully immersed liquid-cooled rack, as it is an experimental system to test it has various hardware across the system. The arrangement of computer hardware will be show in **Table 6-3**:

No. / IP	CPU	Total cores	CPU frequency	Total Memory
101	AMD Opteron 6272	2 x 16	2.1GHz	48GB
102	Intel Xeon E5-2620	2 x 6	2.6GHz	16GB
103	AMD Opteron 6272	1 x 16	2.1GHz	16GB
104	Intel Xeon E5-2620	2 x 6	2.0GHz	32GB
105	Intel Xeon E5-2620	2 x 6	2.0GHz	32GB
106	AMD Opteron 6272	2 x 16	2.1GHz	48GB
107	**Intel Xeon E5-2670**	**2 x 8**	**2.0GHz**	**32GB**
108	Intel Xeon E5-2620	2 x 6	2.0GHz	32GB
109	AMD Opteron 6272	1 x 16	2.1GHz	24GB
110	AMD Opteron 6272	1 x 16	2.1GHz	16GB
111	Intel Xeon E5-2620	2 x 6	2.0GHz	64GB

Table 6-3 Computer component (IT) of in the fully immersed liquid-cooled computer rack, the high-lighted computer node will be latter on involved in another test.

Secondly is the non-IT components in the fully immersed liquid-cooled computer system. The power load reading of these components will be important as well, since they are a part of the supporting parts to run a data centre and will be taken place in the pPUE calculation.

The basic configuration of the in the university lab includes:

Name	model	Quantity	Specification	notes
Power Distribution unit	Avocent PM3000	1X	380V / 3 phase to 220C	Up to 22KW 3KW total
Power Supply unit	Super Macro PWS-1K62P 1R	2X	220V / 1 phase to 12V	1.6KW X2 = 3.2KW
Computer module	Iceotope Module	11X	12V	Vary
Centre heated Pump	GRUNDFOS ALPHA2 L	1X	2.6 m^3/h	
Radiator pump	Wilo Smart A-25/4-130	1X	3.5 m^3/h	

Table 6-4 Basic non-IT component of the fully immersed liquid-cooled computer system

It can be seen from the **Table 6-4** it will need two pumps and two separated water circuits to run a commercial based liquid-cooled computer system. This is the major difference from the thermal test unit in the Iceotope company lab since which has only one water circuit. The reason of such is because the internal cooling water that goes through all computer node needs to be treated and chemically compatible with computer node water jacket, while the external cooling water could be supplied by the data centre facility that may not meet the requirement of compatibility. Obviously a 2-stage cooling water system will have lower thermal efficiency and higher temperature difference, but it is a trade-off between performance and reliability in the real commercial case.

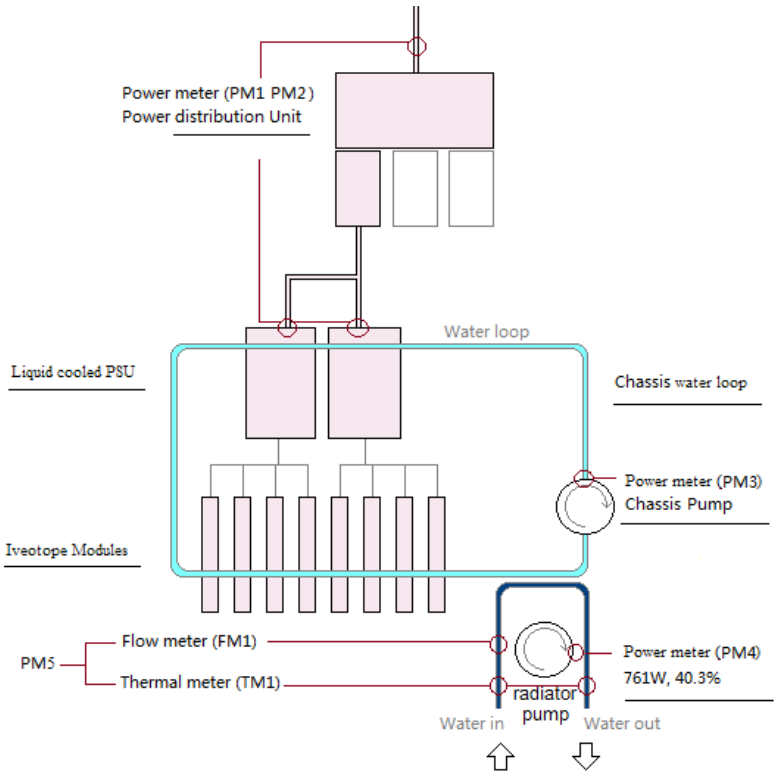

Figure 6-5 Schematic drawing of the fully immersed liquid-cooled computer system layout. 2 pumps and 2 water loops can be seen from the drawing

The **Figure 6-5** also indicates the location of the sensing point and the type of measurements required for the pPUE calculation. The meters and sensing points involved in the test will be:

Name	output	Type	Number	Specification	Model / other
PM1	W	Power meter	1X	Up to 3.2KW380V / 3 phase	Built in Avocent PM3000
PM2	W	Power meter	2X	220V / 1.6KW	
PM3	W	Power meter	1X		Model 2000MU-UK (L61AQ)
PM4	W	Power meter	1X		
FM1	m^3/h	Flow meter	1X	Up to 12L/min	N/a
TM1	^oC (ΔT)	Thermal meter	2X	Up to 80^oC	Center DT610B Thermometer

Table 6-5 List of sensors and meters for the pPUE calculation

Form **Table 6-5** it can be seen there are 7 sensor points / readings will be needed in the pPUE calculation: The PM1 / PM2 are already included in the Avocent PM3000, and the temperature meter can measure both inlet and outlet temperature with 2 thermal-couples, so there are only 5 meters (2X PM2, 1X PM4 and 1X TM1) will be needed in the test.

With the temperature sensor (TM1) and flow meter (FM1), it is possible to calculate the power load carried by the water circuit (PM5). Assume the water Specific Heat Capacity (SHC) is 4.1813

J/kg.ºC, water density (ρ) is 1000kg/m^3, and the temperature difference between water inlet and water outlet is form TM1 (outlet – inlet):

$$\text{water heat load, PM5} = \frac{C_p \cdot FM1 \cdot TM1}{\rho} \qquad 6\text{-}1$$

The PUE stands for: PUE = Total Facility Power / IT Load, where it can be assumed that:

Name	Part	terms
Total Facility Power	Complete system	PM1 +PM3 +PM4
IT Load	Computer components	PM2
pPUE		**(PM1 + PM3 +PM4) /PM2**

Table 6-6 pPUE calculation correlated with the sensing points

From the table above, the PUE of the system can be easily understood. With all the sensors and meters in place, the system thermal test started with running Linpak (windows based) in all computer nodes to achieve 100% power load and continue for 12 hours.

Notice that the only computer node that was involved in the pPUE calculation was the node 107 which is highlighted in the **Table 6-3** and also **Table 6-7**, but all the computer nodes will be switched on and run under the same calculation load. The reason that all nodes need to be switched on for measuring only 1 single node is because all computer nodes share the same water circuit, also the water pump for the liquid-cooled cabinet is a fixed-rate pump that specified optimal running condition to match the full-loaded (11 nodes) system in this case. So having the reading under full load should be closer to the real condition.

Here is the temperature result after 12 hours of continuous running **Table 6-7**.

No./IP	System Temperature	CPU1 /CPU2 Temperature	CPU- System ΔT	CPU1–CPU2 ΔT
101	53 ºC	Medium	N/a	N/a
102	51 ºC	79 ºC / 76ºC	25~27ºC	2 ºC
103	N/a	Medium	N/a	N/a
104	51 ºC	70ºC / 69ºC	19~18ºC	1 ºC
105	52 ºC	75ºC / 69ºC	22~16ºC	6 ºC
106	50 ºC	Low / Low	N/a	N/a
107	**53 ºC**	**70ºC / 69ºC**	**18~16ºC**	**2 ºC**
108	51 ºC	71ºC / 71ºC	20~18ºC	2ºC
109	47 ºC	Medium	N/a	N/a
110	46 ºC	Medium	N/a	N/a
111	51 ºC	73ºC / 69ºC	20~17ºC	3 ºC

Table 6-7 CPU temperature reading from the fully immersed liquid-cooled cabinet after 12 hours run.

Note: The AMD CPUs do not give a detailed temperature reading via SuperMicro IPMI services, instead they only state low, medium, high and overheated.

The power reading from the PDU and power meters for pumps (**Table 6-8**):

Part	Term	Min power	Max power	average
PDU	PM2			(96.5% efficiency) 2128 W
	PM1			2205.1W
Cabinet pump	PM3	75W	85W	78W
Radiator	PM4	16W	16W	16W
total				95W

Table 6-8 Power reading from the PUE and power meters for pumps, notice that the PDU can give the power efficiency of each phase

Now that all the thermal tests for the fully immersed liquid-cooled system have been completed, the sensors and meters reading enable the pPUE of the system to be calculated:

pPUE calculation for the actual fully immersed liquid-cooled system in lab				
PM1	PM2	PM3	PM4	pPUE
2205.1 W	2128 W	78W	16W	1.081
Total load (PM1 + PM3 + PM4)				2300.1 W

Table 6-9 PUE calculation for the actual fully immersed liquid-cooled system in lab

From **Table 6-9** e it can be seen that the pPUE of the actual fully immersed liquid-cooled system in the university lab was very good (slightly lower than 1.1). But this was a small scale system and lacked many components such as UPS that would be required in a typical full scale cabinet.

Thermal test of air-cooled computer node for back door water-cooled computer system

The back door water-cooled computer system was an installation in the HPC department of the university, and responds to the university's academic daily workload. Unlike the liquid-cooled system was a piece of experiment equipment in the lab that can be re-task for any purpose, running thermal tests on a major system like this will significantly affect the daily work in the university. So it will be important to ensure that these only take a small part of the back door water-cooled computer system to establish the thermal test.

The core component of the back door water-cooled computer system is still an air-cooled based computer node, which should be identical to most of other air-cooled system. So the thermal performance of the back door water-cooled solution will still be limited by the air-cooled system.

That also means it would not be necessary to take the complete water-cooled system to the lab for experiment, but only needs a single computer node to finish the task.

Following the previous thermal tests for the liquid-cooled system, one of the computer nodes (node 107) has been taken from the liquid-cooled system and put into an air-cooled system module for in this part of the experiment. Unlike the liquid-cooled system which has only one pump for all computer nodes, the air-cooled unit has individual power-supply and cooling fans so only 1 single computer node can complete the test.

The aim of this experiment is measure the CPUs temperature, inlet air temperature and outlet air temperature. Also it will need to validate the result so the outlet air heat flux will be calculated, which can be obtained by measuring the air flow-rate of the outlet as well. To achieve this a cardboard nozzle was made and regulated the outlet to an axial symmetric shape (round shape), and the diameter of the exhaust pipe is 75mm (**Figure 6-6**)

Figure 6-6 The stand alone computer node with a modify outlet section for the experiment

Figure 6-7 The computer node (node 107) in an air-cooled configuration ready for experiment.

From the photos above (**Figure 6-6** and **Figure 6-7**) it can seen how the air-cooled node was configured, and in this test a SuperMicroCSE-217HQ-R1K62MB rack node was used, with the same computer node (node 107) from the liquid-cooled system. It is also worth to mention that the power supply unit used in this test was the same model (Super Macro PWS-1K62P 1R) as liquid cooled system, but the air-cooled version and liquid-cooled version power supply were not interchangeable.

The test software is identical to the previous test for the liquid-cooled system (Linpack / MS Windows), and when the system is under 100% power load, the mother-board power consumption read from SuperMicro IPMI is 305W.

The exhaust air outlet of the test system is a cylinder section, since the air flow in this section would not be even, so the point velocity and temperature will be measured at different radial.

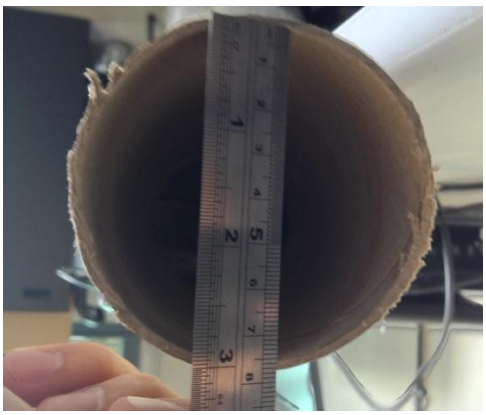

Figure 6-8 Outlet section of the air-cooled experiment system.

The **Figure 6-8** shows the cylindrical shape of the outlet section with a diameter of 75mm.

After about 2 hours of running, the temperature readings become stable, the detail of velocity and temperature reading from the outlet section are given in **Figure 6-9** and **Figure 6-10**:

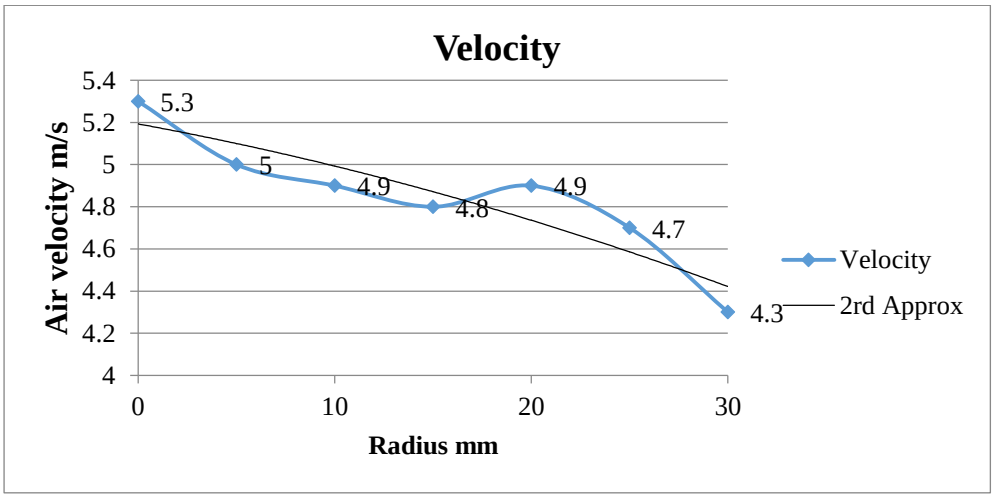

Figure 6-9 Velocity data from the outlet section

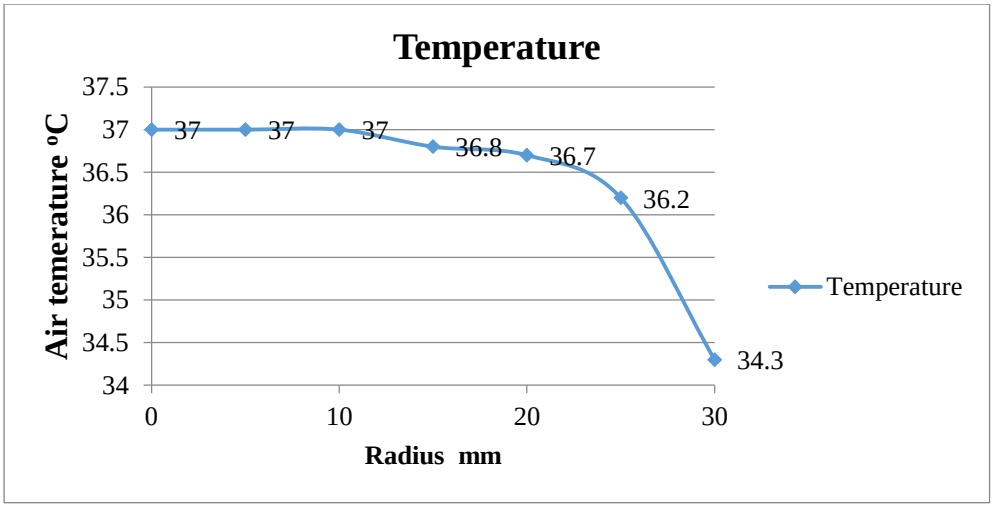

Figure 6-10 Temperature data from the outlet section

Notice: It can be seen from **Figure 6-9** and **Figure 6-10** that the velocity profile has about 15% fluctuation compared to a 2nd orderpolynomial curve approximation, yet the object of such test is to have the average flow velocity reading and the fluctuation would be acceptable.

Here in the temperature cascade of the air-cooled computer node.

Location	Result
Inlet / Ambient	23.8 °C
CPU 1 via IPMI	69 °C
CPU2 via IPMI	70 °C
System via IPMI	36 °C
Average outlet velocity	4.45 m/s
Average outlet temperature	36.34 °C
Temperature delta (inlet to outlet)	12.54 °C
Temperature delta (inlet to CPU)	47.7 °C

Table 6-10 Test result of the air-cooled computer node

From the **Table 6-10**, the temperature difference from the inlet to the CPU chip is about to be 47.7°C, and the temperature delta from the inlet to the outlet is 12.54°C. Consider the air density in 1 atm and 25°C would be about1.160kg/m^3, and the mass flow rate ($\dot{m}$) of the outlet can be calculated as:

$$\dot{m} = \rho \times A_Q \times \bar{v} \qquad 6\text{-}2$$

Where:

ρ is air density (1 atm, 25°C), 1. 160kg/m^3,

A_Q is the surface area of the outlet, 0.00442m^2, and

$\bar{v}$ is the averaged air velocity of the outlet, 4.45 m/s.

As a result, the mass flow rate:

$$\dot{m} = 1.160 \times 0.00442 \times 4.45 = 0.2281 \text{ kg/s} \qquad 6\text{-}3$$

Also the specific heat capacity (*SHC*) of air in 1 atm, 25°C would be 1003.5J/(kg·°C), and the delta temperature from the inlet to outlet ΔT is 12.5°C, where the total heat power $\dot{Q}$that released into the air would be:

$$\dot{Q} = \dot{m} \times C_p \times \Delta T \qquad 6\text{-}4$$

$$\dot{Q} = 0.2281 \times 1003.5 \times 12.54 = 287.4 \text{ W}$$

From the result above, the heat energy released to the air from the system seems to match the energy consumption from the SuperMicro motherboard, therefore the delta temperature across the system should be correct.

Hypothetical model of back door water-cooled and fully immersed liquid-cooled solution for data centre application

In this part of the study, 2 hypothetical systems will be constructed based on the experimental data that obtained from the previous section. They are based on the same computer component and same supporting equipment.

The configuration of both hypothetical system will have 14 cabinets with 48 computer nodes on it. Both systems will be 2x redundancy. The Schematic drawing of the air-cooled based back door water-cooled data centre layout will be (**Figure 6-11**):

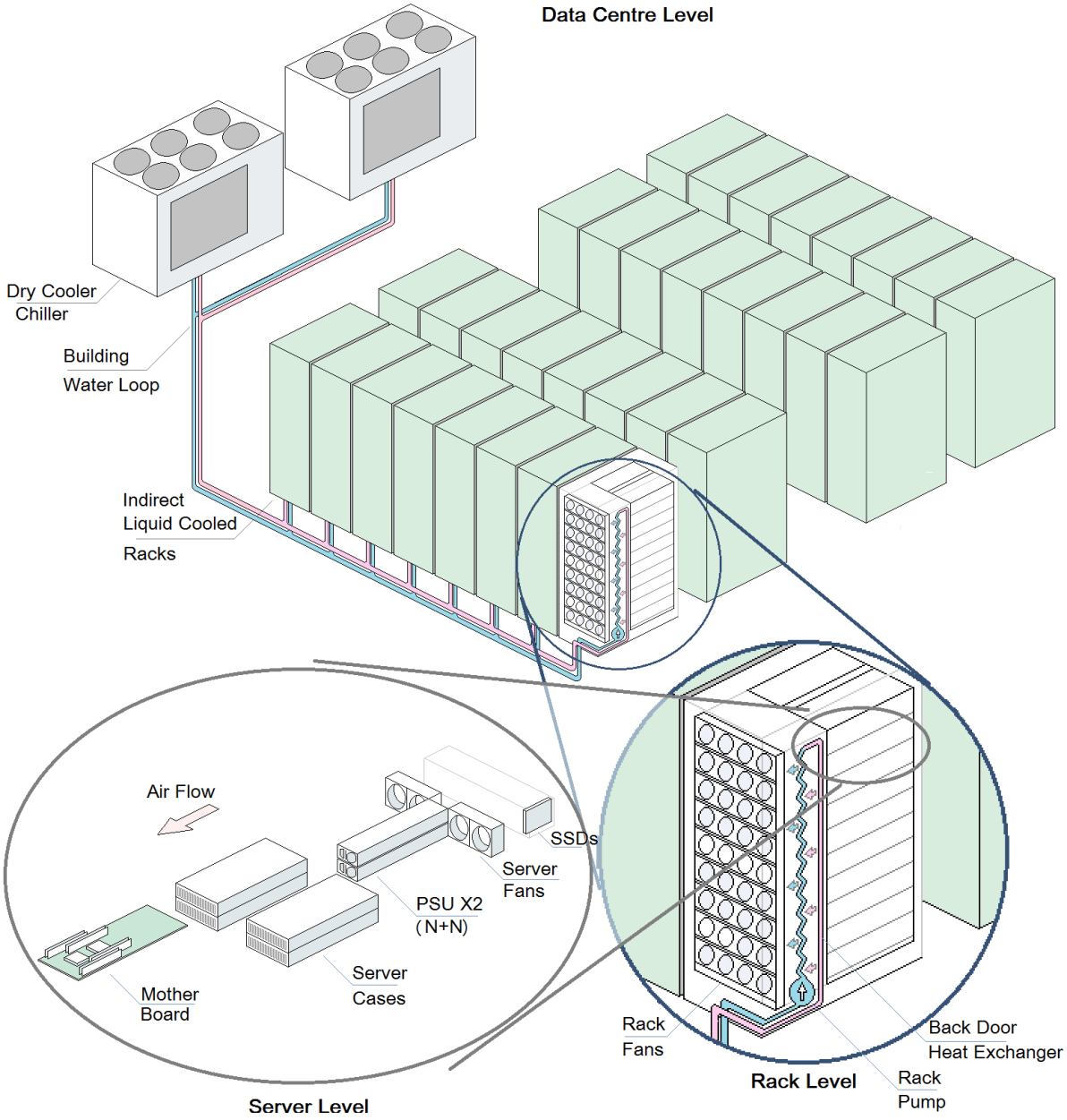

Figure 6-11 Schematic drawing of the back door water-cooled data centre (250 kW system)

A schematic drawing of the fully immersed liquid-cooled data centre is given by **Figure 6-12**:

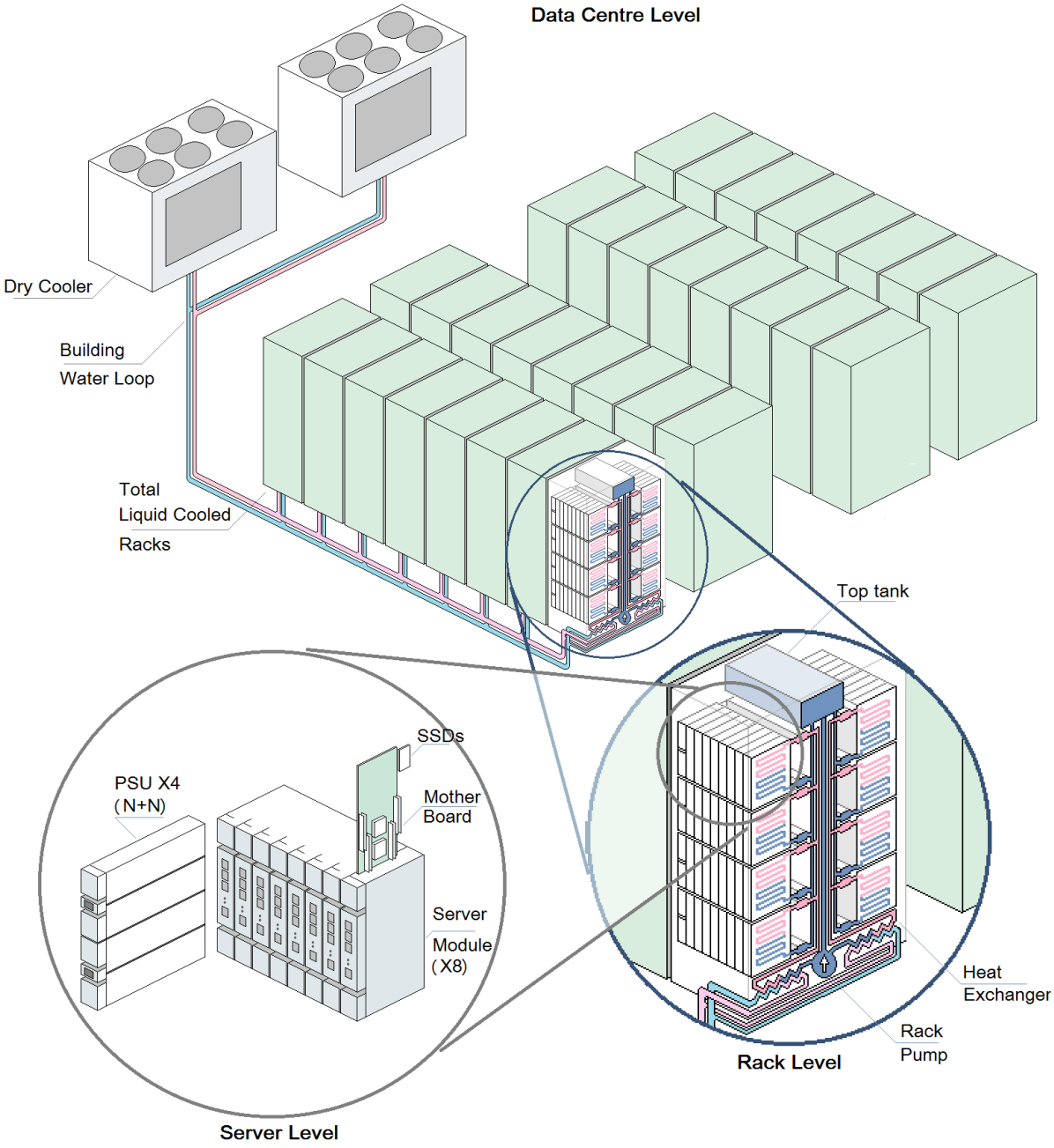

Figure 6-12 Schematic drawing of the fully immersed liquid-cooled data centre (250 kW system)

From **Figure 6-11** and **Figure 6-12** it can be seen that the major difference between the 2 systems is the cooling method for the computer node, and the basic data centre layout is almost identical. One thing should be mentioned as well, though both systems used the same external heat rejection unit, the fully immersed liquid-cooled system does not require the chiller functionality to be switched on, therefore the energy consumption on this part will be different.

The full set of calculated results for the two hypothetical systems will be:

	Part	Model	Load	number	Back door water cooled	Full immerse liquid cooled
Server level /IT load						
Common component	Computer	X9DTT / Intel Xeon E5-2670 X2	305W 306 Gflops	48×14 = 672	204.96kW 205.6Tflops	204.96kW 205.6Tflops
	Storage	Intel SSD 330	0.85W	672	0.571kW	0.571kW
	PSU loss	SuperMicroPWS1K62	7% loss	168	15.67kW	14.43kW
Back door water cooled	PSU Fan	Nidec R40W12BGCA	15.8W	168	2.65kW	
	System Fan	Nidec V80E12BS2	23.4W	672	15.72kW	
			IT component load		223.91kW	206.27kW
Cabinet level						
Common component	Tel-com Equipment	D-Link DGS-1210-48	33.4W	28	0.935kW	0.935kW
	PDU	Avocent PM3000	3.5% loss	28	7.84kW	7.84kW
Back door water cooled	Rack fan	Airedale LogiCoolOnRak LOR6042U-C028-0	161W	14	2.254kW	
Liquid cooled only	Pump	GrundFos Alpha 2L	45W	14		0.63kW
			Rack component load		11.03kW	8.78kW
			Total load		234.94kW	215.05kW
Total Facility Power						
Common component	UPS	APC Symmetra PX 250kW	4% loss	2	9.40kW	8.60kW
Back door water cooled only	Ventilation	Airedale AlpaCoolDF25A / CUS8.5	880W	10	8.8kW	
	CRACs	Airedale Ultima Compact Chiller UCFC250D-8/2	EER= 0.03 Chiller on	2	77.54kW	
Liquid cooled			EER=19.3 Chiller off	2		11.14kW
			Facility component load		95.73kW	19.74kW
			Total load		**330.67kW**	**234.80kW**
			Power saving			95.88kW
			Mflops/W		621.86	875.79
			Total cooling power		98.17kW	11.77kW
			pPUE		**1.477**	**1.138**

Table 6-11 Energy stack-up data of an air-cooled data centre compares to a liquid-cooled data centre (Chi, 2013)

Notice: The energy data from above based on both system running under full load condition.

From **Table 6-11** it can be seen that the fully immersed liquid-cooled solution can achieve a PUE down to 1.138, the back door water-cooled system which could have a PUE about 1.48. In fact from the IT level and rack level the fully immersed liquid-solution does not gain significant energy efficiency improvement by using pumps instead of fans, but in the building level where the back door water-cooled system is switched on the chiller will result in a much poorer thermal efficiency compared to a fully immersed liquid-cooled system.

Because most air-conditioning chillers has an EER (Energy Efficiency Rate) of 3 in the full load condition, this means any system with chillers switched on will have no less than PUE 1.33. In reality The HPC data centre in the University of Leeds requires 100kW of cooling power in summer days when it is full load, which yields a partial PUE of 1.4.

It is also possible to compare the Performance Per Watt (PPW) from these 2 hypothetical systems due to their identical computing hardware. From the table above the air-cooled system rated to 621.86 MFLOPS/W which is close to the 10th (Tianhe-1A) in 2012 green 500 data centres, while the liquid-cooled system rated to 875.79 MFLOPS/W which above the 4th (RIKEN AICS) in the same rating table.

One of the reason that fully immersed liquid-cooled system can avoid using chillers is that it can transfer the heat energy from the computer heat source to the outside environment with lower temperature difference. In fact it can cool down a data centre even with relatively high inlet water temperature so that chiller and refrigeration would not be needed. The temperature data can be seen in the following table:

	Back door water-cooled system			Fully immersed liquid-cooled system		
	medium	Temperature		medium	Temperature	
		in	out		In	out
Ambient	Air		25ºC	Air		25ºC
Chiller	R407c/ water	25ºC	**20ºC**	Water	38ºC	32ºC
Building water	Water	20ºC	22ºC	Water	32ºC	38ºC
Ventilation	Air / water		24ºC			N/a
Rack	Air	24ºC	36ºC	Water	33ºC	39ºC
Computer node	Air		36ºC	Water	33ºC	39ºC
				HFE7300		53ºC
CPU	Air		70ºC	HFE 7300		70ºC
Max delta temperature	CPU to Chiller			CPU to Ambient		
			50ºC			45ºC

Table 6-12 Temperature stack-up data of an air-cooled data centre compares to a liquid-cooled data centre

From **Table 6-12** it can be seen that the back-door water-cooled system requires the chiller to be switched on to have the extra 5ºC temperature delta in order to achieve same 70ºC CPU temperature in this case. On the other hand the fully immersed liquid-cooled system would not require such work because it requires smaller delta temperature to achieve the same cooling effect

This research shows that the liquid-cooled (Iceotope solution) system runs at PUE 1.138 compares to air-cooled system runs at PUE 1.477, about 33.8% more efficient (based on PUE); also the liquid-cooled system has 875.79 MFLOPS/W compared to the air-cooled system with 621.86 MFLOPS/W, which is 40.8% out-performance than the air-cooled system in PPW. Finally the liquid-cooled

system reduced 95.88kW of total power, saves 29% of the total power from the air-cooled system, also saves 88% cooling power from the air-cooled system.

6.2Thermal performance tests of the Iceotope immersed liquid-cooled HPC rack under ASHRAE W5 standard

This thermal performance test follows the ASHRAE W4 (2-45ºC) and W5 (>45ºC) standard by operating fully immersed liquid-cooled HPC system (provided by Iceotope) in the University of Leeds, Mechanical Engineering Department. The American Society of Heating, Refrigerating and Air-Conditioning Engineers (ASHRAE) present a thermal guide line back in 2011 (ASHRAE, 2011) for a liquid /water cooled data centre application. The level of inlet water temperature indicates the re-usability of the heat energy in the water system, and the top line of the standard is the ASHRAE W5 standard, which requires the water inlet over 45ºC and continue running for more than 24 hours.

At the time the liquid-cooled system just finished the mid-life span upgrade so some of the computer nodes were different from the previous test. Also the task of the system was shifted from pure laboratory equipment to a slave machine of the University of Leeds Arc-1 HPC system. At this point the liquid-cooled was taking academic tasks from university students and research staff. The scope of tasks that run in the system was random and various in types, intensity and duration. This means such system is no longer suitable for long term laboratory experiment, but it is also ideal to measure its performance in the real-world condition rather than in laboratory tests.

Overview of the server cabinet setup

Before stepping into the test section there are few points that need to be mentioned. One is the system upgrade IT specs: although most of the computer nodes remain unchanged, 3 AMD nodes have been replaced with new Intel high performance computer nodes. This results in better reliability since the AMD systems has been unreliable in some cases, and better computation speed since the newly installed nodes are significantly faster, but also consumes slightly more power due to the new computer nodes. The following table will highlight the major changes in the IT spec (**Table 6-13**):

Node	CPU	Cores per CPU	Total core	Frequency	Total memory
101	AMDOpteron 6272	16	2 x 16	2.1GHz	48GB
102	Intel Xeon E5-2670	8	2 x 8	2.6GHz	32GB
103	**Intel Xeon E5-2680**	**8**	**2 x 8**	**2.8GHz**	**32GB**
104	Intel Xeon E5-2620	6	2 x 6	2.0GHz	32GB
105	Intel Xeon E5-2620	6	2 x 6	2.0GHz	32GB
106	AMDOpteron 6272	16	2 x 16	2.1GHz	48GB
107	Intel Xeon E5-2620	6	2 x 6	2.0GHz	32GB
108	Intel Xeon E5-2620	6	2 x 6	2.0GHz	32GB
109*	**Intel Xeon E5-2690**	**8**	**2 x 8**	**3.0GHz**	**32GB**
110	**Intel Xeon E5-2670**	**8**	**2 x 8**	**2.6GHz**	**32GB**

Table 6-13 Iceotope rack IT / computer node configuration

Notice that the top spec node 109 is specifically appointed to the Institute of Thermofluids in University of Leeds to run high-intensity CFD tasks. Also the computer node numbering (IP address) was slight shifted, for example the new node 102 in fact was the original node 107 in the previous section of thermal test.

Note also that as a result of a mid-life span upgrade, a simple temperature controller (STC-1000) has been installed in the external water circuit. The STC-1000 temperature controller is a simple cut-off type controller, it can switch-off the power supply of the external water pump when the system reach or exceeds the pre-set temperature and switch back on the pump when below such temperature. In fact it is a 2 way controller that can work for heating and cooling control, but in the following test only cooling control will be used. This controller provides a level of thermal control to the system, and gives it the functionality for the next step of the test. The specification of the STC-1000 temperature controller is given in the following **Table 6-14**:

STC-1000 Specification	
Default lag-temperature	0.2 ^{o}C
Default delay-time	5 min
Accuracy	0.1 ^{o}C

Table 6-14 STC-1000 temperature controller specification

To avoid controller self-oscillation a lag-temperature and delay time could be set. Notice that the default value of lag-temperature and delay time was used in all tests:

The liquid-cooled HPC system is undertaking academic jobs from staff and students which included their research work. As a result the installation, activation and functioning of the temperature controller should not be noticed by the users and must not interrupt the ongoing works. So the implementation of the controller was on an external water loop pump, this would keep the system

running for a short period when the installation has taken place. The sensor of the controller was put to the internal water loop / inlet section, which should be the water section before feeding the computer nodes. The diagram and photo of the controller are shown in the following **Figure 6-13**:

Figure 6-13 Installation and functioning of STC-1000 temperature controller

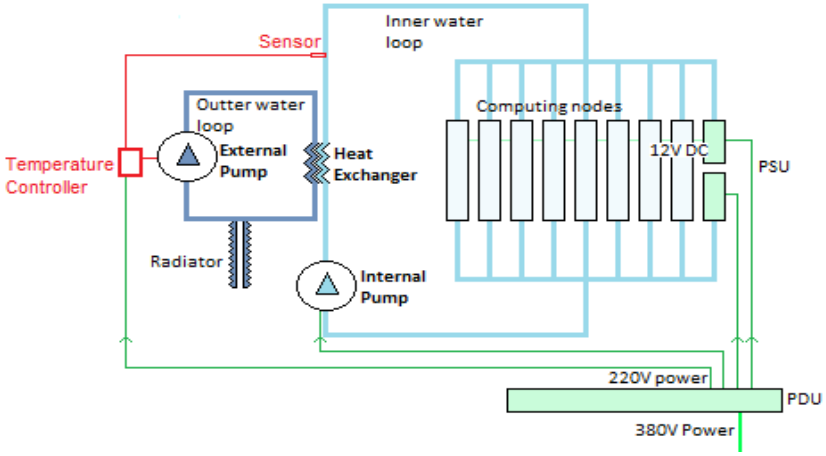

Figure 6-14 liquid-cooled system layout diagram with the temperature controller high-lighted.

There are 2 parts of the test: Firstly there is a long-term test based on the real-world / current state of the system at the time. The primary objective of the long-term change is to increase the system temperature without interfering with the ongoing work of the system. Second part is a short term test based on a bench-mark test by changing / increasing the temperature with a given computing load (StressLinux).

Long term thermal test

The long term test had taken place from 15/4/15 to 13/5/15, a duration of 4 weeks / 28 days. The controller temperature has been reset on every Wednesday at 12:00 and keeps the system running

above the pre-set temperature for 1 week / 7 days. The temperature range starts from 35ºC to the maximum 47.5ºC. The test plan is shown in the following **Table 6-15**:

	Sunday	Monday	Tuesday	Wednesday	Thrusday	Friday	Satusday
April				15	16	17	18
				Long term test (35ºC)			
	19	20	21	22	23	25	25
	Long term test (35ºC)			Long term test (40ºC)			
	26	27	28	29	30	1	2
	Long term test (40ºC)			Long term test (45ºC)			
May	3	4	5	6	7	8	9
	Long term test (45ºC)			Long term test (47.5ºC)			
	10	11	12	13	14	15	16
	Long term test (47.5ºC)			General usage			Maintenance
	17	18	19	20	21	22	23
	Maintenance					General usage	
	24	25	26	27	28	29	30
	General usage				Maintenance		
June	31	1	2	3			
	Maintenance			Short Term Test			

Table 6-15 Liquid-cooled system thermal test schedule

Since the system has been prepared, an e-mail reminder has been setup to send out the mother-board temperature every 2 hours. Notice that the temperature controller does not have data-link and remote functions, and the computer system is running and could not be interrupted, the temperature data from IPMI is the only source of information. The test result is shown in the following figure:

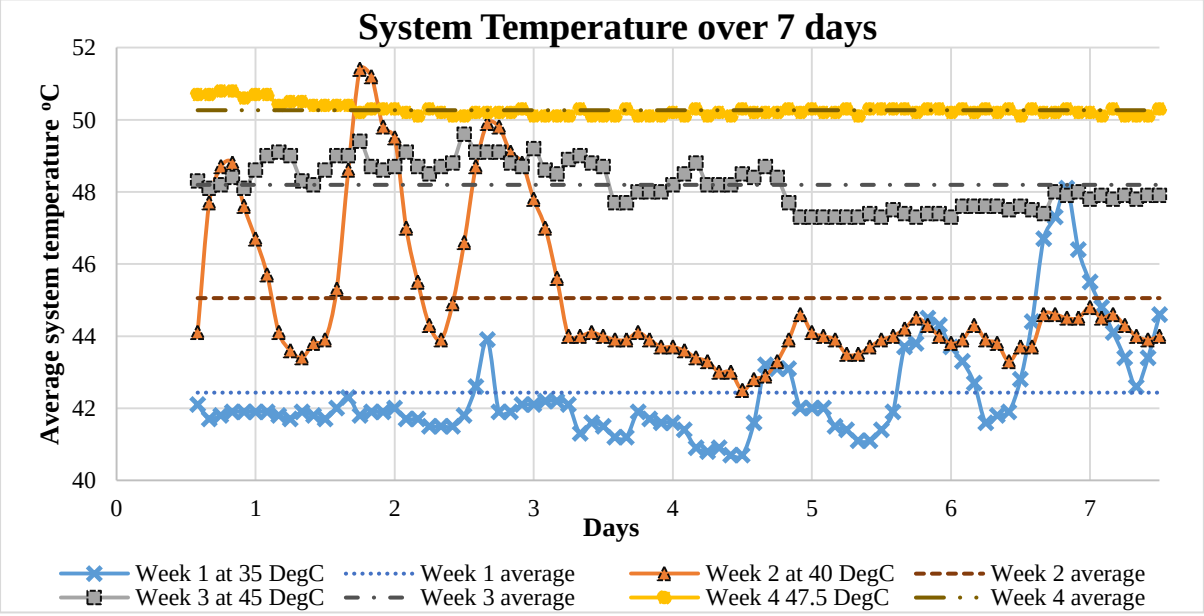

Figure 6-15: System temperature (Mother board) record from every 7 days

From **Figure 6-15** of temperature records it can be seen that the temperature controller has kept the system temperature above a certain level. While the external cooling system is passive and that means the system temperature will be affected by the local temperature. Also all the systems are running random tasks in different time scale / intensity, this results in a fluctuating system running temperature as in the real-world condition.

The result of this test shows how the temperature controller performs, also in the week-4 test the fully immersed liquid-cooled computer system was cooled with an inlet water of 47.5ºC for 7 days without notice by the users.

Short term test

The Short term test is based on a bench-mark software, StressLinux, which can drive the system to the maximum performance and thermal-load in a convenient way. So there are 2 goals for this short test:

The second goal is to measure the temperature response of the system. In most of the mathematics modelling and CFD analysis the cooling performance is assumed to have a linear relationship with the system reference temperature. This is particularly important for Boussinesq approximation and the CTG model presented in the previous chapter. In the other words, if the CPU temperature responds to the controller pre-set temperature non-linearly, the CTG model for natural convection calculation may not be valid for the fully immersed liquid-cooled computer system.

The idea of running the short term test is to measure the power consumption against the temperature increment while the system remains in maximum performance. Ideally a computer should perform equally before the component (CPU) reaching the cut-off temperature. The short term test took place in 3/6/15, when all the daily work of the system was suspended for a few hours to give a time-gap to complete the test. It started from 11:00AM with 37.5ºC pre-set temperature, and steadily increased to 50ºC at 13:00PM. The system remained in 50ºC for 1 hour till 14:00PM, then the test was finished. Here is the table of short-term test (**Table 6-16**):

Pre-set temp		37.5 ºC	40 ºC	42.5 ºC	45 ºC	47.5 ºC	50 ºC	50 ºC
Measure time		11:20	11:45	12:00	12:20	12:45	13:00	14:00
101	CPU 1	medium	medium	medium	medium	High	High	High
	CPU 2	medium	medium	medium	medium	medium	medium	medium
	System	43	45	49	51	54	56	57
102	CPU 1	59	62	64	66	68	71	73
	CPU 2	60	63	65	67	70	72	72
	System	42	46	47	50	53	55	56

103	CPU 1	59	62	64	67	70	72	72
	CPU 2	58	61	63	65	68	70	71
	System	42	45	48	50	53	55	56
104	CPU 1	59	62	64	67	68	70	71
	CPU 2	57	60	61	65	69	70	68
	System	41	45	46	48	51	53	54
105	CPU 1	63	66	68	70	73	71	76
	CPU 2	59	62	64	60	68	71	72
	System	42	43	47	50	52	55	55
106	CPU 1	medium	medium	medium	medium	High	High	High
	CPU 2	medium	medium	medium	medium	medium	medium	medium
	System	44	45	49	52	55	57	57
107	CPU 1	59	62	63	66	68	70	71
	CPU 2	60	62	66	68	72	72	73
	System	42	45	47	50	53	55	56
108	CPU 1	57	60	62	64	67	69	70
	CPU 2	57	60	62	64	66	68	69
	System	40	43	46	48	51	53	54
109	CPU 1	72	75	78	79	81	84	85
	CPU 2	70	74	76	78	80	83	84
	System	44	47	50	53	55	58	58
110	CPU 1	69	72	72	76	79	81	82
	CPU 2	64	67	69	71	74	76	77
	System	45	48	51	53	55	58	59
Total power (kW)		2.36	2.38	2.39	2.42	2.43	2.46	2.47

Table 6-16 Short term thermal test of the fully-immersed liquid-cooled computer system

Table 6-16 shows how the device (CPU / System) temperature against the pre-set controller temperature and the overall power consumption. In order to have a clearer view of the result, here is the plot diagram of power consumption against the device temperature:

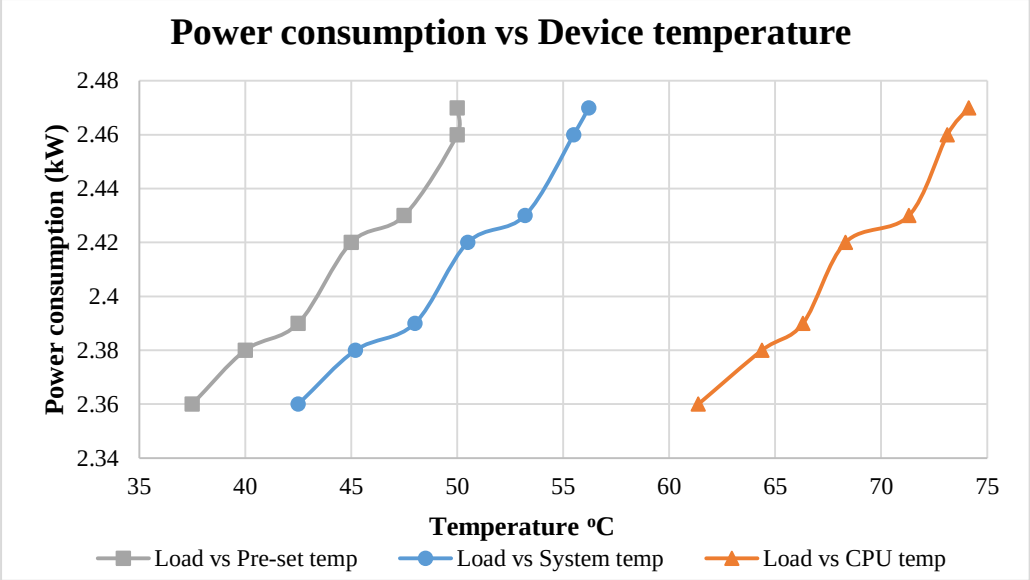

Figure 6-16 Overall system power consumption against the device temperature

From **Figure 6-16** it is interesting to see the overall power-consumption of the whole system (measured when the pump was switched-on) went up following the temperature increment. The tendency of power consumption increase is slightly sharper when the CPU / system temperature is close to the top limit. Since the computer nodes were in almost constant power load before reaching its thermal limit and both internal and external water pump have constant load pumps, the only possibility was the liquid-cooled power supply unit behaving differently under different temperature.

Also for the temperature response, the plot diagram of test result temperature against the set temperature is given by **Figure 6-17**:

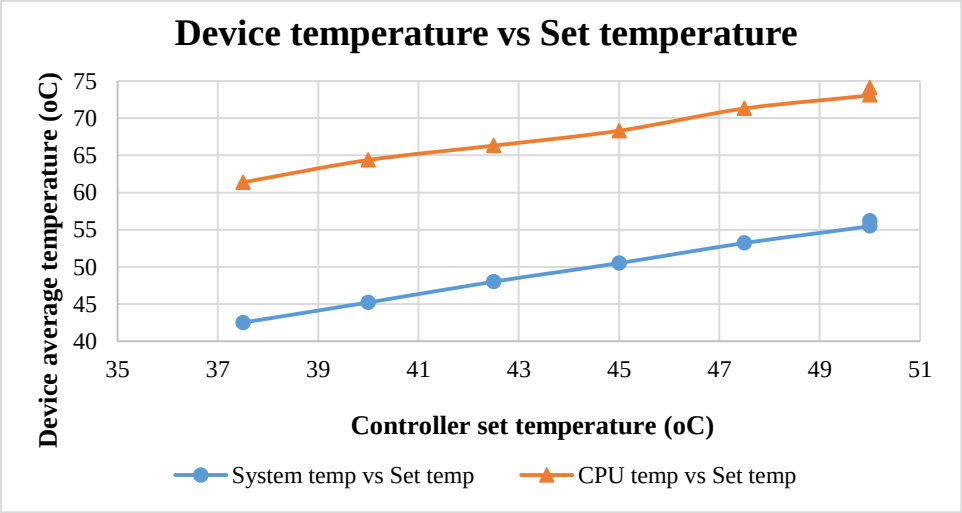

Figure 6-17 CPU and system average temperature against controller set temperature

From **Figure 6-17** it can be seen that the CPU temperature and the system temperature depend linearly on the pre-set temperature of the controller. This simply means the heating part and cooling part of the natural convection is thermally symmetrical. This should fit the Boussinesq approximation since the mathematical difference between heating and cooling part of natural convection under its assumption was only the direction of velocity and positive-negative temperature difference.

6.3 Summary

The thermal test in chapter 5 was more focused on comparing results with the CTG model calculation for specific design problem, however the thermal test in this chapter is more focused on the general performance of the fully-immersed fully liquid-cooled computer design.

With the thermal test result, it is clear that there should be energy advantages and potentials with the fully-immersed fully liquid-cooled computer design, and the advantage on pPUE (less than 1.14, **Table 6-11**) of the liquid-cooled design proof such claim. Also such thermal test will be necessary in further development and improved design stage, since this will be a part of the work flow from predict, analysis to proof the thermal performance of the design and improvement.

7. Conclusion

This chapter highlights the main conclusions of the research undertaken in this thesis.

7.1 Overview of this thesis

This research is based on an advanced technology of Supercomputers and data centre thermal management: the fully immersed liquid-cooled data centre solution. From the test in chapter 6, Such system can achieve a pPUE as low as 1.138 and is currently (up to 2015) one of the most efficient solution for high density computer application, but to further improve the performance of liquid-cooled computer system, it requires intense design work and full understand of density driven natural convection. To achieve this there are few challenges which this research tackles:

One of the difficulty is to solve the Navier-Stokes equations for natural convection flow analytically, because the natural convection flow expression coupled the 2^{nd} order Navier-Stokes equation with another 2^{nd} order Convection-Diffusion equation makes it a 4^{th} order system in mathematical term. This combines with the 2-dimensional flow field and results in even more complex problems for analytical methods. This issue has been addressed in chapter 3 of this thesis by introducing the Constant Thermal Gradient (CTG) model to solve the simplified Navier-Stoke Equation and energy equation.

Another difficult is to find a single characteristic length scale for the natural convection problem. Since it usually combines 2 flow directions, thus the choice of length scale for natural convection flow solutions is problem dependent. Chapter 4 of this thesis has been looked into this problem and came to a conclusion that open cavity and close cavity should have different correlation. Open cavity problem can uses simple linear correlation between X-axis and Y-axis temperature development, which can also converted to general Nusselt correlation $Nu = f(Ra)$. Close cavity problem could be more complex and would require different correlation method.

CFD analysis has been carried out in this thesis as well, which played an important in finding Thermal Gradient Constant CTG in chapter 4 and validating mathematical modelling for practical problem in chapter 5. Although CFD solution may be considered as a convenient tool to solve the natural convection problem, it often has instability and convergence problems. In order to get a converged solution sometimes it will need a very high quality and large size mesh to fulfil the need of resolution on natural convection boundary layer. So it usually results in a task that consumes large amount of time and computing resource to solve the problem.

7.2 Achievements

This PhD project is both an academic research work and an engineering development work that sponsored both by the university and an industrial body (the Iceotope Company). By completing the requirements both from the university and the industry, there are 2 parts of achievements in this thesis, the Academic achievement and Engineering achievement

Academic achievement

Usually Rayleigh number, Prandtl number and Nusselt number are used to describe the natural convection, these are the expressions obtain by non-dimensionalising the Navier-Stokes equation. This thesis uses a slightly different method to obtain the natural convection flow expression by finding the analytical solution (with close form expression) than most convection. And to solve these equations analytically, it can be achieved by simplifying the Navier-Stokes equation and Convection-Diffusion equation for the problem. Though the natural convection problem is a 4th order system of equations, it is still possible to solve these analytically by simplifying the problem with only 1 dimension of velocity term left in the equations – and this is the concept of Constant Thermal Gradient (CTG) model that developed during this research.

For open cavity type of natural convection problem it is possible to obtain simplified analytical solutions using CTG model, this has been discussed in chapter 4 of this thesis. But in the other hand close cavity is a more complex problem rather than open cavity case, it would still be solve with the CTG model but require more sophisticated approximation. General speaking the CTG model is largely based on the closed-form expression of the analytical solution, but still needs at least one approximation value (the thermal gradient constant C_{TG}) to complete the expression. Nevertheless it provides a relative quick solution to predict the natural convection flow behaviour.

Another achievement with the CTG model is that it can rewritten as the general Nusselt number correlation Nu* = f (Ra*) (for open cavity problem). This is particularly straight-forward in the open cavity cases, which the CTG model energy equation can be written as:

$$\mathrm{Nu}^*_h = \left(\frac{1}{2}\right)^{\frac{2}{5}} \cdot \sqrt[5]{\mathrm{CTG}} \cdot \sqrt[5]{\frac{\rho^2 \cdot g \cdot \beta \cdot C_p \cdot \mathrm{Q}^* \cdot h^4}{\mu \cdot \lambda^2}}$$

This could be fitted into the form of Nusselt number correlation that Orhan Aydin, Laila Guessous suggested (Orhan Aydin, Laila Guessous, 2001):

$$\mathrm{Nu}_{local} = C^* \cdot (Gr^* \cdot Pr)^{\frac{1}{5}}$$

Which was interested to see the outcome of the analytical solution from this thesis matches the correlation based on experimental results.

Engineering achievement

The core engineering achievement in this thesis was the development of a work-flow that for natural convection based problem, especially for fully-immersed liquid-cooled computer system. This work-flow has 3 steps. The first step is a quick thermal prediction using the CTG model. The CTG model not only gives a quick view of the heat transfer efficiency of the problem, but also gives a length scale (l^*) for the velocity and temperature field. The second step is the usage of Computer Aided Engineering (CAE) software application such like CFD analysis, which the outcome from previous step provides a view of scope for CFD modelling options, and also provides a length scale (l^*) that could be a guide-line for CFD meshing option. The last step of the work-flow is methodology of doing the laboratory and experimental thermal test to conclude the result. In this step 2 type of figure can be given in thermal test: a PUE value that generally refers to the energy usage figure, and an ASHREA (W5) standard that shows the potential of reusing waste heat.

This thesis also successfully constructed CFD solutions with reasonable resource consumption and accuracy compare to the experimental result. The CFD results also provide a prediction of the new heat sink thermal performance, which was also accepted by the sponsor industrial body as a potentially useful application.

Also the experiments had been completed in thesis were important as well. The case study of fully immersed liquid-cooled data centre solution and the rear door water-cooled data centre solution shows how pPUE could be used in comparing 2 different types of computer system, and provides the evident of fully-immersed liquid-cooled system energy advantage over some conventional design by achieving low PUE figure (pPUE = 1.138). Another experiment in the thesis is to test liquid-cooled system following ASHRAE W5 standard. It proofs not only the ability of reusing waste heat with such system, but also the resilience of the liquid-cooled system can perform sustainably under high ambient temperature and high work load. The result of both experiments has been accepted by the sponsor company as the part of their thermal management white paper (Iceotope, 2013).

Future work

The core value in this thesis is the attempt to fine the analytical solution of Navier-Stokes equation and energy equation in natural convection, and the outcome is the Constant Thermal Gradient (CTG)

model. Thus one of the important future work is to complete the Constant Thermal Gradient (CTG) model in closing the analytical solution. Although the CTG model is largely based on analytical solution, a C_{TG} value still needed from CFD analysis and arguably it was not complete analytical. It might be the case that an experimental constant cannot be avoid since the terms of 'fully developed flow' is somewhat a statement for experimental result, or a complete analytical solution could be achieved by making more assumption. Notice that the energy equation can be rewritten into the general Nusselt number correlation $Nu^* = f(Ra^*)$, that also means the C_{TG} value could be obtained from such correlation done by other authors.

Also another potential of the CTG model is that it could be used in other types of natural convection problem rather than cavity problem. It was not included in this thesis due to the time and effort during the PhD degree, but it did tried the CTG model in a channel flow natural convection problem. With the appropriate DT/DY or C_{TG} value, the same equation set with channel flow boundary condition can give an analytical solution as well, only that the expression of the solution is more complex. Also at the moment the Constant Thermal Gradient (CTG) model can only solve the natural convection case with a vertical wall (along the gravity direction), whether it can solve the problem with a horizontal wall (normal to the gravity direction) will be an interesting question

Last but not least, there is still limitation of using CTG model for natural convection heat transfer prediction, it might be the case that only with 2 constant values (C_{TG} and $K_{coolant}$), and this is not enough to describe the close cavity problem. The close cavity problem is a combination of natural convection and force convection that might not have a simple solution, in fact some assumption such as Nusselt correlation from open cavity problem could not simply 'transplant' to the close cavity problem.

8. Reference

3M, (2015). *3M Novec 7100 Fluid Used in World's Largest Two-Phase Immersion Cooling Project*, 3M Immersion Cooling. [online] Available at: http://solutions.3m.com/wps/portal/3M/en_US/NA-DataCenters/DataCenters/Solutions/EfficiencySustainability/ImmersionCooling/ [Accessed 8 Dec. 2015].

3M, (2015). *3M Thermal management fluids brochure*. 1st ed. 3M electronics Markets Materials Division. [ebook] Available at: http://multimedia.3m.com/mws/media/65495O/3mtm-thermal-management-fluids.pdf [Accessed 8 Dec. 2015].

Airedale, *University of Leeds case study*, Airedale International Air Conditioning Limited, [online] Available at: http://www.airedale.com/web/About-Airedale/The-News-HVAC/University-of-Leeds.htm [Accessed 8 Dec. 2015].

Almoli, A., Thompsion, A., Kapur, N., Summers, J., Thompson, H., Hannah, G., (2012) Computational fluid dynamic investigation of liquid rack cooling in data centres. Appl Energ 2012;89:150–5.

ANSYS Inc., 2010. *ANSYS Fluent 13 Tutorial 7, Modeling Radiation and Natural Convection,* ANSYS, Inc. pp 294

ARK, (2015) ARK, *Your source of Intel Source*, Intel, [online] Available at: www.ark.intel.com [Accessed 8 Dec. 2015].

ASIC.LLNL, (2011) *BlueGene/L*, Advanced Simulation and Computing, Lawrence Livermore National Laboratory, [online] Availabe at: https://asc.llnl.gov/computing_resources/bluegenel/ [Accessed 8 Dec. 2015].

Aydin Orhan, and Guessous Laila, (2001), *Fundamental correlations for laminar and turbulent free convection from a uniformly heated vertical plate*, Int. J. Heat Mass Transfer 44 (2001) 4605-4611

Balance, R. A., Jennings, B., Rajan, M., (2004), Unclassified Systems Available for Alliance Partners, Advanced Simulation & Computing, Sania National Laboratories, [ebook] Available at: https://asc.llnl.gov/content/assets/docs/2004_sandia.pdf [Accessed 8 Dec. 2015].

Batchelor, G.K.,(1967).*An Introduction to Fluid Dynamics* .Cambridge University Press.

Bejan, A., (2013) *Convective Heat Transfer*, Wiley

Bennett, C. O., Myers, J. E. (1962). *Momentum, Heat, and Mass Transfer*. McGraw-Hill.

Bergles, A. E. (1997). *Heat transfer enhancement—the encouragement and accommodation of high heat fluxes*. Journal of Heat Transfer, 119(1), 8-19.

Blodgett, A. and Barbour, D. (1982). *Thermal Conduction Module: A High-Performance Multilayer Ceramic Package*. IBM Journal of Research and Development, 26(1), pp.30-36.

Brady, Gemma A., Nikil Kapur, Jonathan L. Summers, and Harvey M. Thompson. "*A case study and critical assessment in calculating power usage effectiveness for a data centre*." Energy Conversion and Management 76 (2013): 155-161.

Cai Ruixian, and Zhang Na, (2003), *Explicit analytical solution of 2-D laminar natural convection*, Int. J. Heat Mass Transfer 46 (2003) 931-934.

Capozzoli, Alfonso., Primiceria, Giulio,. (2015), *Cooling systems in data centers: state of art and emerging technologies*, 7th International Conference on Sustainability in Energy and Buildings, Energy Procedia 83 (2015) 484 – 493

Chassis-Plans, (2015), *Cooling and Noise in Industrial and Military Computer Systems*, Chassis-Plan, [online] Available at: http://www.chassis-plans.com/whitepapers/cooling-and-noise/ [Accessed 14th January 2015]

Chen, S. (2015). *China shuts down space supercomputer damaged by shockwaves of deadly Tianjin blasts*. South China Morning Post. [online] Available at: http://www.scmp.com/news/china/society/article/1849200/china-shuts-down-space-supercomputer-damaged-shockwaves-deadly [Accessed 8 Dec. 2015].

Chi Y.Q., Summers J., Hopton P., Deakin K., Real A., Kapur N., Thompson H., (2014), *Case study of a data centre using enclosed, immersed, direct liquid-cooled servers* in: Annual IEEE Semiconductor Thermal Measurement and Management Symposium 2014, pp.164-173.

Churchill, S.W. & Chu, H.H.S., (1975), *Correlating equation for laminar and turbulent free convection from a vertical plate*, Int. J. Heat Mass Transfer, 18:1323-1329,

Chu, R.C., Simons, R.E., and Chrysler, G.M., "*Experimental Investigation of an Enhanced Thermosyphon Heat Loop for Cooling of a High Performance Electronics Module*," Proceedings of the 15th IEEE Semiconductor Thermal Measurement and Management Symposium," pp.1-9, 1999.

Computer History Museum, 2015, *Smaller and Faster, the Cray 2 and Cray 3*, [online], available at < http://www.computerhistory.org/revolution/supercomputers/10/68>[Accessed 14th January 2015]

CoolIT Systems, *CoolIT Product Guide.* (2014). CoolIT Systems. [ebook] Available at: http://www.coolitsystems.com/phocadownload/coolit/marketing/771-00012-reva09_coolit-product-guide.pdf [Accessed 8 Dec. 2015].

CRAY, (1988), *The CRAY-2 Series of Computer System Brochure*, CRAY Systems, [ebook] Available at: http://www.craysupercomputers.com/downloads/Cray2/Cray2_Brochure001.pdf [Accessed 8 Dec. 2015].

Dillon H.E., Emery A., Mescher A. (2013). *Analysis of Chaotic Natural Convection in a Tall Rectangular Cavity with Non-Isothermal Walls*. Frontiers in Heat and Mass Transfer, 2(2).

Dongarra., (2013) *TianHe 2 Dongarra Report*. [ebook] Available at: http://www.netlib.org/utk/people/JackDongarra/PAPERS/tianhe-2-dongarra-report.pdf , University of Tennessee, Oak Ridge National Laboratory

Elder, J. (1965). *Laminar free convection in a vertical slot*. J. Fluid Mech., 23(01), p.77.

Fox, R. W., McDonald, A. T., Pritchard, P. J, (2006). *Introduction to fluid mechanics*, 6th ed., Hoboken, NJ: Wiley. p. 213–215. ISBN 9780471735588.

Fujii Tetsu, and Fujii Motoo, (1976), *The dependence of local Nusselt number on Prandtl number in the case of free convection along a vertical surface with uniform heat flux*, Int. J. Heat Mass Transfer 19 (1976) 121-122

Goldstein, R.J., Eckert, E.R.G., (1960), T*he steady and transient free convection boundary on a uniformly heated vertical plate*, Int. J. Heat Mass Transfer 1 pp.208-218

Greenheck, (2015). *The Basics of Fan Performance Tables, Fan Curves, System Resistance Curves and Fan Laws (FA/100-99)*, [online] Available at: http://www.greenheck.com/library/articles/10 [Accessed 8 Dec. 2015].

Habata, S., Yokokawa, <., Kitawaki, S., (2002), *The Earth Simulator System:* NEC Research and Develop, Vol.44, No. 1, January 2003, [ebook] Available at: http://www.egr.unlv.edu/~meiyang/ecg702/proj/theearthsimulatorsystem.pdf [Accessed 8 Dec. 2015].

Heron, S. (2015). *Improvements in the cooling of valves or other moving parts of internal combustion engines that are subject to high temperature*. GB 19230020147 19230807.

Hinze, J. O., (1975). *Turbulence* (2nd ed.). McGraw-Hill.ISBN 0-07-029037-7

Holman, J. P. (2002). *Heat Transfe*r. McGraw Hill

Hopton, P. ; Summers, J., (2013), *Enclosed liquid natural convection as a means of transferring heat from microelectronics to cold plates*, Annual IEEE Semiconductor Thermal Measurement and Management Symposium 2013, pp. 60 – 64

Iceotope (2013), *Typical air-cooled data centre compared to Iceotope's liquid-cooled solution*, [ebook] Available at http://www.iceotope.com/images/upload/files/resources-whitepapers_pdf_424.pdf [Accessed 6 Jun. 2016].

Incropera, Frank P.; DeWitt, David P. (2007). *Fundamentals of Heat and Mass Transfer* (6th ed.). New York: Wiley. p. 514. ISBN 978-0-471-45728-2.

Intel.com, (2015). *PRESS KIT -- Moore's Law 40th Anniversary*. [online] Available at: http://www.intel.com/pressroom/kits/events/moores_law_40th/ [Accessed 8 Dec. 2015].

ITU, (2015). *Individuals using the Internet 2005 to 2014*. International Telecommunication Union, United Nations, [ebook] Available at: https://www.itu.int/en/ITU-D/Statistics/Documents/facts/ICTFactsFigures2014-e.pdf [Accessed 8 Dec. 2015].

Iyengar, M., David, M., Parida, P., Kamath, V., Kochuparambil, B., Graybill, D., Schultz, M., Gaynes, M., Simons, R., Schmidt, R., and Chainer,T., (2012), *Server Liquid Cooling With Chiller-Less Data Center Design to Enable Significant Energy Savings*, 28th IEEE SEMI-THERM Symposium, San Jose, CA, pp. 212–224, March 18–22, 2012

Jurvetson S. T., (2004). *Transcending Moore's Law with Molecular Electronics and Nanotechnology*. [ebook] Available at: http://www.kurzweilai.net/transcending-moore-s-law-with-molecular-electronics-and-nanotechnology , Nanotechnology Law & Business, March, 2004. [Accessed 8 Dec. 2015].

Kakaç, S., Yüncü, H. and Hijikata, H. (1994). *Cooling of electronic systems. Dordrecht*: Kluwer Academic.

Karen Freeman, (1996) *George M. Grover, 81, Inventor Of Popular Heat Transfer Device*, November 03, 1996, New York Times

Kays, W. and Crawford, M. (2004). *Convective heat and mass transfer*. New York: McGraw-Hill.

Kim, Kwang-Soo, Myong-Hee Won, Jong-Wook Kim, and Byung-Joon Back. "*Heat pipe cooling technology for desktop PC CPU*." Applied thermal engineering 23, no. 9 (2003): 1137-1144.

Landahl, M.T., Mollo-Christensen, E. (1992). *Turbulence and Random Processes in Fluid Mechanics*, (2nd ed.), Cambridge

Li, Li., Zheng, Wenli., Wang, Xiaodong., Wang, Xiaorui., (2016), *Data center power minimization with placement optimization of liquid-cooled servers and free air cooling*, Sustainable Computing: Informatics and Systems xxx (2016)

Li, Zheng., Kandlikar, Satish., (2015), *Current Status and Future Trends in Data-Center Cooling Technologies*, *Heat Transfer Engineering*, 36:6, 523-538, DOI: 10.1080/01457632.2014.939032

Merkin, J.H., (1994), *Natural convection boundary layer flow on a vertical surface with Newtonian heating*. Int. J. Heat and Fluid Flow, 15, 392-398.

Moore, G. (1998). *Cramming More Components Onto Integrated Circuits*. Proceedings of the IEEE, 86(1), pp.82-85.

Morton, B. R. (1960). *Laminar convection in uniformly heated vertical pipes*. In: Journal of Fluid Mechanics, Volume 8, Issue 02 Cambridge: Cambridge Journal. p227 - 240.

Munson, B. R., Young, D. F., and Okiishi, T. H., (2002) *Fundamentals of Fluid Mechanics*, John Wiley and Sons. ISBN 0-471-44250-X

Murphy, Dave, 2007, Maintain_Your_Water-Cooling_Setup. *Maximum PC Magazine*: 58–60. [online]. Available at: <http://books.google.com/books?id=OQIAAAAAMBAJ&lpg=PA58&dq=computer%20%22water% [Accessed 8 Dec. 2015].

nVIDIA, (2015), *Tesla- High Performance Computing and Supercomputing*, nVIDIA. [online] Available at: http://www.nvidia.co.uk/object/tesla-high-performance-computing-uk.html [Accessed 8 Dec. 2015].

Ohadi,. MM., Dessiatoun, SV., Choo, K., Pecht, M., Lawler, JV., (2012), *A comparison analysis of air, liquid, and two-phase cooling of data centers*. In :Proceedings of the 28th IEEE SEMI-THERM symposium. San Jose (CA, USA); March 18–22, 2012. p. 58–63.

Pastukhov, V. G., Maidanik, Y. F., Vershinin, C. V., & Korukov, M. A. (2003). *Miniature loop heat pipes for electronics cooling*. Applied Thermal Engineering, 23(9), 1125-1135.

Patterspn, E., (2013), *RoadRunner on the road to Trinity*, National Security Science, April, 2013 : [ebook] Available at: http://www.lanl.gov/discover/publications/national-security-science/2013-april/_assets/docs/road-runner-trinity.pdf [Accessed 8 Dec. 2015].

Pope, S. B., (2003).*Turbulent Flows*, Cambridge: Cambridge University Press

Potter, M., Wiggert, D.C, 2008, *Fluid Mechanics (Schaum"s Series)*, McGraw-Hill (USA), ISBN 978-0-07-148781-8

Qureshi, Z.H., Gebhart, B., (1964), *Transition and transport in a buoyancy driven flow in water adjacent to a vertical uniformly flux heated vertical plate*, AEC Research and Development Report ANL-6835, Argonne National Laboratory, IL, 1964

Qureshi, Z.H., Gebhart, B., (1978), *Transition and transport in a buoyancy driven flow in water adjacent to a vertical uniformly flux surface*, Int. J. Heat Mass Transfer 21 pp.1467-1479

Reay, D. (1982). *The Perkins Tube—a noteworthy contribution to heat exchanger technology*. Journal of Heat Recovery Systems, 2(2), pp.173-187.

Reynolds, Osborne (1883). *An experimental investigation of the circumstances which determine whether the motion of water shall be direct or sinuous, and of the law of resistance in parallel channels*. Philosophical Transactions of the Royal Society 174 (0): 935–982

Rodi, W. (1980) T*urbulence Models and Their Application in Hydraulics - A State of the Art Review*, International Association for Hydraulics Research, Delft, Netherlands.

Seas.upenn.edu, (2015). Penn Engineering - *ENIAC: Celebrating Penn Engineering History*. [online] Available at: http://www.seas.upenn.edu/about-seas/eniac/operation.php [Accessed 8 Dec. 2015].

Sinha, P. C. (1969). *Fully developed laminar free convection flow between vertical parallel plates*. Chemical Engineering Science, Volume 24, Issue 1. London: Elsevier. p33-38.

Solvay (2014), S*olvay Galden PFPE Heat Transfer Fluid*, Solvay Data Sheets, [ebook] Available at: http://www.solvay.com/en/binaries/Galden-PFPE-Heat-Transfer-Fluids_EN-220543.pdf

Sparrow, E.M., Gregg, J.L., (1956), *Laminar free convection form a vertical plate with uniform surface heat flux*, Trans. ASME 78 435-440

SUSLOV, S. and PAOLUCCI, S. (1999). *Nonlinear stability of mixed convection flow under non-Boussinesq conditions. Part 1. Analysis and bifurcations*. J. Fluid Mech., 398, pp.61-85.

SUSLOV, S. and PAOLUCCI, S. (1999). *Nonlinear stability of mixed convection flow under non-Boussinesq conditions. Part 2. Mean flow characteristics.* J. Fluid Mech., 398, pp.87-108.

Tennekes, H. and Lumley, J. (1972). *A first course in turbulence*. Cambridge, Mass.: MIT Press.

The Green Grid, (2007), *The Green Grid Data Center Power Efficiency Metrics: PUE and DCiE White Paper #6*, The Green Grid

Tomkins, J. L., (1999), The ASCI Red Tops Supercomputer, Advanced Simulation & Computing, Sania National Laboratories, [ebook] Available at: http://www.ai.mit.edu/projects/aries/papers/distributed/asci_red_desc.pdf [Ac cessed 8 Dec. 2015]

Top500 SuperComputer site [online], Available at: http://www.top500.org/ [Accessed 8 Dec. 2015].

Tritton D. J., (1977) *Physical Fluid Dynamic*, Claremdon Press, Oxford

Turcotte D. L., Schubert G., (2002), *Geodynamics 2nd edition*. Cambridge University Press

UNFCCC, (1998). *Kyoto Protocol to the United Nations Framework Convention on Climate Change.* [ebook] United Nations Framework Convention on Climate Change. Available at: http://unfccc.int/resource/docs/convkp/kpeng.pdf [Accessed 8 Dec. 2015].

US Department of Energy, 2009, *Data Center Rack Cooling with Rear-door Heat Exchanger*, (PDF document), US Department of Energy, [online], Available at <http://hightech.lbl.gov/documents/data_centers/rdhx-doe-femp.pdf> [Accessed 14th January 2015]

Versteeg, H. K., and Malalasekera, W., (1995) *Computational Fluid Dynamic – The Finite Volume Method*, LongMan,

Varma, D., Best, C Graphics and Solomon, M., (2014), *Oil Submersion Cooling for Today's Data Centers An analysis of the technology and its business implications*, Green Revolution Cooling, [ebook]. Available at: http://www.grcooling.com/wp-content/uploads/2015/06/GRC_WP-CLICK-Oil_Sub_DCc.pdf

[Accessed 8 Dec. 2015].

Weik, Martin H., (1955) *Ballistic Research Laboratories Report No. 971: A Survey of Domestic Electronic Digital Computing Systems*. Aberdeen Proving Ground, MD: United States Department of Commerce Office of Technical Services. p. 41. Retrieved 29 March 2015.

White F.M., (1991).*Viscous Fluid Flow*, McGraw Hill International,

Wilcox C. D., (1998). *Turbulence Modelling for CFD*, (2nd Ed.), DCW Industries, La Cañada

X86-guide, (2015), *X86 CPUs' guide, Intel Pentium, P5 architecture*, [online] Available at: http://www.x86-guide.com/en/cpu/Intel-Pentium/P5-2.html, [Accessed 14th January 2015]

Zitzmann, T; Cook, M; Pfrommer, P; Rees, S; Marjanovic, L; (2005) *Simulation of steady-state natural convection using CFD*. IBPSA 2005 - International Building Performance Simulation Association 2005 pp. 1449-1456

Appendix A

Turbulence in Navier-Stokes equations

Turbulence is a type of chaotic flow in the flow system; it is usually random both in time and space respectively. Generally speaking a turbulent leads to the increase of energy dissipation, heat transfer and fluid mixing. The study of turbulence in physics and mathematics always been important in fluid dynamic (Versteeg and Malalasekera, 1995).

Turbulence research is extremely difficult in many ways, yet this thesis is focussed on the engineering solution and shall avoid in-depth discussion of turbulence mechanism. It starts with simple turbulence modelling method – the Reynolds Averaged Navier-Stokes equation (RANS) approach.

In general engineering assumption, the turbulence in a flow is quantified in terms of velocity fluctuation (ũ) – unpredictable both in time and space. So the total velocity (u) is equivalence to the sum of mean-velocity (ū) plus the derivative (fluctuation) velocity (ũ) (Tennekes and Lumley, 1972)

$$u = \bar{u} + \tilde{u} \tag{0-1}$$

From previous part of Navier-Stokes equation:

$$\rho\left(\frac{\partial \mathrm{u}}{\partial t} + \mathrm{u}\cdot\nabla\mathrm{u}\right) = -\nabla p + \mu\nabla^2\mathrm{u} + \mathrm{f} \tag{0-2}$$

Simplify and combine the viscosity and other tensor force (τ) term, then it became:

$$\rho\left(\frac{\partial \mathrm{u}}{\partial t} + \mathrm{u}\cdot\nabla\mathrm{u}\right) = -\nabla p + \nabla\tau \tag{0-3}$$

Where the velocity, pressure and shear force included the mean term ($\bar{u}, \bar{p}, \bar{\tau}$) and fluctuation term ($\tilde{u}, \tilde{p}, \tilde{\tau}$), then:

$$u = \bar{u} + \tilde{u}, \qquad p = \bar{p} + \tilde{p}, \qquad \tau = \bar{\tau} + \tilde{\tau} \tag{0-4}$$

$$\rho\left(\frac{\partial(\bar{\mathrm{u}} + \tilde{\mathrm{u}})}{\partial t} + (\bar{\mathrm{u}} + \tilde{\mathrm{u}})\cdot\nabla(\bar{\mathrm{u}} + \tilde{\mathrm{u}} + \tilde{\mathrm{u}})\right) = -\nabla(\bar{p} + \tilde{p}) + \nabla(\bar{\tau} + \tilde{\tau}) \tag{0-5}$$

Also it can be written in the partial differential equation (PDE) symbol ∂ instead of del symbol, the equation then become:

$$\rho\left(\frac{\partial(\bar{\mathrm{u}}_\iota + \tilde{\mathrm{u}}_\iota)}{\partial t} + (\bar{\mathrm{u}}_\jmath + \tilde{\mathrm{u}}_\jmath)\cdot\left(\frac{\partial \bar{\mathrm{u}}_\iota}{\partial x_j} + \frac{\partial \tilde{\mathrm{u}}_\iota}{\partial x_j}\right)\right) = -\left(\frac{\partial \bar{p}}{\partial x_i} + \frac{\partial \tilde{p}}{\partial x_i}\right) + \left(\frac{\partial \overline{\tau_{ij}^{\nu}}}{\partial x_j} + \frac{\partial \widetilde{\tau_{ij}^{\nu}}}{\partial x_j}\right) \tag{0-6}$$

By averaging out the equation set **3-23** with time, where:

$$\rho\left(\overline{\frac{\partial(\bar{u}_\iota+\tilde{u}_\iota)}{\partial t}}+\overline{(\bar{u}_J+\tilde{u}_J)\cdot\left(\frac{\partial\bar{u}_\iota}{\partial x_J}+\frac{\partial\tilde{u}_\iota}{\partial x_J}\right)}\right)=\overline{-\left(\frac{\partial\bar{p}}{\partial x_\iota}+\frac{\partial\tilde{p}}{\partial x_\iota}\right)}+\left(\overline{\frac{\partial\overline{\tau_{\iota J}^{(v)}}}{\partial x_J}+\frac{\partial\widetilde{\tau_{\iota J}^{(v)}}}{\partial x_J}}\right) \quad \text{0-7}$$

Simplify the equation **2-24**, where average of a derivative is the same as the derivative of the average:

$$\bar{\bar{x}}=\tilde{\tilde{x}}=0$$

The equation **3-24** eventually becomes:

$$\rho\left(\frac{\partial\bar{u}_\iota}{\partial t}+\bar{u}_J\cdot\frac{\partial\bar{u}_\iota}{\partial x_j}+\overline{\tilde{u}_J\cdot\frac{\partial\tilde{u}_\iota}{\partial x_J}}\right)=-\frac{\partial\bar{p}}{\partial x_i}+\frac{\partial\overline{\tau_{\iota J}^{v}}}{\partial x_j} \quad \text{0-8}$$

Where put the velocity fluctuation term to the right hand side:

$$\rho\left(\frac{\partial\bar{u}_\iota}{\partial t}+\bar{u}_J\cdot\frac{\partial\bar{u}_i}{\partial x_j}\right)=-\frac{\partial\bar{p}}{\partial x_i}+\frac{\partial\overline{\tau_{\iota J}^{(v)}}}{\partial x_j}+\rho\cdot\langle\overline{\tilde{u}_J\cdot\frac{\partial\tilde{u}_\iota}{\partial x_J}}\rangle \quad \text{0-9}$$

Notice that now the velocity fluctuation term written next to the stress term. With the product rule of differential equation, where:

$$\tilde{u}_J\cdot\frac{\partial\tilde{u}_\iota}{\partial x_j}+\tilde{u}_\iota\cdot\frac{\partial\tilde{u}_J}{\partial x_j}=\frac{\partial}{\partial x_j}\tilde{u}_\iota\tilde{u}_J \quad \text{0-10}$$

Flows the mass conservation, where:

$$\nabla u=\nabla\bar{u}+\nabla\tilde{u}=\frac{\partial\bar{u}_j}{\partial x_j}+\frac{\partial\tilde{u}_J}{\partial x_j} \quad \text{0-11}$$

Then:

$$\frac{\partial\bar{u}_j}{\partial x_j}=0,\qquad\frac{\partial\tilde{u}_J}{\partial x_j}=0$$

Which leads to:

$$\rho\left(\frac{\partial\bar{u}_\iota}{\partial t}+\bar{u}_J\cdot\frac{\partial\bar{u}_i}{\partial x_j}\right)=-\frac{\partial\bar{p}}{\partial x_i}+\frac{\partial\overline{\tau_{\iota J}^{(v)}}}{\partial x_j}+\rho\cdot\langle\frac{\partial}{\partial x_j}\overline{\tilde{u}_\iota\tilde{u}_J}\rangle \quad \text{0-12}$$

Or:

$$\rho\left(\frac{\partial\bar{u}_\iota}{\partial t}+\bar{u}_J\cdot\frac{\partial\bar{u}_i}{\partial x_j}\right)=-\frac{\partial\bar{p}}{\partial x_i}+\frac{\partial}{\partial x_j}\left[\overline{\tau_{\iota J}^{(v)}}+\rho\cdot\langle\overline{\tilde{u}_\iota'\tilde{u}_J'}\rangle\right] \quad \text{0-13}$$

Notice that now both the stress tensor term and the velocity fluctuation term are second order terms, they are quite similar to each other therefore the velocity fluctuation term was considered as an 'artificial force' named Reynolds Stress (Hinze, 1975).

By averaging them out, the equations became the Reynolds (time) Average of the Navier-stokes equations (RANS), the only derivative part t) left in the equation is the convective acceleration terms – the Reynolds Stress term, where happen to be the non-linear part of the equations as well. It then leads to an assumption, though not a conclusion, that the turbulence is due to the non-linearity of the Navier-Stokes equations.

Notice that the u_i and u_j stands for 3 dimensional velocities (*u, v, ω*), then the Reynolds Stress term $\rho \cdot \langle \overline{\tilde{u}_i' \tilde{u}_j'} \rangle$ would have 6 components: $\rho\langle\overline{\tilde{u}'\tilde{u}'}\rangle, \rho\langle\overline{\tilde{v}'\tilde{v}'}\rangle,\ \rho\langle\overline{\tilde{\omega}'\tilde{\omega}'}\rangle,\ \rho\langle\overline{\tilde{u}'\tilde{v}'}\rangle,\ \rho\langle\overline{\tilde{v}'\tilde{\omega}'}\rangle$ and $\rho\langle\overline{\tilde{u}'\tilde{\omega}'}\rangle$. This leads to a 'Turbulence Closure Problem' which turbulence modelling seeks to address.

The arises because there are still 3 Navier-Stokes equations with an extra (continuity) equation of incompressible flow, but also 10 unknowns in the equations (3 dimensional velocities, 1 pressure and 6 Reynolds Stresses) which imbalanced the solution.

Introduction of Turbulence Kinetic Energy (TKE)

The origins of turbulence mechanism in an important research area in its own right and only a brief introduction of turbulence mechanism is provide here. The turbulence modelling starts with the Reynolds Stress, where:

$$\tau_{ij} = -\rho\overline{\tilde{u}_i' \tilde{u}_j'} \qquad 0\text{-}14$$

Turbulence process is assumed to have production, then transportation and dissipation which in the same manner as Navier-Stokes equation for general fluid problem. The Turbulence Kinetic Energy usually generated by the force applied on the fluid (control volume), such as shear force (viscosity force) and buoyancy force, which engineering approaches tend to use a turbulence (kinetic energy) production rate to describe this. (Pope, 2003)

Turbulence (kinetic energy) dissipation can be used to describe the dissipation of viscous force, where the kinetic energy is transferred down in the turbulence energy cascade. The eddies in the turbulence break down from large size to small size, and eventually reach the Kolmogorov Scale (Landahl, Mollo-Christensen, 1992) where turbulence motion is dissipated as heat.

Consider the Reynolds Stress with a material time derivative of the non-averaged terms, where:

$$\frac{D(\tau_{ij}')}{Dt} = \frac{D(\rho\widetilde{u_i}'\widetilde{u_j}')}{Dt} = \rho\frac{D(\widetilde{u_i}'\widetilde{u_j}')}{Dt} \quad 0\text{-}15$$

And apply the chain rule it became:

$$\rho\frac{D(\widetilde{u_i}'\widetilde{u_j}')}{Dt} = \widetilde{u_j}'\frac{D(\rho\widetilde{u_i}')}{Dt} + \widetilde{u_i}'\frac{D(\rho\widetilde{u_j}')}{Dt} \quad 0\text{-}16$$

It can finally be rewritten into the general Turbulence Kinetic Energy (TKE) equation as:

$$\widetilde{u_j}'\frac{D(\rho\widetilde{u_i}')}{Dt} + \widetilde{u_i}'\frac{D(\rho\widetilde{u_j}')}{Dt} = \rho\left\{\langle\widetilde{u_j}\frac{\partial\widetilde{u_i}}{\partial t}\rangle + \overline{u_j}\langle\widetilde{u_j}\frac{\partial\widetilde{u_i}}{\partial x_k}\rangle\right\} + \rho\left\{\langle\widetilde{u_i}\frac{\partial\widetilde{u_j}}{\partial t}\rangle + \overline{u_j}\langle\widetilde{u_i}\frac{\partial\widetilde{u_j}}{\partial x_k}\rangle\right\} \quad 0\text{-}17$$

And the Reynolds Stress can be written as:

$$\rho\cdot\langle\widetilde{u_i}'\widetilde{u_j}'\rangle = 2\,\mu\left[S_{ij} - \frac{1}{3}S_{kk}\delta_{ij}\right] \quad 0\text{-}18$$

Where the rate of tensor would be:

$$S_{ij} = \frac{1}{2}\left(\frac{\partial u_i}{\partial x_j} + \frac{\partial u_j}{\partial x_i}\right) \quad 0\text{-}19$$

As been stated in the previous paragraph, the averaged Navier-Stokes equations with the Reynolds Stress term should be:

$$\rho\left(\frac{\partial\overline{u_i}}{\partial t} + \overline{u_j}\cdot\frac{\partial\overline{u_i}}{\partial x_j}\right) = -\frac{\partial\bar{p}}{\partial x_i} + \frac{\partial\overline{\tau_{ij}^{(v)}}}{\partial x_j} + \rho\cdot\langle\frac{\partial}{\partial x_j}\widetilde{u_i}\widetilde{u_j}\rangle \quad 0\text{-}20$$

Then it can finally be rewritten into the general Turbulence Kinetic Energy (TKE) equation as:

$$\begin{aligned}\frac{\partial(\tau_{ij})}{\partial t} + \overline{u_j}\cdot\frac{\partial(\tau_{ij})}{\partial x_k} &= -\left[(\tau_{ik})\cdot\frac{\partial\overline{u_j}}{\partial x_k} + (\tau_{jk})\cdot\frac{\partial\overline{u_i}}{\partial x_k}\right] + \varepsilon_{ij} - \Pi_{ij} \\ &+ \frac{\partial}{\partial x_k}\left[\frac{\mu}{\rho}\frac{\partial(\tau_{ij})}{\partial x_k} + C_{ijk}\right]\end{aligned} \quad 0\text{-}21$$

With the Boussineq eddy viscosity model (Schmitt, 2007), the Reynolds Stress can be written as:

$$\tau_{ij} = -\rho\overline{\widetilde{u_i}'\widetilde{u_j}} = v_t\left(\frac{\partial\overline{u_i}}{\partial x_j} + \frac{\partial\overline{u_j}}{\partial x_i}\right) - \frac{2}{3}k\delta_{ij} = \frac{\mu}{\rho}\left(\frac{\partial\overline{u_i}}{\partial x_j} + \frac{\partial\overline{u_j}}{\partial x_i}\right) - \frac{2}{3}k\sigma_{ij} \quad 0\text{-}22$$

To rewrite the Reynolds Stress term into an equation that coupled with the Navier-Stokes equation, a concept of Turbulence Kinetic Energy (TKE) has been introduced, it generally refers as the mean of the normal stress of the turbulence where:

$$k = \frac{1}{2}\left(\overline{(u')^2} + \overline{(v')^2} + \overline{(\omega')^2}\right) \quad \text{0-23}$$

Notice that now the Turbulence Kinetic Energy became 1/2 of the total sum of Reynolds Stress. So the expression of the turbulence process (production, transportation and dissipation) is:

$$\frac{Dk}{Dt} + \nabla \cdot T' = \mathrm{P}_k - \varepsilon \quad \text{0-24}$$

$\frac{Dk}{Dt}$ is the mean-flow material derivative of Turbulence Kinetic Energy

$\nabla \cdot T'$ is the transportation of Turbulence Kinetic Energy

P_k is production of the Turbulence Kinetic Energy

ε is the dissipation of Turbulence Kinetic Energy

The equations above have somewhat a similar appearance as the general Navier-Stokes equations, so the problem then becomes as how the Turbulence Kinetic Energy equations can be rewritten into a manner that couples with the Navier-Stokes equations.

Now the Turbulence Kinetic Energy (TKE) equation is written in a manner similar as the Navier-Stokes equations, with production, transportation and dissipation terms in it. Set j=1 and k=j of the equation and added the terms together, it became:

$$\rho\frac{\partial k}{\partial t} + \rho\frac{\partial\left(\overline{\mathrm{u}_j}k\right)}{\partial x_j} = -\left(\tau_{ij}\right)\cdot\frac{\partial\overline{\mathrm{u}_j}}{\partial x_j} - \mu\overline{\left(\frac{\partial\widetilde{\mathrm{u}_\iota}}{\partial x_k}\frac{\partial\widetilde{\mathrm{u}_\iota}}{\partial x_k}\right)} + \frac{\partial}{\partial j}\left[\mu\frac{\partial k}{\partial x_j} + \frac{1}{2}\rho\overline{\widetilde{u_\iota}\widetilde{u_\iota}\widetilde{u_j}} - \overline{\tilde{p}\widetilde{u_j}}\right] \quad \text{0-25}$$

By assuming the turbulence is homogenous, a turbulence dissipation ratio ε has been introduced into the equation define as:

$$\varepsilon = \frac{\mu}{\rho}\overline{\left(\frac{\partial\widetilde{\mathrm{u}_\iota}}{\partial x_k}\frac{\partial\widetilde{\mathrm{u}_j}}{\partial x_k}\right)} = -\overline{\widetilde{u_\iota}\widetilde{\mathrm{u}_j}}\cdot\frac{\partial\overline{\mathrm{u}_\iota}}{\partial x_j} \quad \text{0-26}$$

Notice that the ε term is part of viscosity term in Navier-Stokes equations, and it is in fact a damping / diffusion term of the equation.

White (1991) comes to the assumption that based on a physical term that the eddy size scale (l) would move with the speed (u), and the energy dissipated per unit mass then would be:

$$\varepsilon \approx \frac{(drag)\cdot(velocity)}{mass} \approx \frac{(\rho\mathrm{u}^2 l)\mathrm{u}}{\rho l^3} \approx \frac{\mathrm{u}^3}{l} \quad \text{0-27}$$

For small and incompressible flow, the pressure fluctuation terms can be gathered in the same block with a gradient diffusion term as (Wilcox, 1993, Turbulence modelling for CFD, DCW industries. Inc):

$$\frac{\mu_t}{\sigma_k}\frac{\partial k}{\partial x_j} = -\frac{1}{2}\rho\overline{\tilde{u}_i\tilde{u}_i\tilde{u}_j} + \left(\overline{\tilde{p}\tilde{u}_j}\right) \qquad 0\text{-}28$$

Where the σ_k is a closure coefficient (Prandtl-Schmidt number) of k.

Now the equation of Turbulence Kinetic Energy (TKE) can be reduced to:

$$\rho\frac{\partial k}{\partial t} + \rho\frac{\partial\left(\bar{u}_j k\right)}{\partial x_j} = -\left(\tau_{ij}\right)\cdot\frac{\partial\overline{u_k}}{\partial x_j} - \rho\varepsilon + \frac{\partial}{\partial x_j}\left[\mu + \frac{\mu_t}{\sigma_k}\frac{\partial k}{\partial x_j}\right] \qquad 0\text{-}29$$

And the dissipation and eddy viscosity is given as:

$$\varepsilon = C_D\frac{k^{\frac{3}{2}}}{l}, \qquad \mu_t = C_\mu\rho k^{\frac{1}{2}}l = C_\mu\rho\frac{k}{\varepsilon} \qquad 0\text{-}30$$

It is clear now that the turbulence model has introduce 2 more unknowns k and ε, other than this, only the shear stress τ_{ij} and mean velocity ū comes from the Navier-Stokes equations. The rest part of the turbulence model would be approximated with a constant that can measure from experiment. With the Turbulence Kinetic Energy (k) equation there are 4 equations now, however with 3 velocities, 1 pressure, k and ε there are 6 unknowns. As a result and other equation has to be added in to complete the equation sets to form the general solution.

Two equation turbulence model, standard k-ε (kinetic - epsilon) and k-ω (kinetic - omega) turbulent model

As the zero equation turbulence models usually have a constant scalar between velocity scale and length scale, they might be too simple to describe the turbulence in fluid motion. The Turbulence Kinetic Energy has been introduced in the previous part of this work, and as it stated 2 extra equations are needed to complete the description of Turbulence Kinetic Energy (TKE).

Since the derivation of Turbulence Kinetic Energy equation completed in previous chapter, the work here will focus on the second equation of the turbulence model (Wilcox 1998).

In the previous chapter the dissipation ratio ε define as:

$$\varepsilon = \frac{\mu}{\rho}\overline{\left(\frac{\partial\tilde{u}_i}{\partial x_k}\frac{\partial\tilde{u}_j}{\partial x_k}\right)} \qquad 0\text{-}31$$

From the equation:

$$\rho\left\{\frac{\partial \widetilde{u_i}}{\partial t}+\overline{u_j}\cdot\frac{\partial \widetilde{u_i}}{\partial x_j}\right\}=-\frac{\partial \tilde{p}}{\partial x_i}+\frac{\partial \widetilde{\tau_{ij}^{(v)}}}{\partial x_j}-\rho\cdot\widetilde{u_j}\cdot\frac{\partial \overline{u_i}}{\partial x_j}-\left\{\rho\cdot\widetilde{u_j}\cdot\frac{\partial \widetilde{u_i}}{\partial x_j}-\rho\cdot\left\langle\frac{\partial}{\partial x_j}\widetilde{u_i}\widetilde{u_j}\right\rangle\right\} \quad 0\text{-}32$$

Differentiation of this equation with respect to x_k and multiplication by $\partial\tilde{u}_i/\partial x_k$ and average of the equation yields, then it became:

$$\begin{aligned}&\rho\overline{\frac{\partial \widetilde{u_i}}{\partial x_k}\frac{\partial}{\partial x_k}\left(\frac{\partial \widetilde{u_i}}{\partial t}\right)}+\rho\overline{\frac{\partial \widetilde{u_i}}{\partial x_k}\frac{\partial}{\partial x_k}\left(\overline{u_j}\cdot\frac{\partial \widetilde{u_i}}{\partial x_j}\right)}\\&\quad=-\overline{\frac{\partial \widetilde{u_i}}{\partial x_k}\frac{\partial}{\partial x_k}\left(\frac{\partial \tilde{p}}{\partial x_i}\right)}+\overline{\frac{\partial \widetilde{u_i}}{\partial x_k}\frac{\partial}{\partial x_k}\left(\frac{\partial \widetilde{\tau_{ij}^{(v)}}}{\partial x_j}\right)}-\rho\overline{\frac{\partial \widetilde{u_i}}{\partial x_k}\frac{\partial}{\partial x_k}\left(\widetilde{u_j}\cdot\frac{\partial \overline{u_i}}{\partial x_j}\right)}\\&\quad-\left\{\overline{\rho\frac{\partial \widetilde{u_i}}{\partial x_k}\frac{\partial}{\partial x_k}\left(\widetilde{u_j}\cdot\frac{\partial \widetilde{u_i}}{\partial x_j}\right)}-\overline{\rho\frac{\partial \widetilde{u_i}}{\partial x_k}\frac{\partial}{\partial x_k}\left(\frac{\partial}{\partial x_j}\overline{\widetilde{u_i}\widetilde{u_j}}\right)}\right\}\end{aligned} \quad 0\text{-}33$$

And the k and ε equation can be rewritten into a formation that only have mean velocity, pressure, shear force and constant terms:

$$\rho\frac{\partial k}{\partial t}+\rho\frac{\partial\left(\overline{u_j}k\right)}{\partial x_j}=-\frac{\partial}{\partial x_j}\left[\mu+\frac{\mu_t}{\sigma_k}\frac{\partial k}{\partial x_j}\right]+-\left(\tau_{ij}\right)\cdot\frac{\partial \overline{u_i}}{\partial x_j}-\rho\varepsilon \quad 0\text{-}34$$

$$\rho\frac{\partial \varepsilon}{\partial t}+\rho\frac{\partial\left(\overline{u_j}\varepsilon\right)}{\partial x_j}=\frac{\partial}{\partial x_j}\left[\mu+\frac{\mu_t}{\sigma_\varepsilon}\frac{\partial \varepsilon}{\partial x_j}\right]+C_{\varepsilon1}\frac{\varepsilon}{k}\cdot\left(\tau_{ij}\right)\cdot\frac{\partial \overline{u_i}}{\partial x_j}+C_{\varepsilon2}\rho\frac{\varepsilon^2}{k} \quad 0\text{-}35$$

Where the constants are given by experiments (e.g. Rodi, 1980) which:

$$C_{\varepsilon1}=1.44\,,\qquad C_{\varepsilon2}=1.92\,,\qquad C_\mu=0.09\,,\qquad \sigma_k=1.0\,,\qquad \sigma_\varepsilon=1.3 \quad 0\text{-}36$$

Later on, another two-equation turbulence model is k- ω (kinetic - omega) presented by Wilcox (1988) by using a ω equation instead of ε where:

$$\omega=c\frac{k^{\frac{1}{2}}}{l}\propto\frac{\varepsilon}{k},\qquad \mu_t\propto\frac{\rho k}{\omega} \quad 0\text{-}37$$

With the k- ω model the k equation of Turbulence Kinetic Energy remain mostly the same; while the second equation can relate to $\omega \propto \varepsilon/k$ where the ω equation only solve the destruction rate of Turbulence Kinetic Energy (TKE) at the point where the dissipation occurs.

So the general expression of *k-ω* (kinetic - omega) turbulent model can be written as:

$$\rho\frac{\partial k}{\partial t}+\rho\frac{\partial\left(\overline{u_j}k\right)}{\partial x_j}=-\frac{\partial}{\partial x_j}\left[\mu+\frac{\mu_t}{\sigma_k}\frac{\partial k}{\partial x_j}\right]+-\left(\tau_{ij}\right)\cdot\frac{\partial \overline{u_i}}{\partial x_j}-\beta^*\rho k\omega \quad 0\text{-}38$$

$$\rho\frac{\partial\omega}{\partial t}+\rho\frac{\partial\left(\bar{u}_j\omega\right)}{\partial x_j}=\frac{\partial}{\partial x_j}\left[\mu+\frac{\mu_t}{\sigma_\omega}\frac{\partial\omega}{\partial x_j}\right]+\alpha\frac{\omega}{k}\cdot\left(\tau_{ij}\right)\cdot\frac{\partial\bar{u}_i}{\partial x_j}+\beta\rho\omega^2 \qquad 0\text{-}39$$

Where:

$$\alpha=\frac{5}{9}\,,\qquad \beta=\frac{3}{40}\,,\qquad \beta^*=\frac{9}{100}\,,\qquad \sigma_\omega=\frac{1}{2}\,,\qquad \sigma_k=\frac{1}{2} \qquad 0\text{-}40$$

General speaking both k-ε and k-ω model are easy to apply and acceptable accurate in a wide range of cases (from low Reynolds number to high Reynolds number). However the k-ε model, which largely based on the dissipation rate of turbulence, has a weak prediction of turbulence near wall and has to apply a wall treatment / wall function to blend the equation in low Reynolds number cases. In the other hands the k-ω model based on turbulence frequency has a better accuracy in near wall condition and more suitable for lower Reynolds number cases.

Meanwhile the cons of applying *k-ω* model especially *k-ω* (SST) model is that it needs a very fine mesh / grip near wall, this results certain difficulties to generate a mesh in some cases that has a huge amount of surface detail. The other point of *k-ω* (SST) model is that it might take too much computation power and the robustness of the solver engine may be poorer as well.

Notice: *the k-ω (SST) model is generally a k-ω model with a switch that in a certain condition of the flow, the solver would switch to k-ε model in the far-wall section of the flow.*

The k-ω model turbulence model and its variations (i.e. SST model) would be used in part of the case study in this research. Although more complex turbulence could be applied, it is part of the goal in this research to use the limited resource to obtain a reasonably CFD solution for the work.

The turbulence modelling is not all but part of difficulty in solving the problem, as it is a density driven / natural convection problem. The physical nature of this type of problem has more instability in a CFD solution rather than just turbulence. (ANSYS, 2010)

Appendix B

Top listed supercomputers from 1946 to 2013

Super Computer	Year	Capacity	Power consumption	Size	kW/m^2	Location
ENIAC (UPenn)	1946	100 kOPS	**150kW**	167m^2	0.90	U.S.A
Cary 2	1985	3.9GFLOPS	**195kW**	1.4m^2 (1)	**140**	U.S.A
ASCI Red	1999	3.207 TFLOPS	**850kw**	232m^2	3.66	U.S.A
NEC Earth Simulator	2002	35.86 TFLOPS	**3.2 Meta-Watts**	180m^2	**17.8**	Japan
IBM Blue Gene	2007	596.4TFLOPS	**2.32 Mega-Watts**	280m^2	8.28	U.S.A
IBM Road Runner	2008	1.105 PFLOPS	**2.35 Mega-Watts**	560m^2	4.20	U.S.A
TianHe-1	2010	2.566 PFLOPS	**4.04 Mega-Watts**	1000m^2	4.04	China
TianHe-2	2013	33.86 PFLOPS	**17.6 Mega-Watts**	720m^2	**24.4**	China

Table 0-1 Computing performance, Thermal load and space occupation of some top listed supercomputers

(TOP500, 2015), (SEAS. UPEEN, 2015) (CRAY, 1988), (Tomkins, 1999), (Balance, 2004), (Habata, 2003), (ASIC.LLNL, 2011), (Patterspn, 2013), (NSCC, 2011), (Dongarra, 2013), (Chen, 2015).